

**Heterogeneity and scale  
in the rational design  
of an immobilized biocatalyst**

Promotor:  
Prof.dr.ir. J. Tramper  
Hoogleraar in de Bioprocestechnologie, Wageningen Universiteit

Copromotoren:  
Dr. H.H. Beeftink  
Universitair docent, sectie Proceskunde, Wageningen Universiteit  
Dr.ir. C.G.P.H. Schroën  
Universitair docent, sectie Proceskunde, Wageningen Universiteit

Promotiecommissie:  
Prof.dr. J.M.S. Cabral (Instituto Superior Técnico, Lisboa)  
Prof.dr. A. Bruggink (DSM, Heerlen / Radboud Universiteit Nijmegen)  
Prof.dr.ir. R.M. Boom (Wageningen Universiteit)  
Dr. A.A.M. van Lammeren (Wageningen Universiteit)

J.L. van Roon

**Heterogeneity and scale  
in the rational design  
of an immobilized biocatalyst**

PROEFSCHRIFT

TER VERKRIJGING VAN DE GRAAD VAN DOCTOR

OP GEZAG VAN DE RECTOR MAGNIFICUS

VAN WAGENINGEN UNIVERSITEIT,

PROF.DR. M.J. KROPFF,

IN HET OPENBAAR TE VERDEDIGEN

OP VRIJDAG 9 SEPTEMBER 2005

DES NAMIDDAGS TE VIER UUR IN DE AULA.

Roon, J.L. van; 2005.

Heterogeneity and scale in the rational design of an immobilized biocatalyst.

Thesis Wageningen University - with summary in Dutch.

Cover illustration: micrograph of a section through an Assemblase<sup>®</sup> particle. The penicillin-G acylase was immunogold-labeled, silver enhanced and detected with light microscopy in epi-polarization mode. Because the light that reflected from the labels was collected, light regions in the micrograph correspond with section areas of high enzyme densities.

ISBN: 90-8504-246-1

Aan mijn ouders, aan Janet



## Abstract

Assemblase<sup>®</sup> is an industrial biocatalytic particle into which penicillin-G acylase is immobilized. Amongst others, it catalyzes the synthesis of the  $\beta$ -lactam antibiotic cephalexin. Because Assemblase<sup>®</sup>-catalyzed cephalexin synthesis is sub-optimal in terms of yield and selectivity, the behavior of Assemblase<sup>®</sup> was studied with respect to underlying physical and chemical phenomena at various levels of scale. At macro-scale, the diffusion limited behavior of Assemblase<sup>®</sup> was studied and the active enzyme loading was assessed as a function of particle diameter. At micro-scale, the distribution of enzyme was quantitatively determined. At nano-scale, abrupt local deviations of the intra-particle enzyme density were discovered at the particle perimeter and surrounding intra-particle voids, which were subsequently linked to local heterogeneities in the matrix structure. From the combined data (including reactant diffusivities) a mechanistic model was constructed that could describe the behavior of Assemblase<sup>®</sup> well, for conditions ranging from hardly to heavily diffusion limited. The model provides insight in the bottlenecks of the present biocatalytic particle and may be used as a tool for biocatalyst design. Finally, possibilities for future improvement of biocatalysts are discussed for various fields of research.





# Contents

Chapter 1	Introduction	1
Chapter 2	Assessment of intra-particle biocatalytic distributions as a tool in rational formulation	13
Chapter 3	Enzyme distribution derived from macroscopic particle behavior of an industrial immobilized penicillin-G acylase	33
Chapter 4	Novel approach to quantify immobilized-enzyme distributions	59
Chapter 5	Enzyme distribution and matrix characteristics in biocatalytic particles	81
Chapter 6	FESEM analysis of morphology and enzyme distribution within an industrial biocatalytic particle	111
Chapter 7	A multi-component reaction-diffusion model of a heterogeneously distributed immobilized enzyme	129
Chapter 8	Discussion	165
Chapter 9	Epilogue	187
Summary		195
Samenvatting		199
List of publications		203
Nawoord		205
Curriculum vitae		209



---

## Chapter 1 Introduction



## ENZYMATIC BIOCATALYSIS

White biotechnology, the biotechnological production of chemical compounds using enzymes and microorganisms (Jaeger, 2004), has taken an industrial flight. Biotechnological production of desired compounds, which we will call biocatalysis, is now part of the toolbox for the production of a very broad array of (fine) chemicals (Straathof *et al.*, 2002). In search for almost quantitative conversions with low waste streams, chemical industries increasingly invest in life sciences, and biochemists have become accustomed to the use of biocatalysis in new and complex synthesis reactions. Being extremely selective, both simple and complex reactions can be catalyzed with unprecedented chiral and regional selectivity, resulting in highly efficient reactions with few by-products (Schmid *et al.*, 2001). It was estimated that in 10% of the cases, sustainable biocatalysis provides an overall superior synthetic strategy over traditional organic chemistry (Roberts, 2004). It should be realized, however, that the application of the vast array of biocatalytic activities presented by nature is limited. The fact that some enzymes have, besides their natural functions, also a useful application in industry is simply serendipitous (Arnold, 2001). This useful application must be recognized during screening. On top of that, the cost of enzymes may usually not exceed 1-2 % of the final product costs (Cheetham, 1998).

For biocatalytic synthesis of a desired product, whole cells, or one or more isolated enzyme(s), can be used (Thomas *et al.*, 2002). Whole-cell biocatalytic transformations are typically used for complex synthetic redox transformations that require cofactors, because during the conversion the cofactors need to be regenerated, which is a costly task to do *in vitro* (Schmid *et al.*, 2001). Whole-cell biocatalysts and partly purified (crude) enzyme preparations have proved to be very successful in industrial resolutions of racemic mixtures, dynamic kinetic resolutions, or asymmetric synthesis reactions (Schultze and Wubbolts, 1999). In fact, one of the latest scientific developments in biocatalysis is the use of more complex, sometimes living, biocatalytic systems, which catalyze multi-step microbial syntheses of complex chemicals (Schoemaker *et al.*, 2003). Most probably, in time such complex systems will become within reach of industry. In this work, however, we will confine ourselves to the current mainstream

industrial situation: the application of one or more isolated enzymes without cofactor requirement.

## **INNOVATIONS IN ENZYME BIOCATALYSIS**

The diversity of the industrial application is modest. The currently largest industrial biocatalytic processes involve hydrolytic enzymes: proteases for detergent and dairy industries, and carbohydrases for the textile, detergent, and baking industries (Kirk *et al.*, 2002). Panke and colleagues (2004) concluded from 205 relevant industrial patents that the industrial biocatalytic innovations are mainly the continued use of hydrolases (where novel enzymes are available as a result of genomics and high-throughput screening), and the increase in novel oxidoreductases for ketone reductions, aminotransferases, and carbon-carbon bond formation (e.g. Turner, 2003). Also, increasing numbers of oxidative biotransformations are reported (e.g. Burton, 2003). The reason for this limited diversity might have been partly due to the limited enzyme availability, substrate scope, and operational stability (Schoemaker *et al.*, 2003). In this respect, much is expected from the rapid developments in directed evolution (i.e. the mimicked Darwinian evolution in a test tube) by random mutagenesis or *in vitro* gene recombination methods, combined with high-throughput screening (Panke & Wubbolts, 2002). Additionally, the operational stability of enzymes heavily depends on the conditions during storage and during the biocatalytic conversion. The relevance of this issue depends on the price of the enzyme, and on the added value of the product.

## **ENZYME IMMOBILIZATION**

Although enzymes are cheap in some cases (\$10-20/kg protein; Van Beilen and Li, 2002), most of them are expensive, and must be recovered and reused. An industrial demand for absence of enzyme activity in the end product might be another important incentive for the immobilization of enzymes, especially if no thermal or chemical denaturation takes place after the enzymatic conversion. Reuse is often facilitated by immobilization onto a solid support material. The alternative, confinement of free enzyme in a specific volume, by application of e.g. ultra-filtration membranes as a selective barrier, is still an industrial

challenge, because the thermal and mechanical mixing of industrial vessels is not ideal, making the sensitive enzyme more susceptible for degradation in so called “hot-spots”: areas with different temperatures, pH’s or composition, as a result of heterogeneities in the reaction vessel.

Different immobilization technologies have been developed over the last 30 years, including deposition onto hydrophilic inorganic material, encapsulation, covalent linkage to carriers and cross-linking (Christensen *et al.*, 2003). The immobilization method should –amongst other things– stabilize the enzyme, with minimal leakage from the carrier, be cost effective, robust and reproducible. Once immobilized, a thorough analysis should be done on the performance to ensure performance and stability (durability) in the application. The first step would be to compare the macroscopic activity of the immobilized biocatalyst to that of its free (water-) dissolved counterpart. In many cases, this activity will not be the same.

## DESIGN STRATEGY

Two very important questions need to be answered in the optimization of biocatalytic particles. Depending on the answers, different approaches for particle optimization have to be followed. The first question is whether the difference in performance between the immobilized enzyme and the free-enzyme catalyzed bioconversion originates from the (covalent) interaction with the support material, resulting in altered kinetic enzyme behavior, or from mass transfer limitation(s) during the biochemical essay.

### CONFORMATIONAL ENZYME CHANGES

An answer can be obtained by doing a bioconversion with the immobilized enzyme under zero-order condition. This, for instance, can be achieved with high substrate concentrations, or by freezing larger particles and grinding them. If the activity of the immobilized enzyme under zeroth-order conditions is the same as that of the free enzyme, the difference most probably originated from mass-transfer limitation(s) during the conversion. If the activity differs between the two, however, the interaction between the enzyme and its support probably changed the kinetic characteristics of the enzyme. In case these changed characteristics are solely attributed to changes in enzyme conformation, other

support materials or other immobilization methods may have to be used to improve particle performance.

### **MASS-TRANSFER LIMITED PERFORMANCE**

The second question is which type of reaction(s) is (are) considered. Does the bioconversion concern a single reaction of which the desired end-product is the one that is (predominantly) available at the thermodynamic equilibrium? Alternatively it may be a cascade of reactions originating from a single substrate, resulting in a single or multiple end products. Also multiple substrates may be involved, possibly in competing reactions, resulting in multiple (desired and undesired products). It is also possible that the desired product is only accumulated temporarily, i.e. that the conversion is kinetically controlled, instead of thermodynamically. The next paragraphs will give three examples of how the answers to these two questions determine the strategy for particle optimization.

#### ***Single thermodynamically controlled reaction***

Optimization of the biocatalytic particle is relatively straightforward in this case. When the biocatalytic particle is limited by the choice of the support material but not limited by mass transfer, it is a matter of maximizing the amount of enzyme per unit volume in the reactor. After all, every single enzyme has the same amount of all reactants in its immediate surrounding, which is the only factor that determines the turnover of the enzyme during its entire active “life-span”.

When the performance of the biocatalytic particle is hampered by diffusional limitation(s), the situation gets slightly more complicated. If the enzyme costs are low in comparison to other costs (e.g. reactor costs, personal costs, immobilization costs, depreciation) the volumetric productivity (i.e. the vessel capacity) should be optimized. If the enzyme costs are high (due to a high cost-price or a high enzyme inactivation rate) in comparison to other costs, however, optimization should focus on fast (by fine-tuning optimal reaction conditions) and efficient use of every enzyme molecule (i.e. avoid steep gradients of substrates in the biocatalytic particle), during its limited activity. The optimized biocatalytic particle will be a costs-dependent compromise of loading (volumetric productivity), efficient use of enzyme, enzyme distribution, et cetera.

In practice, however, the situation is often not black and white as suggested before. A bioconversion can be influenced by the interaction of the enzyme with



the support material and by mass transfer limitations at the same time. Additionally, any change in enzyme loading and distribution may have an effect on the mass transfer properties of the particle.

### ***Multiple reactions with fixed overall stoichiometry***

Although more substrates are involved in multiple reactions, the situation is quite similar to the example before. As long as the overall stoichiometry remains constant, the ratio of the concentrations of the products is constant. Here also, the substrate concentrations and reaction conditions determine the speed at which the products are formed, and need to be optimized for efficiency, but do not alter the selectivity of the competing reactions or the composition of the products formed.

### ***Multiple reactions with variable overall stoichiometry***

Here the solution becomes less obvious and straightforward. Case-specific kinetics, particle parameters and process parameters each influence the amount of desired end-product that can be obtained, the time consumption per unit mass of product, the selectivity of the product over by-product formation, the yield on each substrate, et cetera. To name some, the development of improved biocatalytic particles involves evaluation of the effects of e.g. particle size, geometry, porosity, tortuosity, hydrophobicity, enzyme loading, enzyme distribution, and process conditions such as temperature, pH, salt concentration, and (ratio's of) substrate concentrations. Summarizing, detailed knowledge on morphology and internal processes is required to rationally optimize the biocatalytic particles in these cases. With this knowledge models can be produced that can be used for a sensitivity analysis. In this way, the design process can be sped-up considerably, by evaluating many different configurations and conditions at the desk, and only testing the most promising ones.

## **RESEARCH SUBJECT: ASSEMBLASE®**

Penicillin-G acylase is an enzyme that catalyzes the coupling of a 7-ADCA nucleus and a phenylglycine amide side chain (PGA) to yield the antibiotic cephalixin (CEX). In addition to this synthesis reaction, the enzyme catalyzes the hydrolysis of CEX, and the hydrolysis of PGA (Figure 1).

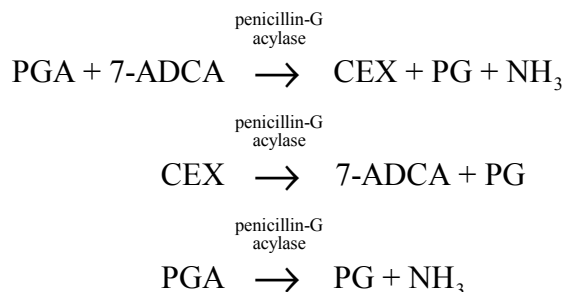


Figure 1. Penicillin-G acylase catalyzed reactions during the synthesis of cephalixin. Besides the coupling reaction of PGA and ADCA, also PGA hydrolysis and CEX hydrolysis take place.

These multiple reactions proceed to a final equilibrium mixture that contains 7-ADCA, PG and  $\text{NH}_3$  only. CEX is formed as an intermediary product only, i.e. its production is kinetically controlled.

On basis of economic considerations and in view of processing boundary conditions, penicillin-G acylase is not deployed as a free enzyme in industry; to facilitate its recovery, the enzyme is immobilized in a chitosan/gelatin support matrix (De Vroom, 1997; Kaasgaard et al., 1992; Harder et al., 1987). This formulation of roughly spherical particles, approximately 0.1 – 0.5 mm in diameter, is referred to as Assemblase®.

As a consequence of immobilization, the overall macroscopic particle performance decreased. Mass transfer limitations entail lowered intra-particle substrate concentrations and higher product concentrations. Because 7-ADCA is the largest (and slowest) substrate and cephalixin the largest reactant (being the coupling product of both substrates), the ratio of PGA over 7-ADCA increases as does the concentration of CEX. The increased CEX concentration leads to increased product hydrolysis. Due to the intrinsic kinetic properties of the enzyme (Schroën *et al.*, 2002), this leads to a change of the individual reaction rates (Fig. 1) and of the overall reaction stoichiometry. This change is reflected in sub-optimal product yields and reduced selectivity.

The above shows that the Assemblase catalyzed synthesis of cephalixin involves multiple kinetically controlled reactions with variable overall stoichiometry. As was explained before, rational particle optimization for such type of biocatalysts requires detailed knowledge on morphology and internal phenomena.

---

## RESEARCH AIM

In literature, an extensive body of data is available on Assemblase<sup>®</sup> catalyzed cephalixin synthesis (Bruggink, 2001). However, this literature only considers a description of external overall kinetics, i.e. Assemblase<sup>®</sup> was regarded as a black box. No information was presented on a mechanistic description of the internal structures and processes involved, which is needed for rational particle optimization. The aim of the research outlined in this thesis is to give a description of the kinetic behaviour of Assemblase<sup>®</sup> in cephalixin synthesis by investigating the internal particle morphology and processes.

A start was made by investigating several particle properties, including particle size and shape, intra-particle enzyme loading, enzyme distribution, matrix morphology, and mass transfer of all reactants. Intrinsic enzyme kinetics were adopted from Schroën *et al.* (2002). From this a physical model was constructed.

The level of complexity of the processes mentioned before is variable, and each process needs to be studied in the proper amount of detail. Which level of detail is needed for the mechanistic description of Assemblase behaviour with the model, however, was not known beforehand. Therefore, we have chosen for a strategy in which phenomena are studied with a progressive level of detail (resolution) to the extent where an adequate description of the system was possible.

## SCALE

Although it may sound obvious that all relevant processes have to be understood in order to rationally optimize a biocatalytic particle, actual determination and understanding is usually complicated. Additionally, the mechanisms involved play at different levels of scale. Centi and Perathoner (2003) considered the processes involved in biocatalytic conversions at three levels of scale. The macroscopic scale, at which e.g. overall performance, particle size and particle geometry play, was already discussed. Distributions of the biocatalyst over the support material (important for mass transfer limited particles), for example, plays at a much more detailed scale, designated the micro-scale. The direct environment of the enzyme, e.g. interactions with the support, the solvent and the

substrates is called the nano-scale. Processes at each of these scales give specific information.

## **THESIS OUTLINE**

The structure of this thesis reflects the progressive analytical resolution mentioned before. The various aspects are finally integrated in a mechanistic model for Assemblase<sup>®</sup> performance in cephalixin synthesis.

### **CHAPTER 2: PREPARATION AND DETECTION TECHNIQUES AT DIFFERENT SCALES**

As a preamble to actual data collection, Chapter 2 gives an overview of various preparation and detection techniques that might allow data collection on biocatalyst characterization, including intra-particle enzyme distribution and support matrix structure. To this end, several light and electron microscopic techniques are reviewed, as well as a number of (immuno-) labeling techniques.

### **CHAPTER 3: MACRO-SCALE ANALYSIS BY EXTERNAL PARTICLE DATA**

The macroscopic kinetic behaviour of Assemblase<sup>®</sup>, formed the basis for a discussion on some simple intra-particle biocatalytic model-distributions. The parameters particle size, enzyme loading and enzyme distribution, which severely determine the macroscopic particle performance, were studied on the basis of macroscopic observations. The relative and total enzyme loadings in Assemblase were found to be inversely correlated with the particle diameter. Preliminary estimates on simple uniform enzyme profiles on basis of macroscopic data were found to be inadequate.

### **CHAPTER 4: MICRO-SCALE ANALYSIS BY LM**

The quantitative intra-particle enzyme distribution of Assemblase<sup>®</sup>, was measured by light microscopy. The intra-particle enzyme distribution was found to be heterogeneous and dependent on particle size. Enzyme gradients could be represented mathematically by an instationary enzyme penetration profile.

### **CHAPTER 5: NANO-SCALE ANALYSIS BY TEM AND CRYO-FESEM**

Transmission electron microscopy (TEM) was used to study intra-particle enzyme distribution at nano-scale resolution. Globally, the size-dependent

enzyme gradient observed with light microscopy was confirmed. Locally, however, abrupt deviations in enzyme concentration were observed. Cryogenic field-emission scanning electron microscopy (cryo-FESEM) related these local heterogeneities to local heterogeneity of the matrix. These regions were expected to have a different matrix composition, which was supported by a basic thermodynamic line of reasoning on polymer demixing.

## **CHAPTER 6: SIMULTANEOUS ANALYSES BY FESEM**

The analysis of various properties with various preparation and detection techniques entails problems in the interpretation of results. In an attempt to circumvent these problems, FESEM was successfully used as a single technique to study both the internal morphology and the intra-particle enzyme distribution of Assemblase<sup>®</sup>.

## **CHAPTER 7: DATA INTEGRATION AND MODEL SYNTHESIS**

Quantitative data from the previous chapters were combined in a physical model for cephalixin synthesis with Assemblase<sup>®</sup>. The model incorporates reactions with a heterogeneous enzyme distribution, electrostatically coupled transport and pH-dependent dissociation behavior of reactants, and the complex interplay between these individual processes. The model was successfully validated against a variety of synthesis experiments and thus may provide a basis for design of optimized particles.

## **CHAPTER 8: DISCUSSION**

A general discussion stresses the paradox that, on one hand, each relevant phenomenon requires dedicated analysis with specialized equipment whereas, on the other hand, the multitude and interdependency of these phenomena would call for their simultaneous analysis in an integrated approach.

Upon identification of bottlenecks in particle performance by model evaluation, a rational choice for further optimization can be made. Examples of possible developments in various disciplines are given.

## **REFERENCES**

- Arnold F.H.** (2001). Combinatorial and computational challenges for biocatalyst design. *Nature* **409**: 253-257.

- Bruggink A.** (2001). Synthesis of  $\beta$ -Lactam Antibiotics: Chemistry, Biocatalysis & Process Integration. Kluwer Academic Publishers, Dordrecht. The Netherlands.
- Burton S.G.** (2003). Oxidizing enzymes as biocatalysts. *Trends Biotechnol.* **21**: 543-549.
- Centi G., and Perathoner S.** (2003). Integrated design for solid catalysts in multiphase reactions. *CATTECH* **7**: 78-89.
- Cheetham P.S.J.** (1998). What makes a good biocatalyst? *J. Biotechnol.* **66**: 3-10.
- Christensen M.W., Andersen L., Husum T.L., and Kirk O.** (2003). Industrial lipase immobilization. *Eur. J. Lipid Sci. Technol.* **105**: 318-321.
- De Vroom, E.** (1997) An improved immobilized penicillin G acylase. *International Patent* WO 97/04086.
- Harder A., De Haan B.R., and Van der Plaats J.B.** (1987) Novel immobilized biocatalysts and their preparation and use. *European Patent* 0222462B1.
- Jaeger K.E.** (2004). Protein technologies and commercial enzymes. White is the hype-biocatalysts on the move. *Curr. Opin. Biotechnol.* **15**: 269-271.
- Kaasgaard S.G., Karlson L.G., and Schneider I.** (1992) Process for separation of two solid components. *International Patent* WO 92/12782.
- Kirk O., Borchert T.V., and Fuglsang C.C.** (2002). Industrial enzyme applications. *Curr. Opin. Biotechnol.* **13**: 345-351.
- Panke, S., and Wubbolts M.** (2002). Enzyme technology and bioprocess engineering. *Curr. Opin. Biotechnol.* **13**: 111-116.
- Panke S., Held, M., and Wubbolts M.** (2004). Trends and innovations in industrial biocatalysis for the production of fine chemicals. *Curr. Opin. Biotechnol.* **15**: 272-279.
- Roberts S.M.** (2004). Biocatalysts in synthetic organic chemistry. *Tetrahedron* **60**: 499-500.
- Schmid A., Dordick J.S., Hauer B., Kiender A., Wubbolts M., and Witholt B.** (2001). Industrial biocatalysis today and tomorrow. *Nature* **409**: 258-268.
- Schoemaker H.E., Mink D., and Wubbolts M.G.** (2003). Dispelling the myths – biocatalysis in industrial synthesis. *Science* **299**: 1694-1697.
- Schulze B., and Wubbolts M.G.** (1999). Biocatalysis for industrial production of fine chemicals. *Curr. Opin. Biotechnol.* **10**: 609-615.
- Schroën C.G.P.H., Fretz C.B., De Bruin V.H., Berendsen W., Moody H.M., Roos E.C., Van Roon J.L., Kroon P.J., Strubel M., Janssen A.E.M., and Tramper J.** (2002). Modeling of the enzymatic kinetically controlled synthesis of cephalixin: influence of diffusion limitation. *Biotechnol. Bioeng.* **80**: 331-340.
- Straathof A.J.J., Panke S., and Schmid A.** (2002). The production of fine chemicals by biotransformations. *Curr. Opin. Biotechnol.* **13**: 548-556.
- Thomas S.M., DiCosimo R., and Nagarajan V.** (2002). Biocatalysis: applications and potentials for the chemical industry. *Trends Biotechnol.* **20**: 238-242.
- Turner N.J.** (2003). Directed evolution of enzymes for applied biocatalysis. *Trends Biotechnol.* **21**: 474-478.
- Van Beilen J.B., and Li Z.** (2002). Enzyme technology: an overview. *Curr. Opin. Biotechnol.* **13**: 338-344.

---

## Chapter 2 **Assessment of intra-particle biocatalytic distributions as a tool in rational formulation**

The contents of this chapter have been published as:

**J. van Roon, R. Beftink, K. Schroën and H. Tramper** (2002). Assessment of intraparticle biocatalytic distributions as a tool in rational formulation. *Curr. Opin. Biotechnol.* **13**: 398-405.

## **ABSTRACT**

In the last decades, research has shown that the intra-particle biocatalytic distribution has extensive effects on the properties of various (industrial) biocatalytic particles and their performance in (bio-) chemical reactions. In recent years, advances in molecular chemistry have led to the development of many different specific (immuno-) labeling and light-microscopic detection techniques. High-quality image-digitizing devices and enhanced computing power have made image analysis readily accessible. This may lead to the assessment and optimization of the internal biocatalyst profile as an integral part of biocatalytic particle optimization.



## INTRODUCTION

Biocatalysts have shown to be of great industrial importance in the past decades. In literature, many new (applications of) biocatalysts can be found, and their number is still expanding rapidly. The development of new biocatalyst particles partly remains to be a craft: usually many alternative formulations are made and the best for the specific application is selected. Recently, however, more attention is given to the rational tailor-made design of industrial biocatalytic particles. An important design parameter is the distribution of biocatalyst within the particle: the precise position of the catalytic enzymes or cells. Knowledge that was obtained in histochemistry can be applied to do this. Here, various detection and labeling methods were developed to characterize the structure and heterogeneity of different structures, as well as the locus of certain compounds, organelles, cell types or (cell) structures within cells and tissues of plants, moulds, animals and micro-organisms (Voronin *et al.*, 2001; Pan *et al.*, 2001; Sugibayashi *et al.*, 1999; Kato *et al.*, 2000; Shores and Hunter, 1999; Denyer *et al.*, 1996).

## PARTICLES

Tramper *et al.* (2001) recently introduced a generic decision strategy to facilitate the choice of ‘when and how to use biocatalysts.’ Immobilization of the costly biocatalytic enzymes or cells facilitates reuse, possibly with extremely high enzyme or cell loadings; it leads to high volumetric activities and creates the possibility to use the biocatalyst in a packed-bed or fluidized-bed reactor (Calsavara *et al.*, 2001).

The properties of the immobilized biocatalysts depend on the properties of both the enzyme or cell and the support material (Tischer and Kasche, 1999). The combination of both can yield biocatalysts with a 100-fold increase or decrease in the activity (Novick and Dordick, 2000). Inside the biocatalytic particle, mass transfer of substrates and products can become limiting, since cells or enzymes are packed tightly into small volumes (or onto small surfaces). Diffusional limitation causes gradients of substrates and or products in the catalyst particle.

Immobilization can lead to various positive effects that are observed in the particle surrounding media. An immobilized biocatalyst can (apparently) be very stable. Many papers report improved operational stability upon immobilization (Novick and Dordick, 2000; Cloix and Wainer, 2001; Jing *et al.*, 2000; Keusgen *et al.*, 2001; Ragnitz *et al.*, 2001; Vertesi *et al.*, 1999; Wang *et al.*, 2001). The same is reported for increased thermal stability upon immobilization (Calsavara *et al.*, 2001; Ragnitz *et al.*, 2001; Vertesi *et al.*, 1999).

Unfortunately, diffusional limitations also cause negative side effects. The effectivity in a biocatalytic particle with diffusion limitation in general is lower than that of the native biocatalyst. Diffusional limitation can also alter the (apparent) substrate specificity (Cloix and Wainer, 2001; Vertesi *et al.*, 1999). In the case of multi-substrate conversions, additional disadvantages can be mentioned. Litjens *et al.* (2001) showed that diffusional limitation causes decreased enantioselectivity and Schroën *et al.* (2002) found that during the production of the semi-synthetic antibiotic cephalixin, a higher enzyme loading results in lowered specificity and effectivity of the reaction.

## INTRAPARTICLE DISTRIBUTIONS

Often, the biocatalyst is assumed to be homogeneously distributed over the particle. Sometimes, efforts are actually made to accomplish this (Handrikova *et al.*, 1996; Polakovic *et al.*, 2001), whereas in other cases a homogenous distribution is simply inferred from the extended contact time during immobilization. Experimental confirmation of this assumption, however, is omitted in nearly all cases. In other cases, the unknown active biocatalyst profiles are estimated from observed kinetic macroscopic data in a fitting procedure (Carvalho *et al.*, 2001).

Hossain and Do (1989) and Do and Hossain (1986) applied the latter procedure by quasi steady state and deactivation analysis. Scharer *et al.* (1992) discussed an increased selectivity and effectivity for pellicular biocatalytic particles, at the cost of diminished stability as compared to homogeneous biocatalyst. Knowledge on the distribution provides inside into these effects. Polakovic *et al.* (2001) determined the effective sucrose diffusivity in supposedly homogeneous biocatalytic particles by measuring the macroscopic product formation rate.

Apart from the question if this assumption is valid, this method cannot be applied to many industrial biocatalytic particles, as they possess an unknown (heterogeneous) distribution. To determine effective diffusivity in this way, knowledge on enzyme distribution is essential.

## **CHARACTERIZATION OF BIOCATALYTIC PARTICLES**

So far, we have seen that immobilization of biocatalyst can be the cause of a variety of positive and negative effects. Recently, research focuses on the specific use of a certain distribution to create a biocatalytic particle that meets the most important design criteria, while minimizing the negative consequences of immobilization.

Therefore, we will discuss recent advances in research on the structure and composition of biocatalytic particles. In particular, we will focus on the determination of the intraparticle distribution, and therefore on various labeling and detection methods. Important parameters are the desired specificity of labeling and the wanted resolution of detection.

In general, assessment of the distribution consists of a few consecutive steps. Usually, the first step is the fixation and preparation of the material. If necessary, the material is embedded to facilitate subsequent sectioning. In the second step, the material is broken or cut into sections to access the internal (of course non-invasive methods do not require this step). Then a labeling step is performed. In this step in particular, resolution is an important issue. What kind of chemical is to be labeled, how specific does it need to be labeled, and which resolution is wanted? Since the choices of the labeling and detection method are interdependent, they are discussed simultaneously. After labeling and final observation, (image) analysis can be performed optionally, where images are subjected to different mathematical algorithms to be able to quantify distributions.

## **PREPARATION, FIXATION AND EMBEDDING**

### **CHEMICAL FIXATION AND EMBEDDING**

Fixation of the biocatalyst can be performed in order to minimize (ultra)structural damage from subsequent procedures. In chemical fixation, proteins can be covalently cross-linked by classic fixates like glutaric dialdehyde and formaldehyde. A general problem with chemical fixation is the potential loss of epitopes (antibody binding sites) for specific labeling. Subsequently, the fixed structures can be embedded to be able to cut sections of the biocatalyst. Usually, one of the first steps in embedding is dewatering of the sample in a series of solvent concentrations.

After dehydration, a resin can be added. Acrylic resins are usually the most suited for subsequent immunolabeling, since epoxy resins can bind covalently to biological materials, particularly with proteins (Kellenberger *et al.*, 1987). Epoxy resins are known to give better preservation of ultrastructural details than acrylic sections, because they are more stable when exposed to an electric beam, and are easier to cut. Brorson (1997, 1998) described some recent methods to improve immunolabeling with epoxy resins.

### **PHYSICAL FIXATION AND EMBEDDING**

Physical particle fixation can be done by freezing. An excellent structure conserving fixation technique is high pressure freezing (200 bar; Wang *et al.*, 2000; Mims *et al.*, 2001); this treatment, however, is not particularly suited for epitope preservation. In cases subsequent labeling is wanted, the sample can alternatively be frozen rapidly at ambient pressures by plunge-freezing in e.g. liquid nitrogen, ethane or propane. This cryo-fixation also serves as an embedding step (in which the frozen water replaces the resin), as the frozen material can be cut into sections by cryo-sectioning, (e.g. Tischer and Kasche, 1999; Oyaas *et al.*, 1995) to study the inner structures with a(n) (ultra-) cryo-microtome. A recently developed technique is cryo-planing by ultra-cryo-microtomy (Nijssse and Van Aelst, 1999), in which the frozen sample is cut with a diamond knife. The sliced sections themselves are ignored, whereas the exposed sample surface is extremely flat and therefore very suitable to be used in (cryo)-Scanning Electron Microscopy (SEM) studies. This is not always possible with older techniques like freeze-breaking, as the plane of fraction can be very

irregular and could be revealing little of the inner structures (Walther and Muller, 1999).

#### **HYBRID FIXATION/EMBEDDING**

A hybrid technique for fixating and embedding is freeze substitution (Thijssen *et al.*, 1998). In this technique, the material is frozen, after which the (amorphous) ice is replaced by a solvent like iso-octane or heptane by application of a specific temperature profile. This has proven to be a reliable technique with an excellent preservation of the ultrastructure of the sample compared to other dehydrating and fixation methods. Another advantage is that the water-soluble components (sugars, amino acids, enzymes, etc) remain inside the sample.

### **LABELING AND DETECTION**

Now that the fixation and preparation of the sample is done, a labeling step can be performed.

Groups of chemically related compounds can be stained. Stains are very efficient, cheap and easy to use. Proteins for instance, can be stained with reagents like Coomassie brilliant blue or naphtol blue black (Tische and Kasche, 1999), fats with phenol red, and phospholipids (in cell membranes) with osmium tetra-oxide or uranyl acetate. There are many more reagents for different kinds of chemical substances. Staining methods, however, are not very specific or selective. In the case of immobilized enzymes for instance, this staining method cannot be used if the carrier material itself contains proteins. Furthermore, the enzyme solution to be immobilized often contains impurities that will be stained as well, and active enzymes cannot be distinguished from denatured, aggregated or precipitated enzymes.

Better selectivity can come from the use of chromogenic reference substrates, which can be used to determine the presence of enzymes that can utilize the chemical as a substrate, as opposed to labeling of all proteins at once (Alkema *et al.*, 1999).

During the last 10 years, developments in the technique of producing (monoclonal) antibodies and the (commercial) availability thereof, has led to an

increase in histochemical publications (Stoward *et al.*, 1998). Antibodies are very specific and therefore used to detect very specific, well-defined molecules. They can be raised in e.g. rabbits, mice, rats and goats. Lately, chickens are immunized more, since their eggs can contain very high titers of antibody in the egg-yolk (IgY's; Tu *et al.*, 2001), which makes bleeding of the animal obsolete. If primary labeling is used, the antibody also contains a specific label in order to make it visible. In secondary labeling, a secondary antibody, raised against the animal in which the first antibody was produced, contains the label for detection. Advantages of primary labeling are the relative high labeling efficiency and the reduced risk of a-specific reactions compared to secondary labeling. Secondary labeling, however, is more flexible, since secondary antibodies raised against all antibodies of a certain animal are readily available with all kinds of labels.

The label attached to the antibody can be an enzyme that performs a specific reaction, from which it can be recognized upon addition of substrate for that enzyme. Alkaline phosphatase is used in many different fields of research, where enzyme distributions in different tissues are established (Voronin *et al.*, 2001; Cheng *et al.*, 2000; Lawrenson *et al.*, 1999). It can hydrolyze naphthol phosphate esters like NBT-BCIP to form phenolic compounds and phosphates. The phenols couple to colorless diazonium salts to produce insoluble azo dyes. The resolution of this procedure is limited, as multiple layers of the precipitated dyes are indistinguishable from monolayers. The coloring reaction can be studied by conventional light microscopy.

Also enzyme anti-enzyme soluble complexes have been routinely employed in histochemical techniques (Kohsaka *et al.*, 2001; Najimi *et al.*, 2001). The soluble complex of peroxidase anti-peroxidase (PAP) consists of three peroxidases and two anti-peroxidase subunits in a cyclic structure. The complex can oxidize a substrate, which produces a brown end product that is highly insoluble in ethanol and other organic solvents.

An ultra-sensitive chemoluminescent imaging system (capable of detecting single photons) for quantitative analysis and visualization of the spatial distribution of biomolecules (such as enzymes) in tissues and cells was presented by Roda *et al.* (1998).

Another common label is gold, often used in combination with electron microscopy. When extremely high resolutions are wanted, detection at molecular level (e.g. single enzymes) is possible by immunogold labeling and subsequent analysis with transmission electron microscopy (TEM; Lovelock and Lucocq, 1998). This requires ultra thin sections of approximately 50-100 nm to yield an electron transparent coupe. Figure 1 shows a TEM photograph of an ultra thin immunogold labeled cross-section of immobilized penicillin-G acylase.

Immunogold labeled sections can alternatively be studied by scanning electron microscopy (SEM). With the latter technique, structural information coming from topographic detection can be combined with localization of enzymes by backscatter detection of a single sample. Immunogold labeling can also be used in light microscopic techniques (Castiglione, 1998). Since the gold particles (usually 10 nm and smaller) are far too small to be detected in the light microscope, a silver-enhancement step is often used. During silver-enhancement (SE), metallic silver is deposited onto ultrasmall (US) gold particles of 1 nm.

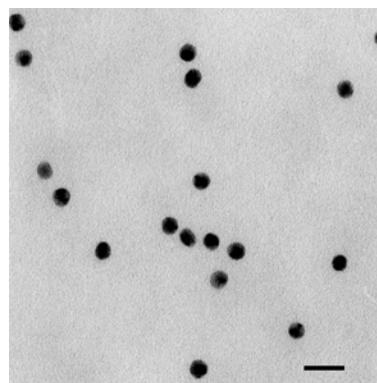


Figure 1. TEM photograph of an ultra-thin immunogold labeled cross-section of immobilized penicillin-G acylase, unpublished work. Bar corresponds to 20 nm.

For industrial biocatalysts, which are usually in the range of 0.1 to several millimeters in diameter, light microscopy with an optical resolution of 200 nm can already yield high detail. Combined with a highly specific labeling technique such as immunogold or alkaline phosphatase labeling, this provides for a powerful tool for quantitative localization of enzymes in industrial biocatalysts: large areas can be viewed in one single image with light microscopy, with relatively cheap and easy accessible equipment. Improvements in digital imaging and analyzing software and in computing power have led to a shift from classical light microscopic techniques (bright field, phase-contrast, differential interference, dark ground and polarization) towards fluorescence and confocal scanning laser microscopy.

The fluorescence microscope usually contains at least two light sources. One provides normal illumination and the other excites the fluorochromes, most commonly by epi-illumination. Components can fluoresce in natural form (primary or autofluorescence) or after treatment with fluorescent dyes.

Fluorescent labels are relatively photostable, photosensitive and may be highly specific when linked to various macromolecules (Spear *et al.*, 1999). Among many others, FITC is a very well known green emitting fluorochrome. When excited, however, it produces free radicals, which can be very harmful to the biocatalyst. Furthermore, FITC is pH sensitive and it bleaches very quickly. More stable and brighter dyes are for example Alexa 488 or Cy2. Also red probes such as Alexa 568, Cy3, Rhodamine, or Texas Red are used frequently. The Green Fluorescent Protein (GFP) is a 27 kDa protein from the jellyfish *Aequorea victoria* which fluoresces in the green upon illumination with UV light. GFP is a tool for labeling cellular proteins to follow their spatial and temporal localization in living cells under a variety of experimental conditions (Margolin, 2000). Many other specific fluorescent labels or combinations of labels can be used. An example is a hybrid label containing a fluorescent label and a gold label for simultaneous fluorescence microscopy and electron microscopy.

Confocal laser scanning microscopy (CLSM) is a very important extension of fluorescence microscopy, because it is a non-invasive technique. As opposed to regular fluorescence microscopy, it analyses the interior instead of the surface of a sample. In confocal microscopy, a laser is used as a light source and the light is focused in a focal place. The plane can be shifted over the depth-axis to scan the sample optically. The advantage is clear: the sample does not need to be cut in sections (with the risk of introducing artifacts by embedding and or cutting; Bougourd *et al.*, 2000).

The fluorescent labels can be introduced into the biocatalytic particles by labeling a biocatalyst with a fluorescent group prior to immobilization. One needs to be convinced, however, that the labeling of biocatalyst does not affect its distribution upon immobilization and this is usually hard to proof/establish. Other disadvantages include the limited penetration depth of CLSM of approximately 100 to 200 micrometers due to scattering and absorption of emitted light from the fluorochrome and fading (quenching and bleaching): the reduction of emission intensity. A third problem is autofluorescence of the



immobilization support material, which can interfere with the fluorescence of the fluorochrom.

Autofluorescence may also be beneficial. Prior *et al.* (1999) used this phenomenon as a tool to section the embedded structure optically prior to actual sectioning with glass knives. In this way, they determined exactly at what depth the structures of interest were localized, so that they would not miss the area of specific interest in the middle of a section. Spieß and Kasche (2001) used a combination of the pH-dependent emission of FITC and the pH-independent emission of TRITC to measure the pH inside the carrier of immobilized enzymes during enzyme catalysis.

## IMAGE ANALYSIS

The data obtained in the labeling experiments can be analyzed by taking (digital) images. Without further manipulations the detection yields a qualitative distribution or localization of the biocatalyst within the particle. When single particles are visible, they can be counted in order to obtain a relative quantitative distribution. When intensity differences are quantified by imaging software in order to obtain a (continuous) quantitative relative distribution, the background should be illuminated homogeneously, or a correction must be made for it. Irregularly shaped particles can complicate the determination of a biocatalyst profile within the particle.

Relative quantitative differences in signal intensity can be combined with the absolute total amount of biocatalyst in the particle to yield an absolute quantitative biocatalyst distribution over the particle. Methods to determine the absolute amount of biocatalyst include activity measurements of the grinded biocatalytic particle (Janssen *et al.*, 2002; Van der Wielen, 1997) and active site titration (Janssen *et al.*, 2002; Rotticci *et al.*, 2000).

## DECISIONS

Research in molecular chemistry has led to the development of many different labeling and detection techniques. The availability of these techniques has provided scientists with a greatly expanded toolbox. In Figure 2, a scheme

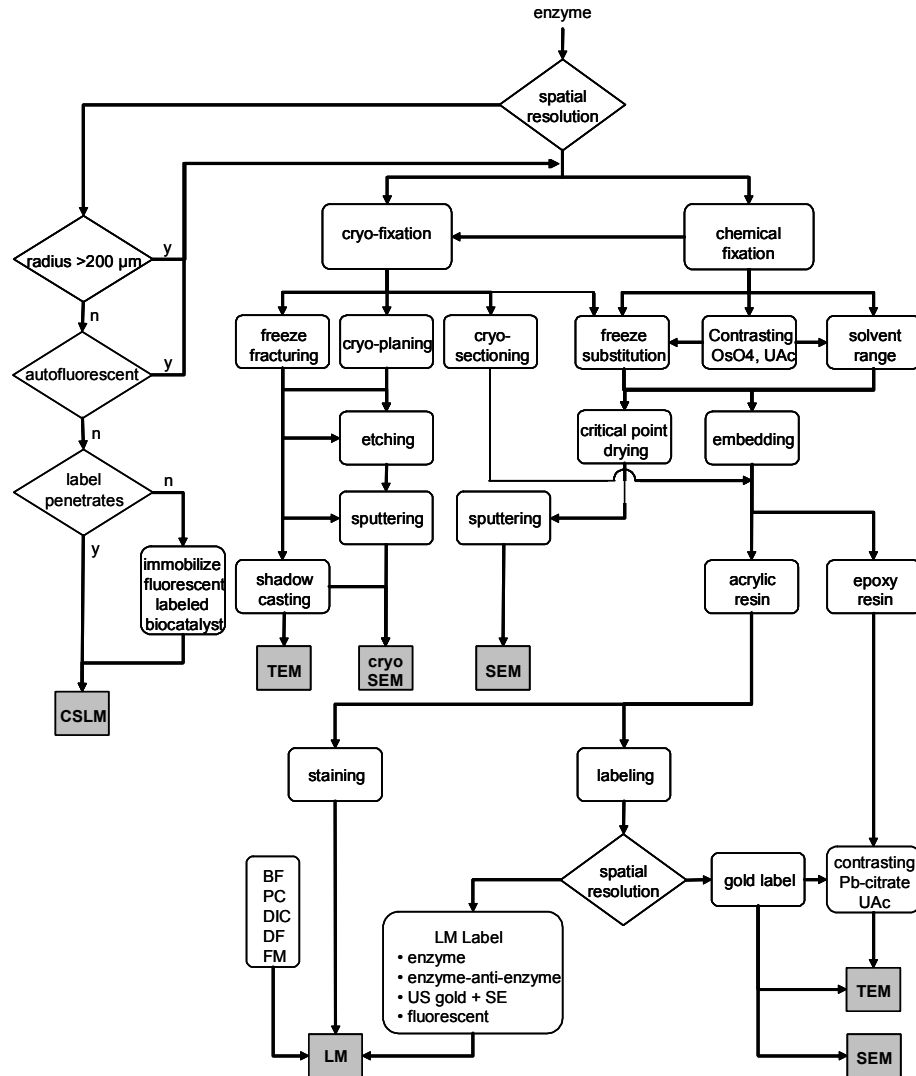


Figure 2a. Decision scheme for choosing a localization technique: detection (see text).

presenting different possibilities for labeling and detection techniques is given. Although incomplete, this could be used as a tool for deciding which labeling and detection method might be used in which case for the localization of enzymes in biocatalytic particles; a similar scheme applies to living cells as well, however.

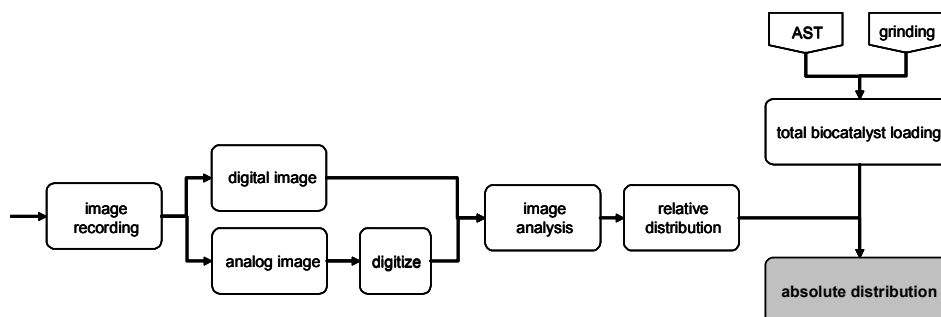


Figure 2b. Decision scheme for choosing a suitable localization technique: image processing (see text).

## APPLICATION OF KNOWLEDGE: CURRENT STATE IN BIOCATALYST

In recent years, more applications of rationally designed biocatalysts are reported on. At present, much research focuses on the development of new supports and on improved or new immobilization methods. Without being complete, some examples are given below.

Jing *et al.* (2000) produced a mesoporous support, with a well-ordered structure. Nanoporous sol-gel glass particles possessing a highly ordered structure were used by Wang and co-workers (2001), to increase biocatalyst stability in organic solvents.

Efforts to improve covalent immobilization onto epoxy supports were made by Mateo *et al.* (2000) by promoting physical adsorption onto the support prior to covalent binding. Carvalho and Cabral (2000) reviewed micelles as promising reaction media for lipases. Tischer and Kasche (1999) recently reviewed immobilization in non-aqueous media, and discuss the advantages of the use of cross-linked enzyme crystals (CLECs). Cao *et al.* (2000; 2001) discuss a procedure of physical aggregation of enzymes, followed by chemical cross-linking to form so called cross-linked enzyme aggregates (CLEA's). They found high volumetric activities combined with high specificity and higher stability and activity in organic solvents compared with the corresponding CLEC.

Recently, research started on the actual control and assessment of the distribution of the biocatalyst in and over particles during immobilization, in order to maximize the performance of (industrial) biocatalysts. Particles with a non-uniform distribution were produced, that showed higher effectivities compared with more uniformly distributed particles at equal Thiele moduli (Ladero *et al.*, 2001). Martin dos Santos (2001) and Martin dos Santos *et al.* (1996) exploited diffusional limitation of oxygen to combine aerobic outer region reactions with anaerobic reactions in the center of the same biocatalytic particle by controlled immobilization of aerobic and anaerobic cells within the same biocatalytic particle (and called the particles “magic beads”). Krastanov co-immobilized two enzymes for continuous phenol removal from waste streams and showed the activities of the two enzymes complement one another (Krastanov, 2000).

Keusgen *et al.* (2001) studied the immobilization of enzymes on PTFE surfaces. They presented a procedure using a spacer molecule with which enzymes can be immobilized under physiological conditions, enzyme multilayers can be achieved, and protein layers are renewable. Mateo *et al.* (2000) reported a fast and relatively simple method to reuse the support material several times by reversible immobilization of industrially relevant enzymes. Mohy Eldin and co-authors (2000) researched the possibility to alter the hydrophobic/hydrophilic nature of the immobilized support by crafting cheap nylon particles. Using graft polymers, enzymes might be more available for reaction than is the case with enzyme entrapped in a gel.

## CONCLUSION

For several decades, much research was conducted on various biocatalytic particles with very different compositions and properties. The optimization of such biocatalytic particles mainly was a craft: many formulations were made by trial and error and the one having the best case-specific properties was selected. This has led to valuable insights on how the distribution of the biocatalyst over the carrier influences its behavior during a reaction.

In recent years, advances in molecular chemistry and histochemistry have led to the development of many different labeling and detection techniques. Highly specific labeling with antibodies has become common practice and a label can be

chosen freely. Combined with the availability of high-quality image digitizing devices (CCD camera's and scanners) and enhanced computing power, light microscopic techniques have become a powerful and readily available tool for the assessment of the internal biocatalyst profile at reasonable efforts and prices. This may lead to the acceptance of the assessment of the internal biocatalyst profile as an integral part of biocatalytic particle optimization.

## ACKNOWLEDGEMENTS

DSM and the Ministry of Economic Affairs of The Netherlands are kindly acknowledged for their financial support. The authors want to thank A.C. van Aelst and H. Kieft of the Wageningen Laboratory of Plant Cell Biology for valuable discussions.

## REFERENCES

- Alkema W.B.L., Floris R., and Janssen D.B.** (1999). The use of chromogenic reference substrates for the kinetic analysis of penicillin acylases. *Anal. Biochem.* **275**: 47-53.
- Bougourd S., Marrison J., and Haselhoff J.** (2000). An aniline blue staining procedure for confocal microscopy and 3D imaging of normal and perturbed cellular phenotypes in mature *Arabidopsis* embryos. *Plant J.* **24**: 543-550.
- Brorson S.H.** (1997). How to examine the antigen-damaging effect of sodium ethoxide on deplasticized epoxy sections. *J. Histochem. Cytochem.* **45**: 146.
- Brorson S.H.** (1998). Antigen detection on resin sections and methods for improving the immunogold labeling by manipulating the resin. *Histol. Histopathol.* **13**: 275-281.
- Calsavara L.P.V., De Moraes F.F., and Zanin G.M.** (2001). Comparison of catalytic properties of free and immobilized cellobiase Novozym 188. *Appl. Biochem. Biotechnol.* **91**: 615-626.
- Cao L., Van Langen L.M., Van Rantwijk F., and Sheldon R.A.** (2001). Cross-linked aggregates of penicillin acylase: robust catalysts for the synthesis of beta-lactam antibiotics. *J. Mol. Catal. B Enzym.* **11**: 665-670.
- Cao L., Van Rantwijk F., and Sheldon R.A.** (2000). Cross-linked enzyme aggregates: a simple and effective method for the immobilization of penicillin acylase. *Org. Lett.* **2**: 1361-1364.
- Carvalho C.M.L., and Cabral J.M.S.** (2000). Reverse micelles as reaction media for lipases. *Biochimie* **82**: 1063-1085.
- Carvalho C.M.L., Aires-Barros M.R., and Cabral J.M.S.** (2001). A continuous membrane bioreactor for ester synthesis in organic media: I. Operational characterization and stability. *Biotechnol. Bioeng.* **72**: 127-135.

- Castiglione M.R.** (1998). Immunogold localization of trans-zeatin riboside in embryo and endosperm during early fruit drop of *Malus domestica*. *Biol. Plant. (Prague)* **41**: 523-532.
- Cheng X.F., Wittich P.E., Kieft H., Angenent G., XuHan X., and Van Lammeren A.A.M.** (2000). Temporal and spatial expression of MADS box genes FBP7 and FBP11 during initiation and early development of ovules in wild type and mutant *Petunia hybrida*. *Plant Biology* **2**: 693-701.
- Cloix J.F., and Wainer I.W.** (2001). Development of an immobilized brain glutamine synthetase liquid chromatographic stationary phase for on-line biochemical studies. *J.Chromatog. A* **913**: 133-140.
- Denyer K., Dunlap F., Thorbjornsen T., Keeling P., and Smith A.M.** (1996). The major form of ADP-glucose pyrophosphorylase in maize endosperm is extra-plastidial. *Plant Physiol.* **112**: 779-785.
- Do D.D., and Hossain Md.M.** (1986). A novel method of determination of the internal enzyme distribution within porous solid supports and the deactivation rate constant. *Biotechnol. Bioeng.* **28**: 486-493.
- Handrikova G., Stefuca V., Polakovic M., and Bales V.** (1996). Determination of effective diffusion coefficient of substrate in gel particles with immobilized biocatalyst. *Enzyme Microb. Technol.* **18**: 581-584.
- Hossain Md.M., and Do D.D.** (1989). General theory of determining intraparticle active immobilized enzyme distribution and rate parameters. *Biotechnol. Bioeng.* **33**: 963-975.
- Janssen M.H.A., Van Langen L.M., Pereira S.R.M., Van Rantwijk F., and Sheldon R.A.** (2002). Evaluation of the performance of immobilized penicillin G acylase using active-site titration. *Biotechnol. Bioeng.* **78**: 425-432.
- Jing H., Li X.F., Evans D.G., Duan X., and Li C.Y.** (2000). A new support for the immobilization of penicillin acylase. *J. Mol. Catal. B Enzym.* **11**: 45-53.
- Kato Y., Ooi R., and Asano Y.** (2000). Distribution of aldoxime dehydratase in microorganisms. *Appl. Environ. Microbiol.* **66**: 2290-2296.
- Kellenberger E., Durrenberger M., Villiger W., Carleman E., and Wurtz E.** (1987). The efficiency of immunolabel on Lowicryl sections compared to theoretical predictions. *J. Histochem. Cytochem.* **35**: 959-969.
- Keusgen M., Glodek J., Milka P., and Krest I.** (2001). Immobilization of enzymes on PTFE surfaces. *Biotechnol. Bioeng.* **72**: 530-540.
- Kohsaka T., Sasada H., Sato E., Bamba K., and Hashizume K.** (2001). Ultrastructural properties and immunolocalization of relaxin in the cytoplasmic electron-dense granules of large luteal cells during pregnancy in the cow. *J. Reprod. Devel.* **47**: 217-225.
- Krastanov A.** (2000). Removal of phenols from mixtures by co-immobilized laccase/tyrosinase and Polyclar adsorption. *J. Ind. Microbiol. Biotechnol.* **24**: 383-388.
- Ladero M., Santos A., and Garcia-Ochoa F.** (2001). Diffusion and chemical reaction rates with nonuniform enzyme distribution: An experimental approach. *Biotechnol. Bioeng.* **72**: 458-467.
- Lawrenson J.G., Reid A.R., Finn T.M., Orte C., and Allt G.** (1999). Cerebral and pial microvessels: differential expression of gamma-glutamyl transpeptidase and alkaline phosphatase. *Anat. Embryol.* **199**: 29-34.

- Litjens M.J.J., Le K.Q., Straathof A.J.J., Jongejan J.A., and Heijnen J.J.** (2001). Diffusion limitation causes decreased enantioselectivity of esterification of 2-butanol by immobilized *Candida antarctica* lipase B. *Biocat. Biotrans.* **19**: 1-19.
- Lovelock C., and Lucocq J.** (1998). Quantitative immunoelectron microscopy reveals alpha 2,6 sialyltransferase is concentrated in the central cisternae of rat hepatocyte Golgi apparatus. *Eur. J. Cell Biol.* **76**: 18-24.
- Margolin W.** (2000). Green fluorescent protein as a reporter for macromolecular localization in bacterial cells. *Methods Orlando* **20**: 62-72.
- Martin dos Santos V.A.P.** (2001). Production and characterization of double-layer beads for co-immobilization of microbial cells. In: Towards the integration of oxidative and reductive activities: application to nitrogen removal by co-immobilized micro-organisms. PhD dissertation. Wageningen The Netherlands pp. 109-129.
- Martin dos Santos V.A.P., Bruijnse M., Tramper J., and Wijffels R.H.** (1996). The magic-bead concept: an integrated approach to nitrogen removal with co-immobilized micro-organisms. *Appl. Microbiol. Biotechnol.* **45**: 447-453.
- Mateo C., Abian O., Fernandez-Lafuente R., and Guisan J.M.** (2000). Reversible enzyme immobilization via a very strong and nondistorting ionic adsorption on support-polyethylenimine composites. *Biotechnol. Bioeng.* **68**: 98-105.
- Mateo C., Fernandez L.G., Abian O., Fernandez L.R., and Guisan J.M.** (2000). Multifunctional epoxy supports: a new tool to improve the covalent immobilization of proteins. the promotion of physical adsorptions of proteins on the supports before their covalent linkage. *Biomacromolecules* **1**: 739-745.
- Mims C.W., Rodriguez L.C., and Richardson E.A.** (2001). Ultrastructure of the host-parasite interaction in leaves of *Duchesnea indica* infected by the rust fungus *Frommeela mexicana* var. *indicae* as revealed by high pressure freezing. *Can. J. Bot.* **79**: 49-57.
- Mohy Eldin M.S., Schroën C.G.P.H., Janssen A.E.M., Mita D.G., and Tramper J.** (2000). Immobilization of penicillin G acylase onto chemically grafted nylon particles. *J. Mol. Catal. B Enzym.* **10**: 445-451.
- Najimi M Bennis M., Moyse E., and Chigr F.** (2001). Distribution of delta sleep-inducing peptide in the newborn and infant human hypothalamus: an immunohistochemical study. *Biol. Res.* **34**: 31-42.
- Nijse J., and Van Aelst A.C.** (1999). Cryo-planing for cryo-scanning electron microscopy. *Scanning* **21**: 372-378.
- Novick S.J., and Dordick J.S.** (2000). Investigating the effects of polymer chemistry on activity of biocatalytic plastic materials. *Biotechnol. Bioeng.* **68**: 665-671.
- Oyaas J., Storro I., Lysberg M., Svendsen H., and Levine D.W.** (1995). Determination of effective diffusion coefficients and distribution constants in polysaccharide gels with non-steady-state measurements. *Biotechnol. Bioeng.* **47**: 501-507.
- Pan J., Suzuki T., Ueda K., Tanaka K., Okubo M., and Pan J.** (2001). Distribution of microbial mass and fibrolytic enzyme activities in different size of feed particles from rumen contents of sheep. *Anim. Sci. J.* **72**: 209-217.
- Polakovic M., Kudlacova G., Stefuca V., and Bales V.** (2001). Determination of sucrose effective diffusivity and intrinsic rate constant of hydrolysis catalysed by Ca-alginate entrapped cells. *Chem. Eng. Sci.* **56**: 459-466.

- Prior D.A.M., Oparka K.J., and Roberts I.M.** (1999). En bloc optical sectioning of resin-embedded specimens using a confocal laser scanning microscope. *J. Microsc.* **193**: 20-27.
- Ragnitz K., Syldatk C., and Pietzsch M.** (2001). Optimization of the immobilization parameters and operational stability of immobilized hydantoinase and L-N-carbamoylase from *Arthrobacter aureus* for the production of optically pure L-amino acids. *Enzyme Microb. Technol.* **28**: 713-720.
- Roda A., Pasini P., Baraldini M., Musiani M., Gentilomi G., and Robert C.** (1998). Chemiluminescent imaging of enzyme-labeled probes using an optical microscope-videocamera luminograph. *Anal. Biochem.* **257**: 53-62.
- Rotticci D., Norin T., Hult K., and Martinelle M.** (2000). An active-site titration method for lipases. *BBA Mol. Cell Biol. Lipids* **1483**: 132-140.
- Scharer A., Hossain Md.M., and Do D.D.** (1992). Determination of total and active immobilized enzyme distribution in porous solid supports. *Biotechnol. Bioeng.* **39**: 679-687.
- Schroën C.G.P.H., Fretz C.B., De Bruin V.H., Berendsen W., Moody H.M., Roos E.C., Van Roon J.L., Kroon P.J., Strubel M., Janssen A.E.M., and Tramper J.** (2002). Modeling of the enzymatic kinetically controlled synthesis of cephalixin: influence of diffusion limitation. *Biotechnol. Bioeng.* **80**: 331-340.
- Shores E.M., and Hunter M.G.** (1999). Immunohistochemical localization of steroidogenic enzymes and comparison with hormone production during follicle development in the pig. *Reprod. Fertil. Dev.* **11**: 337-344.
- Spear R.N., Cullen D., and Andrews J.H.** (1998). Fluorescent labels confocal microscopy and quantitative image analysis in study of fungal biology. *Meth. Enzymol.* **307**: 607-623.
- Spieß A.C and Kasche V.** (2001). Direct measurement of pH profiles in immobilized enzyme carriers during kinetically controlled synthesis using CLSM. *Biotechnol. Prog.* **17**: 294-303.
- Stoward P.J., Nakae Y., and Van Noorden C.J.F.** (1998). The everchanging advances in enzyme histochemistry 1986-1996. *Eur. J. Histochem.* **42 SI**: 35-40.
- Sugibayashi K., Hayashi T., and Morimoto Y.** (1996). Simultaneous transport and metabolism of ethyl nicotinate in hairless rat skin after its topical application: the effect of enzyme distribution in skin. *J. Contr. Release* **62**: 201-208.
- Thijssen M.H., Van Went J.L., and Van Aelst A.C.** (1998). Heptane and isooctane as embedding fluids for high-pressure freezing of *Petunia* ovules followed by freeze-substitution. *J. Microsc.* **192**: 228-235.
- Tischer W., and Kasche V.** (1999). Immobilized enzymes: crystals or carriers? *Trends Biotechnol.* **17**: 326-335.
- Tramper J., Beftink H.H., Janssen A.E.M., Ooijkaas L.P., Van Roon J.L., Strubel M., and Schroën C.G.P.H.** (2001). Biocatalytic production of semi-synthetic cephalosporins: process technology and integration. In: *Synthesis of  $\beta$ -lactam Antibiotics: Chemistry Biocatalysis & Process Integration* (A. Bruggink ed.). Dordrecht: Kluwer Academic Publishers pp. 207:250.
- Tu Y.Y., Chen C.C., and Chang H.M.** (2001). Isolation of immunoglobulin in yolk (IgY) and rabbit serum immunoglobulin G (IgG) specific against bovine lactoferrin by immunoaffinity chromatography. *Food Res. Int.* **34**: 783-789.



- Van der Wielen L.A.M.** (1997). Transients in the heterogeneous enzymatic deacylation of penicillin G. *In: A countercurrent adsorptive fluidised bed reactor for heterogeneous bioconversions*. PhD dissertation Delft The Netherlands. 8.1-8.31.
- Vertesi A., Simon L.M., Kiss I., and Szajani B.** (1999). Preparation characterization and application of immobilized carboxypeptidase A. *Enzyme Microb. Technol.* **25**: 73-79.
- Voronin V., Touraev A., Kieft H., Van Lammeren A.A.M., Heberle B.E., and Wilson C.** (2001). Temporal and tissue-specific expression of the tobacco ntf4 MAP kinase. *Plant Mol. Biol.* **45**: 679-689.
- Walther P., and Muller M.** (1999). Biological ultrastructure as revealed by high resolution cryo-SEM of block faces after cryo-sectioning. *J. Microsc.* **196**: 279-287.
- Wang P., Dai S., Waezsada S.D., Tsao A.Y., and Davison B.H.** (2001). Enzyme stabilization by covalent binding in nanoporous sol-gel glass for nonaqueous biocatalysis. *Biotechnol. Bioeng.* **74**: 249-255.
- Wang Y., Chen Y., Lavin C., and Gretz M.R.** (2000). Extracellular matrix assembly in diatoms (*Bacillariophyceae*). IV. Ultrastructure of *Achnanthes longipes* and *Cymbella cistula* as revealed by high-pressure freezing/freeze substitution and cryo-field emission scanning electron microscopy. *J. Phycol.* **36**: 367-378.



---

## Chapter 3 Enzyme distribution derived from macroscopic particle behavior of an industrial immobilized penicillin-G acylase

The contents of this chapter have been published as:

**J.L. van Roon, M. Joerink, M.P.W.M. Rijkers, J. Tramper, C.G.P.H. Schroën, H. H. Beeftink** (2002). Enzyme distribution derived from macroscopic particle behavior of an industrial immobilized penicillin-G acylase. *Biotechnol.Progr.* **19**: 1510-1518.

## **ABSTRACT**

The macroscopic kinetic behavior of an industrially employed immobilized penicillin-G acylase, called Assemblase<sup>®</sup>, formed the basis for a discussion on some simple intra-particle biocatalytic model-distributions. Assemblase<sup>®</sup> catalyzes the synthesis of the widely used semi-synthetic antibiotic cephalixin. Despite the obvious advantages of immobilization, less cephalixin and more of the un-wanted by-product D-(-)-phenylglycine is obtained due to diffusional limitations when the immobilized enzyme is employed.

In order to rationally optimize Assemblase<sup>®</sup>, the parameters particle size, enzyme loading and enzyme distribution, which severely determine the macroscopic particle performance, were studied on the basis of macroscopic observations.

Laser diffraction measurements showed that the particle sizes in Assemblase<sup>®</sup> vary as much as a 100-fold. The relative and total enzyme loadings in Assemblase<sup>®</sup> and fractions thereof of different sizes were determined by initial-rate D-(-)-phenylglycine amide hydrolysis, cephalixin synthesis experiments, and active-site titration, respectively. These experiments revealed that the loading of penicillin-G acylase in Assemblase<sup>®</sup> was inversely correlated with the particle diameter.

Apart from enzyme loadings, estimates on the intra-particle enzyme distribution came from cephalixin synthesis experiments, where mass transport limitations were present. Although this method cannot provide the level of detail of specific labeling experiments, it is simple, fast and cheap. Within the set of simple model predictions, a heterogeneous enzyme distribution with most biocatalyst present in the outer region of the particle (within outer 100  $\mu\text{m}$ ) gave the best description of the observed behavior, although no exact correlation was established. Highly detailed determination of intra-particle enzyme distributions must come from immuno-labeling.

## INTRODUCTION

The use of immobilized enzymes in biocatalytic processes has been of great industrial interest for many years, since it may offer technical and economical advantages. These include facilitated biocatalyst reuse due to high mechanical and operational (apparent) stability, the possibility to operate at extremely high biocatalyst loadings leading to small reactor sizes, and the possibility to employ the biocatalyst in packed-bed or fluidized-bed reactors. In this way, immobilization may lead to efficient (possibly continuous) conversions with high volumetric productivity and a substantial half-life time (Tramper *et al.*, 2001; Calsavara *et al.*, 2001) .

Classically, much research has focused on the (case-specific) support material of choice and on the best method for immobilizing a particular biocatalyst onto the support material (Borchert and Buchholz, 1984; Vertesi *et al.*, 1999; Mateo *et al.*, 2000; Eldin *et al.*, 2000; Jing *et al.*, 2000; Wolfe and Bryant, 1999).

Apart from the optimal combination between these, also the amount of biocatalyst that is loaded onto or into the particle has extensive effects on its behavior: mass transport could become rate limiting. Diffusional limitation(s) of one or more substrates or products can affect the (apparent) substrate specificity and the effectiveness of these particles usually lies below unity (Vertesi *et al.*, 1999; Cloix and Wainer, 2001; Schroën *et al.*, 2002) . Furthermore, the operational and thermal stability of a biocatalyst can be affected by diffusional limitation (Jing *et al.*, 2000; Keusgen *et al.*, 2001; Novick and Dordick, 2000; Ragnitz *et al.*, 2001; Wang *et al.*, 2001).

The macroscopic particle behavior is a result from kinetic effects and mass transport effects. In systems with relatively straightforward kinetics, e.g. a single substrate, single product reaction, mass transport limitations cause ineffective use of the biocatalyst. Generally, particles with severe mass transport limitations have a low productivity per unit biocatalyst, and a high operational (apparent) stability. Depending on the cost of the immobilized biocatalyst in comparison

with other process costs (capital costs per unit reactor volume), the particle may be optimized for effectiveness or stability.

For more complex systems, in which several reactions occur simultaneously, limitations in mass transport may have additional effects on the macroscopic particle behavior. The diffusive transport rates of the various substrates and products may differ; consequently, the formation of one product may be enhanced over another. Schroën *et al.* showed that diffusional limitations cause lowered selectivity for the synthesis of the semi-synthetic antibiotic cephalexin (Schroën *et al.*, 2002). Similarly, decreased enantioselectivity caused by diffusional limitations was reported on by Litjens *et al.* (2001).

In order to meet process demands, the case-specific optimal biocatalytic particle can be developed by adjusting the enzyme loading as well as the enzyme distribution. Knowledge on the intra-particle biocatalytic distribution is therefore essential in the optimization of biocatalytic particles (Ampon, 1992; Ladero *et al.*, 2001).

## INTRA-PARTICLE DISTRIBUTIONS

Sometimes, a homogeneous distribution is simply inferred from the extended contact time during immobilization (Handrikova *et al.*, 1996; Polakovic *et al.*, 2001). However, experimental confirmation of this assumption is omitted on many occasions. In contrast with the rather blunt assumption of an intra-particle biocatalyst distribution, recent advances in molecular (bio-) chemistry and light-microscopic detection techniques facilitate measurements of intra-particle biocatalyst distributions (Van Roon *et al.*, 2002). Despite the developments in this field, optimizing all consecutive steps from sample preparation to image analysis is not trivial and still very laborious and costly.

Another option is to infer information on the intra-particle biocatalyst distribution from macroscopic particle behavior. Although this procedure provides less detail in comparison with most labeling and detection methods, it is relatively simple and fast. For existing and currently employed (industrial) biocatalytic particles, for which the biocatalyst distribution is usually unknown, prediction of intra-particle biocatalyst distributions on the basis of macroscopic data, which are

usually available (abundantly), can provide insight in the causes for the specific behavior and limitation(s) of the biocatalytic particle. This could facilitate any decisions regarding the strategy for optimization of the current immobilized system or could be the basis for changing the set-up towards other (newly developed) support materials or biocatalysts.

In several papers the intra-particle biocatalytic distribution was fitted from macroscopic data of systems with relatively straightforward kinetics (Do and Hossain, 1986; Scharer *et al.*, 1992; Hossain and Do, 1987, 1989; Hatanaka *et al.*, 1999). To the best of our knowledge, up to now little or no research has focused on the modeling of the intra-particle distribution in systems with complex kinetics under non-steady-state conditions. This is also the case for the modeling of enzyme distributions in non-uniform biocatalytic particles on the basis of macroscopic particle kinetics and particle size distributions.

In the present research, Assemblase<sup>®</sup> is used as a model biocatalytic system in order to investigate its transient kinetic behavior under mass transport limitations. Assemblase<sup>®</sup> is the commercial name of an industrially used immobilized penicillin-G acylase from *E. coli* that catalyzes the condensation reaction of a side chain, D-(-)-phenylglycine amide (PGA), and a nucleus, 7-aminodesacetoxycephalosporinic acid (7-ADCA), to the semi-synthetic cephalosporin antibiotic cephalexin. Besides this desired condensation reaction, also two negative side-reactions can occur. The first one is the irreversible hydrolysis of the activated side chain (PGA) to D-(-)-phenylglycine (PG), and the second one is the irreversible product hydrolysis that generates 7-ADCA and phenylglycine. The kinetics and reaction mechanism are extensively reported upon in several papers (Schroën *et al.*, 1999, 2001, 2002).

This system is of interest since it is a multi-substrate, multi-product set of non-steady-state reactions (that do not have straightforward kinetics), in which mass transport limitations of one or two substrates and of the product occurs during the synthesis reaction, leading to deteriorated activity and selectivity in comparison with the reaction with the freely suspended enzyme. Furthermore, Assemblase<sup>®</sup> consists of a pool of close-to-spherical biocatalytic particles that vary greatly in size: typically the mean diameter is about 400  $\mu\text{m}$ , while the standard deviation approximately 150  $\mu\text{m}$ . The largest particles are over a 100 times larger than the

smallest ones, possibly resulting in large differences in mass transport properties of individual particles.

Assemblase<sup>®</sup> was therefore sieved into four size fractions, and the particle size distributions (PSD) of the unsieved Assemblase<sup>®</sup> and the sieved fractions were determined by laser diffraction. Subsequently, various types of macroscopic behavior of native (unsieved) Assemblase<sup>®</sup> and its sieved fractions were studied.

First, the hydrolysis of D-(-)-phenylglycine amide (PGA) by Assemblase<sup>®</sup> was investigated under conditions where no diffusional limitation was present. The initial PGA hydrolysis rate was taken as a measure for the overall enzyme loading, i.e. the total amount of enzyme per unit mass of biocatalytic particle.

Subsequently, an additional measure of the absolute enzyme loading was obtained from active-site titration (AST). This technique is based on enzyme inactivation by a covalent binding inhibitor (in this case phenyl methyl sulfonyl fluoride, PMSF) and enables a direct estimate of the total molar amount of active enzyme per unit mass of biocatalytic particle (Janssen *et al.*, 2002; Van Langen *et al.*, 2002; Svedas *et al.*, 1997).

Cephalexin synthesis catalyzed by Assemblase<sup>®</sup> comprises of a set of simultaneous desired and undesired reactions. Since substrates and products differ in size and charge, the transport of each component may be hindered differently, resulting in differences in relative reaction rates. In the case of Assemblase<sup>®</sup>, increased mass transport limitations are reflected in a lowered selectivity, that is cephalexin synthesis over phenylglycine formation (hydrolysis) ratio (S/H ratio) (Schroën *et al.*, 2002).

Three independent sets of experiments demonstrated that the particle size was inversely correlated with the enzyme loading. Size-dependent enzyme loading, combined with the macroscopic selectivity of Assemblase<sup>®</sup> and its sieved fractions during cephalexin synthesis, where mass transport limitations do play a significant role, revealed insight in the intra-particle distribution of biocatalyst: calculations based on a constant effectiveness factor (at a certain degree of conversion) showed that a homogeneous enzyme layer (with a constant biocatalyst concentration) of 150  $\mu\text{m}$  gave a reasonable description of the observed behavior.



## MATERIALS AND METHODS

### CHEMICALS

All water used was double distilled. Various batches of D-(-)-phenylglycine amide, D-(-)-phenylglycine, 7-aminodesacetoxycephalosporinic acid (7-ADCA) and cephalexin (the condensation product of D-(-)-phenylglycine amide and 7-ADCA) were supplied by DSM Anti-Infectives (Delft, The Netherlands). Sodium hydroxide (>99%), hydrochloric acid (>99%), and phenyl methyl sulphonyl fluoride (PMSF, >99%) were from Merck (Darmstadt, Germany). Acetonitrile and methanol (HPLC grade) were obtained from Riedel-de Haën (Seelze, Germany). All other chemicals were of analytical grade.

### ENZYME

Assemblase<sup>®</sup> is an in-house biocatalyst of DSM Anti-Infectives (Delft, The Netherlands) and was supplied by this company to conduct this research. These biocatalytic particles consist of isolated (Kaasgaard *et al.*, 1999) penicillin-G acylase from *E. coli*. Immobilization was carried out as described by De Vroom (1997), using gelatin and chitosan as gelling agents and glutaric dialdehyde as cross-linking agent. The immobilization technique was relatively mild. It was shown by Schroën *et al.* (2001), who compared the performance and selectivity of different types of Assemblase<sup>®</sup> and free-suspended enzyme at low temperatures and high substrate concentrations, that the immobilization procedure did neither affect enzyme activity nor the catalytic mechanism. The enzyme activity of this batch of Assemblase<sup>®</sup> was 151 U/g DW. One unit is the amount of enzyme that produces 1  $\mu\text{mol}$  of amoxicillin. $\cdot 3\text{H}_2\text{O}$  (analyses by means of HPLC) from 300 mM 6-amino-penicillic acid and 345 mM hydroxy-phenylglycine methyl ester during one minute at initial pH 6.5 (not controlled during reaction) and 293K. For this research, the more relevant 100 mM PGA hydrolysis reaction rate per gram dry weight at 277K and controlled pH 8.0 was taken as a measure for specific activity (expressed in kat/g DW, see Figures 3 and 4 in the results section).

Fractions, designated <200  $\mu\text{m}$ , 200-400  $\mu\text{m}$ , 400-600  $\mu\text{m}$ , and >600  $\mu\text{m}$ , respectively, were obtained by sieving Assemblase<sup>®</sup> three times on a Retsch AS 200 Control G (Haan, Germany) equipped with appropriate standard sieves (diameter 200 mm; height 50 mm). Enhancement of separation came from water

spraying during sieving and from rinsing the sieves afterwards to remove fines, which were subsequently fed to the next sieve with finer pore diameter.

Prior to use, the immobilized enzyme was washed five times in abundant water (>10 times volume of Assemblase) and filtered over a ZapCap<sup>®</sup> CR (0.45  $\mu$ m nylon filter, Schleicher & Schuell, FP 030/2, Dassel, Germany). Reproducible amounts of wet biocatalytic particles could be weighed in by standardizing the sampling procedure of the biocatalyst: after one minute of continuous suction (to remove inter-particle water) the Assemblase<sup>®</sup> was scraped off the ZapCap<sup>®</sup> and used in subsequent experiments. With this procedure, the dry weight was determined to be 12.6 % of the wet weight.

#### **PARTICLE SIZE DISTRIBUTION**

Particle size distributions of Assemblase<sup>®</sup> and its sieved fractions were determined by a Sympatec Helos laser H0024 diffraction system. With this technique, the distortion of an optical field by particles is assessed. The determined quantity is area. A sample of particles was taken from a vigorously stirred suspension (water) and placed in a stirred cuvette. Particles were illuminated with a He-Ne laser (633 nm) with variable beam expander. Diffracted light was collected by a Helos Topmicron 31-element semi-circular (180°) detector array of the KF ( $f=1000$  mm, range 9 – 1750  $\mu$ m) or the BF ( $f=200$  mm, range 1.8 – 350  $\mu$ m) type, depending on the particle size of the sample. Measuring duration was 10 seconds, with a cycle time of 1000 milliseconds. Measurements were conducted at least in duplicate. In some samples, some agglomerates were detected that were larger than the maximal detection size (out of range), resulting in an erroneous measurement. In these cases, the procedure was repeated after an ultrasonic treatment of the sample, to break up the agglomerates. The cumulative distribution of the third moment (volume) was subsequently calculated by Helos laser diffraction software tool HRLD version 3.2 Release 4.

#### **PHENYLGLYCINE AMIDE HYDROLYSIS**

Measurements of initial phenylglycine amide hydrolysis rates were carried out in temperature-controlled double-walled vessels at 277 K. Prior to enzyme addition, the pH was set to 8.0 by addition of sulfuric acid. During the experiment, the pH was controlled by addition of 1.0 molar hydrochloric acid, using an automatic

titrator (Titrimo 719s, Metrohm). Typical experiments were carried out with 0.3 % w/w Assemblase<sup>®</sup> (0.15% w/w for fraction <200) and 100 mM phenylglycine amide. All components were mixed with a six-blade turbine stirrer in standard geometry at 500 RPM. Depending on the expected reaction rate, experiments were monitored for 60 minutes (taking a sample every five minutes) or for 120 minutes (taking a sample every ten minutes). Note that the time constant for diffusion of PGA in particles of this size is very small (less than one minute), compared to the reaction time, assuring full PGA penetration. All samples were subsequently analyzed by HPLC.

#### **ACTIVE-SITE TITRATION OF ASSEMBLASE<sup>®</sup>**

During active-site titration, the active penicillin-G acylase inside the biocatalysts particles was inhibited with phenyl methyl sulphonyl fluoride (PMSF). PMSF is a serine protease inhibitor and inactivates by binding covalently to a serine residue in the active site of these enzymes (Svedas *et al.*, 1997; Duggleby *et al.*, 1995).

Penicillin-G acylase present in aqueous suspensions of Assemblase<sup>®</sup> and its sieved fractions was partially inactivated overnight by addition of a predefined amount of PMSF. Since PMSF is not particularly stable in aqueous solutions and may be hydrolyzed (James, 1978), the stability of PMSF in water was assessed by addition of 0.10 ml of a 12.5 mM PMSF solution in acetonitrile (stock) and 0.05 ml 2 mg/ml phenol solution (used as an internal standard during HPLC analysis) to 3.85 ml of water. The acetonitrile and the phenol concentration in this mixture were proven not to be harmful for enzyme activity and/or stability. Several of these solutions were incubated at different temperatures to establish the PMSF stability. With HPLC analysis it was shown that the concentration of PMSF reduced to approximately 90 % of the initial concentration in 4 hours at 295 K. At 277 K, however, no significant inactivation was observed in 4 hours. Since diffusional processes inside these biocatalytic particles are of a very different time scale (less than one minute), no correction was made for the hydrolysis of PMSF in water, during enzyme inactivation experiments that were conducted at 277 K.

A known amount of Assemblase<sup>®</sup> was incubated overnight at pH 8.0 and 277 K in a freshly prepared PMSF, phenol and water mixture of known composition to

inhibit part of the active enzymes. The next day, the residual activity was measured in a PGA hydrolysis experiment as explained before. Samples were diluted and subsequently analyzed with HPLC. The relative amount (in  $\mu\text{moles/gram wet biocatalyst}$ ) of PMSF needed to fully suppress all enzyme activity, corresponding to the amount of active enzyme in the biocatalytic particle in a 1:1 ratio, was obtained by linear regression on the data points and extrapolation to the abscissa.

### **CEPHALEXIN SYNTHESIS**

Cephalexin synthesis experiments were conducted under temperature- and pH-controlled conditions. The temperature was set at 293 K and maintained by use of double-walled vessels. Fifty ml substrate solution containing 100 mM phenylglycine amide and 100 mM 7-ADCA was used. Prior to the addition of immobilized enzyme, the pH of the solution containing the two substrates was set to 8.0 using sulfuric acid, ensuring complete dissolving of the substrates. Biocatalyst concentrations varied between 0.5 and 4% w/w, but 3% w/w was used typically. Automated titration of 1 molar hydrochloric acid was used to keep the pH constant during the experiment. All components were mixed using a six-blade turbine stirrer in standard geometry at 500 RPM. At least once every 30 minutes a sample was taken during 3-4 hours: a complete progress curve was measured. Samples were subsequently diluted and analyzed by HPLC.

### **ANALYSIS**

The procedure for sampling during phenylglycine amide hydrolysis experiments and cephalexin synthesis experiments was identical. At pre-defined time intervals, 0.25 ml samples were taken and diluted 200 times in a measuring flask. Approximately 5 ml of the diluted sample was filtered through a 0.45  $\mu\text{m}$  disposable disc-filter (Schleicher & Schuell) of which 20  $\mu\text{l}$  sample was analyzed by HPLC subsequently.

The HPLC (Thermo Separations Products) consisted of an SCM 1000 vacuum membrane degasser, a SpectraSystem P4000 gradient pump, a SpectraSystem AS autosampler and a SpectraSystem UV3000 foto-diode array detector.

For analysis of samples from PGA hydrolysis and cephalexin synthesis experiments, a reversed phase C18 column of 250 by 4.6 mm was used, with a

particle size of 5  $\mu\text{m}$  and a pore size of 10 nm (Bester Prodigy ODS3). The pre-column was of type SGE W5C18RS: reversed phase C18, 10 mm by 4 mm). During analysis, the column and tray temperature were kept constant at 313 and 278 K, respectively. The injection volume varied between 1 and 20  $\mu\text{L}$ . The elution buffer was 18.2 mM  $\text{H}_3\text{PO}_4$  at pH 4.9. During analysis, a gradient of acetonitrile was used to enhance the separation. The first 1.9 minutes the column was eluted with 98% v/v buffer and 2% v/v acetonitrile. During the next two minutes the acetonitrile concentration was linearly increased to 5% v/v and linearly increased again to 9% v/v in another 0.6 minutes. This situation was maintained for 0.8 minutes after which the acetonitrile concentration was increased and maintained for 4 minutes at 15% v/v to clean and regenerate the column. The total elution rate remained constant at 1.25 ml/min. Analysis took place at two wavelengths simultaneously: 220 and 265 nm. All components gave a clear response-signal at 220 nm, whereas the components containing a  $\beta$ -lactam moiety (7-ADCA and cephalexin) also responded clearly at 265 nm. More details on the analysis method are given by Schroën *et al.* (2001).

Analysis of samples from PMSF stability experiments was conducted with the same columns, but operating conditions and used elutes differed. For PMSF analysis, an isocratic water acetonitrile mixture with 0.1% v/v trifluoro acetic acid (TFA) was used as eluate at a constant flow of 1.5 ml/min. The analysis time was reduced to a minimum (9 minutes) in order to prevent PMSF hydrolysis in the vials. Furthermore, samples were not stored in the tray as stability measurements are time dependent, but injected immediately. Detection took place at 254 nm at which the aromatic moiety of PMSF resonated.

## RESULTS AND DISCUSSION

The enzyme loading and activity of Assemblase<sup>®</sup> and its sieved fractions were determined in multiple sets of independent experiments. The initial (maximal) PGA hydrolysis activity of the native Assemblase<sup>®</sup> and its sieved fractions were determined and taken as a measure for their enzyme loading (since internal diffusional limitation was absent during the experiments). Also, the total amount of enzyme present per unit mass of biocatalyst ( $\mu\text{mol enzyme/ gram}$ ), or enzyme loading, was determined by active-site titration for Assemblase<sup>®</sup> and all sieved

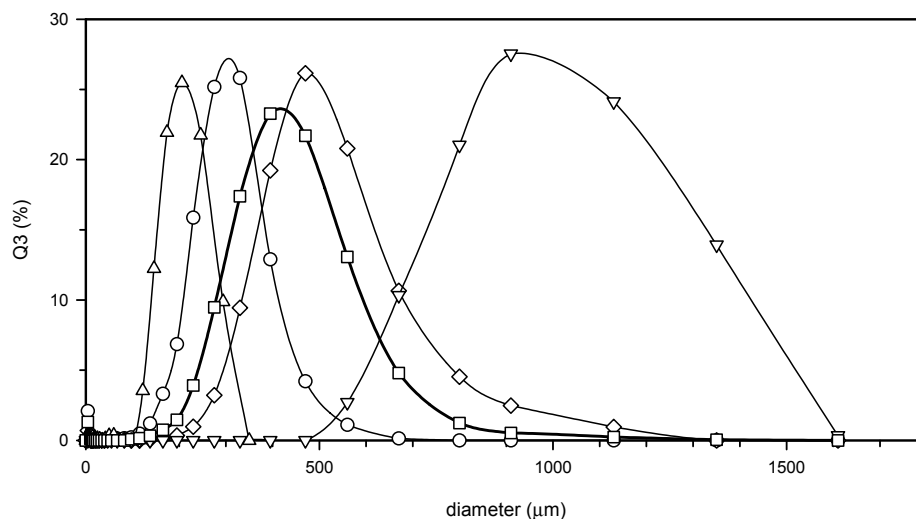


Figure 1. Mean volume-based particle size distribution of Assemblase<sup>®</sup> (□), and sieved fractions thereof; △: <200 μm, ○: 200-400 μm, ◇: 400-600 μm and ▽: >600 μm.

fractions. In a third set of experiments, the cephalixin synthesis capacities of Assemblase<sup>®</sup> and its sieved fractions were determined under conditions where mass transport was limiting. The results were compared to predictions for Assemblase<sup>®</sup>. For the sieved fractions, an effect on the selectivity was expected. In this way, macroscopically observed behavior is linked to the intra-particle distribution of the enzyme.

### PARTICLE SIZE DISTRIBUTION

The volume-based particle size distributions (PSD) of the sieved fractions were determined by laser diffraction. The mean volume distribution as a function of particle diameter is plotted in Figure 1. The volume-based mean diameter (defined as the diameter at which the cumulative volume of the studied sample is 50%) was found to be 409 μm for the unsieved biocatalyst, 183 μm for fraction <200 μm, 288 μm for fraction 200-400 μm, 478 μm for fraction 400-600 μm, and 810 μm for fraction >600 μm. Figure 1 shows that the names of the fractions (<200, 200-400, 400-600, >600 μm) are merely indicative for particle size: e.g. the sample designated as 200-400 μm contains particles ranging from 20 up to 750 μm in diameter. The largest fraction might occasionally contain a cluster of biocatalytic particles, resulting in very large particles, which possibly influences

the PSD of this fraction. The figure also shows that the main volume-contributing fractions in the native biocatalyst are sieved fractions 200-400  $\mu\text{m}$  and 400-600  $\mu\text{m}$ ; hardly any volume in native Assemblase<sup>®</sup> originates from particles smaller than 200  $\mu\text{m}$  or larger than 800  $\mu\text{m}$ .

### PHENYLGLYCINE AMIDE HYDROLYSIS

Since the initial-rates PGA hydrolysis experiments were used as a direct measure of enzyme loading, mass transport limitations had to be avoided. Doubling of enzyme loading would only result in the same increase in the initial PGA hydrolysis rate if mass transport effects were negligible. This was checked by initial PGA hydrolysis experiments, which obey Michaelis-Menten kinetics. Experiments were carried out at 277K and pH 8.0 and the Michaelis-Menten constants were fitted. Values of 8.7 mM and  $7.6 \cdot 10^{-3}$  mmol/(s·gram DW Assemblase<sup>®</sup>) for  $K_m$  and  $V_{\max}$  were found respectively (see Fig. 2). It was decided to use 100 mM in a standard test. The substrate concentration was then over 11 times  $K_m$  (initially a zero-order reaction in PGA) resulting in a reaction rate of more than 93% of the maximum PG formation rate. In this way, mass transport effects are not expected to be significant in initial PGA hydrolysis.

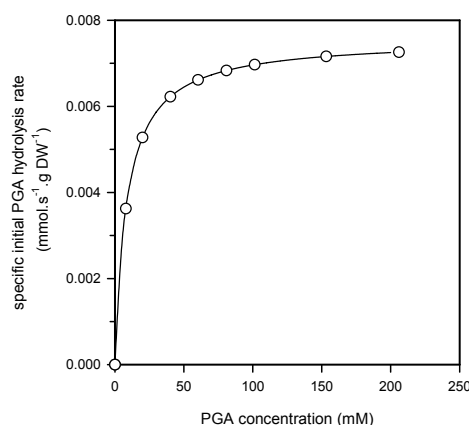


Figure 2. Initial PGA hydrolysis rate as a function of the initial PGA concentration at 277 K and pH 8.0 (●). (—): Model fit with  $K_m = 8.7$  mM and  $V_{\max} = 7.6 \cdot 10^{-3}$  mmol/(s·gram DW Assemblase<sup>®</sup>).

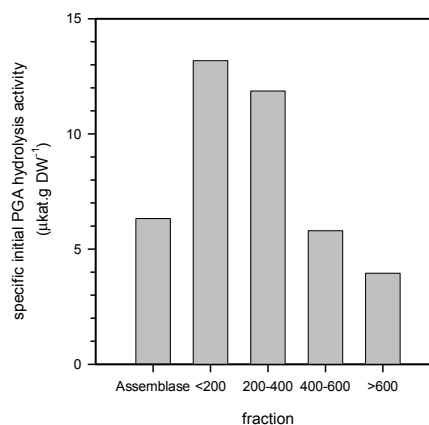


Figure 3. Initial specific PGA hydrolysis activity (U/gram DW biocatalyst) of native Assemblase<sup>®</sup> and its sieved fractions at pH 8.0 and 277 K. One katal (kat) is defined as the amount of enzyme that catalyses 1 mol PG per second from 100 mM PGA at pH 8 and 277 K.

The specific initial PGA hydrolysis rates of native Assemblase<sup>®</sup> (6.3  $\mu\text{kat/g DW}$ ) and its sieved fractions are plotted in Fig. 3. One katal (kat) is defined as the amount of enzyme that catalyses 1 mol PG per second from 100 mM PGA at pH 8 and 277 K. The smallest particles have the highest specific PGA hydrolysis activity ( $1.3 \cdot 10^1 \mu\text{kat/g DW}$ ), the activity of the fraction 400-600 is close to that of native Assemblase<sup>®</sup>, while the activity of the largest particles (>600) is relatively low (3.9  $\mu\text{kat/g DW}$ ). Since diffusional limitation is insignificant during these experiments, also the enzyme loading must be inversely correlated (although not linearly) with the particle diameter. As a check, the initial PGA hydrolysis activity of Assemblase<sup>®</sup>, being a weighed average of that of the sieved fractions, was calculated back by linear combination of the volume shares of the sieved fractions in Assemblase<sup>®</sup> and multiplication with the corresponding enzyme loadings of the sieved fractions. This yielded a calculated initial PGA hydrolysis activity of 99% of the measured activity (data not shown), supporting the measured activities of the sieved fractions.

#### ACTIVE-SITE TITRATION

The absolute amount of enzyme per unit mass of biocatalyst ( $\mu\text{mol enzyme/gram biocatalyst}$ ) was determined by active-site titration. After (partial) inactivation with increasing concentrations of PMSF, the residual hydrolytic activities were

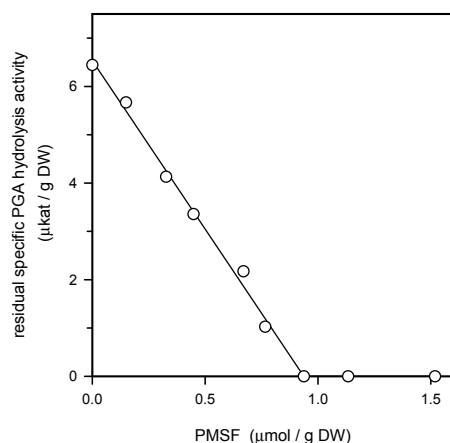


Figure 4. Titration curve for native Assemblase<sup>®</sup>: residual specific PGA hydrolysis activity ( $\mu\text{kat/gram DW}$ ) as a function of the total amount of PMSF added ( $\mu\text{mol/g DW}$ ).

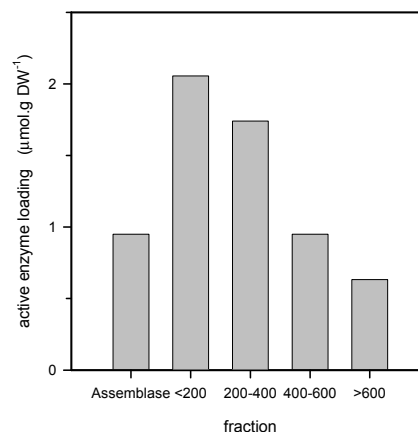


Figure 5. Active enzyme loading ( $\mu\text{mol/g DW}$ ) of Assemblase<sup>®</sup> or sieved fraction, determined by active-site titration.



determined in 100 mM PGA hydrolysis experiments. Note that only the initial hydrolysis rates were measured here: the final conversion was quite low (maximal 3.2%, data not shown). The residual PGA hydrolysis activities were determined for increasing PMSF concentrations (stoichiometrically corresponding to inactivated enzyme) until no residual activity was detected. A typical set of experiments is shown in Figure 4. The absolute active enzyme loading corresponds to the intercept with the abscissa, which was 0.95  $\mu\text{mol}$  of active enzyme per gram dry weight for native Assemblase<sup>®</sup>.

For all experiments, a similar correlation was found (data not shown). The linearity of the residual activity curves for all fractions supports the assumption that measurements were free of diffusional limitation. Since PMSF inhibits from the outside inwards (the particles are partly inactivated by suspending them in a PMSF solution), a growing inactive outer region is expected to be formed as the PMSF concentration increases. Apparently, this does not significantly hamper diffusion of PGA inwards (and of the formed PG outwards), since this would result in a deviation of the residual initial hydrolysis rates away from the ordinate. This was not observed.

In Figure 5, the active enzyme loadings for Assemblase<sup>®</sup> and its fractions are plotted. The average enzyme loading was found to decline with increasing particle diameter. This trend is in excellent agreement with the observations in PGA hydrolysis experiments (see Figure 3).

### **CEPHALEXIN SYNTHESIS**

In contrast to PGA hydrolysis experiments, in which only initial rates were determined, a complete progress curve (resulting from multiple reactions) was monitored during cephalixin synthesis.

PSD measurements showed that particle size varies as much as a factor 100 within native Assemblase<sup>®</sup>. The smallest particles are expected to be less burdened by diffusional limitation because of their size. The effect of enzyme loading was demonstrated for a different type Assemblase<sup>®</sup> with a similar PSD, called Assemblase<sup>®</sup> 7500, containing over double the enzyme loading than the type under investigation here: the S/H ratio at maximum conversion was 1.05 for Assemblase<sup>®</sup> while it was only 0.85 for Assemblase<sup>®</sup> 7500 (data not shown). In

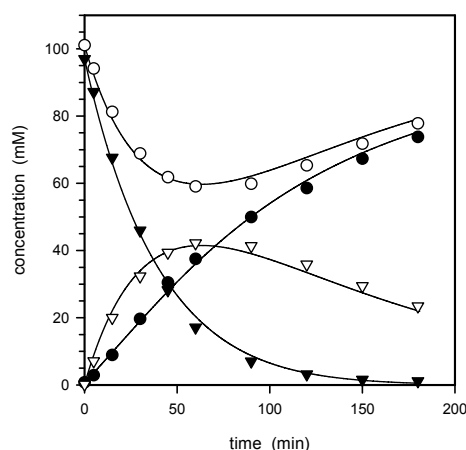


Figure 6. Cephalalexin synthesis for Assemblase<sup>®</sup> <200 fitted with the model of Schroën *et al.* for native Assemblase<sup>®</sup> at 293 K and pH = 8.0 only by adjustment of the enzyme loading per gram of biocatalyst. Measured concentration in mM of ▼: PGA, ○: 7-ADCA, ▽: cephalalexin and ●: phenylglycine. The lines represent the model fit.

the case of Assemblase<sup>®</sup>, the smallest particles also have the highest enzyme loading which may counter-balance the effect of size. It is therefore of interest to examine the selectivity of the sieved fractions during cephalalexin synthesis. It was expected that the S/H ratio would decrease for increasing particle diameter (more mass transport problems), provided that the effects of different enzyme loadings and distributions were not too severe.

However, it was observed that the measured yield on both substrates and the S/H ratio (at any degree of conversion) were very similar for Assemblase<sup>®</sup> and all sieved fractions: the time- dependent concentration profiles of all components could be described with a model presented by Schroën *et al.* (2002), that was derived for native Assemblase<sup>®</sup>, in which the total enzyme loading per unit mass of biocatalytic particles was used as a fit parameter. As a typical example, the measured cephalalexin synthesis data (in this case for fraction <200 µm) and the corresponding model fit is shown in Figure 6.

Moreover, if the enzyme loading was used as a fit parameter, the model fit is in close agreement with the data for every fraction, in spite of the fact that the average particle size of the sieved fractions was significantly different from that in native Assemblase<sup>®</sup> (see Figure 7).

Apparently, the expected increase in mass transport problems due to increasing particle diameter is exactly compensated for by enzyme loading or possibly by enzyme distribution in each sieved fraction. The average enzyme loadings were

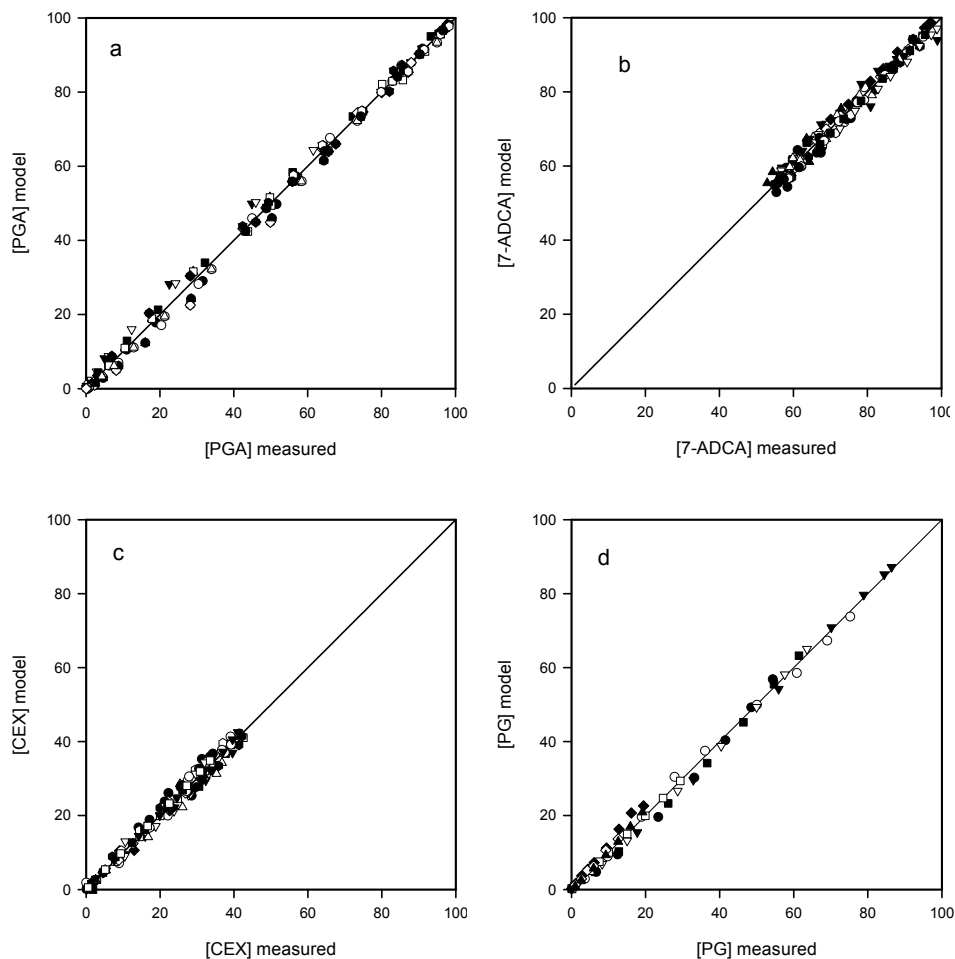


Figure 7a-d. Parity plots for cephalalexin synthesis of PGA (a), 7-ADCA (b), CEX (c) and PG (d) by Assemblase® (●), fraction <200 μm (○), fraction 200-400 μm (▼ and ▽), fraction 400-600 μm (■ and □) and fraction >600 μm (◆, ◇ and ▲).

taken as a measure for synthesis activity and are plotted in Figure 8a. Similar to the observations in PGA hydrolysis experiments and AST, the smallest fractions have a significantly higher synthesis activity and the largest one has a lower cephalalexin synthesis activity in comparison with native Assemblase®.

In Figure 8b, the relative enzyme loading according to AST (Figure 4) is compared to the loading according to PGA hydrolysis (Figure 3) and cephalalexin synthesis experiments (Figure 8a). The figure shows that both methods in which

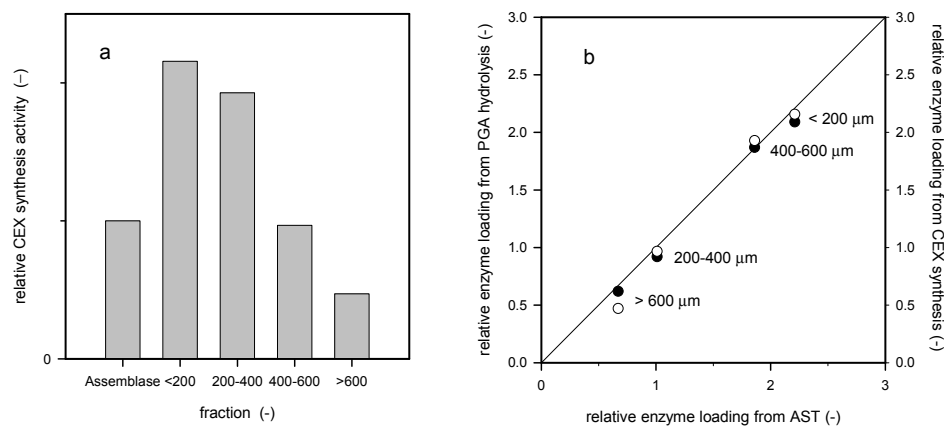


Figure 8. a: Fitted relative cephalixin synthesis activities of Assemblase<sup>®</sup> and its sieved fractions, determined with a 100 mM PGA and 100 mM 7-ADCA substrate solution pH 8.0 at 293 K. A model presented by Schroën *et al.* (2002) was used for fitting the enzyme loadings to the measured progress curves. b: parity plot of the relative enzyme loading according to active-site titration against the loading according to PGA hydrolysis (●) and cephalixin synthesis (○) experiments, respectively.

the activity was taken as a measure for the activity yield the same result as the AST measurement. The (small) variation in activity or enzyme loading for fraction >600  $\mu\text{m}$  could possibly result from clustering of these particles.

It has to be mentioned that in the model only the enzyme loading was adjusted to fit the cephalixin synthesis data. Enzyme distributions that may also affect the impact of mass transport effects with varying particle diameter were not taken into account. During the activation of the empty support material, enzyme diffusion is a transient process. The enzyme penetrates from outward inwards and the intra-particle enzyme loading as well as the intra-particle enzyme distribution depend on the time of activation (unknown for these industrial particles), the diffusivity of enzyme in the carrier and the particle diameter. In other words, these factors do not necessarily only influence enzyme loading, but can also yield intra-particle enzyme profiles. Whether only a different enzyme loading or also a non-homogeneous enzyme distribution caused the observed behavior of the particles of different size classes, is discussed below based on the calculation of the theoretical reduction in enzyme loading that would be required to compensate for increased diameter of homogeneous particles.

A commonly used dimensionless number to compare overall particle performances is the effectiveness factor, which is defined as the ratio of the observed reaction rate divided by the reaction rate at bulk concentration. The overall particle effectiveness factor, the product of the internal and external effectiveness factor, was constant (and equal to that of Assemblase<sup>®</sup>) at any given degree of conversion for native Assemblase<sup>®</sup> and all sieved fractions, since the selectivity of all reactions was the same. As external effectiveness factors for Assemblase<sup>®</sup> and its sieved fractions were assumed constant during cephalixin synthesis, since stirring was standardized and intensified mixing did not enhance the rate of cephalixin formation (data not shown), the internal effectiveness must have been constant as well.

The internal effectiveness factor is often quantified in terms of the Thiele modulus (Van 't Riet and Tramper, 1991). The Thiele modulus describes a ratio between “kinetic rate” and “diffusional rate”. A generalized relation for the Thiele modulus was presented by Aris (1965) and Bischoff (1965), and states that the Thiele modulus is a linear function of the particle diameter and proportional to the inverse square root of the enzyme loading.

In Table 1, the calculated relative homogeneous enzyme loading needed to compensate for the increase in particle size in order to keep the Thiele modulus constant is compared to the measured enzyme loading for Assemblase<sup>®</sup> and its sieved fractions.

The table shows for example that the volume mean particle diameter ( $D_{50}$ ) of the particles larger than 600  $\mu\text{m}$  is over 4 times larger than of particles smaller than 200  $\mu\text{m}$  (1.98/0.45). The calculated difference in the (homogeneous) relative enzyme loading ( $\langle [E]_{\text{rel, calc}} \rangle$ ) needed to compensate for this increased particle

Table 1. Comparison of the calculated enzyme loading ( $\langle [E]_{\text{rel, calc}} \rangle$ ) to compensate for deviating particle diameter of sieved fractions at constant Thiele number in homogeneously loaded spheres and the observed enzyme loading ( $\langle [E]_{\text{rel, obs}} \rangle$ ) in these fractions, relative to Assemblase<sup>®</sup>.  $\langle D_{50} \rangle$  is the relative mean particle diameter at which 50% of the total volume of the fraction is reached.

Fraction	Assemblase <sup>®</sup>	<200	200-400	400-600	>600
$\langle D_{50} \rangle$ (-)	1.00	0.45	0.70	1.17	1.98
$\langle [E]_{\text{rel, calc}} \rangle$ (-)	1.00	5.06	2.07	0.72	0.26
$\langle [E]_{\text{rel, obs}} \rangle$ (-)	1.00	2.53	2.03	1.11	0.73

diameter is a factor 20 (5.06/0.26). However, the actual observed difference in enzyme loading ( $\langle [E]_{\text{rel, obs}} \rangle$ ) is only a factor 4 (2.53/0.73).

Clearly, the theoretically calculated enzyme concentration is not in agreement with the observed concentration. This indicates that the enzyme is most likely not distributed homogeneously over the particle. Recently conducted experiments on the intra-particle distribution, in which the enzyme is specifically labeled with antibodies seem to confirm this.

If the enzymes were mainly located in the outer regions of the carrier and particles of all sizes have similar enzyme distributions in that region, the effect of increasing particle diameter on the mass transport properties would be less pronounced in comparison to particles with homogeneously distributed enzymes.

## DISCUSSION ON INTRA-PARTICLE ENZYME DISTRIBUTION

The most extreme heterogeneous enzyme distribution is a surface loading. If the enzyme would exclusively be present on the surface, the (volume averaged) enzyme loading should be proportional to specific area, i.e. inversely proportional to the particle diameter. This is shown by line 1 in Figure 9. For Assemblase<sup>®</sup> and all fractions the specific surface area was therefore determined by calculation of the weighed average of the specific surface area of the 31 size classes in which the PSD was sub-divided during analysis. These values were compared with the relative activity and loading of the size fractions to evaluate their correlation (see Figure 9), which is discussed later.

The possibility of an enzyme shell with constant thickness (in which the enzyme is distributed homogeneously) was evaluated for various layer-thicknesses. In this type of distribution, a layer of a particular thickness occupies an increasing volume fraction with decreasing particle size. The volume fraction that is occupied by a layer of a certain thickness (lines 2-7 in Figure 9) for a certain sieved particle fraction was compared to the volume fraction occupied by the same layer in the native Assemblase<sup>®</sup> fraction, provided that the layer thickness does not exceed the particle radius. Particles smaller than Assemblase<sup>®</sup> will contain a higher fraction of occupied volume than Assemblase<sup>®</sup> and vice versa.

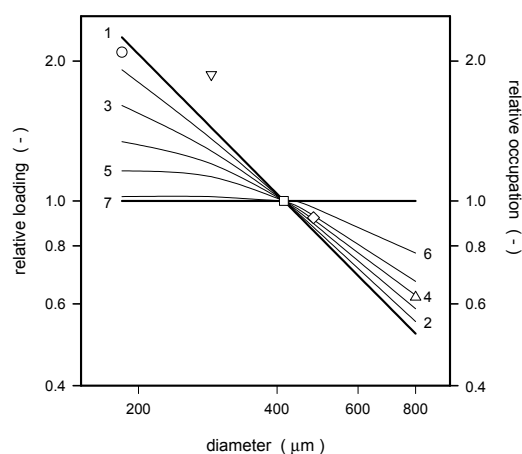


Figure 9. Relative (to Assemblase<sup>®</sup>) enzyme loading (left axis) for size fractions <200  $\mu\text{m}$  (o), 200-400  $\mu\text{m}$  (v), 400-600  $\mu\text{m}$  (◊) and >600  $\mu\text{m}$  ( $\Delta$ ) from PGA hydrolysis and relative fraction of occupied volume for the volume averaged sieved fractions as a function of particle diameter for different homogeneous enzyme layers; 1: surface loading, 2: 25  $\mu\text{m}$ , 3: 50  $\mu\text{m}$ , 4: 75  $\mu\text{m}$ , 5: 100  $\mu\text{m}$ , 6: 150  $\mu\text{m}$  and 7: homogeneous volume distribution.

Figure 9 shows that a surface loading, or a very thin layer of less than 25  $\mu\text{m}$ , covers the differences in average enzyme loading for the smallest particle fraction. For the fraction of 200-400  $\mu\text{m}$ , the correspondence between the relative fraction of occupied volume and the relative activity from AST is poor: even a surface loading does not cover the differences in average enzyme loading. For the largest particle fractions, the relative volume fraction occupied by an enzyme layer of 75-100  $\mu\text{m}$  corresponds to the measured enzyme loading by AST. In other words: under the assumptions made (i.e. a diameter independent layer thickness and constant homogeneous enzyme concentration and distribution within the enzyme layer), there is not one particular layer thickness that describes all measured activity differences between the fractions.

Obviously, the assumptions that were made, lead to extreme enzyme profiles. It is expected that actual enzyme profiles are more gradual. During the activation of the empty support with enzyme, these molecules will reach the center of the particle faster as the particles get smaller. The particle would then no longer act as a semi-indefinite object as the core concentration starts to increase. In that case the enzyme loading for particles smaller than Assemblase<sup>®</sup> is underestimated and is overestimated for particles larger than Assemblase<sup>®</sup>. This is also the trend that was found and that may explain the differences between model and measurements. Future labeling experiments offer the possibility to assess the intra-particle enzyme distribution by specific labeling. Still, the macroscopic measurements have provided valuable additional information on the actual enzyme distribution in Assemblase<sup>®</sup> and have given indications for improvement

of the biocatalyst. E.g. small particles that contain high enzyme loadings can be used without negative effects on the reaction selectivity and thus leads to high volumetric activities. The largest fractions may be sieved out of the support material prior to activation with enzyme.

For preliminary evaluation studies, the discussed macroscopic measurements are valuable tools for optimization. The effects of heterogeneous enzyme distributions can be evaluated to considerable extend. In the later stages of rational biocatalyst design, in which the biocatalyst is optimized, labeling experiments can provide the required detail of information on intra-particle enzyme distributions. From this information, more detailed models can be made for further optimization of Assemblase<sup>®</sup>.

## CONCLUSION

In the previous sections, macroscopically observed particle kinetics (AST, PGA hydrolysis activity and CEX synthesis activity) of Assemblase<sup>®</sup> and its sieved fractions, combined with their PSD's, formed the basis for a discussion on some simple intra-particle model-distributions of penicillin-G acylase in Assemblase<sup>®</sup>. Experiments (AST and PGA hydrolysis) in absence of mass transport limitations showed that the loading of penicillin-G acylase in Assemblase<sup>®</sup> was inversely correlated with the particle diameter. Furthermore, macroscopic experiments where mass transport limitations were present (cephalexin synthesis) revealed additional information on the intra-particle biocatalyst distribution: in Assemblase<sup>®</sup> (and its sieved fractions), the enzyme is distributed heterogeneously over the support material, with most biocatalyst present in the outer region of particle. Recent labeling experiments have shown that detailed discrimination in intra-particle enzyme can actually be made and seem to confirm the findings in this paper (data not shown).

Although the kinetic measurements did not give the same level of detail as labeling experiments can provide for, they are still valuable in the first steps in the rational design of a biocatalyst. These measurements are considerably cheaper and less time consuming than labeling experiments and therefore very suited for preliminary evaluations. For the later stages of rational biocatalyst design, labeling experiments can provide the required level of detail. This



knowledge can be used in accurate models to further optimize these biocatalytic particles.

## ACKNOWLEDGEMENTS

The financial support of DSM and the Ministry of Economic Affairs of the Netherlands is kindly acknowledged. Ruud de Groot (DSM) is acknowledged for his support on wet screening and measurements on particle size distributions. Marten Paasman (DSM) is acknowledged for fruitful discussions on Assemblase<sup>®</sup> formulation and kinetics.

## REFERENCES

- Ampon K.** (1992). Distribution of an enzyme in porous polymer beads. *J. Chem. Technol. Biotechnol.* **55**: 185-190.
- Aris A.** (1965). A normalization for the Thiele modulus. *Ind. Eng. Chem. Fundam.* **4**: 227-229.
- Bischoff K.B.** (1965). Effectiveness factors for general reaction rate forms. *AIChE J.* **11**: 351-355.
- Borchert A., and Buchholz K.** (1984). Improved biocatalyst effectiveness by controlled immobilization of enzymes. *Biotechnol. Bioeng.* **26**: 727-736.
- Calsavara L.P.V., De Moraes F.F., and Zanin G.M.** (2001). Comparison of catalytic properties of free and immobilized cellobiase Novozym 188. *Appl. Biochem. Biotechnol.* **91**: 615-626.
- Cloix J. F., and Wainer I. W.** (2001). Development of an immobilized brain glutamine synthetase liquid chromatographic stationary phase for on-line biochemical studies. *J. Chromatogr. A* **913**: 133-140.
- De Vroom E.** (1997). An improved immobilized penicillin G acylase. PCT/EP96/03253 1-18.
- Do D. D., and Hossain Md.M.** (1986). A novel method of determination of the internal enzyme distribution within porous solid supports and the deactivation rate constant. *Biotechnol. Bioeng.* **28**: 486-493.
- Duggleby H.J., Tolley S.P., Hill C.P., Dodson E.J., Dodson G., and Moody P.C.E.** (1995). Penicillin acylase has a single-amino-acid catalytic centre. *Nature* **373**: 264-268.
- Eldin M.S.M., Schroën C.G.P.H., Janssen A.E.M., Mita D.G., and Tramper J.** (2000). Immobilization of penicillin-G acylase onto chemically grafted nylon particles. *J. Mol. Catal. B Enz.* **10**: 445-451.
- Handrikova G., Stefuca V., Polakovic M., and Bales V.** (1996). Determination of effective diffusion coefficient of substrate in gel particles with immobilized biocatalyst. *Enzyme Microb. Technol.* **18**: 581-584.

- Hatanaka T., Rittirod T., Katayama K., and Koizumi T.** (1999). Influence of enzyme distribution and diffusion on permeation profile of prodrug through viable skin: theoretical aspects for several steady-state fluxes in two transport directions. *Biol. Pharm. Bull.* **22**: 623-626.
- Hossain Md.M., and Do D.D.** (1987). Effects of nonuniform immobilized enzyme distribution in porous solid supports on the performance of a continuous reactor. *Chem. Eng. J.* **34**: B35-B47.
- Hossain Md.M., and Do D.D.** (1989). General theory of determining intraparticle active immobilized enzyme distribution and rate parameters. *Biotechnol. Bioeng.* **33**: 963-975.
- James G.T.** (1978). Inactivation of the protease inhibitor phenylmethanesulphonyl fluoride in buffers. *Anal. Biochem.* **86**: 574-579.
- Janssen M.H.A., Van Langen L.M., Pereira S.R.M., Van Rantwijk F., and Sheldon R.** (2002). Evaluation of the performance of immobilized penicillin-G acylase using active-site titration. *Biotechnol. Bioeng.* **78**: 425-432.
- Jing H., Li X.F., Evans D.G., Duan X., and Li C.Y.** (2000). A new support for the immobilization of penicillin acylase. *J. Mol. Catal. B Enz.* **11**: 45-53.
- Kaasgaard S.G., Karlsen L.G., and Schneider I.** (1992). Process for separation of two solid components. PCT/DK92/00024 1-18.
- Keusgen M., Glodek J., Milka P., and Krest I.** (2001). Immobilization of enzymes on PTFE surfaces. *Biotechnol. Bioeng.* **72**: 530-540.
- Ladero M., Santos A., and Garcia O.F.** (2001). Diffusion and chemical reaction rates with nonuniform enzyme distribution: an experimental approach. *Biotechnol. Bioeng.* **72**: 458-467.
- Litjens M.J.J., Le K.Q., Straathof A.J.J., Jongejan J.A., and Heijnen J.J.** (2001). Diffusion limitation causes decreased enantioselectivity of esterification of 2-butanol by immobilized *Candida antarctica* lipase B. *Biocat. Biotrans.* **19**: 1-19.
- Mateo C., Fernandez L.G., Abian O., Fernandez L.R., and Guisan J.M.** (2000). Multifunctional epoxy supports: a new tool to improve the covalent immobilization of proteins. The promotion of physical adsorptions of proteins on the supports before their covalent linkage. *Biomacromolecules* **1**: 739-745.
- Novick S.J., and Dordick J.S.** (2000). Investigating the effects of polymer chemistry on activity of biocatalytic plastic materials. *Biotechnol. Bioeng.* **68**: 665-671.
- Polakovic M., Kudlacova G., Stefuca V., and Bales V.** (2001). Determination of sucrose effective diffusivity and intrinsic rate constant of hydrolysis catalyzed by *Ca-alginate* entrapped cells. *Chem. Eng. Sci.* **56**: 459-466.
- Ragnitz K., Syldatk C., and Pietzsch M.** (2001). Optimization of the immobilization parameters and operational stability of immobilized hydantoinase and L-N-carbamoylase from *Arthrobacter aurescens* for the production of optically pure L-amino acids. *Enzyme Microb. Technol.* **28**: 713-720.
- Scharer A., Hossain Md.M., and Do D.D.** (1992). Determination of total and active immobilized enzyme distribution in porous solid supports. *Biotechnol. Bioeng.* **39**: 679-687.
- Schroën C.G.P.H., Nierstrasz V.A., Kroon P.J., Bosma R., Janssen A.E.M., Beftink H.H., and Tramper J.** (1999). Thermodynamically controlled synthesis of  $\beta$ -lactam antibiotics. Equilibrium concentrations and side-chain properties. *Enzyme Microb. Technol.* **24**: 498-506.

- Schroën C.G.P.H., Nierstrasz V.A., Moody H.M., Hoogschagen M.J., Kroon P.J., Bosma R., Beftink H.H., Janssen A.E.M., and Tramper J.** (2001). Modeling of the enzymatic kinetic synthesis of cephalexin - Influence of substrate concentration and temperature. *Biotechnol. Bioeng.* **73**: 171-178.
- Schroën C.G.P.H., Fretz C.B., De Bruin V.H., Berendsen W., Moody H.M., Roos E.C., Van Roon J.L., Kroon P.J., Strubel M., Janssen A.E.M., and Tramper J.** (2002). Modeling of the enzymatic kinetically controlled synthesis of cephalexin: influence of diffusion limitation. *Biotechnol. Bioeng.* **80**: 331-340.
- Svedas V.K., Guranda D.F., Van Langen L., Van Rantwijk F., and Sheldon R.** (1997). Kinetic study of penicillin acylase from *Alcaligenes faecalis*. *FEBS Lett.* **417**: 414-418.
- Tramper J., Beftink H.H., Janssen A.E.M., Ooijkaas L.P., and Van Roon J.L.** (2001). Biocatalytic production of semi-synthetic cephalosporins: process technology and integration In: Synthesis of  $\beta$ -lactam Antibiotics: Chemistry Biocatalysis & Process Integration (A. Bruggink Ed.). Kluwer Academic Publishers Dordrecht The Netherlands. pp. 206-249.
- Van 't Riet K., and Tramper J.** (1991). Basic Bioreactor Design. Marcel Dekker Inc., New York. pp 320-341.
- Van Langen L.M., Janssen M.H.A., Oosthoek N.H.P., Pereira S.R.M., Svedas V.K., Van Rantwijk F., and Sheldon R.** (2002). Active site titration as a tool for the evaluation of immobilization procedures of penicillin acylase. *Biotechnol. Bioeng.* **79**: 224-228.
- Van Roon J., Beftink R., Schroën K., and Tramper H.** (2002). Assessment of intraparticle biocatalytic distributions as a tool in rational formulation. *Curr. Opin. Biotechnol.* **13**: 398-405.
- Vertesi A., Simon L.M., Kiss I., and Szajani B.** (1999). Preparation characterization and application of immobilized carboxypeptidase A. *Enzyme Microb. Technol.* **25**: 73-79.
- Wang P., Dai S., Waezsada S.D., Tsao A.Y., and Davison B. H.** (2001). Enzyme stabilization by covalent binding in nanoporous sol-gel glass for nonaqueous biocatalysis. *Biotechnol. Bioeng.* **74**: 249-255.
- Wolfe J., and Bryant G.** (1999). Freezing drying and/or vitrification of membrane-solute-water systems. *Cryobiol.* **39**: 103-129.



---

## Chapter 4 Novel approach to quantify immobilized-enzyme distributions

The contents of this chapter have been published as:

**J.L. van Roon, E. Groenendijk, H. Kieft, C.G.P.H. Schroën, J. Tramper, H.H. Beftink** (2005). Novel approach to quantify immobilized-enzyme distributions. *Biotechnol. Bioeng.* **89**: 660-669.

## **ABSTRACT**

The quantitative intra-particle enzyme distribution of Assemblase<sup>®</sup>, an industrially employed polydisperse immobilized penicillin-G acylase, was measured. Because of strong autofluorescence of the carrier, the generally applied technique of confocal scanning microscopy could not be used; light microscopy was our method of choice. To do so, Assemblase<sup>®</sup> particles of various sizes were sectioned, labeled with antibodies specifically against the enzyme, and analyzed light microscopically. Image analysis software was developed and used to determine the intraparticle enzyme distribution, which was found to be heterogeneous, with most enzyme located in the outer regions of the particles. Larger particles showed steeper gradients than smaller ones. A mathematical representation of the intraparticle profiles, based on in-stationary enzyme diffusion into the particles, was validated successfully for a broad range of particle sizes using data for volume-averaged particle size and enzyme loading. The enzyme gradients determined in this work will be used as input for a physical model that quantitatively describes the complex behavior of Assemblase<sup>®</sup>. Such a physical model will lead to identification of the current bottlenecks in Assemblase and can serve as a starting point for the design of improved biocatalysts that also may be based on intelligent use of enzyme gradients.

## INTRODUCTION

The use of immobilized enzymes is widespread. More and more, enzymes become an integral part of the (bio) chemist's toolbox. Optimization of reactions carried out with immobilized enzymes is straightforward as long as single reactions are concerned. If the enzyme activity is not sufficient, more biocatalytic particles can be added or the amount of enzyme per particle (loading) can be increased. As long as no diffusion limitation occurs both alternatives should result in the same observed enzyme activity. However, if this is not the case, the biocatalyst with the highest enzyme load will exhibit the lowest activity as a result of diffusion effects.

For multiple reactions, the situation becomes more complex because not all reactions will be influenced in the same way by diffusion limitation (Keusgen *et al.*, 2001; Leenen *et al.*, 1997; Litjens *et al.*, 2001; Novick and Dordick, 2000; Ragnitz *et al.*, 2001; Wang *et al.*, 2001). An illustrative example is the enzymatic synthesis of cephalexin, a semi-synthetic  $\beta$ -lactam antibiotic. When Assemblase<sup>®</sup>, which is an industrially used immobilized penicillin-G acylase, is used for the synthesis of cephalexin, the selectivity of the wanted synthesis reaction over the unwanted hydrolysis side-reaction depends on the enzyme loading of the biocatalyst. In the case of Assemblase<sup>®</sup>, the wanted synthesis reaction is hampered more, resulting in an unfavorable decrease in the synthesis/hydrolysis ratio as the enzyme loading increases (Schroën *et al.*, 2002).

Up till now, only the total enzyme loading was discussed. To which extend the biocatalytic particle is affected by the reduced local substrate concentrations depends, amongst others, on the local enzyme loading, i.e. on the enzyme distribution. Therewith, the enzyme distribution (which is often overlooked) can severely influence the macroscopic particle dynamics. In fact, for Assemblase<sup>®</sup> previous experiments on its external macroscopic kinetic behavior indicated a heterogeneous enzyme distribution, but the actual distribution could not be derived from these measurements (Van Roon *et al.*, 2003).

Therefore, the quantitative intra-particle distribution of penicillin-G acylase in Assemblase<sup>®</sup> had to be measured. Recently, much work is done by optical sectioning of biocatalytic particle interiors, e.g. by confocal scanning laser microscopy (Bougourd *et al.*, 2000; De Beer *et al.*, 1997; De Smet *et al.*, 1997; Laca *et al.*, 1999; Linden *et al.*, 1999; Prior *et al.*, 1999; Spear *et al.*, 1999). This method has some limitations, (Booth and Wilson, 2001; van Roon *et al.*, 2002) and cannot be used for Assemblase<sup>®</sup> because of strong auto-fluorescence of the carrier material and the relatively large size of the particles. In the present work epi-polarization light-microscopy was used on physical sections of the biocatalytic particles. The particles were embedded in a resin, sectioned, and labeled with antibodies specific against Penicillin-G acylase, which is not a trivial task. Furthermore, multiple sections of a single particle were studied, from which the 3D-intra-particle enzyme distribution was calculated. This yielded a heterogeneous radius-dependent enzyme concentration profile that had the mathematical shape of in-stationary diffusion. The actual enzyme diffusivity in the carrier was found to be close to literature estimates. It was shown that enzyme profiles of other differently-sized Assemblase<sup>®</sup> particles could be predicted well.

These data will be used to construct a physical model for Assemblase<sup>®</sup>, in which mass transfer, enzyme loading, and enzyme distribution are accounted for separately. Because such a model gives physical understanding of the processes involved and current bottlenecks, it can be used as a starting point for particle optimization and opens the door to rationally designed processes (for other antibiotics) around the biocatalyst and vice versa.

## **MATERIALS AND METHODS**

All methods were developed specifically for the present work and are therefore described in adequate detail.

### **CHEMICALS**

All water used was double distilled. Polyclonal rabbit immunoglobulin-G against *E. coli* penicillin-G acylase was generously donated by Dr. C.F. Sio (Department of Pharmaceutical Biology, University of Groningen, The Netherlands), and was used as a primary antibody. Secondary antibodies were GAR (goat anti-rabbit)



polyclonals to which an ultra-small (<1nm) gold particle was attached (Aurion, Wageningen, The Netherlands). Silver enhancement was done with an Aurion R-Gent SE-EM silver-enhancement kit. All other chemicals were at least of analytical grade.

#### ENZYME IMMOBILIZATION

Assemblase<sup>®</sup> is an in-house biocatalytic particle of DSM Anti-Infectives (Delft, The Netherlands); a single batch was donated for the present research. In all instances where the trademark Assemblase<sup>®</sup> is used, this refers to this particular preparation. These biocatalytic particles contained immobilized *E. coli* penicillin-G acylase. In patents by De Vroom (1997) and Harder *et al.* (1982), the immobilization procedure is described. For this specific batch, the enzyme was loaded onto the support material from the exterior after bead formation. Although activation times can vary considerably depending on many different process conditions such as ambient temperature, biocatalyst concentration and agitation speed, it was approximately 1.9 hours for this research. Immobilization was relatively mild: previous research showed the enzyme activity and kinetic mechanism to be unaffected (Schroën *et al.*, 2002). The enzyme activity of this specific batch of Assemblase<sup>®</sup> was 3800 U per kg of particle dry weight (1 U produces 1 g of amoxicillin trihydrate - as analyzed by HPLC - from 300 mM 6-aminopenicillanic acid and 345 mM hydroxy-phenylglycine methyl ester in 1 hour at pH 6.5 and 293 K).

Assemblase<sup>®</sup> size fractions (<200 µm, 200-400 µm, 400-600 µm, and >600 µm) were obtained by sieving the native biocatalyst three times on a Retsch AS 200 Control G (Haan, Germany) with appropriate standard sieves (200 x 50 mm). Separation was enhanced by water spraying during sieving and by rinsing the sieves to remove fines, which were subsequently fed to the next sieve with finer pore diameter. Prior to use, immobilized enzyme particles were washed five times in abundant water (>10 times volume of Assemblase<sup>®</sup>) and filtered over a ZapCap<sup>®</sup> CR (0.45 µm nylon filter, Schleicher & Schuell, FP 030/2, Dassel, Germany). Reproducible amounts of wet biocatalytic particles could be weighed in by standardizing the sampling procedure of the biocatalyst: after one minute of continuous suction to remove inter-particle water, the Assemblase<sup>®</sup> was scraped off the ZapCap<sup>®</sup> and used in the experiments.

### **EMBEDDING**

To allow inspection of their interior, the sub-millimeter particles had to be cut in smooth slices of reproducible thickness. Prior to slicing, therefore, particles were embedded in BMM (40 mL butylmethacrylate, 10 mL methylmethacrylate, 0.25 g benzoin ethylether and 0.08 g DTT, stripped of oxygen by continuous nitrogen flushing; (Baskin et al., 1992). Proper particle dehydration and penetration of water-insoluble resin proved crucial for a good embedding. Particles were washed three times in abundant water and then dehydrated by washing for 30 minutes each in a series of 10, 30 and 50% ethanol with 10 mM of the reducing agent dithiothreitol (DTT). Subsequently, beads were washed two times 30 minutes in 70% ethanol with 10 mM DTT and left overnight in a shaker at 277 K in 70% ethanol with 10 mM DTT. The next day, washing was continued at 277 K in 96 and 100% ethanol with 10 mM DTT for one hour each. Ethanol was then replaced by three ethanol:BMM mixtures (ratios of 5:1, 3:1 and 1:1) for 2 hours each at 277 K. After leaving the samples overnight in a 1:3 mixture, infiltration was continued the next day at 1:5 (3 hours) and three times by a 100% BMM (1 hour each). Samples were left overnight at 277 K and then transferred into BEEM capsules (EMS, Washington, USA) the next day. Polymerization of the BMM under black-light ultra-violet lamps was done for 48 hours at 253 K, since the exothermic polymerization would be too fast without cooling.

### **SECTIONING**

After resin polymerization, BEEM capsules were removed and the plastic-embedded Assemblase<sup>®</sup> particles were cut in a series of subsequent 2.75- $\mu$ m sections at various positions within a single particle. To this end, an LKB 2088 Ultratome V was used (LKB Bromma, Stockholm, Sweden), fitted with glass knives (LKB 7801 knifemaker, LKB, Stockholm, Sweden). Sections were put onto a water drop on a microscope glass slide and stretched with chloroform vapor, after which water was vaporized by placing the slide onto a heated plate of approximately 323 K allowing the sections to stick to the microscopic slide.

### **LABELING**

For reasons of label flexibility and limited primary-antibody availability, a two-step labeling procedure was adopted. Prior to labeling, BMM was removed by washing the sections 2 times 7 minutes in 100% acetone, after which the solvent was removed by washing in PBS (8 g NaCl, 0.2 g KCl, 0.2 g KH<sub>2</sub>PO<sub>4</sub> and 1.41 g

Na<sub>2</sub>HPO<sub>4</sub> dihydrate in 1 liter water, pH 7.4). To avoid a-specific epitope binding, sections were treated with 0.1 M hydroxyltetraammonium chloride in PBS (5 min), washed in PBS (5 min), and treated with 1% w/v bovine serum albumine (BSA fraction V, Merck, Darmstadt, Germany) in PBS (30 min), followed by 0.01% acetylated BSA (BSA-c, Aurion) in PBS for 3 x 5 min. Incubation with the primary antibody was done overnight at 277 K, followed by washing with 0.01% BSA-c (4 x 15 min) at 295 K. Sections were then incubated with GAR-type secondary antibody containing an ultra-small 1 nm gold particle as a label (2 h at 310K). Subsequently, sections were washed with 0.01% BSAc (4 x 15 min, 293 K), fixated in 2% w/v glutaric dialdehyde in PBS (5 min), and washed with water (3 x 5 min). Silver enhancement (label enlargement by silver deposition onto the gold particles) was done with a standard kit (Aurion) until an appropriate label size (approximately 30-40 nm diameter).

Three negative control experiments were done in triplicate. In the first, the primary antibody was omitted from the labeling procedure to check for a-specific binding of the secondary antibody. In the second, empty support particles without penicillin-G acylase were labeled with both antibodies, to check for a-specific affinity of one or both antibodies to the support material. Finally, a normal rabbit serum was used in combination with the second (GAR-type) antibody, to check for affinity of the rabbit serum to the penicillin-G acylase. In all negative control experiments, no gold label whatsoever was visible under the microscope after silver enhancement. Additionally to the negative control experiments, a positive control experiment was performed in triplicate with both antibodies, showing abundant label presence. From this, it was concluded that the chemicals used in the embedding and labeling procedure did not destroy (all) the highly specific epitope structures of the penicillin-G acylase; all labeling experiments were therefore carried out according to this procedure. Whether or not the enzyme was still fully functional after this treatment was irrelevant, since only detection of their presence was of importance in the labeling experiment.

For both antibodies, saturation tests were conducted to ensure antibody under-saturation in all experiments. In all cases, less than 1% of the label concentration at which saturation effects became visible under the microscope was employed. Furthermore, silver enhancement was stopped immediately after proper contrast became visible in the microscope, minimizing the label size (30-40 nm diameter).

Because the observed label intensity in the microscope heavily depends on the lighting, on diaphragm and collector settings, on the set of lenses used and magnification used, it is impossible to relate absolute light intensities to enzyme concentrations. However, with the applied precautions, the relative label signal intensity can safely be assumed to be proportional to the relative enzyme density within a single sample.

### **DETECTION**

The label of particle sections was measured in an epi-polarisation microscope with an IGS filter block (Optiphot, Nikon, Tokyo, Japan). Filtered light from a mercury lamp was reflected by the silver-enhanced gold particles. Although the particles themselves are below the microscope resolution, their polarized reflection was detectable. Particle section micrographs were recorded by a digital 24-bits 3 CCD video camera (Sony dxp 950c, Tokyo, Japan) and were digitized with an image recorder (Sony DKR700) for subsequent image analysis.

### **IMAGE ANALYSIS**

A Matlab<sup>®</sup> procedure was written for the analysis of label densities in the micrographs of the particle sections. The procedure consists of multiple routines that will be outlined shortly below. Figure 1 shows an example of a micrograph as it is loaded into Matlab<sup>®</sup>.

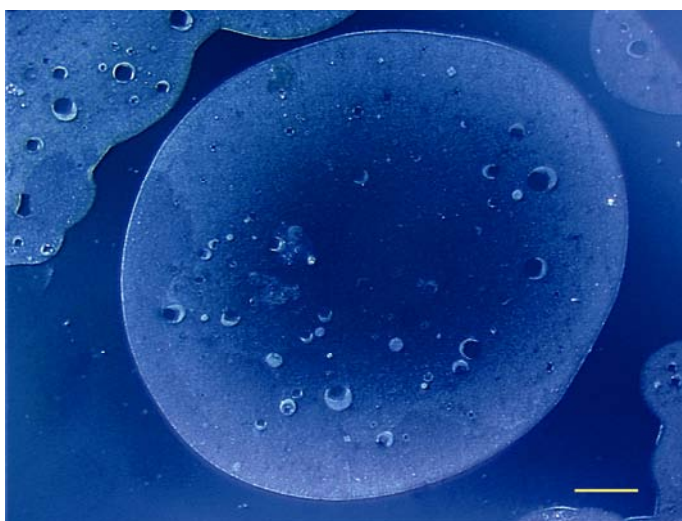


Figure 1. Epipolarization micrograph of a section through Assemblase. High light intensities in the outer regions of the section are caused by high label (enzyme) densities. Note the holes, which were natively present in the biocatalytic particle. The bar corresponds to 50  $\mu\text{m}$ .

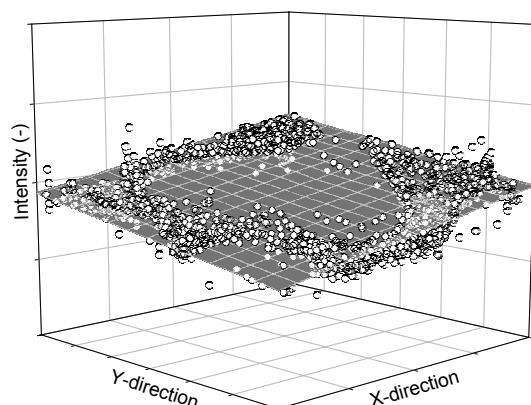


Figure 2. Fit of background intensity for the micrograph presented in Figure 1. As an example, the Figure shows one of the three fitted RGB intensity planes (blue in this case) in gray.

First, light intensities of the micrograph were thresholded to establish a particle section perimeter. Filters were written to reconstruct incomplete perimeters and remove all noise after thresholding. The resulting matrix with all perimeter coordinates was used to distinguish between object pixels (particle section) and background pixels.

#### UNEVEN IMAGE EXPOSURE

Mathematical expressions for the possibly uneven background intensity within a micrograph were obtained by fitting three planes through the red, green and blue (RGB) intensities, respectively, of all background pixels, which were situated outside the particle perimeter. All pixels belonging to the particle were neglected in this stage (note the local absence of intensity data in the section in Figure 2). The resulting expressions for the intensity gradient of the background, which corresponds to the fitted intensity plane (gray plane in Figure 2) though all background intensity data (○ in Figure 2), were then subtracted from all the RGB intensity values in the complete original micrograph (background and particle). Remaining intensity differences in the resulting micrograph were thus exclusively generated by label density differences.

#### SECTION INTENSITY PROFILES

For every pixel within an Assemblase<sup>®</sup> section, the distance to every perimeter pixel of that section was calculated; its minimum value was stored as the pixel's distance to the section perimeter. Distances to the perimeter were then translated

to a radial position  $r_s$  within the section by defining a surface-equivalent section radius ( $R_s$ ), based on the total number of pixels in the slightly non-circular section. Particles and sections with pronounced deviations from circularity were ignored. For all pixels at a certain radial position  $r_s$  within the section, the average pixel intensity  $I(r_s)$  was calculated. Plotting these averaged intensities against position within a section yielded the intensity profile of a single section. Since overall micrograph exposure (illumination) varied between sections, section intensity profiles were normalized with respect to their perimeter intensity, i.e.  $I(r_s)/I(r_s)$ .

### PARTICLE INTENSITY PROFILES

Radial positions within a particle section ( $r_s$ ) were converted to particle positions ( $r_p$ ) with a simple pythagorean algorithm; it was applied to two sections at a time through a single purportedly spherical particle (Figure 3, sections a and b). As an input to this algorithm, the distance  $d$  between both sections was obtained from counting cuts in the sectioning procedure ("Sectioning", 2.75  $\mu\text{m}$  per cut); from this distance and the section radii  $R_{s,a}$  and  $R_{s,b}$ , the particle radius  $R_p$  was calculated. For a minimum of three sections through a single particle, the final particle radius was calculated as the average particle diameters obtained from all possible combinations of section pairs in the above routine. In Figure 3, both sections are above the center of the particle, which was not known in advance.

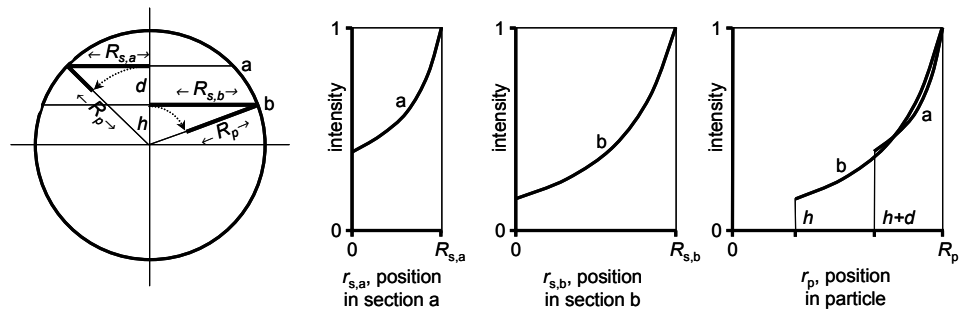


Figure 3. Schematic representation of normalized intensity profiles of 2 sections with radii  $R_{s,a}$  and  $R_{s,b}$  through the top half of a single particle with radius  $R_p$ . Section "a" originated near the surface and has a relatively flat intensity profile in comparison with section "b", which originated near the center of mass of the particle. The particle radius and the distances from the center of mass of the particle the sections originated from ( $h$  and  $h+d$  for sections b and a, respectively, see left drawing) are used to calculate the normalized intra-particle enzyme distribution (right).

Therefore, for each pair of sections, two particle radii were calculated, assuming the particle center to be either in between or outside the two sections. The physically appropriate radius was then selected manually.

### **SHRINKAGE**

Particle shrinkage due to embedding was investigated by measuring particle diameters of approximately 50 beads with a binocular before (native, swollen state) and after dehydration and BMM penetration (dehydrated shrunken state). The average final radial shrinkage was 32% with a standard deviation of 2.4% (0.024), which was used to correct all distances relative to the center of the particle: only shrinkage-corrected data are shown in the rest of the paper.

### **NUMERICAL SOLUTION PROFILES**

The numerical solution of the partial differential equation describing the intra-particle enzyme profiles was calculated by discretization with the method of lines. A standard set of boundary conditions was used. It is assumed that, the particles are freely suspended in a semi-infinite continuum with constant enzyme concentration. The continuum approaches infinite turbulence, which implies that the resistance for mass-transfer is only situated internally; no external diffusional limitation occurred). Further, radial symmetry for the concentrations of all components was assumed in the particle center: all gradients and mass fluxes in the particle center were nil. The resulting set of equations was solved with Matlab<sup>®</sup> version 13 (ODE 15s solver variable-order Runge-Kutta algorithm with variable time-step) for an enzyme penetration time of 1.9 hours and the outcome was compared to the measured intra-particle enzyme gradients. The enzyme diffusivity was fitted to the experimental data by minimizing the squared differences. The only fit parameter was the enzyme diffusivity.

## **RESULTS AND DISCUSSION**

### **MICROSCOPIC DETECTION**

To study the particle interior, sections were made through Assemblase<sup>®</sup> particles. As an example, Figure 4a-e shows five different sections through a single particle with a (calculated) radius of 167  $\mu\text{m}$ . The radius of the section increased in Figures 4a and 4b, indicating that the subsequent sections came closer to the particle center, and diminished again in Figures 4c to 4e as the sections moved

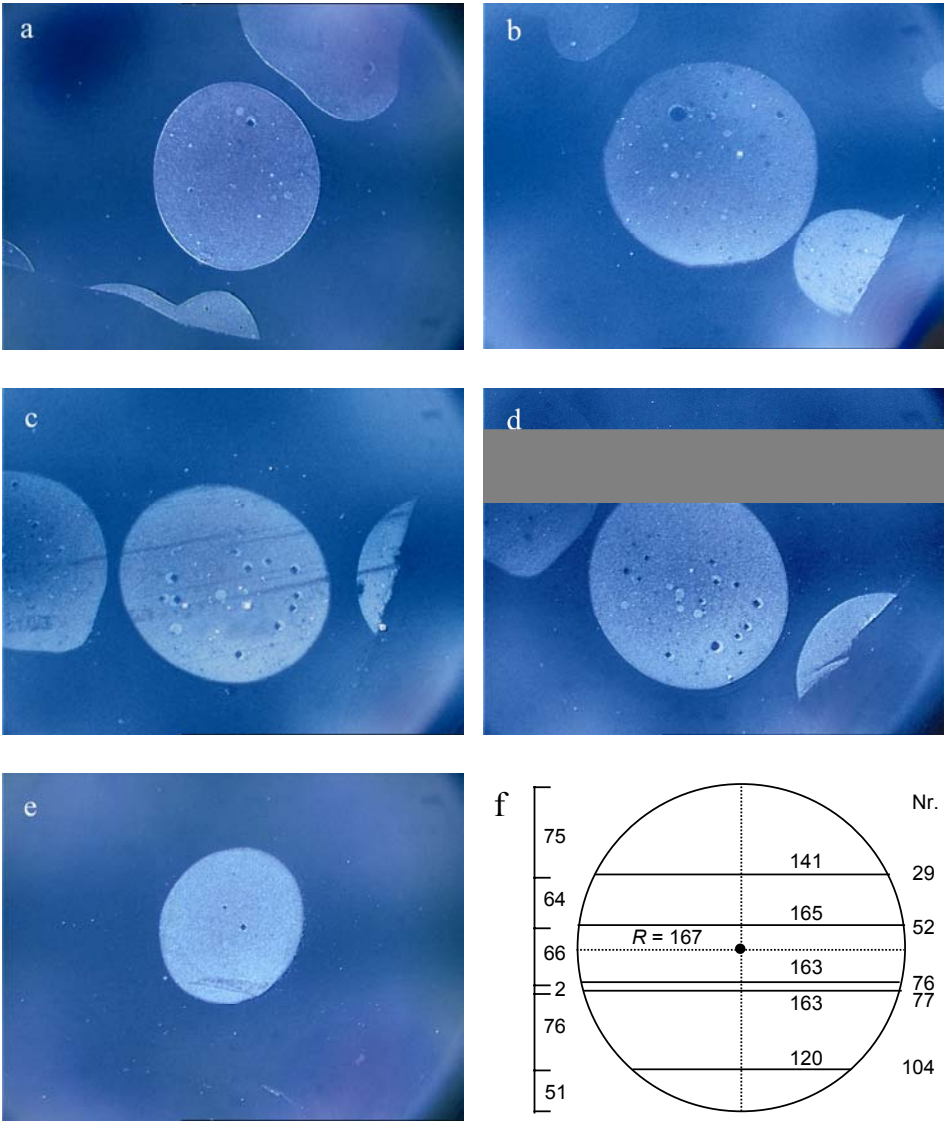


Figure 4. a-e: Micrographs of section numbers 29, 52, 76, 77 and 104 through a single Assemblase® particle with a calculated radius of 167  $\mu\text{m}$ . The first two sections are situated above the center of mass of the particle and the last three sections below the center. f: Schematic representation of the positions at which the sections (numbers in right scale) were made, their mutual distances in  $\mu\text{m}$  (left scale) and the section radii in  $\mu\text{m}$ .



away from the middle of the particle. Figure 4f shows a schematic representation of the size and position of the sections within the particle (determination according to the material and method section).

The micrographs of labeled sections (Figures 4a-e) all show a radial intensity gradient: at the perimeter of the sections, the light intensity (proportional to the local enzyme density) is higher, whereas the signal intensity is lower near the center of the section, indicating less enzyme was present there. Furthermore, intensity profiles were more pronounced in central sections (Figures 4b-d) in comparison with the more peripheral sections (Figures 4a and 4e). This is in agreement with in-stationary enzyme diffusion into the empty support material during the preparation of the biocatalytic particles.

Figure 4 also shows some abrupt local intensity changes in certain regions of the labeled sections. Near the surface (e.g. in Figure 4a) and around holes in the sections (which were not introduced by cutting, but were already present in the native material), a step-wise intensity increase was observed. Also image analysis confirmed the presence of abrupt intensity peaks at the perimeter of some sections, for example in section 29 (Figure 5a) and also surrounding some intra-particle holes. This corresponds to an abrupt high (surface) loading, which may become important for future particle development. Unfortunately, the resolution of the presently used technique is not sufficient to study this effect in detail. Therefore, the rest of this paper will focus on the overall enzyme gradient over the entire particle, which accounts for the greater part of the enzyme. The surface phenomena are currently investigated with high-resolution equipment.

#### **INTENSITY PROFILE OF A SINGLE PARTICLE**

In an intra-particle intensity plot, only a section exactly through the center of mass of the particle would reveal information on the entire intra-particle distribution. Peripheral sections reveal only a part of the enzyme concentration as a function of particle radius, i.e. the intra-particle enzyme gradient. An example is given in Figure 5a, where the normalized light intensity is plotted as a function of the radial position within a section (section 29, Figure 4a, section radius 141  $\mu\text{m}$ ). The enzyme distribution was normalized to the intensity that the surface would have if no abruptly elevated surface loading was present, i.e. extrapolation of the global continuous gradient for the most outer 2  $\mu\text{m}$  (Figure 5a). This was

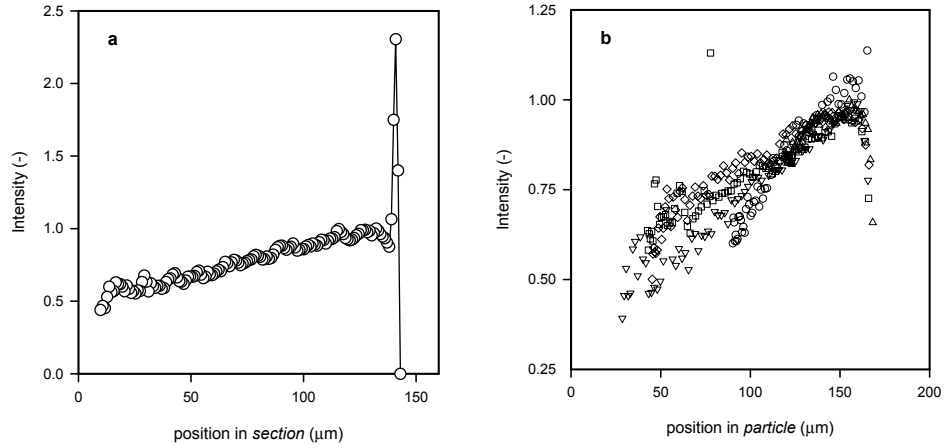


Figure 5. a: Normalized relative intra-section intensity profile as a function of radial section position in section 29. b: Normalized relative intra-particle intensity profiles through the single Assemblase® particle presented in Figure 4 (radius 167  $\mu\text{m}$ ) calculated from section profiles 29 ( $\circ$ ), 52 ( $\nabla$ ), 76 ( $\square$ ), 77 ( $\diamond$ ) and 104 ( $\triangle$ ), respectively.

done, because normalization to discontinuous, abruptly elevated surface loadings would result in incorrectly amplified (stretched) distributions. The straightforward geometrical (Pythagorean) conversion from a section position (radius 141  $\mu\text{m}$ ) to the corresponding radial particle position (radius 167  $\mu\text{m}$ ) was done according to the procedure explained in the materials and methods; the result of this is plotted in Figure 5b for section 29 ( $\circ$ ) and all other sections originating from the same particle, which were presented in Figure 4.

Sections 76 and 77 (Figures 4d and 4e, respectively), which were adjacent, were used as a control of the image analysis routine. Visually, the original micrographs of the sections show large differences in micrograph brightness and contrast and in the background gradient. Furthermore, section 76 contains artifacts due to sectioning (dark lines in Figure 4c). Despite these differences, the intensity profile of the two sections after image analysis is almost identical, as shown in Figure 5b ( $\square$  and  $\diamond$ ). This indicates that compensations for micrograph brightness and uneven micrograph exposure were done consistently and that small artifacts of the sections caused by cutting did not significantly influence the intensity profile (the intensities were averaged over a radial shell).

Figure 5b indicates that although not every section yielded information over the same distance inwards the object, all profiles were equivalent and seemed to indicate a single relative intra-particle enzyme profile. The figure shows that the intensity in the central regions of the particle is more prone to scattering. In central regions, fewer pixels are available to calculate the average intensity, which is already low. Furthermore, in-homogeneities, such as small holes in the bead, cutting artifacts or salt crystals will result in increased data scattering in these regions.

### SIZE-DEPENDENT INTENSITY PROFILES

So far, the relative enzyme gradient within a single particle (Figure 5b) was presented. As indicated before, Assemblase<sup>®</sup> consists of a pool of close-to-spherical biocatalytic particles that considerably vary in size. For this batch, the mean diameter is just over 400  $\mu\text{m}$ , while the standard deviation is approximately 150  $\mu\text{m}$ . Since the enzyme is loaded into the carrier material after particle formation, the gradients in particles of different sizes are expected to be different too. As a matter of fact, large particles are expected to show a steeper intra-particle enzyme gradient in comparison with smaller ones. This was investigated by analysis of the intra-particle enzyme distribution of multiple Assemblase<sup>®</sup> particles of different diameter.

As an example, Figure 6 shows the normalized relative intra-particle enzyme gradient of a relatively small, a medium-sized, and a relatively large biocatalytic

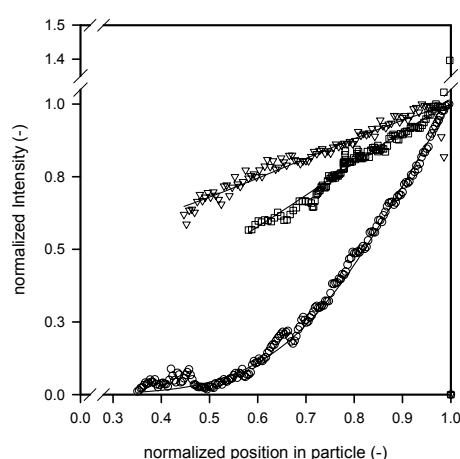


Figure 6. Intra-particle normalized relative intensity profiles for a small ( $\nabla$ ,  $r = 167 \mu\text{m}$ ), medium-sized ( $\square$ ,  $r = 205 \mu\text{m}$ ) and a large particle ( $\circ$ ,  $r = 268 \mu\text{m}$ ) as a function of the dimensionless particle position and model fits ( $\text{—}$ ) according to Equation [4.1].

particle, each plotted as a function of the relative radial position. For each particle, the intra-particle enzyme profile in this figure was an average resulting from multiple sections of the particle under consideration (of which an example was given in figure 5b).

Figure 6 shows that in this example, no intensity data near the center of mass of the particle were obtained, since no sections were analyzed in that region. As expected, the figure indicates that the intra-particle intensity profile is more fully penetrated (less steep profiles) for smaller particles. For the largest particle (radius 268  $\mu\text{m}$ ), the label intensity at 60% penetration depth (160  $\mu\text{m}$  into the particle) was only 5-10% of its surface intensity. At these and greater depths, almost no enzyme was present, suggesting an inactive core for the larger biocatalytic particles. With a radius of 167  $\mu\text{m}$  for the small particle in Figure 6, no such inactive core was found for the samples that were investigated.

#### MATHEMATICAL REPRESENTATION OF PROFILES

So far, the general shape of the intra-particle intensity profiles (e.g. in Figure 6) qualitatively resembled in-stationary diffusion profiles. This observation was verified by adopting a mass-balance for in-stationary enzyme diffusion into a spherical support material. The expression describes intra-particle enzyme profiles as a function of the intra-particle enzyme diffusivity, the particle radius and the diffusion time of the enzyme during preparation. In its dimensionless form, the equation expresses relative concentrations as a function of the Fourier number for mass transfer ( $Fo$ ), which is the quotient of the process time and the characteristic diffusion time. Its numeric value indicates the progress of an in-stationary diffusion process towards equilibrium and reflects the shape of the intra-particle enzyme gradient. The dimensionless concentration can be replaced by the relative (dimensionless) label intensity. The resulting equation is:

$$\frac{\partial i}{\partial Fo} = \frac{\partial^2 i}{\partial \rho^2} + \frac{2}{\rho} \frac{\partial i}{\partial \rho} \quad [4.1]$$

with  $Fo = D_E^{\text{ip,eff}} t / R_p^2$ , with  $D_E^{\text{ip,eff}}$  the intra-particle effective enzyme diffusivity ( $\text{m}^2/\text{s}$ ),  $R_p$  the particle radius (m),  $t$  the time (s),  $i$  the normalized intensity  $I / I_p$ , and  $\rho$  the relative position in the sphere  $r_p / R_p$ . The definition of the intra-particle enzyme diffusivity requires some additional comments.

In this case, the intra-particle enzyme diffusivity was defined as a pseudo-effective diffusivity: a single homogeneous particle interior was assumed into which no discrimination was made between the enzyme diffusivity into the water and solids inside the support material. Furthermore, possible enzyme adsorption to the support material, prior to chemical (covalent) linkage by glutaric aldehyde, is incorporated in the diffusivity constant according to Vieth (2003). Such lumping into a single ‘pseudo’-diffusivity constant requires that enzyme adsorption to the support material should be rapid in comparison with diffusion, and, secondly, adsorption should obey a linear adsorption isotherm. Both requirements seem reasonable, since protein diffusion is usually very slow and because similar particles could be prepared with approximately ten times higher enzyme loading, respectively. Mathematically, this means that the effective diffusivity constant is replaced by a pseudo-effective diffusivity in which adsorption is integrated. The result is that the shapes of the in-stationary profiles do not change: only the time that is needed for a penetration profile to develop is longer, since the support material functions as an active ‘sink’ of enzyme.

Equation 1 was discretized and simultaneously fitted to the measured intra-particle enzyme distributions of a small, medium-sized, and large particle for an activation time of 1.9 hours. The exact fitting procedure was already described in the materials and methods section. The result is plotted in Figure 6 for a diffusivity of  $5.0 \cdot 10^{-13} \text{ m}^2/\text{s}$  and shows that the enzyme profiles for small, medium-sized, and large particles could excellently be described with equation 1.

The intra-particle enzyme profiles of other particles were used to validate the fitted pseudo-effective diffusivity. To do so, the Fourier numbers representing the measured profiles of all other particles were compared with the Fourier numbers that were predicted by the above relation for the fitted diffusivity (Figure 7). This was done for particle sizes ranging from 340  $\mu\text{m}$  to 570  $\mu\text{m}$  in diameter, which is the main volume-contributing size range in native Assemblase<sup>®</sup> (Van Roon *et al.*, 2003).

The figure shows that the Fourier numbers that were obtained from the measured intra-particle enzyme gradient were very close to the predicted ones, which were based on an activation time of 1.9 hours and a fitted pseudo-effective diffusivity of  $5.0 \cdot 10^{-13} \text{ m}^2/\text{s}$ . All data lie well within the 95% confidence interval. All intra-

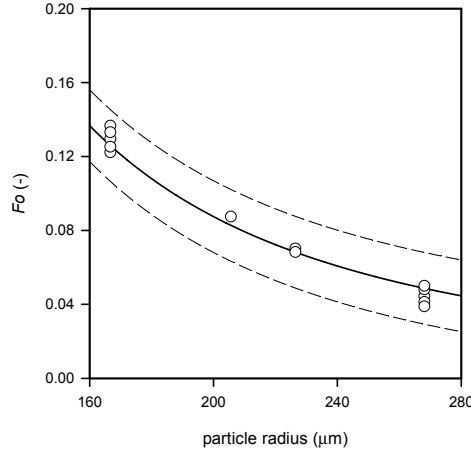


Figure 7. The Fourier number for mass transfer as a function of the particle radius for multiple sections of different-sized particles (○). The solid line represents the regression curve of the Fourier number (—) and the corresponding 95% confidence intervals (- -). The intra-particle enzyme-profile corresponds with a Fourier number of  $8.2 \cdot 10^{-2}$  (-). The data clearly indicate the correlation between the Fourier number and the particle diameter is applicable to this heterogeneous system.

particle enzyme profiles have the (same) mathematical shape of an in-stationary diffusion process and can be described with their radius-dependent Fourier number only.

Because the fitted pseudo-effective diffusivity provided no information on the influence of adsorption (and no data are available on adsorption rates), the actual diffusivity (without adsorption) was estimated by substituting the Vonk equation (1994) for solute retardation due to limited matrix porosity into the Wilke–Chang relation. This yields:

$$D_E^{\text{ip,eff}} = \frac{5.9 \cdot 10^{-17} (\phi_S M_S)^{1/2} T}{\eta_S V_E^{0.6}} \cdot e^{-\sqrt{\varepsilon}(r_E/r_C)} \quad [4.2]$$

where  $D_E^{\text{ip,eff}}$  represents the effective intra-particle diffusivity of the enzyme in the porous biocatalyst ( $\text{m}^2/\text{s}$ ),  $\phi_S$  is an association factor of the solvent that accounts for hydrogen bonding, and is 2.26 (-) for water,  $M_S$  is the molar weight of the solvent ( $\text{kg/mol}$ ),  $T$  the temperature (293 K),  $\eta_S$  the viscosity of the solvent ( $1.0 \cdot 10^{-3} \text{ Pa}\cdot\text{s}$  at 293 K),  $V_E$  the molar volume of the enzyme ( $\text{m}^3/\text{mol}$ ),  $\varepsilon$  the solidity (-) of the biocatalytic particle and  $r_E$  and  $r_C$  the radii (m) of the solute and the polymer chain, respectively. The solidity  $\varepsilon$  of this batch of Assemblase<sup>®</sup> was reported to be 0.13 (-) (Van Roon et al., 2003). Van der Wielen estimated the polymer chain radius to be 0.3 nm for Separase<sup>®</sup>, which uses a similar support material as Assemblase<sup>®</sup> (VanderWielen, 1997). With an enzyme radius of

approximately 3 nm (Duggleby et al., 1995), a molecular weight of 86 kDa, and an estimated density of  $1350 \text{ kg/m}^3$  (typical protein density), the enzyme diffusivity in Assemblase<sup>®</sup> was estimated to be  $5.3 \cdot 10^{-13} \text{ m}^2/\text{s}$ , i.e. 3% of the free-water diffusivity.

Because the values of the fitted pseudo-effective diffusivity ( $5.0 \cdot 10^{-13} \text{ m}^2/\text{s}$ ) and the estimated effective diffusivity ( $5.3 \cdot 10^{-13} \text{ m}^2/\text{s}$ ) are close to each other, the effect of adsorption is not expected to be very important for the dynamics of enzyme loading during activation. With equation 1, the intra-particle enzyme distribution of Assemblase can be predicted for any given particle size and loading time.

## CONCLUSION

The intra-particle penicillin-G acylase distribution of Assemblase<sup>®</sup> was visualized after particle sectioning of multiple particles of different sizes by highly specific immunological labeling and image analysis, which was specifically developed for this purpose. This showed that the intra-particle enzyme distribution in Assemblase<sup>®</sup> was heterogeneous, with most enzyme located in the outer regions of the particle. Larger particles showed steeper gradients than smaller ones, as was expected from in-stationary enzyme diffusion during enzyme loading of the empty support material and subsequent chemical fixation.

A simple mass balance, assuming enzyme diffusion into empty support material, quantitatively confirmed that the shape of the measured intra-particle enzyme profiles mathematically matched in-stationary enzyme diffusion. Moreover, the mathematical representation, which was successfully validated for a broad range of particle sizes, showed that the differences in intra-particle profiles resulted from differences in particle size only. The description can therefore be used as a hand-on tool to produce any desired diffusion-based intra-particle distribution into the empty support material for any particle size.

The measured intra-particle enzyme gradient will be used as input for a physical model for cephalixin synthesis, catalyzed by Assemblase<sup>®</sup>. In this dynamic model, all input parameters, like mass transfer of reactants and products, enzyme

kinetics, enzyme loadings, and the enzyme distribution (that was measured in this paper) are independently incorporated. Such a mechanistic model can provide insight in current bottlenecks in Assemblase<sup>®</sup>, and therewith lead to rational design of new, improved biocatalysts. For this design process, the ability to quantitatively measure the intra-particle enzyme distributions of present and future biocatalytic particles is indispensable.

## ACKNOWLEDGEMENTS

DSM (Delft, The Netherlands) is kindly acknowledged for their financial support and valuable discussions. DSM Research (Geleen, The Netherlands) is kindly acknowledged for sieving Assemblase<sup>®</sup> fractions and determining their particle size distributions by laser diffraction. The Ministry of Economic Affairs of the Netherlands is kindly acknowledged for their financial support. Mr. Boudewijn van Veen (Wageningen University) is kindly acknowledged for his expert help in digital image processing.

## REFERENCES

- Baskin T.I., Busby C.H., Fowke L.C., Sammut M., and Gubler F.** (1992). Improvements in immunostaining samples embedded in methacrylate: localization of microtubules and other antigens throughout developing organs in plants of diverse taxa. *Planta* **187**: 405-413.
- Booth M.J., and Wilson T.** (2001). Refractive-index-mismatch induced aberrations in single-photon and two-photon microscopy and the use of aberration correction. *J. Biomed. Opt.* **6**:266-272.
- Bougourd S., Marrison J., and Haselhoff J.** (2000). An aniline blue staining procedure for confocal microscopy and 3D imaging of normal and perturbed cellular phenotypes in mature *Arabidopsis* embryos. *Plant J.* **24** :543-550.
- De Beer D., Stoodley P., and Lewandowski Z.** (1997). Measurement of local diffusion coefficients in biofilms by microinjection and confocal microscopy. *Biotechnol. Bioeng.* **53**: 151-158.
- De Smet S.C., Meyvis T.K.L., Demeester J., Van Oostveld P., Blonk J.C.G., and Hennink W.E.** (1997). Diffusion of macromolecules in dextran methacrylate solutions and gels as studied by confocal scanning laser microscopy. *Macromolecules* **30**: 4863-4870.
- De Vroom E.** (1997). Gist-brocades N.V. An improved immobilized penicillin G acylase. *International Patent Application Gist-brocades* WO 97/04086.



- Duggleby H.J., Tolley S.P., Hill C.P., Dodson E.J., Dodson G., and Moody P.C.E.** (1995). Penicillin acylase has a single-amino-acid catalytic centre. *Nature* **373**: 264-268.
- Harder A., De Haan B.R., and Van der Plaats J.B.** (1987). Gist-brocades N.V. Novel immobilized biocatalysts and their preparation and use. *International Patent Application Gist-brocades* EP 0222462B1.
- Keusgen M., Glodek J., Milka P., and Krest I.** (2001). Immobilization of enzymes on PTFE surfaces. *Biotechnol. Bioeng.* **72**: 530-540.
- Laca A., Garcia L.A., Diaz M.** (1999). Protein diffusion in alginate beads monitored by confocal microscopy. The application of wavelets for data reconstruction and analysis. *J. Ind. Microbiol. Biotechnol.* **23**: 155-165.
- Linden T., Ljunglöf A., Kula M.-R., and Thömmes J.** (1999). Visualizing two-component protein diffusion in porous adsorbents by confocal scanning laser microscopy. *Biotechnol. Bioeng.* **65**: 622-630.
- Litjens M.J.J., Le K.Q., Straathof A.J.J., Jongejan J.A., and Heijnen J.J.** (2001). Diffusion limitation causes decreased enantioselectivity of esterification of 2-butanol by immobilized *Candida antarctica* lipase B. *Biocat. Biotrans.* **19**: 1-19.
- Novick S.J., and Dordick J.S.** (2000). Investigating the effects of polymer chemistry on activity of biocatalytic plastic materials. *Biotechnol. Bioeng.* **68**: 665-671.
- Prior D.A.M., Oparka K.J., and Roberts I.M.** (1999). En bloc optical sectioning of resin-embedded specimens using a confocal laser scanning microscope. *J. Microsc.* **193**: 20-27.
- Ragnitz K., Syldatk C., and Pietzsch M.** (2001). Optimization of the immobilization parameters and operational stability of immobilized hydantoinase and L-N-carbamoylase from *Arthrobacter aurescens* for the production of optically pure L-amino acids. *Enzyme Microb. Technol.* **28**: 713-720.
- Schroën C.G.P.H., Fretz C.B., De Bruin V.H., Berendsen W., Moody H.M., Roos E.C., Van Roon J.L., Kroon P.J., Strubel M., Janssen A.E.M., and Tramper J.** (2002). Modelling of the enzymatic kinetically controlled synthesis of cephalixin: influence of diffusion limitation. *Biotechnol. Bioeng.* **80**: 331-340.
- Spear R.N., Cullen D., and Andrews J.H.** (1999). Fluorescent labels, confocal microscopy, and quantitative image analysis in study of fungal biology. *Meth. Enzymol.* **307**: 607-623.
- Van Roon J.L., Beftink H.H., Schroën C.G.P.H., and Tramper J.** (2002). Assessment of intraparticle biocatalytic distributions as a tool in rational formulation. *Curr. Opin. Biotechnol.* **13**: 398-405.
- Van Roon J.L., Joerink M., Rijkers M., Tramper J., Schroën C.G.P.H., and Beftink H.H.** (2003). Enzyme distribution derived from macroscopic particle behavior of an industrial immobilized penicillin-G acylase. *Biotechnol. Prog.* **19**: 1510-1518.
- Van Der Wielen, L.A.M.** (1997). Transients in the heterogeneous enzymatic deacylation of penicillin G. In: A countercurrent adsorptive fluidized bed reactor for heterogeneous bioconversions. Dissertation, Delft University of Technology, The Netherlands. Delft: p 1-35.
- Vieth W.R.** (2003). Diffusion in and through Polymers: Principles and Applications. New York: Oxford University Press.

- Vonk, P.** (1994). Geometrical hindering of diffusion In: Diffusion of large molecules in porous structures. Dissertation, University of Groningen, The Netherlands. Groningen: p 101-128.
- Wang P., Dai S., Waezsada S.D., Tsao A.Y., and Davison B.H.** (2001). Enzyme stabilization by covalent binding in nanoporous sol-gel glass for nonaqueous biocatalysis. *Biotechnol. Bioeng.* **74**: 249-255.

---

## Chapter 5 Enzyme distribution and matrix characteristics in biocatalytic particles

The contents of this chapter have been accepted for publication as:

**J.L. van Roon, R.M. Boom, M.A. Paasman, J. Tramper, C.G.P.H. Schroën, and H.H. Beeftink** (2005). Enzyme distribution and matrix characteristics in biocatalytic particles. *J. Biotechnol.*, <http://dx.doi.org/10.1016/j.jbiotec.2005.04.012>.

## **ABSTRACT**

In a study of Assemblase<sup>®</sup>, an industrial immobilized Penicillin-G acylase, various electron microscopic techniques were used to relate intra-particle enzyme heterogeneity with the morphological heterogeneity of the support material at various levels of detail. Transmission electron microscopy was used for the study of intra-particle Penicillin-G acylase distribution in Assemblase<sup>®</sup> particles of various sizes; it revealed an abrupt increase in enzyme loading at the particle surface (1.4-fold) and in the areas (designated halo's) surrounding internal macro-voids (7.7-fold). Cryogenic field-emission scanning electron microscopy related these abrupt local enzyme heterogeneities to local heterogeneity of the support material by revealing the presence of dense top layers surrounding both the particle exterior and the internal macro-voids. Furthermore, it showed a very distinct morphological appearance of the halo. Most probably, all these regions contained relatively more chitosan than gelatin (the polymers Assemblase<sup>®</sup> was constructed of), which suggested local polymer demixing during particle production. A basic thermodynamic line of reasoning suggested that a difference in hydrophilicity between the two polymers induced local demixing. In the future, thermodynamic knowledge on such polymer interactions resulting in matrix heterogeneity may be used as a tool for biocatalyst design.

## INTRODUCTION

Currently, the development of biocatalytic particles usually is both an intuitive and experimental craft, in which knowledge and experience in fields of both biocatalysts and support materials are combined (Burton *et al.*, 2002; Moulijn *et al.*, 2003). After initial selection of an appropriate biocatalyst and support material, often multiple formulations are produced with various methods of immobilization under different conditions (Berger *et al.*, 2004; Fernandez-Lafuente *et al.*, 1998; Hennink and Van Nostrum, 2002; Juang *et al.*, 2002; Kaneko *et al.*, 2004; Taqieddin and Amiji, 2004); of these, the performance is usually evaluated from macroscopic kinetic essays (Hossain and Do, 1989; Scharer *et al.*, 1992). Such trial-and-error approach is time consuming and leaves uncertainty about whether or not a truly optimal formulation was produced, because only a limited number of particles and reaction conditions can be evaluated.

Computer models based on enzyme kinetics and reactant mass transfer can be used to speed up this process, because they facilitate the at-the-desk evaluation of numerous process conditions and biocatalytic particle configurations. Whenever mass transfer limitations come into play, also the intra-particle enzyme distribution is an important parameter for the overall particle performance: at the core of the particle, mass transfer limitations are expected to be most severe. However if the core has a low enzyme loading, these limitations will not influence the overall performance of the biocatalyst too much. It is obvious that variation of the distribution provides the engineer with an extra degree of freedom to design the optimal particle configuration. The production of heterogeneous enzyme distributions in practice, however, is all but trivial, since it calls for methods to introduce heterogeneity in intra-particle enzyme distributions.

An important means to govern the intra-particle enzyme distribution is by controlling the matrix properties of the particle: local differences in matrix morphology (heterogeneity of the support material) can result in local differences in biocatalyst binding affinity or capacity (biocatalyst heterogeneity). Doing so,

however, requires extensive knowledge on the structure-function relations of the matrix material (e.g. binding capacity and permeability of different types of support materials with various morphology) and on the mechanisms of matrix formation. In this paper, the intra-particle enzyme heterogeneity was successfully related to support material heterogeneity by various microscopic techniques for an immobilized biocatalytic system of which the enzyme distribution was known to be heterogeneous: Assemblase<sup>®</sup>, which is an industrially used immobilized penicillin-G acylase that catalyzes the synthesis of the  $\beta$ -lactam antibiotic cephalexin (Van Roon *et al.*, 2003).

As a first step, the global intra-particle enzyme distribution of Assemblase<sup>®</sup> was investigated with transmission electron microscopic (TEM) analysis on sections through differently sized particles, of which the penicillin-G acylase was specifically labeled with colloidal gold particles. The global intra-particle enzyme distribution, which was previously determined with light-microscopic experiments (Van Roon *et al.*, 2005), was confirmed to be heterogeneous and had the mathematical shape of in-stationary diffusion profiles (most enzyme present in the outer region of the particles). It was shown that this method yielded the same distribution as the LM-based experiments, but without the need of extensive image analysis.

The previously conducted LM-based experiments additionally suggested the presence of local regions in which the enzyme loading was elevated significantly (the limited resolution of the technique prevented further study on this phenomenon). In this work, a high-resolution electron microscopic study was therefore done on Assemblase<sup>®</sup> particles. TEM on ultra-thin sections of the particles revealed abruptly increased local enzyme densities (up to a factor 8) at the particle surface and in eccentrically shaped structures around internal macrovoids, called halos. Also, the local support material densities in these areas were found to be elevated. To study the local morphology of these areas in greater detail, frozen and cryo-planed particles were analyzed with field-emission scanning electron microscopy (FESEM). This revealed the presence of a very thin (1  $\mu$ m) but dense top-layer at the particle surface and surrounding intra-particle voids. Furthermore, the latter were found to be surrounded by halos, which were also observed with TEM.

Combination of the locally elevated enzyme loadings in the top layers and halos and of the morphological properties observed with FESEM and TEM in the same regions suggested local chitosan enrichment (one of the two polymers the support material of Assemblase<sup>®</sup> is made of), which contains most of the binding sites. This implies that some local relative movement of the two polymers (gelatin and chitosan) must have been possible during particle formation. This was confirmed by a thermodynamic evaluation that indicated that both polymers have had a tendency to demix which can result in matrix heterogeneity.

This knowledge on the composition and the formation of matrix heterogeneity can be seen as the first step towards the control of the enzyme heterogeneity by rationally adjusting the intra-particle matrix morphology. Eventually, it may lead to a new approach to biocatalyst design that uses matrix heterogeneity as a tool for biocatalyst optimization.

## MATERIALS AND METHODS

### CHEMICALS

All water used was double distilled. Polyclonal rabbit immunoglobulin-G against *E. coli* penicillin-G acylase was generously donated by Dr. C.F. Sio (Department of Pharmaceutical Biology, University of Groningen, The Netherlands), and was used as a primary antibody. Secondary antibodies were GAR (goat anti-rabbit) polyclonals to which a 10-nm gold spherical particle was attached (Aurion, Wageningen, The Netherlands). All other chemicals were at least of analytical grade.

### BIOCATALYTIC PARTICLES

Assemblase<sup>®</sup> is an in-house biocatalytic particle of DSM Anti-Infectives (Delft, The Netherlands); a single batch was donated for the present research. In all instances where the trademark Assemblase<sup>®</sup> is used, this refers to this particular preparation. Although several combinations of polymers, non-solvents, and cross-linking agents are suitable and applied for industrial particle preparation, in this case gelatin and chitosan were contacted with non-solvent and chemically cross-linked with glutaric di-aldehyde according to Harder *et al.* (1987) and De Vroom (1997). For this specific batch, the penicillin-G acylase was isolated and purified from *E. coli* according to Kaasgaard *et al.* (1992), and was loaded onto

the support material from the exterior after bead formation. Although activation times can vary considerably depending on many different process conditions such as ambient temperature, biocatalyst concentration and agitation speed, it was 1.9 hours for this research. Immobilization was relatively mild: previous research showed the enzyme activity and kinetic mechanism to be unaffected (Schroën *et al.*, 2002). The enzyme activity of this specific batch of Assemblase<sup>®</sup> was 3800 U per kg of particle dry weight (1 U produces 1 g of amoxicillin trihydrate - as analyzed by HPLC - from 300 mM 6-aminopenicillanic acid and 345 mM hydroxy-phenylglycine methyl ester in 1 hour at pH 6.5 and 293 K). Some particles were not activated for reference purposes (negative control).

## TRANSMISSION ELECTRON MICROSCOPY

### *Embedding*

Assemblase<sup>®</sup> particles are relatively large objects that subsequently have to be sectioned for the high-resolution study of the particle interior. To assure optimal section quality (smooth surface and reproducible thickness), fine-tuning of standard embedding procedures was required. The procedures are therefore explained in some detail. The particles were embedded in BMM (40 mL butylmethacrylate, 10 mL methylmethacrylate, 0.25 g benzoin ethylether and 0.08 g dithiothreitol (DTT), stripped of oxygen by continuous nitrogen flushing) before cutting (Baskin *et al.*, 1992). Proper dehydration of and resin penetration into the biocatalytic particles proved crucial for a good embedding result. First, the samples were washed three times in abundant water. Next, the beads were dehydrated by washing for 30 minutes each in a series of 10, 30 and 50% ethanol with 10 mM of the reducing agent (DTT), after which the beads were washed two times 30 minutes in 70% ethanol with 10 mM DTT. The beads were left in a shaker overnight at 277 K in 70% ethanol with 10 mM DTT; the next day, washing continued at 277 K in 96 and 100% ethanol with 10 mM DTT for one hour each. Subsequently ethanol was replaced by ethanol:BMM mixtures at 277 K in mixture ratio's of 5:1, 3:1 and 1:1 for 2 hours each at 277 K. After leaving the samples overnight in a 1:3 mixture, infiltration was continued the next day at 1:5 (3 hours) and three times by a 100% BMM (1 hour each). Samples were left overnight at 277 K and were transferred into BEEM<sup>™</sup> capsules (EMS, Washington, USA) the next day. Polymerization of the BMM under black-light



ultra-violet lamps was done for 48 hours at 253 K, since the polymerization is exothermic and would go too fast without cooling.

### ***Shrinkage***

Particle shrinkage due to embedding was investigated by measuring the particle diameter of approximately 50 beads with a binocular in the native, swollen state, after dehydration, and after BMM penetration (dehydrated shrunken state). The final average radial shrinkage was 32%, which was used to correct all distances relative to the center of the particle: only for shrinkage corrected data are shown in the rest of the paper.

### ***Sectioning***

After resin polymerization, the BEEM<sup>TM</sup> capsules were removed and the formed plastic with the embedded biocatalytic particles was cut in a series of sections of 2.75  $\mu\text{m}$  thickness with an LKB 2088 Ultratome V (LKB Bromma, Stockholm, Sweden), fitted with glass knives (LKB 7801 knifemaker, LKB, Stockholm, Sweden). Approximately one out of every five sections was put onto a water droplet on a glass microscope slide and stretched with chloroform vapor, after which the water was vaporized by placing the slide onto a heated plate of approximately 323 K to stick the section to the microscopic slide. Sectioning was repeated until a nice smooth surface without cutting damage was obtained and large sections through particles were visible. Subsequently the planed resin was transferred to an ultra-microtome (Reichert Ultracut-S, Seefeld, Germany) and ultra-thin sectioning was started (section thickness was estimated at approximately 80 nm from the color on water surface). The ultra-thin sections were transferred onto hexagonal 200 mesh nickel grids for subsequent labeling.

Particle sections were generally off-centre. Radial positions within an off-centre section, however, were converted to radial positions in the purportedly spherical biocatalytic particle (i.e. to positions in a central section). To do so, two or more sections from a series of subsequent sections with known thickness and mutual distance through a single particle were combined in a simple Pythagorean procedure (Van Roon *et al.*, 2005).

***Labeling***

For reasons of label flexibility and limited primary antibody availability, a two-step labeling procedure was applied to ultra-thin sections. Prior to labeling, BMM was removed by washing the sections 2 times 7 minutes in 100% acetone, after which the solvent was removed by washing in PBS (8 g NaCl, 0.2 g KCl, 0.2 g  $\text{KH}_2\text{PO}_4$  and 1.41 g  $\text{Na}_2\text{HPO}_4$  dihydrate in 1 liter water, pH 7.4). To avoid a-specific epitope binding, sections were treated with 0.1 M hydroxyltetraammonium chloride in PBS (5 min), washed in PBS (5 min), and treated with 1% w/v bovine serum albumine (BSA fraction V, Merck, Darmstadt, Germany) in PBS (30 min), followed by 0.01% acetylated BSA (BSA-c, Aurion) in PBS for 3 x 5 min. Incubation with the primary antibody was done overnight at 277 K, followed by washing with 0.01% BSA-c (4 x 15 min) at 295 K. Next, sections were incubated (2 h at 310 K) with the GAR-type (goat anti-rabbit) secondary antibody, which contained a 10 nm spherical gold particle as label. Subsequently they were washed with 0.01% BSAC (4 x 15 min at 293 K) and fixated (chemical binding of enzymes and antibodies) with 2% w/v glutaric dialdehyde in PBS (5 min). Finally, the samples were washed with water (3 x 5 min) and air-dried.

Three negative control experiments were done in triplicate. In the first, the primary antibody was omitted from the labeling procedure to check for a-specific binding of the secondary antibody. In the second, support particles without penicillin-G acylase were labeled with both antibodies, to check for a-specific affinity of one or both antibodies to the support material. Finally, a normal rabbit serum was used in combination with the second (GAR-type) antibody, to check for affinity of the rabbit serum to the penicillin-G acylase. In all negative control experiments, no gold label whatsoever was visible under the microscope. In the actual experiments, with both antibodies, label was abundantly present. From this, it was concluded that the labeling was specific for penicillin-G acylase, and that the chemicals used in the embedding and labeling procedure did not destroy (all) their highly specific epitope structures.

***Detection***

Label detection in sections took place in a transmission electron microscope (JEOL JEM 1200 EXII, Tokyo, Japan) at an acceleration voltage of 80 kV. Micrographs were made at magnifications of typically 10.000 – 15.000 times for

gold particles to be counted and approximately 50.000 times for detailed analysis. Negatives were scanned and thresholded to count individual gold particles and to calculate their area density. The amount of label was assumed to be proportional to the amount of enzyme. Radial positions within TEM sections were converted to radial positions within the particle (Van Roon *et al.*, 2005; *cf.* Sectioning). Finally, the discretely measured enzyme distribution was fitted to continuous instationary enzyme diffusion patterns by the least squares method.

### FIELD-EMISSION SCANNING ELECTRON MICROSCOPY

Low temperature field-emission scanning electron microscopy (cryo-FESEM) was used to study the morphology of the biocatalytic particles. Samples of an Assemblase<sup>®</sup> suspension in water were transferred onto 3-mm aluminium pins, plunge-frozen in liquid propane, transferred to liquid nitrogen, and then mounted in a pre-cooled screw-clamp holder in a pre-cooled ultra-microtome (Reichert Ultracut E/FC4D) equipped with a cryo stage. Planing was started with a glass knife and finished with a diamond knife (Histo no trough, 8 mm 45°, Drukker International, The Netherlands) at a specimen temperature of 183 K and a knife temperature of 173 K. After planing, samples were stored in liquid nitrogen (77 K). For analysis, samples were transferred to a cryo-transfer unit (Oxford CT 1500 HF, Oxford instruments, Oxford, UK), mounted onto a cryo-FESEM (JEOL JSM-6300F, Tokio, Japan) with an Oxford cryo-chamber. The surface was etched for 5 min at 184 K and  $10^{-4}$  Pa, sputter-coated in a dedicated preparation chamber (Oxford CT 1500 HT) with 5 nm platinum, and analyzed at 5 kV.

Additional morphological experiments were done with critical-point dried samples. For this, Assemblase<sup>®</sup> particles were dehydrated in a seven-graded series of ethanol and critical-point dried with carbon-dioxide (Wergin and Stone, 1981). The dried particles were sputter-coated with 10 nm platinum in a dedicated preparation chamber (Oxford CT 1500 HT) and examined at 5 kV with the cryo-FESEM.

## RESULTS AND DISCUSSION

### GLOBAL EFFECTS: INTRA-PARTICLE ENZYME GRADIENT

Transmission electron microscopy (TEM) was used to evaluate global enzyme distributions within sections through biocatalytic Assemblase<sup>®</sup> particles (Fig. 1).

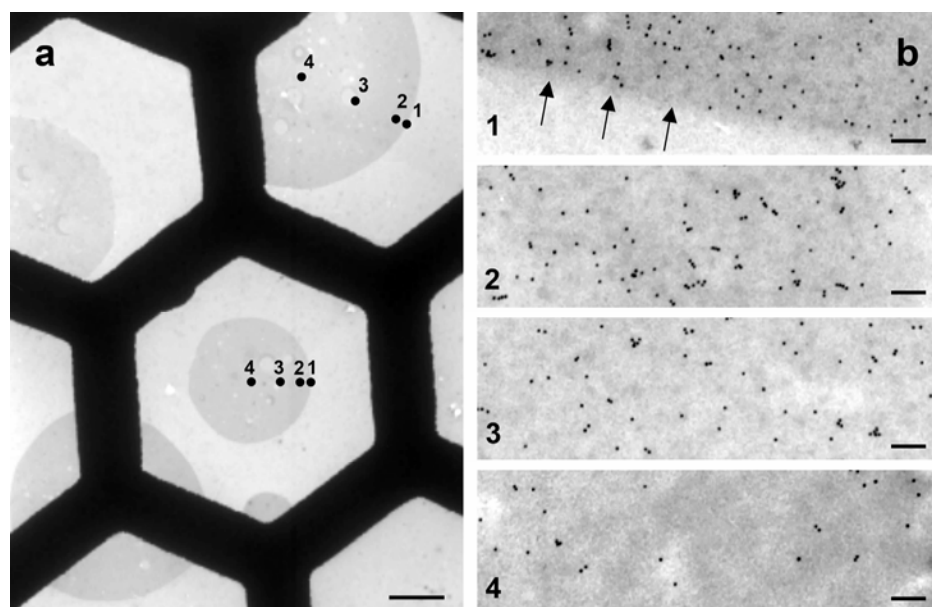


Figure 1. **a:** Arbitrary transmission electron microscopic (TEM) micrograph of a section through Assemblase<sup>®</sup> particles at low magnification (bar = 50  $\mu$ m). The nickel hexagonal grid onto which the section was placed is clearly visible. In this example, the enzyme density through two sections was examined at the particle surface (1), just below the surface (2), halfway the particle center (3) and in the particle center (4). **b:** Example of high-magnification micrographs (bar = 100 nm) of a 10-nm immuno-gold labeled Assemblase<sup>®</sup> particle at positions 1 to 4 (Fig. 1a), respectively. Visual inspection instantly shows that the gold-label density was higher at the particle perimeter (micrograph 1, the particle surface is indicated by the arrowheads) than in the particle center (micrograph 4).

Within each section, micrographs were made at positions 1, 2, 3 and 4, i.e. at the section perimeter, just below the section perimeter, halfway its interior, and in the section center. Higher magnifications at these positions showed the 10-nm colloidal gold particles that were used to label individual Penicillin-G acylase molecules (Fig. 1b for positions 1 to 4, respectively). The gold particle densities (number per unit area) directly correspond to the local enzyme densities and multiple of these local discrete measurements gave a discrete enzyme distribution over the section. In the top micrograph of Fig. 1b, the outer perimeter of the particle is visible (arrowheads). Outside the particle, no gold-particles were present, illustrating the absence of a-specific antibody binding to the resin.

Visual inspection instantly showed that the enzyme density was higher at the particle perimeter (top micrograph in Fig. 1b) than in the particle center (bottom micrograph in Fig. 1b). Because most particle sections were off-centre, radial positions within individual sections were converted (Van Roon *et al.*, 2005) into radial positions within the biocatalytic particle, and the corresponding normalized enzyme densities were plotted as a function of the intra-*particle* radial positions (Fig. 2a). The relative enzyme densities were normalized to that at position 2, because at the particle surface (position) the enzyme loading was increased rather abruptly. This phenomenon was evaluated separately and will be discussed later in this section; for now the focus will be on the overall intra-particle enzyme gradient. Fig. 2a confirms that more enzyme was present at the outside of the particle in comparison to its interior. Because the section in the example was not positioned at the center of mass of the particle, experimental data on the enzyme distribution in this section only partially reveal the intra-particle enzyme distribution.

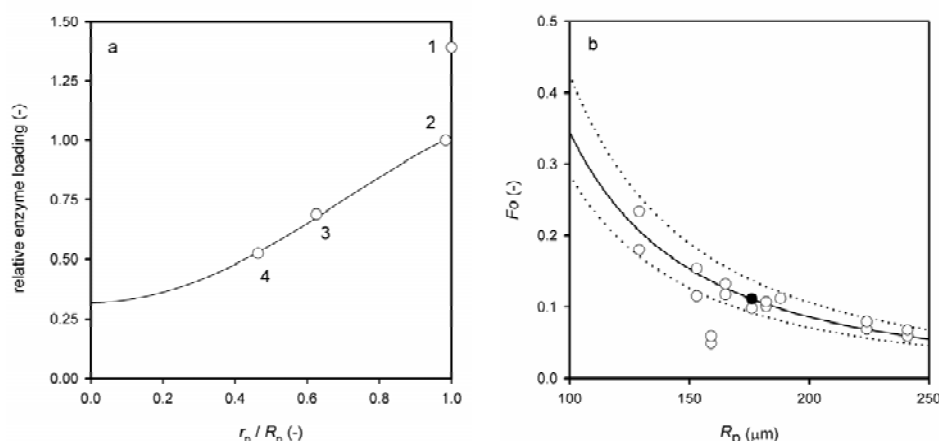


Figure 2. a: Relative enzyme loading ( $\circ$ ) at positions 1 to 4 for the particle depicted in Figures 1b (radius  $177\ \mu\text{m}$ ) and the fitted (—) intra-particle enzyme profile for  $\text{Fourier} = 0.11$  based on Van Roon *et al.*, (2005). b: Fourier numbers fitted to experimental enzyme densities ( $\circ$ ) from TEM micrographs of differently sized particles ( $\bullet$ : Fourier number of particle used in Figure 2a) and comparison with the expected model correlation of the Fourier number with the particle radius (—). The dotted lines are obtained for particles with a 10% larger or smaller particle radius.

A continuous intra-particle enzyme distribution of this particular batch of Assemblase<sup>®</sup> was previously determined with light microscopy (LM) and described with a model. A comparison between the present discrete

measurements and the previous continuous LM measurements for an equally sized particle (354  $\mu\text{m}$ , — in Fig. 2a) shows that both methods yield the same intra-particle heterogeneous enzyme distribution with most enzyme in the outer region.

#### **GLOBAL EFFECTS: FOURIER ANALYSIS**

Although specific local aberrations in enzyme densities were observed (*cf.* 3.3 and 3.4), the global shape of each discretely measured intra-particle enzyme gradient was in agreement with previous findings (Van Roon *et al.*, 2004). The global enzyme profile was assumed to reflect a halted instationary penicillin-G acylase penetration into the particle: the glutaric aldehyde in the activated matrix quickly binds the passing Penicillin-G acylase during diffusive particle activation, but enzyme penetration from the external enzyme solution was only allowed for 1.9 hours, which was not enough to ensure a homogeneous intra-particle enzyme distribution .

Mathematically, the progress of such a diffusive enzyme penetration may be expressed by the dimensionless Fourier number for mass transfer, which is the quotient of process time and diffusion time. The larger the Fourier number, the further the diffusion process is towards the homogeneous enzyme distribution that might have been attained for very long enzyme penetration times. The calculation assumes a homogeneous Assemblase<sup>®</sup> matrix; it neglects the quite local deviations from homogeneity (polymer composition) that are discussed elsewhere (*cf.* 3.3 and 3.4). The value of the Fourier number (0.11, Fig. 2a) was obtained by fitting a mathematical Fourier relation (Van Roon *et al.*, 2005) to the measured intra-particle enzyme profile. In this way the Fourier numbers of all TEM measurements on particles with different sizes were determined. Doing so facilitated a convenient one-parameter evaluation of the diameter-dependency of the intra-particle enzyme distribution, as well as a comparison with previous LM-based model predictions (Fig. 2b). Fig. 2b shows a consistent decline in the Fourier number for increasing particle radii: the progress of the enzyme diffusion process into the particle is further towards completion for smaller particles, and the Fourier relation that was derived for the description of the previously measured continuous LM gradients as a function of particle size, also fully applies for the present measurements. Because the calculated particle radius varied a little depending on the set of sections chosen (less than 10% difference

in radius was found in all cases), the dotted lines in Fig. 2b indicate the Fourier numbers for a 10% deviation of the model particle radius.

Although one has to invest in fine-tuned embedding procedures, skills for ultra-thin sectioning, and obviously a TEM in order to use the technique to the fullest, there are some important advantages of using TEM to study the intra-particle enzyme distribution in comparison to LM. Firstly, TEM offers some practical advantages over LM for the global determination of intra-particle enzyme distributions, while both methods yield the same results. No complicated and labor-intensive image analysis is needed (that often needs to be so specific that it requires case-specific development): the contrast in the TEM micrographs between the gold particles and the background is large enough to automatically assess the gold-particle density by a single automated threshold-step with virtually any graphic software package.

Additionally, the ultra-high resolution that TEM offers facilitates study on various local phenomena within the same sample. In the next sections, local deviations from the global (continuous) intra-particle enzyme distributions of Assemblase<sup>®</sup> particles will be described and these will be related to matrix morphology. The next sections will indicate the benefits of such knowledge for rational particle design, which is only attainable with high-resolution equipment.

#### **LOCAL EFFECTS: ELEVATED SURFACE LOADING**

One interesting local phenomenon is the observation of an abrupt label intensity increase at the surface of the biocatalytic particles. In previous work, image analysis on light-microscopic sections already occasionally showed abruptly elevated signal intensities in these areas. However, due to the limited resolution of the latter technique, this could not be established quantitatively. In the present work, this presumed increased surface loading was evaluated by comparison of the gold-particle density at the surface of the section and a few micrometers (typically 3  $\mu\text{m}$ ) inward, indicated by positions 1 and 2, respectively, in Fig. 1a. For this particular example, the gold particle density at the surface (top micrograph; Fig. 1b) was found to be 1.39 times higher than that 3  $\mu\text{m}$  inward (second micrograph; Fig. 1b). This increase is much more pronounced than the (very) small increase that was expected on the basis of the local slope in enzyme loading at position 2 (Fig. 2a). The approximately 20 sections that were analyzed

in this manner showed that on average the enzyme density in the outer 3  $\mu\text{m}$  of the section was elevated by a factor 1.4 (standard deviation 0.2).

#### LOCAL EFFECTS: ELEVATED INTRA-PARTICLE LOADING

Another local phenomenon that was studied in detail with TEM was the enzyme density around internal holes: the latter will be referred to as macro-voids. Surrounding these macro-voids, a distinct concentric to sickle-shaped structural element ranging from 2 to 20  $\mu\text{m}$  was observed (Fig. 3a), which will be referred to as “halo” in this work. High magnification of the halo (Fig. 3b) showed a vast local increase in gold particle density. Furthermore, the high enzyme loading inside the halo very sharply falls towards the much lower enzyme loading of the surroundings. Analysis of 8 different sections of multiple particles showed that the mean enzyme density in the halo was 7.7 times higher than in the immediate surroundings of the halo (standard deviation 1.3). This is much higher than the local abrupt increment in enzyme loading at the surface of the particles.

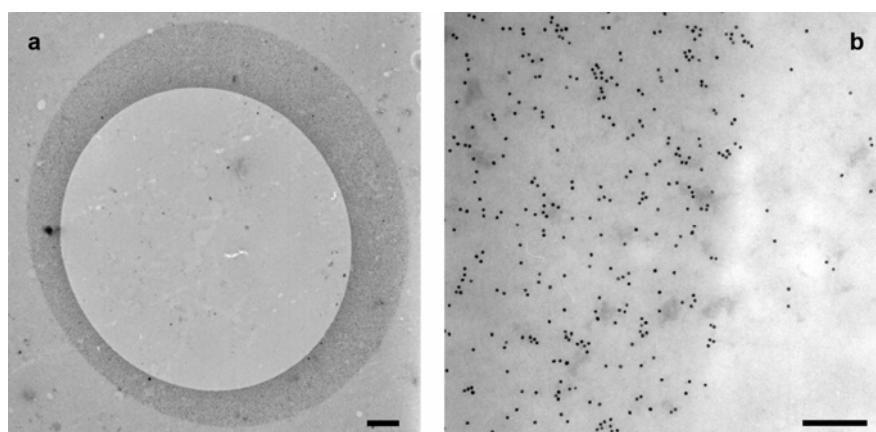


Figure 3. a: TEM micrograph of a halo surrounding a macro-void. The bar corresponds to 2  $\mu\text{m}$ . b: Detail of Figure 3a. The enzyme density (black spots are 10-nm gold labels) inside the halo (left) is much higher than that outside the halo (right). The transition between the enzyme densities in the two areas is sharp. Also the matrix material (background color) in the halo is electron denser (darker) in comparison to the surroundings. The bar corresponds to 100 nm.

The elevated local enzyme concentrations are likely caused by a local change in the properties of the support material that resulted in an increased number of (favorable) enzyme binding sites. This may have been caused by a local density increase of support material, i.e.: a locally more densely packed polymeric



network without any alterations in polymeric composition (only water excretion). Alternatively, the local composition of the support material could have been changed resulting in enzyme binding-site enrichment. Also a combination of both is possible.

If it is assumed that the density increase of the halo resulted from the emerging macro-void, a density increase of maximally a factor 2 could be expected, as the halo volume is approximately equal to the void volume. However, the enzyme loading in the halo was found to be increased about eight-fold. A local density increase without any compositional changes in the halo is therefore improbable as the only mechanism.

It seems likely therefore that the large increase in enzyme density in the halo was for the largest part caused by a compositional difference of the support material. More specifically, the extremely high enzyme density in the halo suggests chitosan enrichment, because chitosan theoretically has a much higher enzyme binding capacity per unit mass than gelatin: chitosan contains one primary amino group (for enzyme binding) per sugar residue, whereas gelatin only contains approximately one basic residue (for enzyme binding) for every thirty amino acids in its chain. Because the density of chitosan (estimated at 1.5 – 1.6 g/ml) is higher than that of gelatin (estimated at approximately 1.3 g/ml), a higher chitosan fraction in the polymeric network would simultaneously increase the local density. Fig. 3b indicates that the material of the halo indeed contained a higher (electron) density: the background material of the halo is darker (i.e. less electron transparent) than the surrounding material. The morphological properties of these local areas with elevated enzyme loading were investigated in more detail and related to the production of the particles in an effort to understand the process(es) that caused the formation of the areas.

## **PARTICLE MORPHOLOGY: CRYO-FESEM**

### ***Composition and structure of the external top layer***

Morphological analysis was done by cryogenic Field Emission Scanning Electron Microscopy (cryo-FESEM) on cryo-planed surfaces of frozen samples, which each contained sections through several particles. Fig. 4a shows the small aluminum pin onto which a small amount of biocatalytic particle-in-water suspension was frozen by immersion in liquid propane and subsequent cryo-

planing. On the left, the flat cryo-planed surface is visible with sections through the biocatalytic particles, which contrasts with the irregularly shaped surface of the freeze-broken area (the classically applied technique) on the right side. An example of a cryo-planed surface through one particle (embedded in ice) is given in Fig. 4b.

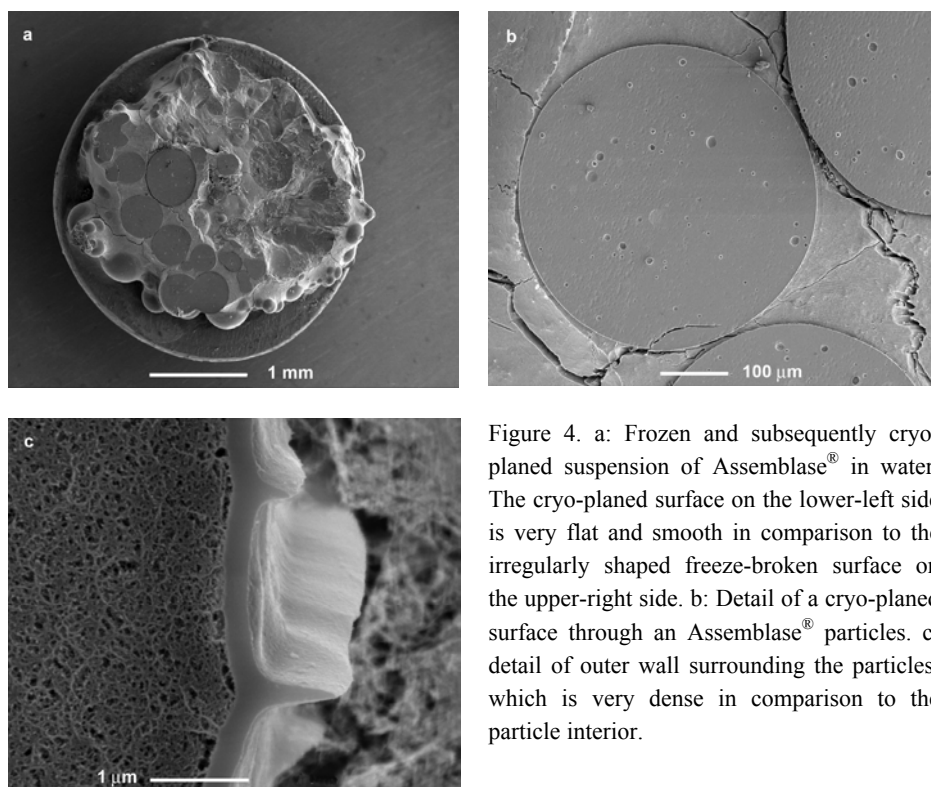


Figure 4. a: Frozen and subsequently cryo-planed suspension of Assemblase<sup>®</sup> in water. The cryo-planed surface on the lower-left side is very flat and smooth in comparison to the irregularly shaped freeze-broken surface on the upper-right side. b: Detail of a cryo-planed surface through an Assemblase<sup>®</sup> particles. c: detail of outer wall surrounding the particles, which is very dense in comparison to the particle interior.

The particle interior is typically a porous matrix. At the particle perimeter, a compact layer of approximately 0.5 - 1  $\mu\text{m}$  thickness was observed (Fig. 3c) with a jagged outer surface. As opposed to the particle interior, no substructure or porosity was visible within this apparently dense outer layer. Lack of substructure theoretically could have resulted from rapid amorphous freezing without formation of ice crystals. In this case, however, this is highly unlikely. If amorphous freezing would have been relevant, its extent or significance should depend on the position within the frozen lump of material and should decrease with the distance to the lump surface. The dense layers surrounding biocatalytic

particles featured very discrete borders and were identical throughout the entire preparation and were therefore expected to be natively present in Assemblase<sup>®</sup>.

Final proof of the native presence of the dense surface layer came from analysis of samples that were critical point dried. With this technique, no gas-liquid interface was present during drying and no cryo-fixation (freezing) was needed to study the samples, which makes it a good preservation technique. An example of the appearance of critically dried Assemblase<sup>®</sup> particles onto which no further manipulations were conducted is given in Fig. 5a. The bottom-right of the micrograph shows that some particles have smaller particles attached to them (partial coalescence), which must have happened during the production of these particles. The central particle in the micrograph shows scars of smaller particles that were detached at some stage. These scar areas reveal the particle interior. A magnification of such an area is given in Fig. 5b. It shows that the inner structure consisted of more porous material in comparison to the dense surface layer, which hardly showed any sub-structure (Fig. 4b). This led to the conclusion that the relatively dense top-layer layer that transitioned sharply with the particle interior was present natively and not an artifact of sample preparation.

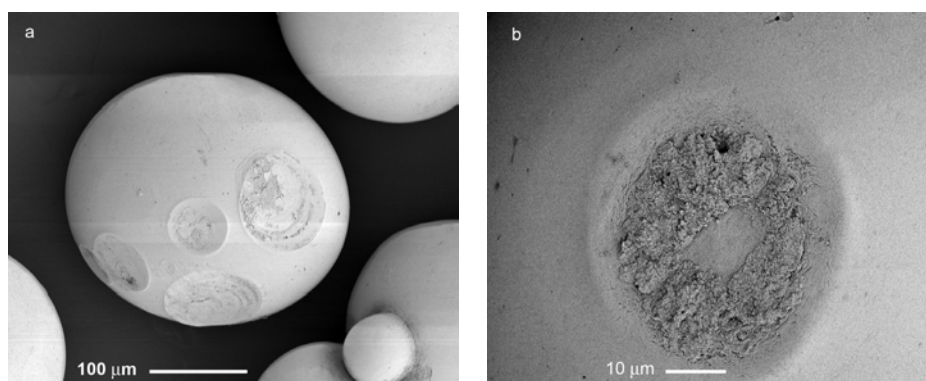


Figure 5. a: Super Critically Dried (SCD) Assemblase<sup>®</sup> particles. The central particle shows scars of other particles that were detached during particle preparation. b: Detail of Figure 5a. The region where the particle detached reveals particle interior. The particle surface is quite dense in comparison to the particle interior.

This does not imply that the dense top layer observed with cryo-FESEM (Fig. 4c) was not influenced by the freezing process: areas where relatively little “free-water” is present (i.e. water that is not bound to the support molecules) result in

relatively dense areas after freezing, because locally the low free-water content results in the formation of only small (structure disrupting) crystals during freezing. This indicates local chitosan enrichment in the top layers, because this polymer swells less in comparison to gelatin (e.g. Yin *et al.*, 1999), which also corresponds with the higher enzyme loading that was found in these areas by TEM (due to the higher binding capacity of chitosan per unit mass in comparison to gelatin).

#### **COMPOSITION AND STRUCTURE OF THE INTERNAL TOP LAYER AND THE HALO**

Analogous to the morphological study on the particle exterior, the internal characteristics of the support material were investigated on the same cryo-planed particle sections (Fig. 6a). A micrograph of a macro-void within the particle shows it to be surrounded by two structures that differ from the more or less “bulk” particle interior: (1) a dense top layer at the macro-void border, and (2) an eccentric halo, which has a courser, more porous structure (Figs. 6b and 6c, respectively). Both the top layer and the halo resemble earlier observations in size and shape. The top-layer surrounding the macro-voids had a similar density, structure and thickness (approximately 0.5 – 1.0  $\mu\text{m}$ ) as the one observed with FESEM at the particle surface (Fig. 4c) and the sickle-shaped halo had a maximal thickness of 5-10  $\mu\text{m}$ , which was in line with TEM observations on ultra-thin sections (Fig. 3a).

The similar morphology between the top layers surrounding the particles and the ones surrounding the macro-voids, suggest a similar composition. Like the top layer at the exterior particle surface, also the dense layer of matrix material surrounding the internal macro-voids is thought to be locally enriched in chitosan, which would result in increased local enzyme binding capacity and in a decreased local swelling.

The composition of the matrix material in the halo, however, remains unclear at the moment. Both the 8-fold enzyme-binding capacity and the high material density in TEM suggest chitosan enrichment. The morphology of the halo area in cryo-FESEM, however, is even more porous than the surrounding “normal” support material (2 versus 3 in Fig. 6c). This was not implicitly expected from chitosan rich material, given the low swelling value of chitosan. Although these seem to be conflicting observations at first hand, chitosan enrichment still seems

the only plausible mechanism given the huge increase of the number of enzyme binding sites per unit volume (or mass).

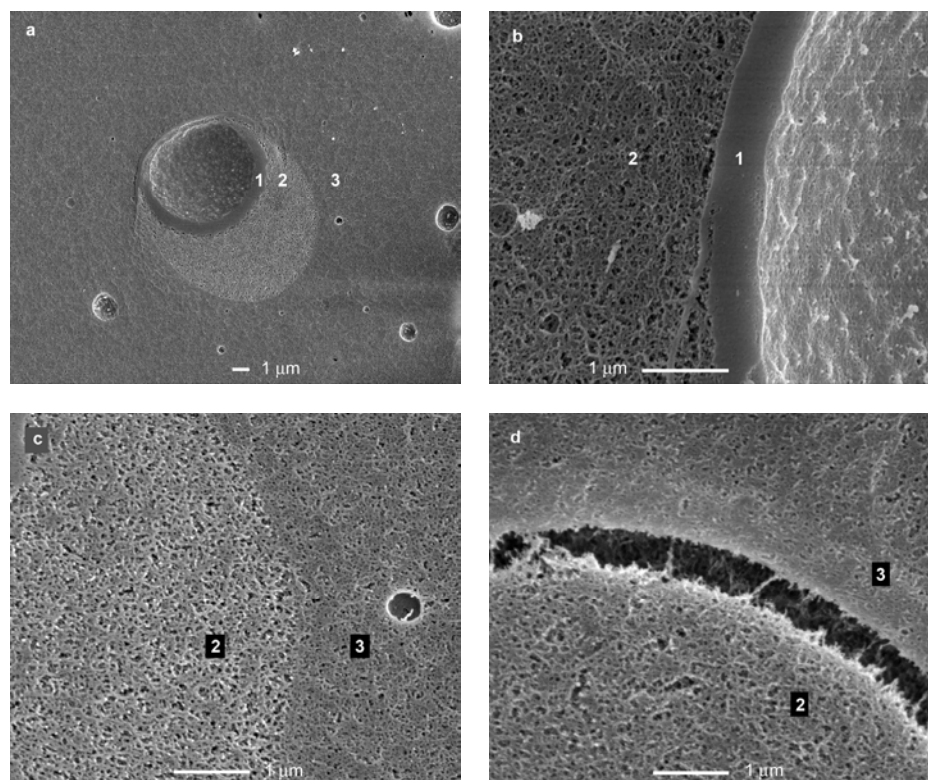


Figure 6. a: Section through a macro-void within an Assemblase® particle, consecutively surrounded by a dense wall (1), a halo (2) and the surrounding matrix material (3). b: Detail of the boundary between the wall (1) and halo (2). c: Detail between the halo (2) and the surroundings (3). d: As Figure 6c, only here the halo (2) has detached from the surrounding material (3) during freezing, indicating compositional differences.

It is clear that Assemblase® consists of areas with very different properties, which have different structural arrangements and vary considerably in enzyme loading. The enzyme loading and mass transfer properties of a biocatalyst heavily depend on the matrix morphology. It is therefore important to know the characteristics of the different areas of the support material, for which a start was made in the previous sections. However, for the eventual production of improved biocatalysts in the future, it is also important to understand the underlying mechanisms for the formation of these different areas.

## POLYMER DEMIXING

### *Driving force*

In order to obtain more insight in the morphological diversity of Assemblase<sup>®</sup>, the polymers involved and the conditions during particle preparation were considered in detail. Depending on the pH, chitosan, which is a poly-cation below its pKa of approximately 6.5, and gelatin, which is a poly-anion above its isoelectric point of approximately 4.6, can have a strong ionic interaction, resulting in a polyelectrolyte complex (PEC; e.g. Mao *et al.*, 2003; Mao *et al.*, 2004). Such strong interactions generally prevent the polymers to diffuse away from each other; they cause associative phase separation, during which complex coacervation of the polymers occurs (i.e. the polymers stay together and only water is excluded during gelling; Walstra, 2003). In the case of Assemblase<sup>®</sup>, it is possible that polyelectrolyte linking of the two polymers contributed to overall associative phase behavior; both cryo-FESEM and TEM micrographs showed a well-mixed overall particle matrix. Besides this, the areas that are supposedly enriched in chitosan do not have enough volume to account for all chitosan present.

However, areas with very different morphology were present locally (Figs. 4, 5 and 6). The high enzyme loading in these areas suggests chitosan enrichment, which would imply: (i) that there was a driving force for polymer demixing during particle preparation, and (ii) that actual polymer movement along this gradient was possible during particle production.

The presence of a driving force was investigated with a thermodynamic line of reasoning. The sole purpose of these calculations was to see whether there might be a thermodynamic driving force for polymer demixing. Whether actual segregation takes place depends on the physical ability of the polymers to do so and will be discussed in the next paragraph. Without going into details of the calculations, the phase behavior of the ternary water/gelatin/chitosan system was described with the standard form of the Flory-Huggins theory (Flory, 1964).

As a start, a description of the swelling behavior of gelatin and chitosan films as measured by Yin *et al.* (1999) was attempted. This is shown in the lower left of

Fig. 7, in which the experimental swelling data of Yin *et al.* are plotted with the calculated swelling lines for different values for the interaction parameter between gelatin and chitosan. The agreement between experimental data and the calculated curves is adequate, especially given the rough assumptions that were made regarding the presence of physical cross-links and regarding the complex and inhomogeneous nature of the interactions between the two polymers and water. The deviation of the experimental points from the calculated curves was expected, given the strong hydrogen-bonding present in the system: this often results in concentration-dependent interaction parameters (Altena and Smolders, 1982).

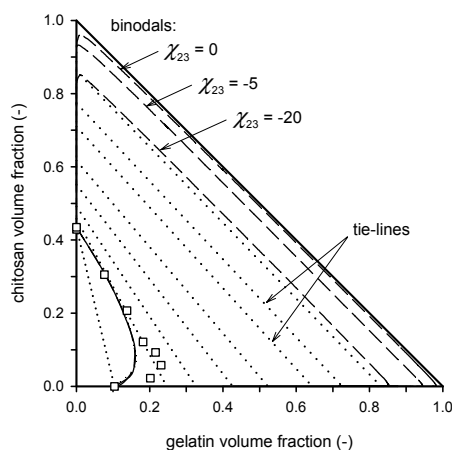


Figure 7. Comparison of experimental swelling data by Yin *et al.* (1999; □) of gelatin (2) - chitosan (3) films in water (1) with calculated swelling lines, for  $\chi_{12} = 0.539$  and  $\chi_{13} = 0.718$  and for  $\chi_{23} = 0, -5$ , and  $-20$ , respectively (lines overlap). The binodals (—) are plotted for 3 different gelatin-chitosan interaction parameters ( $\chi_{23}$ ). The tie-lines (· · ·); lines that connect equilibrium compositions) shown are valid for all three binodals: there was no discernable difference between the tie lines for the three binodals. The figure indicates that the two polymers have a driving force for almost complete demixing for a large range of compositions.

Apparently, the swelling behavior of ternary films of chitosan, gelatin, and water can be predicted relatively well on the basis of water/gelatin and water/chitosan interaction parameters ( $\chi_{12}$  and  $\chi_{13}$ , respectively), while gelatin/chitosan interaction ( $\chi_{23}$ ) plays a minor role. A large change in  $\chi_{23}$  from 0 (representing gelatin/chitosan interaction that is just as strong as between gelatin molecules themselves and between chitosan molecules themselves) to  $-20$  (representing a gelatin/chitosan interaction that is enormously stronger than the internal interactions gelatin/gelatin and chitosan/chitosan) does not result in a change of the calculated swelling curve. Apparently, the polymer/solvent interactions are predominant in the swelling behavior.

With the resulting interaction parameters, the ternary phase equilibria were calculated. Solutions were looked for in which two demixed phases would have different compositions but identical chemical potentials for each of the three components. Solutions were obtained by nonlinear numerical minimization of the squares of the differences in the Flory-Huggins equations for the chemical potential for each component (Boom *et al.*, 1994a, 1994b) .

Subsequently, the binodals of the system were calculated as a function of the gelatin/chitosan interaction parameter  $\chi_{23}$ . The binodal represents the border of the miscibility gap: beyond the binodal, compositions are stable, whereas in the area enclosed by the swelling line and the binodal, homogeneous compositions are unstable and may separate into two phases.

For three  $\chi_{23}$  values, binodals are given in Fig. 7. The miscibility gap, i.e. the area between the swelling line and the binodal, is found to be very large for all values of  $\chi_{23}$ . Without physical or electrolyte interactions holding them together, the polymers will have a clear tendency to demix in two phases, each almost exclusively containing one of the two polymers (the tie lines end almost completely at the horizontal and vertical axis, respectively). Even an extreme gelatin/chitosan interaction ( $\chi_{23} = -20$ ) does not preclude polymer segregation: the only influence of  $\chi_{23}$  is the shifting of the binodal towards somewhat higher water concentrations.

Tie lines were found to be independent of the value of  $\chi_{23}$ , due to the difference in hydrophilicity ( $\chi_{12} - \chi_{13}$ ) between the polymers. The very low entropy of mixing between the polymers implies that the system can gain significant entropy by water-polymer mixing. Separation in two phases (i.e. introducing polymer-water interactions at the expense of polymer-polymer interactions) therefore leads to a gain in the Gibb's free energy of mixing.

The calculations thus show that both polymers exhibit an entropical thermodynamic driving force for segregative phase separation during which each polymer forms a separate phase with the solvent. This is found to hold for almost all compositions, and is more or less independent of mutual enthalpic polymer interactions. It is, in fact, widely acknowledged that proteins and carbohydrates do not mix, unless there is an associative interaction (e.g. charge effects; Walstra,



2003). Although this hypothesis may give a thermodynamic explanation for (partial) segregative polymer demixing at a micron-scale, the actual extent of demixing depends on the freedom of motion of the polymers, which may be restricted by polyelectrolyte interactions and physical cross-links.

As shown in Figs. 4, 5 and 6, a PEC did not prevent relative polymer movement in areas with different morphology. As shown in the thermodynamical treatment above, a chemical potential gradient may have caused this movement. Apparently, the presense of a PEC did not prevent polymer movement. If the pH during the production of the particles (its exact value is unknown because the particles were produced in industry) differed from the electrical equivalence pH (EEP, the pH at which the polymers carry equal but opposite charges; depending on polymer charge density and mass ratio), there may have been polymers that were not restricted for movement by the presence of the PEC, but could have diffused through the solvent, accompanied with their salt counter-ions. Locally, this may have resulted in thermodynamically driven polymer segregation, and resulted in heterogeneities of the support material.

Besides ionic restrictions, also physical restriction can prevent polymer movement. It is expected that relative polymer movement is possible in freshly dispersed polymeric droplets. Following polymer dispersion, however, solidification takes place and polymer movement becomes more difficult. Later on, polymer movement is completely stopped by addition of glutaric di-aldehyde, which interconnects the polymer chains.

#### **FORMATION OF A TOP-LAYER AT THE PARTICLE EXTERIOR**

The above suggests two alternative mechanisms for top layer formation during particle production. In the first, the top-layer is formed during gelling or after transfer of the beads to an aqueous phase. The PEC and the physical cross-links that emerge during gelling may have not yet been able to completely immobilize the polymers and some small-scale migration may occur. Due to the thermodynamic driving force, the polymers will demix to a certain extent. Initiation of the demixing of a meta-stable solution may take place against an interface, which could be the non-solvent phase. Because chitosan is the more hydrophobic of the two polymers, gelatin would in that case diffuse away from the interface, into the droplet. As a result, a higher chitosan concentration near

the surface, and an increased gelatin concentration just below the top layer would be expected.

Alternatively, the same effects may occur during particle suspension in the aqueous phase. Once again, small-scale demixing takes place, but now gelatin will probably diffuse into the aqueous phase. The aqueous phase (in which the particles are present before chemical cross-linking with glutaric aldehyde, see Materials and Methods) may impose a strong driving force for gelatin movement into the aqueous phase, leaving behind a chitosan-enriched layer. Local chitosan enrichment will decrease the local swelling; consequently, gelatin movement through that layer will be hindered and will stop eventually (Walstra, 2003). In this case, the gelatin concentration below the top layer is not expected to be higher than normal.

At this stage it is not possible to distinguish between these two mechanisms. However, the fact that an excess concentration of gelatin was not observed just below the top layer would point to the second mechanism. It is also possible that both mechanisms played a role. In any case, the mutual diffusion between the polymers is expected to be virtually stopped by chitosan enrichment in the emerging top layer, which compacts the local matrix and drastically diminishes gelatin diffusivity. A small decrease in gelatin concentration would decrease the local hydrophilicity, and would lead to significant expulsion of water and a much higher resulting local polymer concentration (Fig. 7). Additionally, the small chemical cross-linking agent glutaric di-aldehyde may have started to fixate the matrix (chemically bind the chitosan and gelatin together). Combination of these two effects may have rapidly stopped the initial phase separation, with only a thin top layer formed. The fact that phase separation is responsible for the formation of the top layer explains the very sharp transition between a typical top layer and the underlying gel phase: two very different compositions are at (local) equilibrium with each other.

#### **FORMATION OF A TOP-LAYER SURROUNDING MACRO-VOIDS**

A second phenomenon observed was the top layer surrounding the macro-voids in the particle interior. They have a very similar morphology as the ones surrounding the particle and are also thought to be a result of phase-separation during particle formation. Possibly, a droplet of non-solvent was included in the

polymeric mixture during its preparation, which could have resulted in similar phase contact as was present at the particle perimeter. This would lead to the formation of similar structures.

#### **FORMATION OF A HALO SURROUNDING MACRO-VOIDS**

The halos were predominantly eccentrically located around an internal top-layer surrounding a macro-void, and were most probably significantly enriched in chitosan. At this point, their formation is not understood. An explanation might be that they originated from remnants of small, poorly dissolved patches of chitosan. Such “lumps” obviously would contain much chitosan, would be denser, would have an extreme high binding capacity, and could have a very distinct appearance in the FESEM, for instance by electrostatic repulsion of the positively charged chitosan strands. Possibly, a droplet of non-solvent may have been caught on the interface between the relatively hydrophobic chitosan patch and the surrounding polymeric solution. This non-solvent droplet can then act as a nucleus for a small-scale local phase separation process, as described above for the particle exterior. The result may be a partial melting of the chitosan lump with the non-solvent droplet.

Alternatively, the halo structures might result from inclusion of non-solvent droplets in the polymeric matrix. Immediately upon inclusion, the shape of these droplets may be non-spherical. Interfacial tension, however, will tend to re-shape the droplets, especially the highly curved parts, into sphericity. This process is time-consuming due to the high medium viscosity. During curvature changes, phase separation takes place, as was the case for the outside of the biocatalytic particles. Contrary to the situation on the outside of the particles, the interface now recedes during phase separation. Although chitosan is expected to accumulate at the interface, as on the exterior surface of the particle, it is pulled with the receding interface and may not be allowed to form a dense layer. A more open, eccentrically placed halo structure might be the result. Only if the interface reaches its equilibrium curvature, the polymers may be able to form dense structures such as the thin, dense layer on the inside of the halo. If the non-solvent droplets are very small, they will be spherical due to the high Laplace pressure, which may be an explanation for the absence of halos around the smallest voids.

The above shows that it is not yet possible to unambiguously attribute all observed matrix heterogeneity to specific mechanisms, although some important characteristics of these structures were identified. Locally, the enzyme loading was found to deviate from the global enzyme profile, which reflects diffusion of enzyme into the particle during loading. These deviations were attributed to matrix morphology. Combined data suggested that it is very likely that these deviating areas are enriched in chitosan, thus indicating polymer segregation during particle production. A basic thermodynamic treatment supported this assumption and showed the polymers to be subject to a segregative driving force, assuming there are no physical constraints. Control of demixing may be a starting point for a new rational optimization of biocatalytic particles, in which fundamental polymer properties are exploited to impose desired matrix-related enzyme heterogeneity or heterogeneous mass transfer properties.

## CONCLUSION

The ultra-high resolution of TEM facilitates its use at various levels of detail within a single particle. In this work, TEM was used for the analysis of global and local phenomena in Assemblase<sup>®</sup>. Global analysis revealed the intra-particle enzyme distribution of Assemblase<sup>®</sup> particles of various sizes. The results showed that the distribution was equivalent with the one found in previous light microscopic work, albeit without the need for complicated image analysis.

Several local phenomena were investigated as well. TEM quantitatively revealed an abruptly elevated enzyme loading at the particle perimeter and surrounding macro-voids. It was found that the enzyme loading in the halos, which eccentrically surrounded the top-layers around the macro-voids, was increased almost eight-fold. TEM additionally revealed a local increase in material density in these regions.

A cryo-FESEM study, which is very well suited for the high-resolution morphological study of the particle interior, related abrupt local enzyme heterogeneity to local heterogeneity of the support material of Assemblase<sup>®</sup>. Analysis revealed the presence of top-layers at the surface of Assemblase<sup>®</sup> particles and in the top-layers surrounding internal macro-voids. Furthermore, it showed that the halo's contained a very distinct morphological appearance. The

detail provided by the combination of cryo-planing and subsequent analysis with cryo-FESEM gave strong indications that the local composition of the top-layers and the halos was enriched in chitosan.

Local enrichment of one of the constituents implies local demixing had occurred. The possibility for such demixing was hypothesized on. Based on an adequate description of the swelling behavior of gelatin/chitosan films with single interaction parameters, the ternary phase behavior of gelatin/chitosan solutions was interpreted with the standard form of the Flory-Huggins theory. It was found that both polymers have a clear tendency to demix. Resulting segregative phase separation could explain the local sharp transitions of the top layers and their significantly elevated enzyme binding capacity. Knowledge on the mechanisms that are responsible for the formation of these structures can be a useful tool for the rational design of future biocatalytic particles.

## ACKNOWLEDGEMENTS

DSM (Delft, the Netherlands) and The Ministry of Economic Affairs of The Netherlands are kindly acknowledged for their financial support. Dr. S. Arendsen (DSM Food Specialties, Delft, The Netherlands) and dr. E.J.A.X van de Sandt (DSM Anti-Infectives, Delft, The Netherlands) are kindly acknowledged for valuable discussions. Mr. Boudewijn van Veen (Wageningen University) is kindly acknowledged for his expert help in digital image processing.

## REFERENCES

- Altena F.W., and Smolders C.A.** (1982). Calculation of liquid-liquid phase separation in a ternary system of a polymer in a mixture of a solvent and a nonsolvent. *Macromolecules* **15**: 1491-1497.
- Baskin T.I., Busby C.H., Fowke L.C., Sammut M., and Gubler F.** (1992). Improvements in immunostaining samples embedded in methacrylate: Localization of microtubules and other antigens throughout developing organs in plants of diverse taxa. *Planta* **187**: 405-413.
- Berger J., Reist M., Mayer J.M., Felt O., Peppas N.A., and Gurny R.** (2004). Structure and interactions in covalently and ionically crosslinked chitosan hydrogels for biomedical applications. *Eur. J. Pharm. Biopharm.* **57**: 19-34.

- Boom R.M., Reinders H.W., Rolevink H.H.W., Van den Boomgaard Th., and Smolders C.A.** (1994<sup>a</sup>). Equilibrium thermodynamics of a quaternary membrane-forming system with two polymers. 2. Experiments. *Macromolecules* **27**: 2041-2044.
- Boom R.M., Van den Boomgaard Th., and Smolders C.A.** (1994<sup>b</sup>). Equilibrium thermodynamics of a quaternary membrane-forming system with two polymers. 1. Calculations. *Macromolecules* **27**: 2034-2040.
- Burton S.G., Cowan D.A., and Woodley J.M.** (2004). The search for the ideal biocatalyst. *Nat. Biotechnol.* **20**: 37-45.
- De Vroom E.** (1997). An improved immobilized penicillin G acylase. International patent WO 97/04086.
- Fernandez-Lafuente R., Rosell C.M., Caanan-Haden L., Rhodes L., and Guisan J.M.** (1998). Facile synthesis of artificial enzyme nano-environments via solid-phase chemistry of immobilized derivatives: dramatic stabilization of penicillin acylase versus organic solvents. *Enzyme Microb. Technol.* **24**: 96-103.
- Flory P. J.** (1964). Principles of Polymer Chemistry. Cornell University Press Ithaca.
- Harder A., De Haan B.R., and Van der Plaats J.B.** (1987). Novel immobilized biocatalysts and their preparation and use. European patent 0222462B1.
- Hennink W.E., and Van Nostrum C.F.** (2002). Novel crosslinking methods to design hydrogels. *Adv. Drug Deliv. Rev.* **54**: 13-36.
- Hossain Md.M., and Do D.D.** (1989). General theory of determining intraparticle active immobilized enzyme distribution and rate parameters. *Biotechnol. Bioeng.* **33**: 963-975.
- Juang R.S., Wu F.C., and Seng R.L.** (2002). Use of chemically modified chitosan beads for sorption and enzyme immobilization. *Adv. Environ. Res.* **6**: 171-177.
- Kaasgaard S.G., Karlsen L.G., and Schneider I.** (1992). Process for separation of two solid components. International patent WO 92/12782.
- Kaneko T., Hamada K., Chen M.Q., and Akashi M.** (2004). One-step formation of morphologically controlled nanoparticles with projection coronas. *Macromolecules* **37**: 501-506.
- Mao J.S., Cui Y.L., Wang X.H., Sun Y., Yin Y.J., Zhao H.M., and De Yao K.** (2004). A preliminary study on chitosan and gelatin polyelectrolyte complex cytocompatibility by cell cycle and apoptosis analysis. *Biomaterials* **25**: 3973-3981.
- Mao J.S., Wang X.H., De Yao K., Shang Q.X., and Yang G.H.** (2003). Studied on a novel human keratinocyte membrane delivery system in vitro. *J. Mater. Sci.* **15**: 2283-2290.
- Moulijn J.A., Perez-Ramirez J., Van Diepen A., Kreutzer M.T., and Kapteijn F.** (2003). Catalysis engineering on three levels. *Int. J. Chem. React. Eng.* **1**: 1-17.
- Scharer A., Hossain Md.M., and Do D.D.** (1992). Determination of total and active immobilized enzyme distribution in porous solid supports. *Biotechnol. Bioeng.* **39**: 679-687.
- Schroën C.G.P.H., Fretz C.B., De Bruin V.H., Berendsen W., Moody H.M., Roos E.C., Van Roon J.L., Kroon P.J., Strubel M., Janssen A.E., and Tramper J.** (2002). Modelling of the enzymatic kinetically controlled synthesis of cephalixin: influence of diffusion limitation. *Biotechnol. Bioeng.* **80**: 331-340.
- Taqiuddin E., and Amiji M.** (2004). Enzyme immobilization in novel alginate-chitosan core-shell microcapsules. *Biomaterials* **25**: 1937-1945.

- Van Roon J.L., Groenendijk E., Kieft H., Schroën C.G.P.H., Tramper J., and Beeftink H.H.** (2005). Novel approach to quantify immobilized-enzyme distributions. *Biotechnol. Bioeng.* **89**: 660-669.
- Van Roon J.L., Joerink M., Rijkers M., Tramper J., Schroën C.G.P.H., and Beeftink H.H.** (2003). Enzyme distribution derived from macroscopic particle behavior of an industrial immobilized penicillin-G acylase. *Biotechnol. Prog.* **19**: 1510-1518.
- Walstra P.** (2003). *Physical Chemistry of Foods*. Marcel Dekker Inc., New York.
- Wergin W.P., and Stone A.R.** (1981). Techniques for preparation and examination of plant parasitic nematodes in the scanning electron microscope. *Scanning* **3**: 169-176.
- Yin Y.J., Yao K.D., Cheng G.X., and Ma J.B.** (1999). Properties of polyelectrolyte complex films of chitosan and gelatin. *Polym. Int.* **48**: 429-432.





---

## Chapter 6 FESEM analysis of morphology and enzyme distribution within an industrial biocatalytic particle

The contents of this chapter have been accepted for publication as:

**J.L. van Roon, A.C. van Aelst, C.G.P.H. Schroën, J. Tramper and H.H. Beeftink** (2005). FESEM analysis of morphology and enzyme distribution within an industrial biocatalytic particle. *Scanning* **27**: 181-189.

## **ABSTRACT**

Field-emission scanning electron microscopy (FESEM) was used in a technical feasibility study to obtain insight in the internal morphology and the intra-particle enzyme distribution of Assemblase<sup>®</sup>, an industrial biocatalytic particle containing immobilized penicillin-G acylase. The results were compared to previous studies based on light and transmission electron microscopic techniques. The integrated FESEM approach yielded the same quantitative results as the microscopic techniques used previously. Given this technical equivalence, the integrated approach offers several advantages. First, the single preparation method and detection system avoids interpretation discrepancies between corresponding areas that were examined for different properties with different detection techniques in different samples. Second, the specimen size suitable for whole particle study is virtually unlimited, which simplifies sectioning and puts less stringent demands on the embedding technique. Furthermore, the sensitivity towards enzyme presence and distribution increases because the epitopes inside thick sections become available for labeling. Quick and unambiguous analysis of the relation between particle morphology and enzyme distribution is important because this information may be used in the future for the design of enzyme distributions in which the particle morphology can be used as a control parameter.

## INTRODUCTION

Enzymes are biocatalysts that efficiently catalyze specific reactions. Their industrial application has grown rapidly over the last two decades (Straathof *et al.*, 2002). In view of reuse and stability, enzymes are often immobilized into biocatalytic particles. The enzyme distribution within these particles is important for overall performance if diffusion limitation occurs (Schroën *et al.*, 2002; Scharer *et al.*, 1992; Hossain and Do, 1989). Mass transfer within biocatalytic particles is largely determined by the steric morphology of the particle material. In addition, the chemical nature of the particle support material also determines the amount of enzyme it binds as well as the interactions between the biocatalyst and the support material (Van Roon *et al.*, 2005<sup>b</sup>). Intra-particle heterogeneities of the support material can cause heterogeneities in the intra-particle enzyme distribution. Because the support morphology influences both reactant mass transfer and the intra-particle enzyme distribution, understanding the relationship between the internal particle morphology and enzyme density is important. Such knowledge may provide a starting point for designed enzyme distributions in biocatalytic particles for which morphological properties of the support can be used as a control parameter.

A model example of a biocatalytic system with complex kinetics in which mass transfer limitations occur is Assemblase<sup>®</sup>, an industrially used immobilized penicillin-G acylase that is used for the production of e.g. the semi-synthetic antibiotic cephalexin (Tramper *et al.*, 2001 and Schroën *et al.*, 2001). Previously, the global intra-particle enzyme distribution of Assemblase<sup>®</sup> was measured by light microscopy (LM) on labeled particle sections (Van Roon *et al.*, 2005<sup>a</sup>). Because the size distribution of Assemblase<sup>®</sup> particles is very broad, this procedure had to be performed for particles of various sizes to obtain the intra-particle enzyme distribution as a function of the particle diameter. The results showed that the particles contained various heterogeneous enzyme distributions resulting from in-stationary enzyme penetration during biocatalytic activation of the empty particles.

A study on local heterogeneities in enzyme density was performed by discrete measurement of gold labeled sections of Assemblase<sup>®</sup> with transmission electron microscopy (Van Roon *et al.*, 2005<sup>b</sup>). Abrupt local heterogeneities in enzyme density (up to a factor 8) were found at the particle perimeter and around internal macro-voids. Low-temperature field-emission scanning electron microscopy (cryo-FESEM) on liquid-propane frozen and cryo-planed Assemblase<sup>®</sup> particles showed that the local morphology of the support material was different from the global (average) matrix morphology in the corresponding areas. Conclusions were drawn on the local composition of the matrix material in these areas in relation to the local enzyme density, and on the genesis of these morphologically distinct areas (Van Roon *et al.*, 2005<sup>b</sup>).

Characterization of the enzyme distribution and matrix morphology at different levels of detail required complementary microscopic techniques that each involved unique sample preparations (Van Roon *et al.*, 2002, 2005<sup>b</sup>). Because the Assemblase<sup>®</sup> particles were relatively large (up to 1 mm), each preparation was amended to obtain optimal results. Consequently, sample preparation was laborious. Moreover, these procedures had to be conducted on different samples, which complicated the interpretation of the results.

This paper evaluates the feasibility of FESEM as a single method for the simultaneous study of morphological particle properties and intra-particle enzyme distribution in Assemblase<sup>®</sup>.

## **MATERIALS AND METHODS**

### **BIOCATALYTIC PARTICLES**

Assemblase<sup>®</sup> is a biocatalytic particle of DSM Anti-Infectives (Delft, The Netherlands); a single batch was provided for the present research. In all instances the trademark Assemblase<sup>®</sup> refers to this preparation. Although several combinations of polymers, non-solvents, and cross-linking agents are suitable and applied for industrial particle preparation, gelatin and chitosan were contacted with a non-solvent and chemically cross-linked with glutaric dialdehyde according to Harder *et al.* (1987) and De Vroom (1997). For this specific batch, isolated and purified penicillin-G acylase from *Escherichia coli* (Kaasgaard *et al.*, 1992) was loaded for 1.9 hours onto the support material from

the exterior after bead formation. Some particles were not activated to provide a negative control. Immobilization was relatively mild: previous research showed the enzyme activity and kinetic mechanism to be unaffected (Schroën *et al.*, 2002). Further details on this specific batch of Assemblase® were previously given (Van Roon *et al.*, 2002).

### CHEMICALS

All water was double distilled. Polyclonal rabbit immunoglobulin-G against *E. coli* penicillin-G acylase was generously donated by Dr. C.F. Sio (Department of Pharmaceutical Biology, University of Groningen, The Netherlands), and used as a primary antibody. Secondary antibodies were GAR (goat anti-rabbit) polyclonals to which 10-nm gold spherical particles were attached (Aurion, Wageningen, The Netherlands).

### EMBEDDING

The particles were embedded in BMM (40 mL butylmethacrylate, 10 mL methylmethacrylate, 0.25 g benzoin ethylether and 0.08 g dithiothreitol (DTT) done under a nitrogen atmosphere according to Baskin *et al.* (1992). Dehydration and resin penetration were done with two 5-graded series with ethanol/DTT and BMM, respectively. Samples were subsequently transferred into BEEM™ capsules (EMS, Washington, USA). Polymerization of the BMM under black-light ultra-violet lamps was done for 48 hours at 253 K.

### SECTIONING

After resin polymerization, the BEEM™ capsules were removed and the embedded biocatalytic particles were sectioned at 3 µm thickness with an ultramicrotome (Reichert Ultracut-S, Seefeld, Germany) fitted with glass knives (LKB 7801 knifemaker, LKB, Stockholm, Sweden). Approximately one out of every ten sections was placed onto a water droplet on a glass microscope slide and expanded with chloroform vapor, and then the water was vaporized by placing the slide onto a hot plate (approximately 323 K). These sections were examined with LM to determine the position of the sections under study in the particle and to determine the size of the particle. Adjacent sections were put onto carbon foil (EMS, Washington, U.S.A.), treated the same as those put onto the microscopic slides and analyzed in the FESEM. For each preparation, a series of approximately 80 sections were made.

**LABELING**

Prior to labeling, BMM was removed by washing the sections 2 times for 7 minutes in 100% acetone. The acetone was removed by washing in PBS (8 g NaCl, 0.2 g KCl, 0.2 g  $\text{KH}_2\text{PO}_4$  and 1.41 g  $\text{Na}_2\text{HPO}_4$  dihydrate in 1 liter water, pH 7.4). A two-step labeling procedure was applied to the sections (Van Roon *et al.*, 2005<sup>a</sup>). After labeling, the samples were washed with water (3 x 5 min) and air-dried. Three negative control experiments were done each in triplicate. In the first, the primary antibody was omitted from the labeling procedure to check for a-specific binding of the secondary antibody. In the second, “empty” support particles without penicillin-G acylase were labeled with both antibodies, to check for a-specific affinity of one or both antibodies to the support material. Finally, normal rabbit serum was used in combination with the second (GAR-type) antibody, to check for affinity of the rabbit serum to the penicillin-G acylase. In all negative control experiments, no gold label was visible. In experiments with both antibodies, label was abundantly present (Van Roon *et al.*, 2005<sup>a</sup>). The detected amount of label was found to be proportional to the relative enzyme density within a single sample (Van Roon *et al.*, 2005<sup>a</sup>).

**DETECTION**

A standard bright-field microscope (Optiphot, Nikon, Tokyo, Japan) was used to measure the radii of the untreated sections on the glass slides to determinate the position that the section under study with FESEM occupied in the original particle and its diameter. All sections that were labeled on carbon foil were mounted onto brass holders with double-sided sticky carbon tape (EMS, Washington, U.S.A.). Subsequently, they were transferred uncoated into a FESEM (JEOL JSM-6300F, Tokyo, Japan) via a dedicated pre-chamber (Oxford Instruments CT 1500 HF, Eynsham, England). The uncoated samples were analyzed and recorded with BSE and SE detection at 12 kV with 15 mm working distance to the objective pole piece and with 9 mm detection distance to the BSE detector. BSE recording was done by a retractable Autrata YAG crystal detector (AutraDet, Brno, Czechoslovakia). The optimum BSE and SE signal/noise ratio was detected empirically at 12 kV. After the uncoated analyses, the sample was retracted into the preparation chamber and sputter coated with 10 nm platinum (DC magnetron sputter head, Denton Vacuum, Moorestown, USA), recorded with a thickness monitor (Cressington MTM 10, Cressington Scientific Instruments, Watford, England). After coating the sample was replaced into the

FESEM and re-analyzed morphologically at a working distance of 8 mm, with SE detection at 5 kV, where the signal/noise ratio of the platinum coated samples was optimal. All images were recorded digitally (Orion, 6 E.L.I. sprl., Charleroi, Belgium) at a scan rate of 100 seconds (full frame) at the size of 1264 x 1015 pixels, with 8-bit depth. The images were optimized and resized for publication by Adobe Photoshop 8.0.

### **CORRECTION OF MEASUREMENTS**

Particle shrinkage due to embedding was investigated by measuring the particle diameter of approximately 50 beads with a binocular in the native, swollen state, after dehydration, and after BMM penetration (dehydrated shrunken state). The final average radial shrinkage was 32% (Van Roon *et al.*, 2005<sup>a</sup>), which was used to correct all distances relative to the center of the particle: only shrinkage-corrected data are shown in the paper.

## **RESULTS AND DISCUSSION**

### **LABEL DETECTION**

An undiluted secondary antibody solution (10 nm gold) on a Formvar-coated

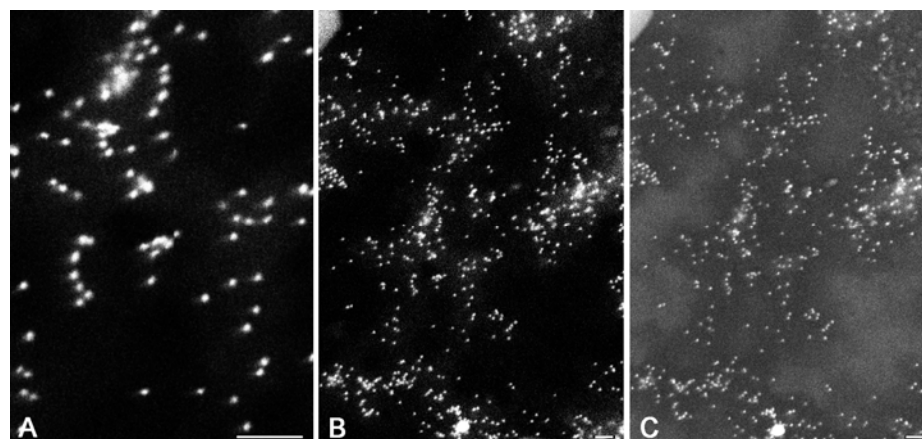


Figure 1. a: 10 nm Immuno-gold labeled antibodies attached on a TEM grid and detected with FESEM in back-scatter electron mode (BSE). The bright spots are the 10 nm gold labels. b: 10 nm gold labeled section of Assemblase<sup>®</sup> attached to carbon foil, detected with FESEM in BSE mode. c: The same section as in Figure 1c, now detected with FESEM in secondary-electron (SE) mode. Bar = 100 nm.

TEM grid was examined in backscatter electron (BSE) and secondary electron (SE) modes in the FESEM for reference purposes: for this sample, the signal-to-noise ratio was expected to be near its maximum. The bright spots indicate the 10 nm gold particles (Figure 1a). Assemblase<sup>®</sup> sections attached to carbon foil were also analyzed in BSE and SE modes (Figures 1b and 1c, respectively). In all samples, the gold particles were clearly visible. Because topographic information makes orientation and navigation within the Assemblase<sup>®</sup> sections easier, the samples were detected in BSE and SE modes and recorded in SE mode throughout the experiment.

### DETERMINATION OF PARTICLE SIZE AND SECTION POSITION

The gold particle distribution is a function of the position of the section within the purportedly spherical biocatalytic particle. Only sections through the center of mass of the particle reveal its total spatial enzyme distribution, whereas off-center sections reveal only a part of the intra-particle enzyme distribution. Consequently, for off-center sections all distances of a position within that section to its rim is larger than the distance to the actual particle surface and all

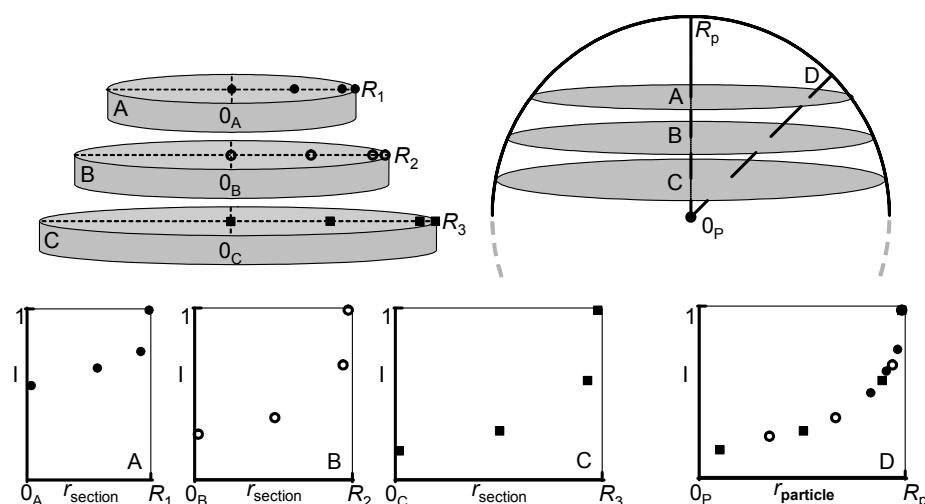


Figure 2. Schematic representation of the intensity profile of three different sections A, B and C, with respective radii  $R_1$ ,  $R_2$  and  $R_3$ . The intensity profiles were discretely measured at the section rim,  $3\ \mu\text{m}$  inward, halfway the sections and in the section center ( $0_A$ ,  $0_B$ , and  $0_C$ , respectively). The three section profiles were transformed to a particle profile (from  $0_p$  to  $R_p$ ). Note that section A gives less information on the total intra-particle enzyme distribution compared to section C, which is closer to the center of mass of the particle.



section positions need to be converted into positions in the original particle. This procedure was described previously (Van Roon *et al.*, 2005<sup>a</sup>) and is schematically shown in Figure 2.

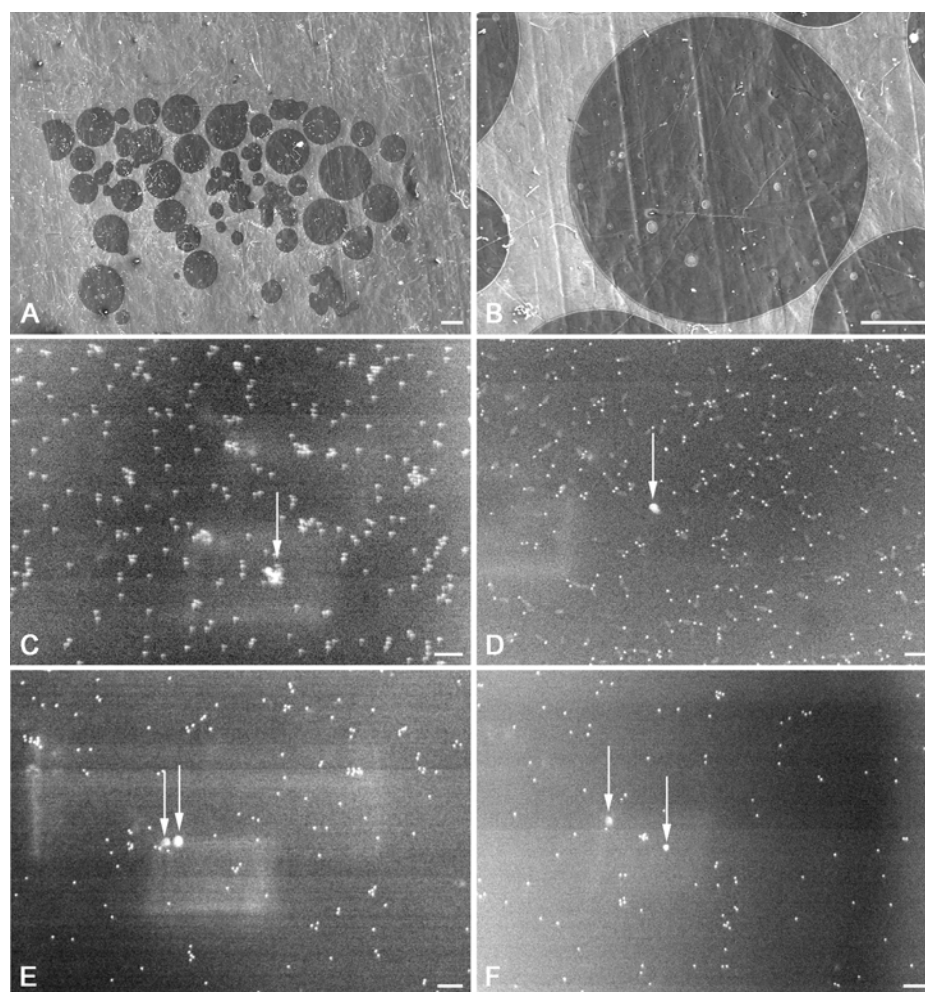


Figure 3. Micrographs of a resin section through Assemblase<sup>®</sup> particles. The section was attached to carbon foil and detected with FESEM in SE mode. a: Low-magnification overview of a resin section through many Assemblase<sup>®</sup> particles. Bar = 100  $\mu\text{m}$ . b: Detail of the largest section in the overview. Bar = 100  $\mu\text{m}$ . c-f: High-magnification micrographs of the section presented in Figure 3b. The penicillin-G acylase was labeled with 10 nm gold particles and micrographs were taken at the surface, 3  $\mu\text{m}$  inwards, halfway the section, and in the center of the section, respectively. Contamination spots, due to dwell time at high magnification, are clearly distinguishable (arrows). Bars = 100 nm.

Neither the exact section position within the particle, nor the size of the originating particle was known beforehand: Assemblase<sup>®</sup> is polydisperse and many different sized particles were embedded within a single sample (Figure 3a). Therefore, the section adjacent to the one observed with FESEM was placed on a glass microscopic slide and located by LM. Its radius was measured and this process was repeated for the other sections at different positions throughout the particle (all on glass microscopic slides). Because the distance between these sections was accurately known, the particle radius and the position of the FESEM section within the particle could be calculated (Van Roon *et al.*, 2005<sup>a</sup>). From this, the section enzyme profile that was observed with FESEM could be translated into an intra-particle enzyme profile (Figure 2). Because of the broad particle size distribution of Assemblase<sup>®</sup>, several different sized particles had to be recorded and analyzed by FESEM.

#### **FESEM AS AN LM ALTERNATIVE: GLOBAL ENZYME HETEROGENEITY**

Measurement of the section enzyme distribution was done at specific locations within a section: at high magnification the 10 nm gold particles were individually visible. This results in a small area that is covered within a single micrograph. Within this area, differences in label density were assumed to be absent. As an example, Figures 3c-3f show micrographs of the enzyme densities at the positions indicated schematically in Figure 2, i.e. at the rim of a section, just under the rim (2-3  $\mu\text{m}$  inward), halfway through the section, and in the center of the section, respectively. Within one micrograph, no differences in label density are observed. On the other hand, the heterogeneity in enzyme density is clearly evident. At the rim of the cross section (Figure 3c), the label density is higher than inside the particle (Figure 3d). The enzyme density decreases further inside

Figures 3c-f show that the intra-particle enzyme distribution matches previous findings in qualitative terms (Van Roon *et al.*, 2005<sup>a</sup>, Van Roon *et al.*, 2005<sup>b</sup>) and are expected to be quantitatively identical. This assumption was checked for multiple particles, of which one example is given in Figure 4. The enzyme densities at the four positions in the section (Figures 3c-f) were converted into positions in the original particle, and subsequently compared to the model prediction for the intra-particle enzyme profile of an equally-sized particle, based on the previous LM work (Van Roon *et al.* 2005<sup>a</sup>). Figure 4 shows that the quantitative agreement between the measurements and the model prediction is

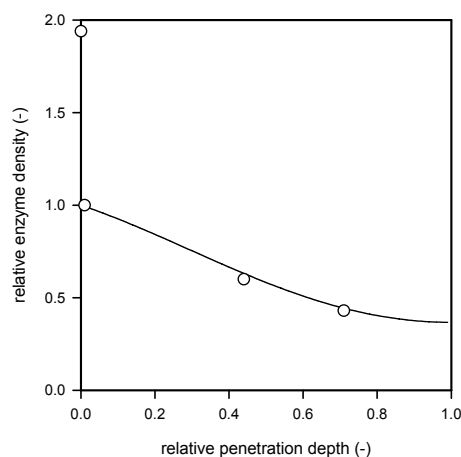


Figure 4. Example of a surface-normalized *particle* enzyme density profile calculated from the measured *section* gold-label densities presented in Figures 3c-f, i.e. at the particle perimeter, 3  $\mu\text{m}$  inward, halfway the section and in the center of the section, respectively (○). The particle radius (173  $\mu\text{m}$ ) was calculated from the measured section radius (168  $\mu\text{m}$ ). The data are in close agreement with the model prediction (—) from previous LM-based work (Van Roon *et al.*, 2004).

good. Note that the model is only valid inside the particle and does not cover the elevated concentration at the particle perimeter.

#### FESEM AS A TEM ALTERNATIVE: LOCAL ENZYME HETEROGENEITY

Previous TEM experiments showed that the enzyme density was abruptly elevated at the particle surface and in the immediate surroundings of intra-particle holes (Van Roon *et al.*, 2005<sup>b</sup>). The areas of increased enzyme density surrounding these macro-voids were designated as “halos”.

Figure 4 showed that the enzyme surface density of the particle was abruptly elevated and approximately 2 times higher than that just a few micrometers inside the particle. This distribution is in agreement with the TEM experiments, in which a similar increase was found near the particle surface. Also the area surrounding the macro-voids (the halo) was found to be abruptly enriched in enzyme. As an example, the enzyme density observed with the FESEM measurements inside the halo was compared to the normal “average” surrounding area in Figures 5a and 5b, respectively. The enzyme density in the halo was found to increase rather abruptly by almost a factor 6 compared with its immediate surroundings. This result is in good agreement with previous TEM experiments that showed abrupt enzyme density increases inside the halo of a factor 4 to 8 (Van Roon *et al.*, 2005<sup>b</sup>).

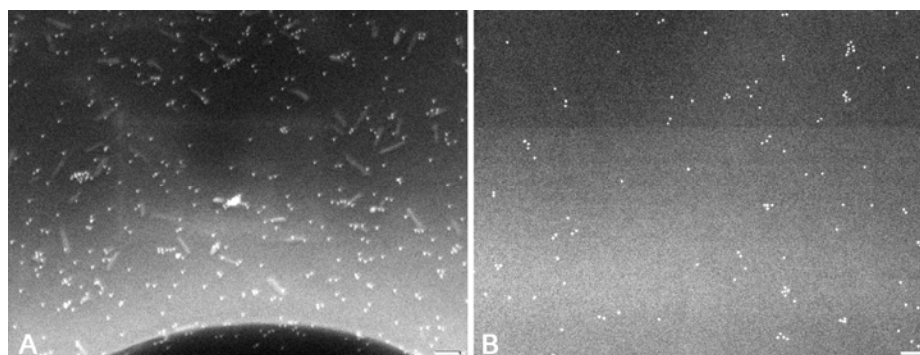


Figure 5. Example of micrographs of an Assemblase<sup>®</sup> section near a macro-void, detected with FESEM in SE mode. The enzyme density in the area directly surrounding the macro-void (black hole at the bottom of the micrograph in Figure 5a) is almost 6 times higher than that in the area just outside the halo (Figure 5b). See also Figure 6 for a micrograph on the morphology of the halo). Bars = 100 nm.

As far as the detection of the enzyme densities is concerned, FESEM is very well suited to quantitatively determining intra-particle enzyme heterogeneity at various levels of detail within a single sample. The global enzyme heterogeneity, i.e. the overall intra-particle enzyme distribution, was in good agreement with previous LM results, and local deviations of this gradient, i.e. the high-resolution local enzyme heterogeneities, were also in agreement with TEM results.

#### **FESEM AS A CRYO-FESEM ALTERNATIVE: MATRIX MORPHOLOGY**

To study the morphology of the Assemblase<sup>®</sup>, the carbon foil with the labeled sections was removed from the microscope, sputter coated with approximately 10 nm platinum and observed again in SE mode in the FESEM. Figure 6a shows the platinum-coated section that was previously shown in Figure 3b. Two areas were investigated in detail: the rim of the section and the area surrounding internal macro-voids. In Figure 6b, which depicts the rim of the section, at the left side of the micrograph the carbon-foil onto which the section is attached is visible; at the right side of the micrograph, the interior of the particle section is visible. At the rim of the section, a structure is observed of approximately 1  $\mu\text{m}$  thickness that protrudes above the plane of section. Because the matrix-supporting resin (BMM) was washed away before labeling, and all water was removed from the labeled sections during air-drying, the elevated matrix level at the particle surface indicates that the total solid fraction (polymer content) was locally higher (and,

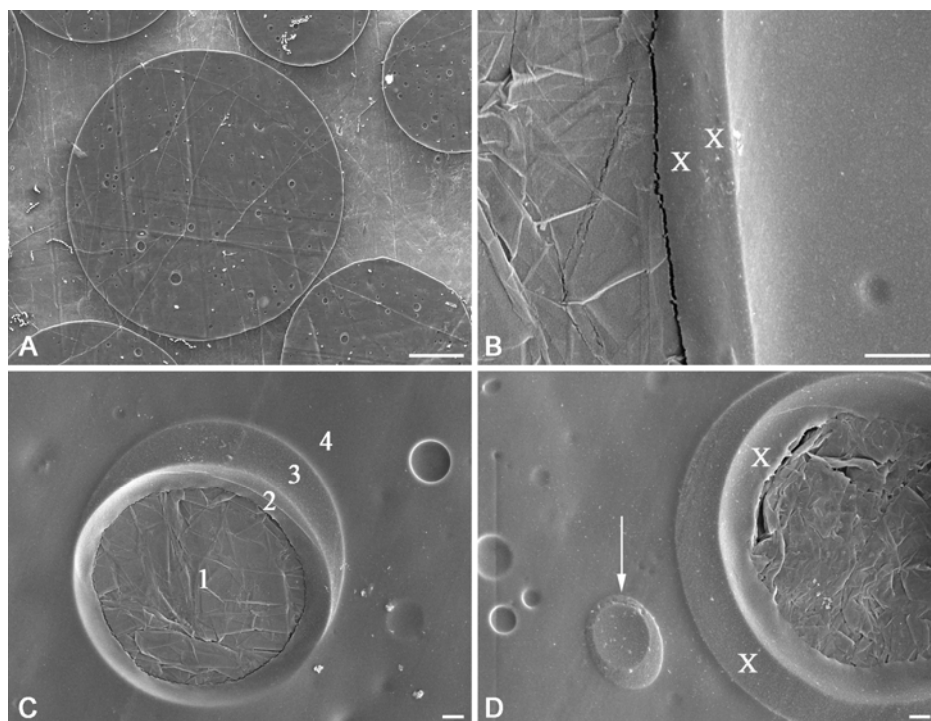


Figure 6. Platinum-coated Assemblase<sup>®</sup> section, detected with FESEM in SE mode. a: Overview of the sputter-coated section (the enzyme distribution of this was previously investigated in Figure 3). Bar = 100  $\mu\text{m}$ . b: Detail of the section (right) onto the carbon foil (left). At the rim of the section, a top layer of approximately 1  $\mu\text{m}$  is visible that is elevated above the plane of the internal “average” support material (X-signs). Bar = 1  $\mu\text{m}$ . c: Immediately surrounding the internal macrovoids (the carbon foil is visible in the center of the micrograph; 1) the support material is abruptly elevated again (2), and continues in a somewhat lower but still elevated level in the halo (3). At the end of the halo the matrix level abruptly drops to the average matrix level (4). Bar = 1  $\mu\text{m}$ . d: The void in the lower left corner (arrow) ends in the section (no carbon foil is visible) and is completely surrounded with the material the halo is made of. Bar = 1  $\mu\text{m}$ .

correspondingly, the water fraction was lower). This agrees with our previous results: it was shown with ambient-temperature FESEM on critical point dried samples that the water content at the surface of the particles was lower natively (Van Roon *et al.*, 2005<sup>b</sup>). It was concluded therefore that the observed density increase in the frozen samples of this study, was not caused (exclusively) by radial shrinkage, but reflect real density differences.

The interior of the particle showed a homogeneous composition. The only exception to this observation was found near the internal macro voids where the same halo-shaped structures were observed as with the previous cryo-FESEM experiments on cryo-planed samples (Van Roon *et al.*, 2005<sup>b</sup>). In Figure 6c, a typical example of such a macro-void and its surrounding matrix structure is depicted. The center of the micrograph depicts a macro-void with a diameter of approximately 9  $\mu\text{m}$ . In its center, the carbon-foil onto which the section was attached is visible (1). In the peripheral region of the micrograph, the general (average) matrix is visible (4). Immediately surrounding the macro-void, the level of the matrix material rapidly increases and rises above that of the average matrix level (2). Then the level drops a little, but continues to be elevated throughout the sickle-shaped halo area (3). This elevated matrix level then abruptly drops to the average level at the end of the halo (the “rim” of the halo can clearly be distinguished). Similar to the elevation of the matrix level at the particle perimeter, the elevated level of the matrix material surrounding the internal macro-voids indicates a higher local solid content. This observation is in agreement with previous studies (Van Roon *et al.*, 2005<sup>b</sup>).

The elevated dry matter content pointed in the direction of chitosan enrichment (Van Roon *et al.*, 2005<sup>b</sup>). Being the most hydrophobic polymer, chitosan binds less water in swollen state in comparison with gelatin (Yin *et al.*, 1999). Due to this low swelling value, chitosan enriched areas are expected to settle less upon drying (water removal) of the sample than the continuous average matrix material, leaving them elevated above the average matrix surface. Local chitosan enrichment, as an explanation for the local increase in dry matter content, corresponds to the significantly elevated enzyme density in these areas: chitosan is expected to have a much higher enzyme binding capacity per unit mass than gelatin. Chitosan contains one primary amino group for enzyme binding per sugar residue, whereas gelatin only contains approximately one basic residue for enzyme binding for every thirty amino acids in its chain. Chitosan enrichment would therefore result in a simultaneous increase in dry matter content and in enzyme binding capacity. Therefore, this is expected to be the dominant causal mechanism.

In some cases, the halo surrounds the entire macro-void (Figure 6d): in the lower-left corner a section (arrow) was cut just through the lowest part of a macro-void.

The void ends within the section of 3.00  $\mu\text{m}$  thickness (no carbon-foil is visible) and is completely surrounded by the halo, the level of which is elevated above that of the surrounding matrix material. Figures 6b and 6d show (x signs) that the elevation of the matrix material is not abrupt, but progresses. This supposedly happened during the drying of the labeled sections. The bottom of the sections was presumably firmly attached to the carbon foil, which resulted in progressive shrinkage during drying of the section.

#### **COMPATIBILITY OF THE METHOD FOR DETERMINATION OF STRUCTURE-FUNCTION RELATIONS**

FESEM shows that immunological and morphological aspects of Assemblase<sup>®</sup> particles could be evaluated adequately within one sample. This integrated approach simplifies the determination of the relation between these (often very local) properties because no complicating comparison between equivalent areas in different samples, which have undergone different preparations, is necessary. The integrated approach used in this study accelerates the characterization process considerably, because only the development of a single sample preparation and detection procedure is required.

#### **ADDITIONAL FESEM ADVANTAGES**

Obviously, a single-method preparation and detection avoids the interpretation problems that hamper analysis in case of multiple preparation and detection. For highly heterogeneous systems, such as Assemblase<sup>®</sup>, this approach simplifies the analysis of morphology-enzyme density relations. Further advantages result from FESEM being a scanning technique. The applicable specimen size in a FESEM study is virtually unlimited and no interfering signals are present from the metal grid bars underneath TEM samples. This is a clear advantage for the large Assemblase<sup>®</sup> particles. In contrast to TEM, the sections for FESEM do not have to be ultra-thin. Embedding, which is difficult for large particles like Assemblase<sup>®</sup>, is therefore less critical. Additionally, in thick samples the sensitivity increases towards the presence of enzyme and towards differences in enzyme loading, because also epitopes inside the entire volume of the section are available for labeling.

## CONCLUSION

This paper demonstrated that FESEM detection is well suited for the quantitative determination of the global intra-particle enzyme gradient of Assemblase<sup>®</sup>. The analysis of the enzyme density at discrete positions resulted in an identical global intra-particle enzyme profile compared to previous LM work. Also, the local heterogeneities in enzyme density were observed and were interchangeable with the TEM experiments.

In addition, the morphology of the same sample was observed with the same equipment, without any further sample manipulations (apart from sputter coating), and was compared to the previously cryo-FESEM observed morphology of cryo-fixated and cryo-planed samples. Although the structural detail of the Assemblase<sup>®</sup> interior that was observed with the present method was not as discrete as that observed with cryo-FESEM, the elevated areas at the particle surface and surrounding the internal macro-voids were identical in size and shape.

Furthermore, the same conclusions were drawn regarding the composition of these areas: they are enriched in chitosan. The relation that exists between the heterogeneity in enzyme loading and heterogeneity in particle morphology in Assemblase<sup>®</sup> particles that could only be established after extensive combination of TEM and cryo-FESEM experiments, became evident using only the integrated FESEM experiments.

Another advantage of the use of FESEM is that the sample size that can be studied is virtually unlimited. Due to the relative unimportance of the section thickness, the technique puts fewer constraints on the embedding and sectioning procedures, which can be a big advantage for relatively large samples such as Assemblase<sup>®</sup>. Additionally, in depth enzyme labeling in the relatively thick sections would make the method more sensitive than TEM on ultra-thin sections. Obviously, this integrated approach only requires a FESEM, without the need of a cryo-stage or an additional TEM. These aspects make the analysis of the relation between (local) particle morphology and (local) enzyme distribution relations easier and quicker. Insight in these types of relations is important, because it may be used for future design of enzyme distributions in which the particle morphology can be used as a(n) (extra) control parameter.



## ACKNOWLEDGEMENTS

Mr. Marten Paasman (DSM Anti Infectives) is kindly acknowledged for valuable discussions. DSM and The Ministry of Economic Affairs of the Netherlands are kindly acknowledged for their financial support. Mr. Henk Kieft (Wageningen University) is kindly acknowledged for his expert help in sample preparation.

## REFERENCES

- Baskin T.I., Busby C.H., Fowke L.C., Sammut M., and Gubler F. (1992). Improvements in immunostaining samples embedded in methacrylate: Localization of microtubules and other antigens throughout developing organs in plants of diverse taxa. *Planta* **187**: 405-413.
- De Vroom E. (1997). An improved immobilized penicillin G acylase. *International patent application* WO 97/04086.
- Harder A., De Haan B.R., and Van Der Plaat J.B. (1987). Novel immobilized biocatalysts and their preparation and use. *International Patent Application Gist-brocades* EP 0222462B1.
- Hossain, Md.M., and Do D.D. (1989). General Theory of Determining Intraparticle Active Immobilized Enzyme Distribution and Rate Parameters. *Biotechnol. Bioeng.* **33**: 963-975.
- Kaasgaard S.G., Karlsen L.G., and Schneider I. (1992). Process for separation of two solid components. *International patent application* WO 92/12782.
- Scharer A., Hossain, Md.M., and Do D.D. (1992). Determination of total and active immobilized enzyme distribution in porous solid supports. *Biotechnol. Bioeng.* **39**: 679-687.
- Schroën C.G.P.H., Nierstrasz V.A., Moody H.M., Hoogschagen M.J., Kroon P.J., Bosma R., Beeftink H.H., Janssen A.E.M., and Tramper J. (2001). Modeling of the enzymatic kinetic synthesis of cephalixin - Influence of substrate concentration and temperature. *Biotechnol. Bioeng.* **73**: 171-178.
- Schroën C.G.P.H., Fretz C.B., De Bruin V.H., Berendsen W., Moody H.M., Roos E.C., Van Roon J.L., Kroon P.J., Strubel M., Janssen A.E.M., and Tramper J. (2002). Modelling of the enzymatic kinetically controlled synthesis of cephalixin: influence of diffusion limitation. *Biotechnol. Bioeng.* **80**: 331-340.
- Straathof A.J.J., Panke S., and Schmid A. (2002). The production of fine chemicals by biotransformations. *Curr. Opin. Biotechnol.* **13**: 548-556.
- Tramper J., Beeftink H.H., Janssen A.E.M., Ooijkaas L.P., Van Roon J.L., Strubel M., and Schroën C.G.P.H. (2001). Biocatalytic production of semi-synthetic cephalosporins: process technology and integration. In: *Synthesis of  $\beta$ -lactam Antibiotics: Chemistry, Biocatalysis & Process Integration* (A. Bruggink, ed.). Kluwer Academic Publishers, Dordrecht.
- Van Roon J.L., Beeftink H.H., Schroën C.G.P.H., and Tramper J. (2002). Assessment of intraparticle biocatalytic distributions as a tool in rational formulation. *Curr. Opin. Biotechnol.* **13**: 398-405.

- Van Roon J.L., Groenendijk E., Kieft H., Schroën C.G.P.H., Tramper J., and Beftink H.H.** (2005<sup>a</sup>). Novel approach to quantify immobilized-enzyme distributions. *Biotechnol. Bioeng.* **89**: 660-669.
- Van Roon J.L., Boom R.M., Paasman M., Tramper J., Schroën C.G.P.H., and Beftink H.H.** (2005<sup>b</sup>) Enzyme distribution and matrix characteristics in biocatalytic particles. *J. Biotechnol.*, accepted for publication.
- Yin Y.J., Yao K.D., Cheng G.X., and Ma J.B.** (1999). Properties of polyelectrolyte complex films of chitosan and gelatin. *Polym. Intern.* **48**: 429-432.

---

## Chapter 7 A multi-component reaction-diffusion model of a heterogeneously distributed immobilized enzyme

The contents of this chapter have been submitted for publication as:

**J.L. van Roon, M.M.H.D. Arntz, A.I. Kallenberg, M.A. Paasman, J. Tramper, C.G.P.H. Schroën, H.H. Beftink** (2005). A multi-component reaction-diffusion model of a heterogeneously distributed immobilized enzyme. *Appl.Microbiol.Biotechnol.*

## ABSTRACT

A physical model was derived for the synthesis of the antibiotic cephalexin with an industrial immobilized penicillin-G acylase, called Assemblase<sup>®</sup>. In reactions catalyzed by Assemblase<sup>®</sup>, less product and more by-product is formed in comparison with a free-enzyme catalyzed reaction. The model incorporates reaction with a heterogeneous enzyme distribution, electrostatically coupled transport and pH-dependent dissociation behavior of reactants and is used to obtain insight in the complex interplay between these individual processes leading to the sub-optimal conversion. The model was successfully validated with synthesis experiments for conditions ranging from heavily diffusion limited to hardly diffusion limited, including substrate concentrations from 50 to 600 mM, temperatures between 273 and 303 K and pH's between 6 and 9. During the conversion of the substrates into cephalexin, severe pH gradients inside the biocatalytic particle, which were previously measured by others, were predicted. Physical insight in such intra-particle process dynamics may give important clues for future biocatalyst design. The modular construction of the model may also facilitate its use for other bioconversions with other biocatalysts.

## INTRODUCTION

Because biocatalyst costs usually are relatively important in bioconversions, they are often immobilized to enhance their stability and facilitate their reuse or continuous utilization (Tramper *et al.*, 2001). During a biocatalytic conversion with an immobilized enzyme, the net fluxes of substrates and products in and out the biocatalytic particles, are –in case of a diffusion-controlled transport– driven by radial concentration gradients of the reactants. The local steepness of these gradients is determined by a balance between conversion rates, and transport rates and therefore depends on particle size, enzyme loading, particle porosity and intra-particle reactant diffusivity. As a result of intra-particle reactant gradients, the immobilized biocatalyst operates at concentrations that differ from external bulk liquid concentrations, which is often reflected in the effectiveness factor of a biocatalytic particle. If, however, multiple reactions are involved, differences in reactant diffusivities may additionally cause a shift in the relative reaction rates, promoting or inhibiting wanted and unwanted reactions. An example of a system in which such phenomena are relevant is the Assemblase<sup>®</sup>-catalyzed cephalixin synthesis (Fig. 1).

Assemblase<sup>®</sup> is an in-house biocatalytic particle of DSM Anti-Infectives (Delft, The Netherlands). It contains an immobilized penicillin-G acylase that catalyzes,

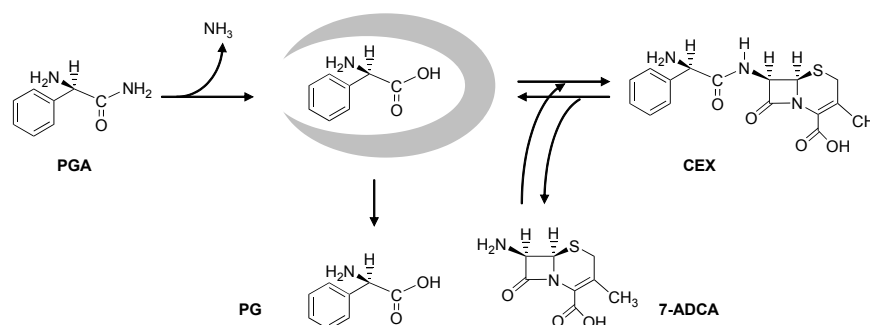


Figure 1. Production of cephalixin (CEX) from D-(-)-phenylglycine (PGA) and 7-amino deacetoxy cephalosporinic acid (7-ADCA) via an enzyme phenylglycine complex (gray). Besides the CEX synthesis reaction, the enzyme also catalyzes two unwanted side-reactions: PGA and CEX hydrolysis respectively.

among others, the synthesis of the widely used semi-synthetic antibiotic cephalixin. A single batch was donated for the present research and in all instances where the trademark Assemblase<sup>®</sup> is used, this refers to this particular preparation. The CEX synthesis reaction catalyzed by Assemblase<sup>®</sup> is kinetically controlled, and the reaction is stopped before thermodynamic equilibrium is reached (Schroën *et al.*, 2001), implying the need for a transient description of the reaction progress. Cephalixin (CEX) synthesis (Fig. 1) involves a 2-step coupling reaction of an amide-activated phenylglycine (PGA) with 7-amino deacetoxy cephalosporinic acid (7-ADCA), via an enzyme-phenylglycine complex. The enzyme also catalyzes two unwanted side reactions. In the first, PGA is hydrolyzed to the inactive by-product D-(-)-phenylglycine (PG). In the second, CEX is hydrolyzed to yield 7-ADCA and PG. Schroën *et al.* showed that transport of multiple reactants limited each reaction differently (2002). Overall, it was shown that diffusion limitations in Assemblase<sup>®</sup> cause a reduced cephalixin production rate, a reduced yield on substrate, and an increased formation rate of the un-wanted by-product PG in comparison with the free enzyme (Schroën *et al.*, 2002). On top of that, the intra-particle enzyme distribution of Assemblase<sup>®</sup> was found to be heterogeneous (Van Roon *et al.*, 2005<sup>a</sup>), which is expected to have a severe impact on the macroscopic particle behavior as well.

In order to describe the behavior of the immobilized biocatalyst, various types of models can be used, which may differ in the amount of detail in which physical and chemical processes are accounted for. Schroën and co-workers (2002) adapted their own model for free penicillin-G acylase kinetics to one for Assemblase<sup>®</sup> by lumping all relevant phenomena of the biocatalytic particle into a new set of fitted pseudo-kinetic constants. Although their description of macroscopically observed kinetics was quite good, the fitted constants are only valid for the reaction conditions and biocatalyst preparation they were derived for. Such lumped models are not suited for rational design of new biocatalytic particles, since the constants relate to multiple effects simultaneously. It is obvious that for this specific purpose, a physical model, which accounts for reaction kinetics and mass transfer separately, should be used. This requires extensive knowledge on all the relevant processes in the system, which may be time consuming, but is indispensable for rational biocatalyst design.

In this paper we present a model that is based on enzyme kinetics of free enzyme, mass transfer in the biocatalytic particle and the enzyme gradient that is present inside the biocatalytic particle. All these aspects were studied and the obtained constants are truly independent of each other, unlike the constants in the lumped model.

Intrinsic kinetic constants and activation enthalpies (temperature dependence) for the freely suspended form of penicillin-G acylase were adopted from Schroën *et al.* (2002). The activity of the free enzyme as a function of the pH was measured and included in our Assemblase<sup>®</sup> model. Effective diffusivities of all substrates and products were measured. The enzyme loading and enzyme distribution in the Assemblase<sup>®</sup> particles were previously measured as a function of the particle radius (Van Roon *et al.*, 2003), which led to the definition of a single, spherical particle with a characteristic size, enzyme loading and enzyme distribution.

An aspect that also is of importance is that all reactants in cephalixin synthesis are weak electrolytes. The charge of the reactants depends on the local pH in the biocatalytic particle. Duggleby (1995) and Svedas (1980) showed that the enzyme has a single amino acid catalytic center and uses one particular charged form of the reactant only. Because the dissociation constants (pKa values) of substrates and products are different, local enzymatic conversion will result in a change in pH. The fact that all reactants are weak electrolytes also implies that their transport is coupled electrostatically. Electrostatic interactions were modeled by using the Nernst-Planck flux equation for each charged component (e.g. Perry and Green, 1997). Based on local transport of reactants and local enzyme kinetics, the pH-gradients were predicted, which were used to calculate the local average charge of each weak electrolyte and the local enzyme activity.

The phenomena mentioned before, enzyme kinetics, mass transfer, enzyme distribution and dissociation effects, give an impression of the phenomena needed to be modeled for the dynamic description of cephalixin synthesis. In literature, several papers are published that focus on some of these phenomena. Intrinsic kinetic parameters have been published by Schroën *et al.* (2002). In literature, papers on all sorts of reaction-diffusion systems can be found. Van der Wielen and co-workers (1997) modeled the enzymatic deacylation of penicillin G into phenylacetic acid and 6-aminopenicillanic acid taking coupled electrostatic transport of ionic species into account. The influence of heterogeneous enzyme

distributions in systems with non-ionic reactants and with relatively simple enzyme kinetics (zero<sup>th</sup> order, first order and Michaelis-Menten) was investigated by Do and Hossain (1989 and 1986), who fitted some extreme intra-particle enzyme distributions to macroscopic data sets.

To the best of our knowledge, all these aspects are now brought together for the first time for one immobilized biocatalytic system. The prediction of the macroscopic course of the reaction was successfully validated against experimental data for various temperatures, external pH's, enzyme loadings, and substrate concentrations. The model was used to evaluate the effects of various alterations to the biocatalytic particles, such as alternative enzyme loadings and distributions. In this light, the potential use of the model for biocatalyst improvement is discussed.

## MODEL

### DEFINITION OF A MODEL SYSTEM

As stated previously, the model is based on enzyme kinetics, enzyme distribution inside the biocatalytic particle and mass transfer of all reactants. Since we are dealing with charged components, also dissociation has to be taken into account. For cephalixin synthesis with Assemblase<sup>®</sup>, the terms for mass transfer, association/dissociation and enzyme kinetic rates are stated in Equation [7.1]:

$$\left( \frac{dc_{\text{CEX}^-}}{dt} \right)_{\text{in}} = M_{\text{CEX}^-} + r_{\text{CEX}} + R_{\text{CEX}^-} \quad [7.1]$$

The change of the concentration of (negatively charged) cephalixin  $c_{\text{CEX}^-}$  (mol·m<sup>-3</sup>) in time  $t$  (s) involves a mass transport rate of the (negatively charged) cephalixin  $M_{\text{CEX}^-}$  (mol·m<sup>-3</sup>·s<sup>-1</sup>), the dissociation rate  $r_{\text{CEX}}$  of cephalixin (mol·m<sup>-3</sup>·s<sup>-1</sup>), and the conversion rate  $R_{\text{CEX}^-}$  of the (negatively charged) cephalixin. In order to understand the mechanisms resulting in Assemblase<sup>®</sup> behavior (in comparison with the reaction catalyzed by the free enzyme), each of these three contributing rates will be discussed in greater detail in this section. Before we do so, some basic particle characteristics are defined first.



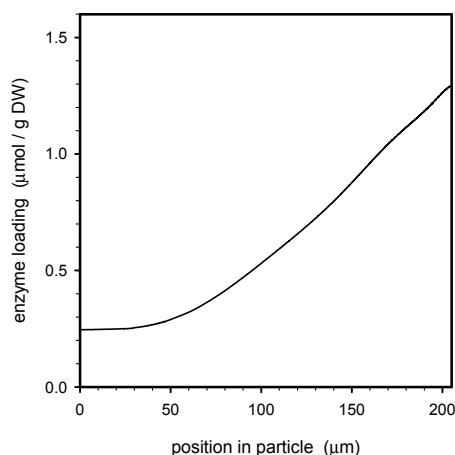


Figure 2. Characteristic intra-particle enzyme profile for the characteristic Assemblase particle. The enzyme profile corresponds with a Fourier value 0.082 with an average enzyme loading of 0.95  $\mu\text{mol/g DW}$ .

## PARTICLE

### *Geometry and particle size*

In previous work it was shown that Assemblase<sup>®</sup> particles are polydisperse (Van Roon *et al.*, 2003) and, to some extent, polymorph (Van Roon *et al.*, 2005<sup>b</sup>). A formal treatment of mass transfer processes in such particles would involve an exact three-dimensional analysis of each particle and its contribution to the total volume (or mass) of biocatalytic particles, which is extremely laborious. Instead, spherical particle geometry was assumed; Scanning Electron Microscopic (SEM) micrographs of super-critically dried Assemblase<sup>®</sup> particles (Chapter 5, Fig. 5a) illustrate that this assumption is not too far off. From the particle size distribution (Van Roon *et al.*, 2003), a characteristic particle was defined as particle the at the 50% point of the cumulative volume distribution (205  $\mu\text{m}$  radius). Assemblase<sup>®</sup> was modeled as if it consisted of spherical particles of this radius exclusively.

### *Enzyme loading and enzyme distribution*

Previously, the enzyme loading and distribution was measured for multiple particle sizes (Van Roon *et al.*, 2005<sup>a</sup>). It was shown that all size-dependent intra-particle enzyme profiles of Assemblase<sup>®</sup> had the mathematical shape of stationary enzyme diffusion and could be described with a Fourier relation as a function of the particle radius. Based on this, the actual enzyme gradient was interpolated for the particle with the characteristics size. This relative distribution

was combined with the measured active enzyme loading of 0.95  $\mu\text{mol/g}$  dry weight (DW) and a solidity (g dry weight per g wet weight) of 0.13 (Van Roon *et al.*, 2003) to obtain the quantitative active enzyme distribution of the characteristic particle (Fig. 2). The enzyme gradient in Fig. 2 corresponds with a Fourier value of  $8.2 \cdot 10^{-2}$  (-) with a standard deviation of  $9.7 \cdot 10^{-3}$  (-) and is in very good agreement with the gradient that was measured for a particle of 210  $\mu\text{m}$  radius (Van Roon *et al.*, 2003).

## KINETICS

### *Intrinsic enzyme kinetics*

Schroën *et al.* derived kinetic equations for product and by-product formation using the King-Altman approach (Schroën *et al.*, 2002). Duggleby and Svedas *et al.* (1995 and 1980, respectively) found that the enzyme only binds the PGA and 7-ADCA if the amino-group is neutral (the carboxylic acid group can be either negatively charged or neutral). For this, the rates are expressed in terms of concentrations of the active form:

$$\begin{aligned} R_{\text{PGA}^0} &= (-k_1 k'_2 c_{\text{PGA}^0} - k_1 k_3 c_{7\text{-ADCA}^-} c_{\text{PGA}^0}) \cdot E_0 / \Sigma \\ R_{\text{CEX}^-} &= (k_1 k_3 c_{\text{PGA}^0} c_{7\text{-ADCA}^-} - k'_2 k_{-3} c_{\text{CEX}^-}) \cdot E_0 / \Sigma \\ R_{\text{PG}^0} &= (k_1 k'_2 c_{\text{PGA}^0} + k'_2 k_{-3} c_{\text{CEX}^-}) \cdot E_0 / \Sigma \\ \Sigma &= k_1 c_{\text{PGA}^0} + k'_2 + k_3 c_{7\text{-ADCA}^-} + k_{-3} c_{\text{CEX}^-} \end{aligned} \quad [7.2]$$

with  $R_{\text{PGA}^0}$ ,  $R_{\text{CEX}^-}$  and  $R_{\text{PG}^0}$  the net rates for neutral  $\text{PGA}^0$ , negatively charged  $\text{CEX}^-$  and neutral  $\text{PG}^0$  production ( $\text{mol} \cdot \text{m}^{-3} \cdot \text{s}^{-1}$ ), respectively, and  $E_0$  the initial enzyme concentration (g enzyme per g total). The enzyme can only convert substrates with a neutral amino-group. Being weak electrolytes, the fraction of a particular reactant that is present in its active form depends on the local pH via its dissociation constant  $K_a$  ( $\text{mol} \cdot \text{m}^{-3}$ ). As an example, Equation [7.3] shows the dissociation of  $\text{CEX}^0$  into  $\text{CEX}^-$ :



The concentrations of  $\text{CEX}^0$  and  $\text{CEX}^-$  are related via the equilibrium constant  $K_{\text{CEX}}$  ( $\text{mol}\cdot\text{m}^{-3}$ ):

$$K_{\text{CEX}} = \frac{c_{\text{CEX}^-} c_{\text{H}^+}}{c_{\text{CEX}^0}} \bigg|_{\text{eq}} \quad [7.4]$$

Obviously, for all other reactants, similar equations hold and should be taken into account in the model (see also Table 1). Other components present are  $\text{Na}^+$ , which is the counter ion, and  $\text{NH}_3$ , which is liberated during the binding step of PGA with the enzyme.

### ***Temperature and pH dependency of the enzyme***

For the temperature dependency of all reaction rate constants, the Arrhenius equation was used (Van 't Riet and Tramper, 1991), because the activation enthalpies (reaction enthalpies) were assumed to be constant. Data for free enzyme were taken from Schroën *et al.* (2002):

$$k_{k,T} = k_{k,T_{\text{ref}}} e^{\frac{-\Delta H_k}{R} \left( \frac{1}{T} - \frac{1}{T_{\text{ref}}} \right)} \quad [7.5]$$

with  $k_{k,T}$  the reaction rate constant at temperature  $T$ ,  $k_{k,T_{\text{ref}}}$  the reaction rate constant at reference temperature ( $T_{\text{ref}}$ ) 293 K, and  $\Delta H_k$  the reaction enthalpy ( $\text{kJ}\cdot\text{mol}^{-1}$ ).

The enzyme activity as a function of pH was investigated with free suspended penicillin-G acylase. The relative activity was assessed between 6.0 and 9.0 (with 0.5 pH unit intervals) in cephalixin synthesis experiments from 100 mM PGA and 100 mM 7-ADCA at 293 K containing 0.59  $\mu\text{M}$  penicillin-G acylase. Between 6.0 and 8.0, the relative activity was constant (data not shown). At pH 9.0, 80% residual activity (compared to pH 8.0) remained; the enzyme activity in the model was adjusted accordingly.

### **MASS TRANSFER**

The diffusivities of the reactants were measured at 293K. At other temperatures, the diffusivities were corrected by application of the generally applied Stokes-Einstein relation (e.g. Bird *et al.*, 1960). Based on the measured diffusivities at

293 K, this equation was first used to estimate the hydrodynamic reactant radius. Subsequently, combination with tabulated values of the dynamic viscosity of water (e.g. Handbook of Chemistry and Physics, 1980) as a function of temperature led to an estimate of the diffusivity at other temperatures.

### ***Location of mass transfer resistance***

It was determined whether there were large differences in the internal and external mass transfer resistance. If so, the model only needs to describe the processes in the most limited region. The Biot (Bi) number of an arbitrary component describes the dimensionless ratio of the internal and external mass transfer resistance the component  $k$  encounters in the system, and is defined as:

$$Bi_k = \frac{k_{l,k} d_p}{D_{\text{eff},k}} = Sh_k \frac{D_{l,k}}{D_{\text{eff},k}} \quad [7.6]$$

with  $k_{l,k}$  the mass transfer coefficient of component  $k$  in the stagnant layer surrounding the particles,  $d_p$  the particle diameter (m),  $D_{\text{eff},k}$  and  $D_{l,k}$  the intra-particle effective and external free-solution diffusivities of component  $k$  ( $\text{m}^2 \cdot \text{s}^{-1}$ ), respectively, and  $Sh$  the dimensionless Sherwood number for mass transfer, which is the ratio of total mass transfer and diffusive mass transfer in the continuous phase surrounding the particles. The value of the Sherwood number was estimated from the dimensionless Reynolds number. Because the reactor was vigorously stirred turbulent flow was assumed, and Reynolds was therefore estimated to be at least 1000 (Van 't Riet and Tramper, 1991). The Sherwood number was calculated with the empirical relation by Ranz and Marshall, which applies for  $Re > 30$  (Van 't Riet and Tramper, 1991):

$$Sh_k = 2 + 0.57 \sqrt{Re} \left( \frac{\eta_l}{\rho_l D_{l,k}} \right)^{0.33} \quad [7.7]$$

with  $Re$  the dimensionless Reynolds number (-),  $\rho_l$  the water density ( $1000 \text{ kg} \cdot \text{m}^{-3}$ ), and  $\eta_l$  the dynamic viscosity of the continuous phase ( $1 \cdot 10^{-3} \text{ Pa} \cdot \text{s}$ ). With a cephalixin diffusivity of  $4.3 \cdot 10^{-10} \text{ m}^2 \cdot \text{s}^{-1}$  (see Table 2), this resulted in  $Sh=235$ . From equation [7.6] it follows that Biot = 404, i.e. the resistance for mass transfer

was located almost exclusively inside the biocatalytic particle. External mass transfer resistance was therefore neglected in the model.

Because the resistance for mass transfer is situated in the particle interior also the diffusivities of the reactants inside the particles were measured. This was done with a portion of the same preparation of Assemblase<sup>®</sup> particles that was not activated with enzyme. A known amount of these wet sieved (Van Roon *et al.*, 2003) particles was incubated overnight at 277 K and pH 8.0 in a solution in which a known amount of reactant was dissolved. Then the equilibrium concentration of the reactant in the continuous phase was analyzed by HPLC (Van Roon *et al.*, 2003) to check for partitioning. A portion of these particles was transferred into a known amount of water that was vigorously stirred. Immediately, particle-free samples were taken (by use of filters) and the concentration was measured with HPLC. From this, the diffusivity was estimated by fitting a standard parabolic differential equation for Fickian diffusion (e.g. Bird *et al.*, 1960) out of a known mass of spheres of 205  $\mu\text{m}$  radius. As an example, the measured concentrations and fitted concentration profile of PG is given in Fig. 3. The effective PG diffusivity that fitted the data best was  $4.7 \cdot 10^{-10} \text{ m}^2 \cdot \text{s}^{-1}$ . The diffusivities of the other reactants were fitted analogous and their value is given in Table 1.

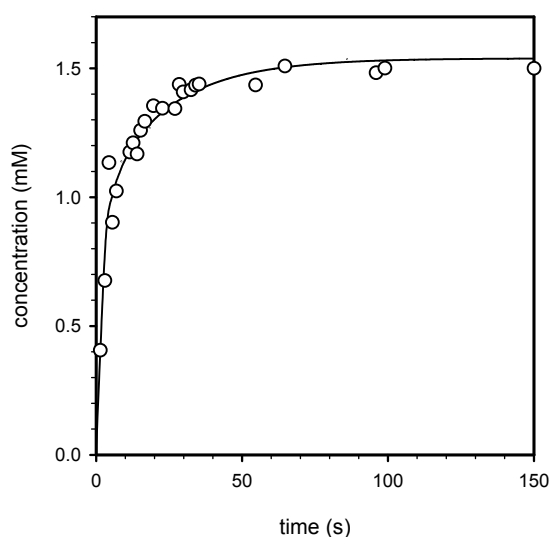


Figure 3. Measured PG concentration in the continuous phase in time (points) and the fitted concentration profile for an effective intra-particle PG diffusivity of  $4.7 \cdot 10^{-10} \text{ m}^2 \cdot \text{s}^{-1}$  at an initial intra particle PG concentration of 19 mmol/kg WW (13% solidity) and 7% w/w particle hold-up

**Mass transport rate and flux equations**

Because the particles are assumed to be spherical, radial symmetry can be assumed and the mass balances can be solved one-dimensionally (along the radial axis). The rate equation for diffusion of species  $k$  into a spherical particle along the space coordinate  $x$  (m):

$$M_k = \frac{1}{x^2} \frac{d}{dx} (x^2 J_k) \quad [7.8]$$

with  $M_k$  the rate of the concentration change of component  $k$  ( $\text{mol}\cdot\text{m}^{-3}\cdot\text{s}^{-1}$ ) and  $J_k$  the mass flux of component  $k$  ( $\text{mol}\cdot\text{m}^{-3}\cdot\text{s}^{-1}$ ). For all components the Nernst-Planck equation was used, which describes the flux of a charged component as a function of a concentration gradient and a potential gradient:

$$J_k = D_{k,\text{eff}} \left( \frac{dc_k}{dx} + z_k c_k \frac{F}{RT} \frac{d\Phi}{dx} \right) \quad [7.9]$$

with  $J_k$  the flux of component  $k$  ( $\text{mol}\cdot\text{m}^{-3}\cdot\text{s}^{-1}$ ),  $z_k$  is the charge of component  $k$  (-),  $F$  the Farraday constant ( $\text{C}\cdot\text{mol}^{-1}$ ),  $R$  the gas constant ( $\text{J}\cdot\text{mol}^{-1}\cdot\text{K}^{-1}$ ),  $T$  the temperature (K), and  $\Phi$  the electrical potential (V). For uncharged components ( $z_k = 0$ ), Equation [7.9] reduces to the Fickian flux equation. The potential gradient was eliminated from the system by assuming a zero net electrical current:

$$\sum_{k=1}^N z_k J_k = 0 \quad [7.10]$$

where  $N$  equals the total number of components (-). From equations [7.9] and [7.10], it can be derived that:

$$\frac{d\Phi}{dx} = - \frac{RT}{F} \frac{\sum_{k=1}^N z_k D_{k,\text{eff}} dc_k / dx}{\sum_{k=1}^N z_k^2 D_{k,\text{eff}} c_k} \quad [7.11]$$

which can be substituted in equation [7.9]:

$$J_k = D_{k,\text{eff}} \left( \frac{dc_k}{dx} - z_k c_k \frac{\sum_{k=1}^N z_k D_{k,\text{eff}} dc_k / dx}{\sum_{k=1}^N z_k^2 D_{k,\text{eff}} c_k} \right) \quad [7.12]$$

### INTERNAL MASS BALANCES

Now all parts of Equation [7.1] have been discussed in more detail, we will focus on the association and dissociation reactions. The (de-)protonation rate ( $r_{\text{CEX}}$ ) from Equation [7.1] is extremely fast in comparison with the enzymatic reaction rates ( $R_{\text{CEX}^-}$  in Equation [7.1]). The different time constants for both processes dramatically increases the stiffness of the system of mass balances and may result in long calculation times or even in numerical instabilities. Therefore, fast (de-)protonation rates were eliminated taking convenient linear combinations of the differential mass balances and regarding the (de-)protonation rates to be infinitely fast in comparison with the enzymatic conversion rates, analogue to the procedure by Van der Wielen (1997). For the example given in Equation [7.1], a suitable linear combination is:

$$\begin{aligned} \left( dc_{\text{CEX}^-} / dt \right)_{\text{in}} &= M_{\text{CEX}^-} + r_{\text{CEX}} + R_{\text{CEX}^-} \\ \left( dc_{\text{CEX}^0} / dt \right)_{\text{in}} &= M_{\text{CEX}^0} - r_{\text{CEX}} \end{aligned} \quad [7.13]$$

The equation illustrates that the neutral form of cephalixin cannot be formed by the enzyme. By addition of these two equations, the fast association rates cancel out. With the assumption of infinitely fast de-protonation reactions, the concentration of neutral cephalixin is instantly dictated by the association constant of cephalixin, and the concentrations of negatively charged cephalixin and protons equation [7.4] and the rate equation becomes:

$$\left( \frac{dc_{\text{CEX}^-}}{dt} \right)_{\text{in}} = \frac{M_{\text{CEX}^-} + M_{\text{CEX}^0} + R_{\text{CEX}^-} - \frac{c_{\text{CEX}^-}}{K_{\text{CEX}}} \frac{dc_{\text{H}^+}}{dt}}{1 + c_{\text{H}^+} / K_{\text{CEX}}} \quad [7.14]$$

Equation [7.14] shows that the concentration change of  $\text{CEX}^-$  in time is not only affected by its enzymatic conversion and the flux of itself, but also by the flux of

Table 1. Dissociation constants for weak electrolytes involved in CEX synthesis and effective intra-particle enzyme diffusivities of reactants at 298 K.

	$\text{PGA}^+/\text{PGA}^0$	$\text{NH}_4^+/\text{NH}_3$	$7\text{-ADCA}^0/7\text{-ADCA}^-$	$\text{CEX}^0/\text{CEX}^-$	$\text{PG}^0/\text{PG}^-$	$\text{H}^+$	$\text{OH}^-$	$\text{Na}^+$	$\text{Cl}^-$
pKa $\text{RNH}_2$ (-)	7.2	9.4	4.9	7.6	9.0	-	-	-	-
pKa $\text{RCOOH}$ (-)	< 1.0	-	3.0	2.6	2.0	-	-	-	-
$D_{\text{eff}}$ ( $10^{-10} \text{ m}^2/\text{s}$ )	4.3 <sup>1</sup>	15 <sup>2</sup>	3.0 <sup>1</sup>	2.5 <sup>1</sup>	4.7 <sup>1</sup>	70 <sup>2</sup>	40 <sup>2</sup>	10 <sup>2</sup>	15 <sup>2</sup>

<sup>1</sup>: measured in this study (see also Figure 2)<sup>2</sup>: estimated at 75% of the free-water diffusion coefficient at infinite dilution (Cussler, 2002).

its uncharged counterpart  $\text{CEX}^0$ . Furthermore, it is also directly affected by the local pH and the pH gradient. The example given above also applies for the other weak electrolytes. The pKa values of all the components in the model are summarized in Table 1.

In all association/dissociation reactions protons are bound or released. For all weak electrolytes, the internal pH-gradient is influenced by all these equilibria and vice versa. An exception to this is 7-ADCA, of which the pKa values are so low that its charge is almost exclusively negative in the pH regions where the reactions take place. Therefore, 7-ADCA is conveniently regarded as a strong electrolyte with a negative charge. Because protons are released or used in the de-protonation and protonation reactions of every weak electrolyte, respectively, the mass balance becomes complex; it is therefore given in the appendix (A1).

#### EXTERNAL MASS BALANCES

The mass balances over the continuous phase surrounding the particles were derived analogous to the internal mass balances. The two differences are the obvious absence of enzyme in the continuous phase of the reactor, and the time dependent volume increase of the water phase, which is a result of titration with hydrochloric acid during the conversion in order to keep the external pH constant. In equations [7.15] and [7.16], the external mass balances for  $\text{PGA}^0$  and  $\text{PGA}^+$  are given:



$$\left( \frac{dc_{\text{PGA}^0}}{dt} \right)_{\text{ex}} = M_{\text{PGA}^0} + r_{\text{PGA}} - \frac{c_{\text{PGA}^0}}{V_c} \frac{dV_c}{dt} \quad [7.15]$$

$$\left( \frac{dc_{\text{PGA}^+}}{dt} \right)_{\text{ex}} = \frac{dc_{\text{PGA}^0}}{dt} = M_{\text{PGA}^+} - r_{\text{PGA}} - \frac{c_{\text{PGA}^+}}{V_c} \frac{dV_c}{dt} \quad [7.16]$$

with  $V_c$  the volume of the continuous (water) phase ( $\text{m}^3$ ). Linear combination of these equations to eliminate the fast association/dissociation rates (analogous to Equation [7.14]) results in:

$$\left( \frac{dc_{\text{PGA}^0}}{dt} \right)_{\text{ex}} = \frac{M_{\text{PGA}^0} + M_{\text{PGA}^+} - \frac{c_{\text{PGA}}}{K_{\text{PGA}}} \frac{dc_{\text{H}^+}}{dt} - \frac{1}{V_c} \frac{dV_c}{dt} (c_{\text{PGA}^+} + c_{\text{PGA}^0})}{1 + c_{\text{H}^+}/K_{\text{PGA}}} \quad [7.17]$$

The titration with hydrochloric acid during the synthesis reaction introduces chloride ions in the system (which will subsequently diffuse into the carrier and were therefore incorporated in the summation term of the internal and external Nernst-Planck flux equations. The chloride ions are considered inert in the model; only electrostatic diffusion of chloride into the particles was accounted for. The volume increase is calculated and used in all external equations. Both equations are given in the appendix ([7.24] and [7.25], respectively). For the external chloride mass balance this results in:

$$\left( \frac{dc_{\text{Cl}^-}}{dt} \right)_{\text{ex}} = M_{\text{Cl}^-} + \frac{c_{\text{titrant}}}{V_c} \frac{dV_c}{dt} - \frac{c_{\text{Cl}^-}}{V_c} \frac{dV_c}{dt} \quad [7.18]$$

### BOUNDARY CONDITIONS

Because radial symmetry was assumed in all particles, all concentration profiles are symmetric around the particle center. Consequently, all concentration gradients in the particle center are zero, which results in a zero net mass flux through the particle center:

$$\left( dc_k/dx \right) \Big|_{x=0} = 0 \quad [7.19]$$

At the particle-bulk interface, no accumulation can take place: the net flux of reactants leaving the continuous phase equals the net flux of reactants entering the combined volumes of the first slabs of the particles. Because external diffusion limitation could be neglected, it follows that:

$$\left( V_c \frac{dc_{k,c}}{dt} \right)_{\text{ex}} = A_p n_p \left| \frac{1}{x^2} \frac{d}{dx} \left( x^2 D_{k,\text{eff}} \left( \frac{dc_k}{dx} - z_k c_k \frac{\sum_{k=1}^N z_k D_{k,\text{eff}} \frac{dc_k}{dx}}{\sum_{k=1}^N z_k^2 D_{k,\text{eff}} c_k} \right) \right) \right|_{x=R_p} \quad [7.20]$$

with  $V_c$  the volume of the continuous (water) phase ( $\text{m}^3$ ),  $A_p$  the surface area of a single particle ( $\text{m}^2$ ),  $n_p$  the number of particles (calculated from mass hold-up and particle density) and  $c_{k,c}$  the concentration of component  $k$  in the continuous (water) phase ( $\text{mol} \cdot \text{m}^{-3}$ ).

#### NUMERICAL SOLUTION OF MASS BALANCES

In order to numerically solve the parabolic partial differential equations for combined mass transfer and enzyme kinetics, the system of equations was discretized with respect to the spatial coordinate. A schematic representation of the spatial grid is depicted in Fig. 4. At the left side of the Fig., the particle center is drawn and the particle perimeter with the surrounding continuous phase is drawn at the right-hand side. An arbitrary transient gradient of a reactant with its highest concentration near the particle surface is drawn in Fig. 4. The gradient is approximated by dividing the particle interior in several volume elements that were each regarded as ideally mixed CSTR's (finite volume method).

The volume of all elements was chosen constant (equivolumetric grid) to save calculation time, without precision loss. Consequently, the model can make do with fewer internal grids in comparison with an equidistant grid. Because the innermost grid covers quite a large distance from the center of the particle, it was refined with equidistant sub-grids. Fig. 4 illustrates that the concentration gradient (slope) of the arbitrary concentration profile of the reactant at the particle center is zero and that the surface concentration ( $c_n$ ) equals the bulk concentration because external diffusion limitation was neglected.

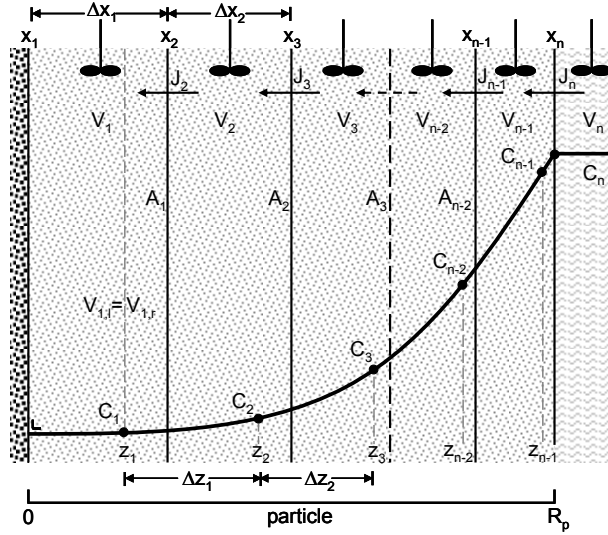


Figure 4. Grid used for numerical solution of the differential equations. Equi-volumetric volume elements are considered ideal mixers with concentration  $C_i$  located at the volumetric centre of the grid  $z_i$ . Mass fluxes ( $J$ ) enter and leave at the borders of the volumetric element ( $x_i$ ) across an area  $A_i$ . External diffusion limitation is neglected and the continuous phase is considered ideally mixed.

The average concentration in each element ( $V_i$ ) is situated at the positions where 50% of the volume of that particular volume element was reached. This concentration is affected by the inflow and outflow of mass (the fluxes are indicated by the arrows) through the boundary areas ( $A_i$ ) on both sides of the element and by enzymatic and by association/dissociation reactions, as was explained previously. Two different grids were introduced: one to define the locations of the average concentrations ( $z$ -grid) and the other to define the locations of the interfaces through which the fluxes take place ( $x$ -grid). Consequently,  $\Delta z_i \neq \Delta x_i$  and both grid-vectors were used during solving.

A central difference approximation of the second order was used to approximate the concentration derivatives in the mass balances. An example is given for the central difference approximated concentration gradient of arbitrary non-ionic reactant  $k$  in Fig. 4 at position  $z_2$  in volume element  $V_2$ :

$$\frac{dc_{k,2}}{dz} \approx \frac{J_{k,3}A_2 - J_{k,2}A_1}{V_2} = \frac{D_{k,\text{eff}} \left( \frac{c_{k,3} - c_{k,2}}{\Delta z_2} A_2 - \frac{c_{k,2} - c_{k,1}}{\Delta z_1} A_1 \right)}{V_2} \quad [7.21]$$

The spatially discretized system of the mass balances was solved for all components by use of the ODE-15s solver of Matlab (version 6.5.0). This solver

is especially useful to solve stiff systems to which end it uses a variable order Runge-Kutta algorithm with adaptive time-step to approximate the solution. The concentrations of the conjugated forms of the biocatalytically active weak electrolytes were subsequently calculated by the dissociation constant in each time step. For control purposes, the total charge in the system was calculated for each time step. With the applied precision (32 digit calculation and tolerance settings), the total charge imbalance always remained below  $10^{-12}$  (mol·m<sup>-3</sup>), which is very low, even in comparison with the proton concentrations.

## RESULTS

Prior to validation of our model with data on Assemblase<sup>®</sup> catalyzed reactions, we tested it on the enzyme kinetics only. This was done by increasing the diffusion coefficients to very high values. The model should now predict the reaction carried out by free enzyme. The result is shown in Fig. 5a for a reaction previously done for 100 mM of both substrates at 293 K and pH 8.0 (Schroën *et al.*, 2002). The model and the measured data are in good agreement therewith indicating that the kinetics were implemented correctly in the model.

### EXTERNAL COURSE OF THE REACTION: MODEL VALIDATION

Cephalexin (CEX) synthesis experiments at various PGA and 7-ADCA concentrations, pH values, and temperatures were done to check the predictions of the model.

#### *Synthesis with various substrate concentrations*

Subsequently, the proper diffusivities were used to check whether the model could predict syntheses reactions catalyzed by Assemblase<sup>®</sup>. Fig. 5b shows that for the same reaction conditions used in the free enzyme experiment the model prediction is in close agreement with the experimental data and the effect of mass transfer during the synthesis was predicted well. When compared with the free enzyme reaction (Fig. 5a), less CEX and more phenylglycine (PG) is formed during the synthesis with Assemblase<sup>®</sup>. The model could also predict the course of the reaction for other substrate concentrations (Figs. 5c and 5d). Both at medium-high and very high substrate concentrations, the model was found to predict the experimental data well, therewith indicating that in the current model mass transfer is also implemented correctly, together with the enzyme gradient.

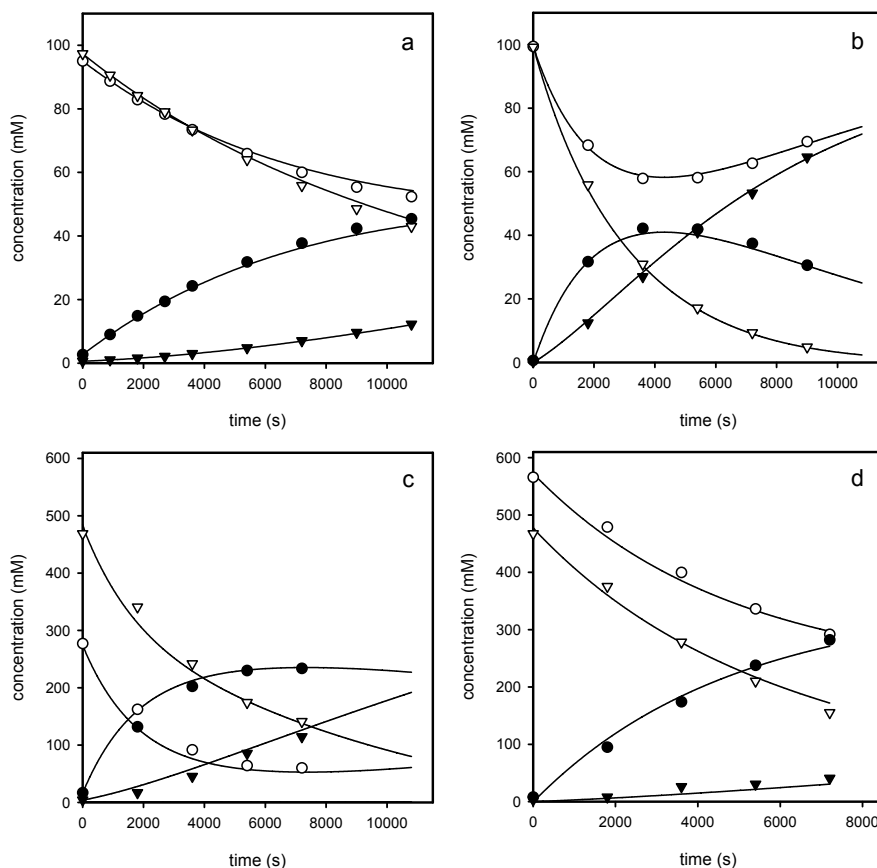


Figure 5. Predicted (lines) and measured (dots) total concentrations of PGA, 7-ADCA, CEX and PG during cephalixin synthesis at 293 K and pH 8.0. a: Model prediction for unrealistically high reactant diffusivities and experimental values for a CEX synthesis with free enzyme from 100 mM of both substrates. b: Experimental data and model prediction for CEX synthesis from 100 mM of both PGA and 7-ADCA. c: Experimental data and model prediction for CEX synthesis from 500 mM PGA and 300 mM 7-ADCA. d: Experimental data and model prediction for CEX synthesis from 500 mM PGA and 600 mM 7-ADCA. All graphs:  $\nabla$ : PGA;  $\blacktriangledown$ : PG;  $\bullet$ : CEX;  $\circ$ : 7-ADCA.

The main difference with the previously published model (Schroën *et al.*, 2002) is that now actually a prediction on the basis of independent physical and chemical phenomena is obtained rather than a description based on pseudo-kinetic parameters that were fitted to the experimental data.

### *Synthesis experiments at various temperatures*

The temperature influences both the rates of reaction and of diffusion. Temperature corrections for the rates of enzymatic reactions were made with the Arrhenius equation, while the temperature-dependencies of diffusivities were based on the Stokes-Einstein equation (see Model section). In order to check whether temperature effects were correctly implemented, it was tested whether the model predicted reactions carried out between 273 and 303 K correctly.

For the entire temperature range correct predictions were obtained as is illustrated by the result of the two extremes (Fig. 6). With equal amounts of Assemblase<sup>®</sup>, the CEX synthesis at 273 K (Fig. 6a) is approximately 4.3 times slower than at 293 K (Fig. 5b). At 303 K (Fig. 5b), the CEX synthesis is 1.9 times faster than at 293 K for equal enzyme amounts (Fig. 5b). The maximum CEX concentration is highest at lower temperatures: 56 mM at 273 K (Fig. 6a) and 36 mM at 303 K (Fig. 6b). The reason is that the kinetic reaction is more temperature dependent than diffusion: a low-temperature synthesis is therefore less diffusion limited.

### *Synthesis experiments at various pH's*

At the pH that was used until now (8.0) the model predicted the course of the reactions correctly. Now the model is tested at pH's between 6.0 and 9.0.

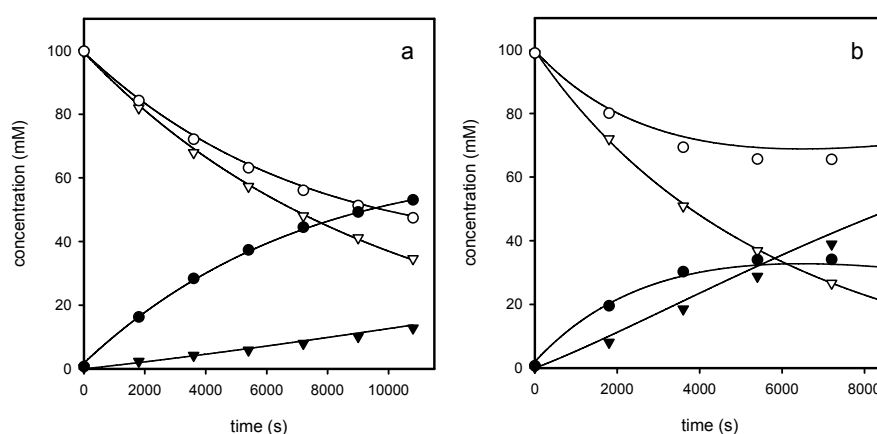


Figure 6. Predicted (lines) and measured (dots) total concentrations of PGA, 7-ADCA, CEX and PG during cephalixin synthesis at from 100 mM PGA and 100 mM 7-ADCA, pH 8.0 at 273 K (a) and 303 K (b), respectively. All graphs:  $\nabla$ : PGA;  $\blacktriangledown$ : PG;  $\bullet$ : CEX;  $\circ$ : 7-ADCA.

Because the enzyme only uses a specifically charged state of the weakly electrolytic reactants (see Model section), the ambient pH determines the availability of reactants for reaction and influences the electrostatically coupled transport of electrolytes. Because the pH continuously changes in space and time, prediction of the overall reaction progress is challenging. This can be illustrated by the fact that the course of the reaction at  $\text{pH} < 7$  could not be described by the lumped model we presented previously (Schroën *et al.*, 2002).

The model predicted the course of the CEX synthesis well for the entire range of pH's. Once again, the predictions for the two extremes are shown ( $\text{pH} 6.0$  and  $\text{pH} 9.0$  in Figs. 7a and 7b, respectively). For  $\text{pH} 9.0$ , the situation is comparable to  $\text{pH} 8.0$  for as far as diffusion limitation is concerned, and these effects are predicted correctly. At  $\text{pH}=6.0$ , the solubility of the substrates is limited and the experiment was conducted with approximately 50 mM of both substrates. Fig. 7a shows that with the physical model, the prediction of the course of the reaction is good. The fact that reactions are slow at  $\text{pH} 6.0$  is not only caused by a reduced enzyme activity at this pH, but is a result of the reduced amounts of reactive PGA and CEX (Schroën *et al.*, 2002). Because the conversion rates are reduced, the particle is less diffusion limited at lower pH. In this case, the course of the reaction is similar to one carried out with free enzyme. As opposed to the

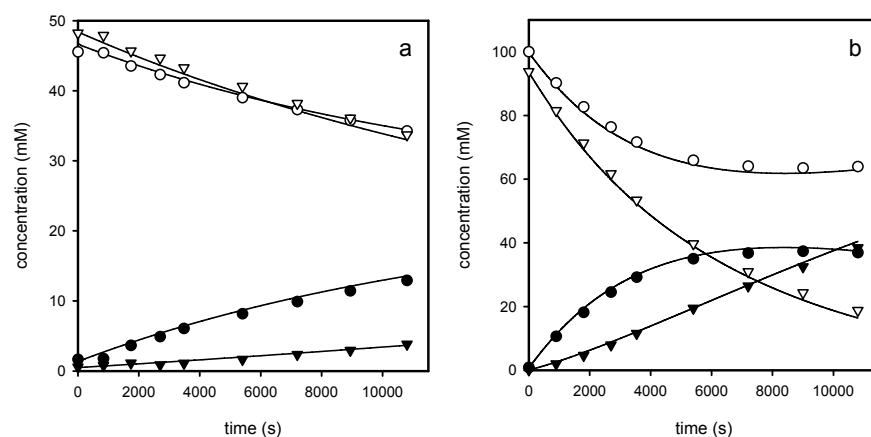


Figure 7. Predicted (lines) and measured (dots) total concentrations of PGA, 7-ADCA, CEX and PG during cephalixin synthesis at from PGA and 7-ADCA, 293 K at  $\text{pH} 6.0$  (a), and  $\text{pH} 9.0$  (b), respectively. In case of  $\text{pH} 6.0$ , 50 mM of both substrates was used because of solubility limits. All graphs:  $\nabla$ : PGA;  $\blacktriangledown$ : PG;  $\bullet$ : CEX;  $\circ$ : 7-ADCA.

pseudo-kinetic model by Schroën *et al.* (2002), the present physical model quantitatively predicts these effects ranging from situations that are heavily diffusion limited to situations that are hardly diffusion limited.

#### **INTERNAL COURSE OF THE REACTION: UNDERSTANDING PARTICLE BEHAVIOR**

Until now, the model was successfully validated by comparing the prediction of the external course of the synthesis reaction with the experimental synthesis data. This gives confidence in the validity of the predicted internal gradients of reactants during the conversion (which are very difficult to measure due to their dynamic character). Because insight in intra-particle phenomena can greatly improve our understanding of the biocatalytic system, Fig. 8 gives an overview of dynamic intra-particle gradients of some reactants during the conversion of 100 mM of both PGA and 7-ADCA at pH=8 and 293 K (Fig. 5b).

Immediately upon the addition of the Assemblase<sup>®</sup> particles (start of the reaction), the mobile sodium ion (Fig. 8a) and PGA (Fig. 8e), of which only a part is ionic at pH 8.0, penetrate the particle along their concentration gradient. This transport must be accompanied by influx of negative ions. Anionic transport is accounted for by 7-ADCA, which penetrates into the carrier along its concentration and electrical gradient (Fig. 8b), but also by the relatively mobile chloride ions (Fig. 8f), for which only an electrical gradient exists (i.e. no concentration gradient). Accumulation of chloride ions in the carrier by this electrical gradient generates an opposed concentration gradient, i.e. electrostatic interactions cause chloride to diffuse temporarily against its concentration gradient.

As a result of the substrate fluxes the substrate concentration in the outer regions of the particle rises quickly. Combined with the presence of a relatively high enzyme concentration in the outer region, the cephalixin production rate is relative high there. Because hardly any cephalixin is yet present in the interior or in the continuous phase, the formed cephalixin temporarily diffuses in both these directions (Fig. 8c). Because of the volume of the continuous phase, the driving force for transport towards this phase remains high in comparison with the much smaller particle interior (where cephalixin will be generated as well). Internally, the CEX production rate rises as substrates become more available, and the concentration gradient becomes directed towards the bulk phase (Fig 8c.).



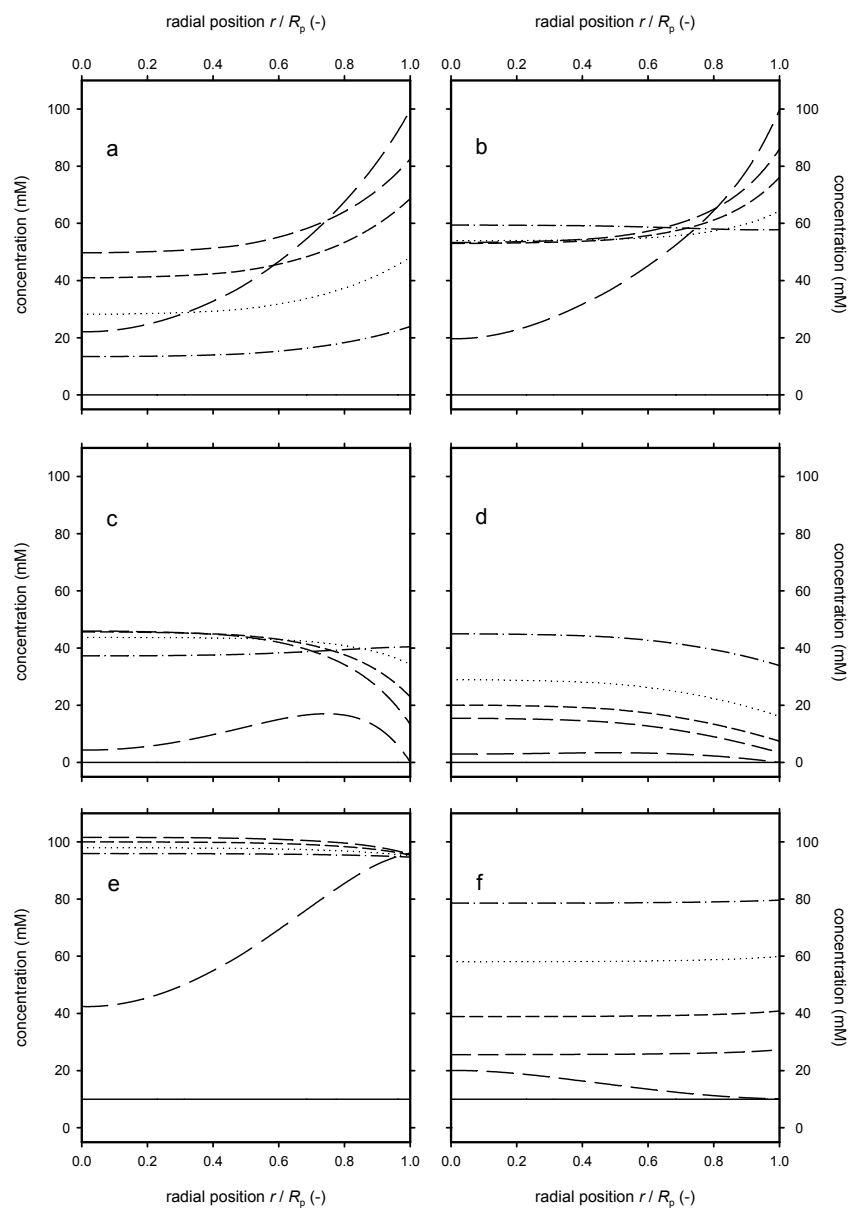


Figure 8. Model predictions for a 100 mM PGA and 7-ADCA conversion by Assemblase<sup>®</sup> at 293 K. During the experiment, the external pH was kept at 8.0 by 0.5 M HCl titration. a-f: Prediction of the internal total concentration profiles of PGA, 7-ADCA, CEX, PG, Na<sup>+</sup> and Cl<sup>-</sup> after 0 (—), 10 (— — —), 1000 (— · — · —), 2000 (— · — · —), 4000 (·····), and 8000 seconds (— · — · —).

After the maximum CEX concentration in the bulk is reached (as was shown in Fig. 5b, this happens after approximately  $4.5 \cdot 10^3$  seconds), the total CEX hydrolysis rate becomes higher than the CEX production rate, and the concentration gradient reverses again toward the inner regions of the particle (net CEX flux into the particle).

For the by-product of the syntheses, PG, the same happens as with CEX. A temporary accumulation followed by bi-directional diffusion, and subsequently the concentration gradient becomes directed towards the outside of the particle (Fig. 8d). This effect is smaller than for CEX, occurs at a later moment in time, and is situated more internally. Given the temporary cephalixin maximum, this could be expected; CEX will partly be hydrolyzed by the enzyme to form phenylglycine (secondary hydrolysis). Because the equilibrium of the reaction lies completely on the PG side, the total PG production rate remains positive, and the concentration gradient of PG remains directed towards the continuous phase.

Upon binding of PGA to the enzyme,  $\text{NH}_3$  is formed. Being the strongest base in the system with a pKa value of 9.4, it will take up protons and form  $\text{NH}_4^+$ , which will cause the local pH to rise. Fig. 9a shows that the model predicts an initial

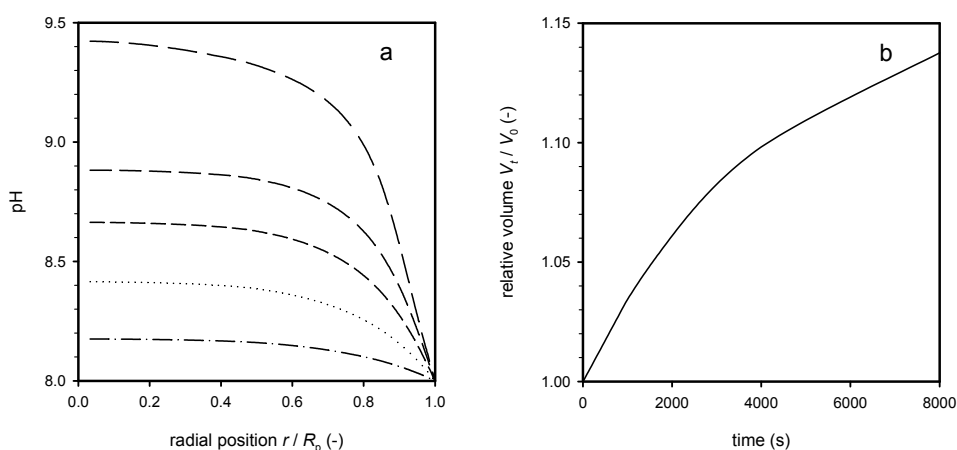


Figure 9. a: Predicted internal pH profiles during a 100 mM PGA and 7-ADCA conversion by Assemblase® at 293 K after 0 (—), 10 (— — —), 1000 (— — —), 2000 (— · — · —), 4000 (·····), and 8000 seconds (— · — · —). During the experiment, the external pH was kept at 8.0 by 0.5 M HCl titration (see also Fig. 8). b: Predicted total volume during the conversion. See also Figure 5b for external concentrations.

increase in pH in the particle center of almost 1.5 pH unit, which quickly diminishes to 0.5 – 1 pH unit. These values are comparable to values reported by Spieß and Kasche (2001) for CEX synthesis reactions carried out with Assemblase®.

Fig. 9b shows that the volume of the bulk phase increases because of the external HCl addition for pH control. In the experiment, a moderate titrant concentration of 0.5 M was used in order to prevent “hot spots” in the reactor. Fig. 9b shows that during the synthesis of cephalixin, the rate of HCl addition is continuously decreased. This is in accordance with Fig. 5b that showed that PGA conversion, and therewith the NH<sub>3</sub> production rate, decreases. The effect from this on pH overrules the effect of the increased PG production rate.

#### **TOWARDS PARTICLE OPTIMIZATION: DESIGN PARAMETERS**

Fig. 8 showed an example of the predicted internal reactant dynamics during CEX synthesis. The internal production rates are lowered as a result of diffusional limitations of multiple reactants. Because the CEX production rate is hampered more than the PG production rate, and the produced CEX remains longer in the carrier, the macroscopic particle behavior of Assemblase® is sub-optimal for CEX synthesis when compared with free-enzyme catalyzed reactions. In order to obtain an idea of the sensitivity of the Assemblase® system for variations in parameters of the biocatalytic particle, their effect is evaluated in terms of the cephalixin yield on 7-ADCA and the selectivity for product formation (S/H ratio at maximum conversion). The predicted effects of particle size, enzyme loading and the distribution of enzyme for some hypothetical situations (model extrapolations) are summarized in Table 2.

Table 2 shows that, with all other parameters identical, smaller particle sizes are favorable for both the product yield and the selectivity for CEX synthesis, as was expected. To keep all other parameters constant, a homogeneous enzyme distribution was used. Similarly, particles with a lower enzyme loading, i.e. average enzyme concentration over the particle, perform better in terms of product yield and S/H, because particles with low enzyme concentrations are less diffusion limited. For heterogeneously loaded particles, the combination of particle size, enzyme loading and the enzyme distribution determines the overall yield and selectivity.

In Assemblase<sup>®</sup> with the enzyme predominantly situated in the outer regions of the particle (Van Roon *et al.*, 2005<sup>a</sup>), the yield and selectivity are better than that of a particle with a homogeneous enzyme distribution and much better than one with an active core (Table 2). This results from an improved supply of 7-ADCA to the enzyme and the reduced secondary hydrolysis of the ‘slow’ CEX for the case of Assemblase<sup>®</sup>. Obviously, the yield and selectivity obtained with surface-loaded particles are equal to those of free enzyme, because no diffusional limitations are present.

Industrial application of such hypothetical new biocatalytic particles can be hampered, however, by several aspects. On the one hand, there is no production process available to produce the theoretical particles with the properties described above. On the other hand, there are practical limitations to the application of such new particles. For instance, depending on the maximal enzyme binding capacity, it may not be possible to immobilize enough enzyme on the surface of the particles and keep the particle hold-up within practical limits at the same time. The enzyme on surface-loaded particles may also be more sensitive to chemical (hot spots) or mechanical degradation. Additionally, very small particles may not be suitable for industrial application.

Table 2. Model prediction of the yield of cephalixin on 7-ADCA ( $Y_{\text{CEX},7\text{-ADCA}}$ ) and selectivity for CEX over PG formation (S/H) for particles with different radii ( $R_p$ ), enzyme loadings (average moles of enzyme per gram DW,  $E_{\text{avg}}$ ) and enzyme distributions. All simulations were done with 100 mM of both substrates at 293 K and pH 8.0. The S/H was evaluated at the maximal CEX concentration (maximal conversion).

$R_p$ ( $\mu\text{m}$ )	$E_{\text{avg}}$ ( $\mu\text{mol/gDW}$ )	Distribution	$Y_{\text{CEX},7\text{-ADCA}}$ (-)	S/H (-)
5	0.95	Homogeneous	0.48	1.93
50	0.95	Homogeneous	0.47	1.80
250	0.95	Homogeneous	0.37	0.98
500	0.95	Homogeneous	0.31	0.71
205	0.50	Homogeneous	0.42	1.31
205	0.95	Homogeneous	0.39	1.10
205	2.00	Homogeneous	0.36	0.90
205	5.00	Homogeneous	0.32	0.71
205	0.95	Surface loading	0.48	1.93
205	0.95	Assemblase <sup>®</sup>	0.41	1.19
205	0.95	Homogeneous	0.39	1.10
205	0.95	Active core (50 $\mu\text{m}$ )	0.09	0.15

The present model describes effects in terms of underlying fundamental processes. The fact that in this specific case the enzyme should be situated at the particle surface as much as possible may sound trivial, but is actually dictated by the diffusivities of the reactants. Because of the relatively low diffusivity of 7-ADCA in comparison with that of PGA, the internal concentration ratios of these substrates shifts towards an unfavorably high PGA predominance, which is known to increase PGA hydrolysis and to reduce CEX synthesis (Schroën *et al.*, 2002). Moreover, because the formed CEX is the slowest diffusing reactant, its prolonged contact times with the enzyme increase secondary hydrolysis rates. However, in other bioconversions with other biocatalysts where multiple diffusion-limited reactions are in competition, other enzyme gradients (perhaps with an active core region) may be favorable. For such systems, the present modular physical model can easily be adapted for the specific geometry, kinetic parameters, flux equations and mass balances at hand.

Besides enzyme loading, the intra-particle enzyme distribution and the particle radius, also the ability of the reactants to diffuse through the particle influences the particle performance. Understanding the precise mechanisms that determine the diffusivity of reactants into the matrix material is all but trivial, let alone the production of matrix structures with defined/designed resistances for mass transfer of specific reactants. Before even beginning to explore such possibilities in practice, it would be a good idea to establish the possible gain by model calculations. In this paragraph, the influence of (theoretical) alterations in reactant diffusivities was studied. For all reactants, one at a time, the reference diffusivity at 293 K (see Table 1) was increased or decreased by a factor 5, to evaluate the (predicted) effect on the CEX synthesis. Changes as a result of variation in diffusivities were found to be most noticeable for 7-ADCA, PGA and CEX; therefore these are only listed (Table 3).

Table 3 shows that when the diffusivity of 7-ADCA decreases, also the CEX yield and selectivity decrease. Low 7-ADCA diffusivities lead to low internal 7-ADCA/PGA ratios, which is known to reduce CEX formation and to increase PGA hydrolysis (Schroën *et al.*, 2002). The opposite happens when the diffusivity of 7-ADCA was increased to its value in water.

When the PGA diffusivity was decreased, however, the yield and selectivity also decreased. In view of the line of reasoning just given for the 7-ADCA diffusivity,

Table 3. Model prediction for the yield of cephalixin on 7-ADCA ( $Y_{\text{CEX},7\text{-ADCA}}$ ) and selectivity for CEX over PG formation (S/H) for diffusivities of 7-ADCA, PGA and CEX for values 5 times lower than their reference values as indicated in Table 1 and the (estimated) free water diffusivities, respectively. All simulations were done with 100 mM of both substrates at 293 K and pH 8.0. The S/H was evaluated at the maximal CEX concentration (maximal conversion).

	20% of $D_{\text{eff}}$ $10^{-10}$ ( $\text{m}^2/\text{s}$ )	$Y_{\text{CEX},7\text{-ADCA}}$ (-)	S/H (-)	$D_{\text{free}}$ $10^{-10}$ ( $\text{m}^2/\text{s}$ )	$Y_{\text{CEX},7\text{-ADCA}}$ (-)	S/H (-)
PGA	0.86	0.36	1.12	$7.0^3$	0.42	1.20
7-ADCA	0.60	0.38	0.94	$5.7^2$	0.41	1.25
CEX	0.50	0.35	0.81	$4.3^1$	0.42	1.33
reference		0.41	1.19		0.41	1.19

<sup>1</sup> Adopted from Van der Wielen (1997). <sup>2</sup> Estimated equal to  $D_{\text{free}}$  of the similar component 6-aminopenicillinate from Van der Wielen (1997). <sup>3</sup> Estimated equal to  $D_{\text{free}}$  of the similar component phenylacetate from Van der Wielen (1997).

this was counter-intuitive. Further investigation showed that the intra-particle PGA concentrations were reduced when the PGA diffusivity was lowered, as expected. At the same time, however, the pH gradients in the particle became very pronounced. Due to the absence of PGA (the main buffering component in the particle interior,  $\text{pK}_a=7.2$ ), the internal pH went up to 9.5 over a large portion of the particle interior. These high pH values are known to decrease CEX yield and selectivity (Schroën *et al.*, 2002). Oppositely, when the PGA diffusivity was increased to the value in free water, the CEX yield and selectivity increased and the pH remained below 8.4 within the entire particle.

Table 3 shows that a lowered CEX diffusivity has a strong negative impact on both the yield after CEX formation, which increases the risk of secondary hydrolysis. When the CEX diffusivity was increased, the opposite was observed, albeit that the effect is mainly on prevention of secondary hydrolysis (S/H increases, while the yield only increases slightly).

With the current model, we were able to pinpoint macroscopic behavior of biocatalysts to specific processes that occur inside the biocatalyst. Therewith important guidelines for future biocatalyst design were obtained. Besides for the specific case of Assemblase<sup>®</sup> that we used in this study, we expect that our approach will also be useful for other biocatalysts and biocatalytic conversions.

Ideally, the model will facilitate the process of biocatalyst production from a more or less trial and error approach to a truly rational design.

## CONCLUSION

A physical model for mass transfer and enzyme kinetics was derived for the transient Assemblase<sup>®</sup>-catalyzed synthesis of the semi-synthetic antibiotic cephalixin. Mass transfer was accounted for by implementation of electrostatically coupled diffusive transport of all reactants, and enzyme kinetics were assumed to obey the previously published mechanism for free-enzyme kinetics. All parameters specific for Assemblase<sup>®</sup>, including enzyme loading and enzyme distribution, were measured separately and independently, and incorporated into this framework.

The model validation was successful: the course of the reaction of CEX synthesis experiments was predicted accurately for a broad range of substrate concentrations (between 50 and 600 mM and temperatures (between 273 and 303K). In contrast with our previous (purely macroscopic) model where mass transfer and enzyme kinetics were lumped into a set of fitted pseudo-kinetic constants (Schroën *et al.*, 2002), the present physical model could also predict the course of the reaction at all pH's between 6 and 9, which ranges from almost free of diffusional limitation (pH 6) to severely diffusion limited (pH 9).

Apart from an accurate description of the macroscopic reaction, the model gave insight in the highly transient processes occurring in the particle. The model showed how diffusion limitation of substrates and products lead to sub-optimal conversions in terms of yield and selectivity during the CEX synthesis. It further predicted the presence of large intra-particle pH gradients, which were experimentally found and reported by Spieß and Kasche (2001). Because the model gives an accurate description of the Assemblase<sup>®</sup> catalyzed CEX synthesis on the basis of physical and chemical phenomena that occur on a micro-scale inside the particle, it is very well suitable for the rational design of new biocatalysts for CEX production. The effects of particle size and enzyme distribution were evaluated. The modular design of the physical model facilitates its application in other systems. These may involve completely different reactions, catalyzed by other biocatalysts in other geometries.

## ACKNOWLEDGEMENTS

Dr. Ruud van de Sman (Wageningen University) is kindly acknowledged for valuable discussions on process physics. Dr. Dimitris Stamatialis and Prof. Matthias Wessling from Twente University (The Netherlands) are acknowledged for fruitful discussions on mass transport of electrolytes. DSM and The Ministry of Economic Affairs of the Netherlands are kindly acknowledged for their financial support.

## REFERENCES

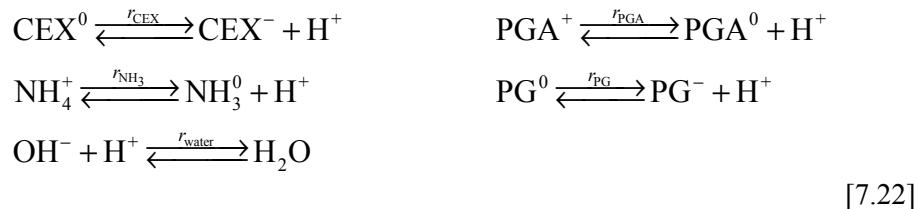
- Bird R.B., Stewart W.E., and Lightfoot E.N.** (1960). Transport Phenomena. New York: John Wiley & Sons. Ch.16, p 495-518.
- Bird R.B., Stewart W.E., and Lightfoot E.N.** (1960). Transport Phenomena. New York: John Wiley & Sons. Ch.19, p 592-625.
- Cussler E.L.** (2002). Diffusion. Mass Transfer in Fluid Systems. 2<sup>nd</sup> ed., New York: Cambridge University Press. Ch 8, p 142-184.
- Do D.D., and Hossain Md.M.** (1986). A novel method of determination of the internal enzyme distribution within porous solid supports and the deactivation rate constant. *Biotechnol. Bioeng.* **28**: 486-493.
- Duggleby H.J., Tolley S.P., Hill C.P., Dodson E.J., Dodson G., and Moody P.C.E.** (1995). Penicillin acylase has a single-amino-acid catalytic centre. *Nature* **373**: 264-268.
- Hossain Md.M., Do D.D.** (1989). General theory of determining intraparticle active immobilized enzyme distribution and rate parameters. *Biotechnol. Bioeng.* **33**: 963-975.
- Perry R., and Green D.W.** (1997). Perry's Chemical Engineers Handbook, 7<sup>th</sup> ed. New York: McGraw-Hill.
- Schroën C.G.P.H., Nierstrasz V.A., Moody H.M., Hoogschagen M.J., Kroon P.J., Bosma R., Beftink H.H., Janssen A.E.M., and Tramper J.** (2001). Modeling of the enzymatic kinetic synthesis of cephalixin - Influence of substrate concentration and temperature. *Biotechnol. Bioeng.* **73**: 171-178.
- Schroën C.G.P.H., Fretz C.B., De Bruin V.H., Berendsen W., Moody H.M., Roos E.C., Van Roon J.L., Kroon P.J., Strubel M., Janssen A.E.M., and Tramper J.** (2002). Modeling of the enzymatic kinetically controlled synthesis of cephalixin: influence of diffusion limitation. *Biotechnol. Bioeng.* **80**: 331-340.
- Spieß A.C., and Kasche V.** (2001). Direct measurement of pH profiles in immobilized enzyme carriers during kinetically controlled synthesis using CLSM. *Biotechnol. Prog.* **17**: 294-303.
- Svedas V.K., Margolin A.L., and Berezin I.V.** (1980). Enzymatic synthesis of  $\beta$ -lactam antibiotics: a thermodynamic background. *Enzyme Microb. Technol.* **2**: 138-144.
- Tramper J., Beftink H.H., Janssen A.E.M., Ooijkaas L.P., Van Roon J.L., Strubel M., and Schroën C.G.P.H.** (2001). Biocatalytic production of semi-synthetic cephalosporins: process technology and integration. In: Bruggink A, editor, Synthesis



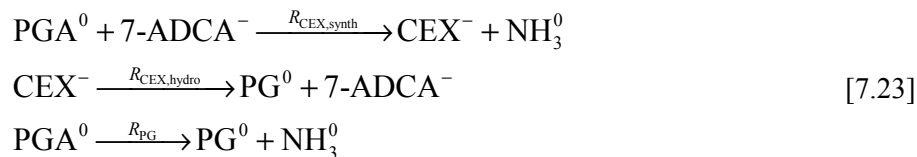
- of  $\beta$ -Lactam Antibiotics: Chemistry, Biocatalysis & Process Integration. Dordrecht: Kluwer Academic Publishers, pp 206-249.
- Van der Wielen L.A.M.** (1994). Transients in the heterogeneous enzymatic deacylation of penicillin G. In: Van der Wielen LAM. A Countercurrent Adsorptive Fluidized Bed Reactor for Heterogeneous Bioconversions. PhD dissertation. Delft University of Technology, Delft, pp 8.1-8.31.
- Van Roon J.L., Boom R.M., Paasman M., Tramper J., Schroën C.G.P.H., and Beftink H.H.** (2005<sup>b</sup>). Enzyme distribution and matrix characteristics in biocatalytic particles. *J. Biotechnol.*, accepted for publication.
- Van Roon J.L., Groenendijk E., Kieft H., Schroën C.G.P.H., Tramper J., and Beftink H.H.** (2005<sup>a</sup>). Novel approach to quantify immobilized-enzyme distributions. *Biotechnol. Bioeng.* **89**: 660-669.
- Van Roon J.L., Joerink M., Rijkers M., Tramper J., Schroën C.G.P.H., and Beftink H.H.** (2003). Enzyme distribution derived from macroscopic particle behavior of an industrial immobilized penicillin-G acylase. *Biotechnol. Prog.* **19**: 1510-1518.
- Van 't Riet K., and Tramper J.** (1991). Basic Bioreactor Design. New York: Marcel Dekker. p 320-341.
- Weast R.C., and Astla M.J.** (1980). Handbook of Chemistry and Physics, 61<sup>st</sup> ed. Boca Raton: CRC Press.

## APPENDIX

The dissociation reactions that were considered are:



In addition, the following enzyme-catalyzed reactions were assumed:



with  $r_k$  the (fast) association/dissociation reaction rate of component  $k$  ( $\text{mol}\cdot\text{m}^{-3}\cdot\text{s}^{-1}$ ),  $R_k$  the enzymatic reaction rate, which only takes place inside the biocatalytic particle ( $\text{mol}\cdot\text{m}^{-3}\cdot\text{s}^{-1}$ ). The total enzymatic rate of cephalaxin

formation  $R_{\text{CEX}}$  is defined as the sum of the rates of CEX synthesis,  $R_{\text{CEX,synth}}$ , and CEX hydrolysis,  $R_{\text{CEX,hydro}}$ . In this work, the following assumptions were made:

The batch reactor is ideally and turbulently mixed, i.e., no concentration gradients of any component is present in the continuous bulk phase;

The immobilization process of penicillin-G acylase in Assemblase<sup>®</sup> does not alter the intrinsic kinetics of the enzyme. This was also found by Schroën and co-workers (2002);

The polydisperse Assemblase<sup>®</sup> particles can be represented by an equal volume of monodisperse spherical particles, which possess a single characteristic size, enzyme loading and enzyme distribution;

All resistance for mass transfer is located in the particle interior, i.e. no external diffusion limitations are present;

Uniform mass transfer properties are assumed throughout the particle. This implicates that all transient processes, i.e. (electrostatic) diffusion and reaction, are radially symmetrical and can therefore be modeled in one dimension (along the radial axis);

The flux of components inside the biocatalytic particles can be described with the Nernst-Planck flux equation for the ionic components (diluted solutions); for non-ionic components, this reduces to the Fick flux equation.

As was mentioned in the main text, the internal pH is altered by the enzymatic conversion (substrates and products have different pKa values). The arising mass and electrostatic gradients are a driving force for the fluxes of charged and uncharged components, of which the fluxes of the ionic components are electrostatically coupled. The fluxes of all electrolytes, in turn, influence the local pH via local association/dissociation equilibria of all weak electrolytes. These rather complex interactions are incorporated in the proton balance. The balance for the continuous (water) phase is given (volume changes from titrant addition, no enzymatic conversion). Each  $M$  in equations [7.24] and [7.25] refers to the

mass balance as was given in eq. [7.8] in the main text into which the suitable flux equation (Eq. [7.9] for electrolytes) was substituted:

$$\left( \frac{dc_{H^+}}{dt} \right)_{\text{ex}} = \left[ \begin{aligned} & M_{H^+} - M_{OH^-} - M_{PGA^0} - M_{NH_3} - M_{CEX^-} - M_{PG^-} \\ & + \frac{1}{V_c} \frac{dV_c}{dt} (-c_{H^+} + c_{OH^-} + c_{PGA^0} + c_{NH_3} + c_{CEX^-} + c_{PG^-} + c_{\text{titrant}}) \\ & + \frac{M_{PGA^+} + M_{PGA^0} - \frac{1}{V_c} \frac{dV_c}{dt} (c_{PGA^+} + c_{PGA^0})}{1 + c_{H^+}/K_{PGA}} \\ & + \frac{M_{NH_4^+} + M_{NH_3} - \frac{1}{V_c} \frac{dV_c}{dt} (c_{NH_4^+} + c_{NH_3})}{1 + c_{H^+}/K_{NH_3}} \\ & + \frac{M_{CEX^0} + M_{CEX^-} - \frac{1}{V_c} \frac{dV_c}{dt} (c_{CEX^0} + c_{CEX^-})}{1 + c_{H^+}/K_{CEX}} \\ & + \frac{M_{PG^0} + M_{PG^-} - \frac{1}{V_c} \frac{dV_c}{dt} (c_{PG^0} + c_{PG^-})}{1 + c_{H^+}/K_{PG}} \end{aligned} \right] \quad [7.24]$$

$$1 + \frac{K'_w}{c_{H^+}^2} + \frac{c_{PGA^0}}{K_{PGA} + c_{H^+}} + \frac{c_{NH_3}}{K_{NH_3} + c_{H^+}} + \frac{c_{CEX^-}}{K_{CEX} + c_{H^+}} + \frac{c_{PG^-}}{K_{PG} + c_{H^+}}$$

with  $K'_w = c_{H^+} c_{OH^-}$ . With a constant pH in the continuous water phase, i.e.  $(dc_{H^+}/dt)_{\text{ex}} = 0$ , the volume change in time follows from Equation [7.24]:

$$\frac{dV_c}{dt} = \frac{1}{V_c} \left[ \begin{aligned} & -M_{H^+} + M_{OH^-} + M_{PGA^0} + M_{NH_3} + M_{CEX^-} + M_{PG^-} - \\ & \frac{M_{PGA^+} + M_{PGA^0}}{1 + c_{H^+}/K_{PGA}} - \frac{M_{NH_4^+} + M_{NH_3}}{1 + c_{H^+}/K_{NH_3}} - \frac{M_{CEX^0} + M_{CEX^-}}{1 + c_{H^+}/K_{CEX}} - \frac{M_{PG^0} + M_{PG^-}}{1 + c_{H^+}/K_{PG}} \end{aligned} \right] \quad [7.25]$$

The external mass balance for PGA was given in the main text; the ones for the other (weak) electrolytes,  $CEX^-$ ,  $NH_3$  and  $PG^-$  are more straightforward:

$$\left( \frac{dc_{CEX^-}}{dt} \right)_{ex} = \frac{M_{CEX^0} + M_{CEX^-} - \frac{c_{CEX^-}}{K_{CEX}} \frac{dc_{H^+}}{dt} - \frac{1}{V_c} \frac{dV_c}{dt} (c_{CEX^0} + c_{CEX^-})}{1 + c_{H^+}/K_{CEX}} \quad [7.26]$$

$$\left( \frac{dc_{NH_3^0}}{dt} \right)_{ex} = \frac{M_{NH_3^0} + M_{NH_4^+} - \frac{c_{NH_3^0}}{K_{NH_3}} \frac{dc_{H^+}}{dt} - \frac{1}{V_c} \frac{dV_c}{dt} (c_{NH_3^0} + c_{NH_4^+})}{1 + c_{H^+}/K_{NH_3}} \quad [7.27]$$

$$\left( \frac{dc_{PG^-}}{dt} \right)_{ex} = \frac{M_{PG^-} + M_{PG^0} - \frac{c_{PG^-}}{K_{PG}} \frac{dc_{H^+}}{dt} - \frac{1}{V_c} \frac{dV_c}{dt} (c_{PG^-} + c_{PG^0})}{1 + c_{H^+}/K_{PG}} \quad [7.28]$$

The conjugated counter forms of these biocatalytically active components were calculated from their respective equilibrium constants. For hydroxide ions, it follows from the water equilibrium that:

$$\left( \frac{dc_{OH^-}}{dt} \right)_{ex} = K'_w \frac{d(1/c_{H^+})}{dt} = \frac{K'_w}{c_{H^+}^2} \frac{dc_{H^+}}{dt} \quad [7.29]$$

As a result of the addition of hydrochloric acid in the continuous (water) phase, the concentration of the inert chloride ions increases:

$$\left( \frac{dc_{\text{Cl}^-}}{dt} \right)_{\text{ex}} = M_{\text{Cl}^-} + R_{\text{HCl}} - \frac{c_{\text{Cl}^-}}{V_c} \frac{dV_c}{dt} \quad [7.30]$$

The rate at which HCl is added in order to keep the external pH at its set point is:

$$R_{\text{HCl}} = \frac{c_{\text{HCl}}}{V_c} \left( \frac{dV_c}{dt} \right)_{\text{ex}} \quad [7.31]$$

of which the last part was already declared in equation [7.25].

The internal mass balances are almost the same as the external ones. The differences are the presence of enzyme, i.e. enzymatic conversion terms ( $R_k$ ), and the absence of volume changes. As a final example, the internal mass balances for PGA and 7-ADCA are given:

$$\left( \frac{dc_{\text{PGA}^0}}{dt} \right)_{\text{in}} = M_{\text{PGA}^0} + r_{\text{PGA}} - R_{\text{CEX}^-} - R_{\text{PG}^0} \quad [7.32]$$

$$\left( \frac{dc_{\text{7-ADCA}^-}}{dt} \right)_{\text{in}} = M_{\text{7-ADCA}^-} - R_{\text{CEX}^-} \quad [7.33]$$



---

## Chapter 8 Discussion

## **ABSTRACT**

Multiple phenomena are involved in conversions by immobilized biocatalysts. A paradox is identified between analytical desires on one hand and analytical boundary conditions on the other: while the study of interdependent phenomena would call for their simultaneous analysis in an integrated context, the available experimental options may impose a series of separate and dedicated analyses.

From this, bottlenecks in particle performance may be identified, if possible supported by a mechanistic model and performance criteria. Subsequently, a strategy for further biocatalyst development may be chosen.

Some examples of recent developments in enzyme and matrix characteristics, reactor operation, and micro-technology are discussed.



---

**PARALLEL VS. SERIAL ANALYSIS**

As illustrated in the previous chapters, a large array of disciplines and techniques are involved in the characterization of biocatalytic particles at various levels of scale. Most probably, additional disciplines will be involved in the next step in particle design: i.e. the optimization of the biocatalytic activity in new immobilized systems. The high resolution at which some phenomena needed to be analyzed called for delicate preparation techniques and sensitive equipment operating under well-defined conditions. For such analysis, protocols for sample preparation may have to be fine-tuned (e.g. Chapters 4 until 6) for optimal results. Moreover, setting up and executing the analyses often requires experience and craftsmanship.

The need for such specialized analyses, however, presents a paradox for rational biocatalyst particle design. At the one hand, multiple morphological and biochemical aspects of the biocatalytic particle at micro- and nano-scale, e.g. particle size and enzyme loading and distribution, each influence the macro-scale particle performance, but are also interrelated. In practice, it is often difficult to optimize for a specific macroscopic particle characteristic (by adjusting parameters at the micro- and nano-scales) without influencing or making concessions to other macroscopic particle properties. This calls for an optimization approach in which the effects of several key parameters are studied and optimized simultaneously.

In case data on key parameters are required at high resolution and detail, on the other hand, the analysis requires highly specialized preparation methods and dedicated detection equipment. The specificity of these analyses will often preclude a study of other phenomena in the same sample at the same time. The need for specificity and resolution implicates serial analyses, rather than parallel ones, thus entailing great investments in time and resources. Additionally, preparation and analysis methods may restrain the range of sample variations that, in principle, might have been suitable in the study of structure-function relations. It is therefore not surprising that literature on integral rational particle design coming from system-specific knowledge on structure-function relations is

scarce. In practice, development is often done by treating different samples with different sample preparation methods and by detection with dedicated hardware for single properties. This approach presents problems in data interpretation, since data come from different samples that have undergone different pre-treatments.

Preferably, the array of complex interdependent phenomena is analyzed with robust analysis methods that can be applied to study several phenomena at the same time. In Chapter 6, Field-Emission Scanning Electron Microscopy was used to simultaneously analyze the overall enzyme gradient, local areas of increased enzyme loading, and the corresponding complex matrix morphology. It was concluded that FESEM may be a powerful tool in particle design, because such analysis directly provides information on structure-function relations of (heterogeneous regions in) samples.

There is a lot to be gained from robust methods that can accurately and efficiently give information on biocatalyst loading and distribution onto or into support materials, and can relate this to morphological aspects of the support material. Modern techniques for elemental analysis of the sample under investigation, such as energy-dispersive X-ray spectrometry (EDX; e.g. Modi *et al.*, 2004) or atomic absorption spectrometry (AA; e.g. Pereira-Filho *et al.*, 2002), are good examples of promising recent developments, which will extend the possibilities of current electron microscopic techniques. In addition, tomography (i.e. virtual sectioning) with high-voltage transmission electron microscopes may prove to become a very valuable tool for non-invasive three-dimensional in-situ analysis at high resolution, especially with the large increase in computing power over the last decade (e.g. Bouwer *et al.*, 2004 and Ulrike *et al.*, 2002).

The development and maturation of confocal scanning laser microscopy (CSLM) provides scientists with a powerful method to study (fluorescent) structures in systems. Because it is non-invasive, this technique can be used to study dynamics of molecules, and to study phenomena in living systems. There are still some major scientific drawbacks to tackle, i.e. limited penetration depth, requirement of uniform refractive index, and signal disturbances caused by the sample above the focal plane. In the near future, a significant part of these problems might be solved by the design of clever software (run on fast hardware).

Recently, Van Roon and co-workers described what preparation and detection methods can be used and combined for the description and eventual optimization of biocatalytic particles as a function of their size and the desired scale of detection (Chapter 2). Whatever the set of detection methods used, integration of such multi-disciplinary knowledge of the immobilized biocatalyst into models can be used in the rational design of biocatalytic particles. Especially physical models that contain independent physical and chemical key parameters can greatly enhance our understanding of complex systems and can give information on the system's behavior and its sensitivity towards variations in input variables. Such models can speed up the design process considerably, by evaluating many new possibilities and configurations at the desk. Scientific publications on such research, however, are scarce at best. Possibly, the integrated knowledge on all combined disciplines, which is needed for the actual development of an efficient biocatalytic particle, is present in industry, where economical efficiency and durability are major incentives for developing new biocatalysts with improved characteristics. Publication of such knowledge, however, will most probably be omitted to protect industrial (intellectual) property.

What the properties of the most cost-effective biocatalyst (and accompanying process) should be, is very case-specific. When a conversion is done with expensive enzymes, i.e. when biocatalyst costs are significant (which usually is the case; Straathof, 2001), operational stability for extensive reuse is important for process economics. For applications in which cheap enzymes are used in large-scale conversions, the volumetric productivity may be more important, which calls for large amounts of enzyme within a single particle. In systems with multiple reactions, however, high enzyme loadings may aggravate the diffusion limitation(s) of one or more substrates or products. For Assemblase<sup>®</sup>-catalyzed synthesis of CEX, an increase in enzyme loading and diffusion limitation leads to a reduced product yield and reaction selectivity (Schroën *et al.*, 2002). Others have reported a reduced (apparent) substrate specificity (Vertesi *et al.*, 1999; Cloix and Wainer, 2001) and shifts in temperature optima (Jing *et al.*, 2000; Keusgen *et al.*, 2001; Novick and Dordick, 2000; Ragnitz *et al.*, 2001; Wang *et al.*, 2001) because of an increase in diffusion limitation.

Once the specific areas of innovation are selected, preferably assisted by a model-based sensitivity analysis, an appeal is made to the specialists to come up

with an improved product or process, given a set of specifications. Obviously, the parallel multi-disciplinary approach is difficult maintain here: research for new functionalities, and the development of robust methods to characterize functional properties, is highly specialistic work. From this point onwards, therefore, future developments are case-specific, which makes it very difficult to predict the major developments in biocatalysts design to be expected in the near future. Nonetheless, some interesting developments, coming from different disciplines, are given in the next paragraph.

## **DEVELOPMENTS IN BIOCATALYST DESIGN**

A lot of effort is put into the search for new or improved enzyme functionalities, new (polymeric) supports for immobilization, new methods to immobilize enzymes, and for improvements in biocatalyst efficiency. Geneticists, for example, are continuously looking for enzymes with improved characteristics, or improve existing enzymes by altering their structure, improving thermal, chemical or mechanical stability (e.g. Eijssink *et al.*, 2004), altering substrate affinities. In thermodynamics, research on polymer interactions with their environment is done, from which improved resins are developed to immobilize the biocatalysts on (e.g. Fuentes *et al.*, 2004). Polymer scientists are working on the development of new, stable, open networks, with specified hydrophilicity, and mechanical strength, and 3-dimensional structure (e.g. Wooley *et al.*, 2000). Together with application scientists, research is done to control the size, shape and structure of new carrier materials and make them a stable platform onto or into which all types of biocatalysts can easily and firmly be attached with sufficient loading capacity. Also in reactor design, there is an ongoing quest for new reactor concepts and processing options. Besides this, in the new field of micro technology, radical new approaches to process design may become available.

### **ENZYME KINETICS**

Rapid developments over the last decades have greatly extended the possibilities in genetics and molecular biology. Enzyme sequencing and proteomics are used more commonly to unravel secondary and tertiary structures of enzymes, thus providing scientist with mechanistic understanding of the catalytic mechanisms, the amino acids that are involved in the catalytic reaction, and their position with

respect to each other and the substrate during the conversion. Additionally, such knowledge may facilitate the prediction of the affinity of the enzyme for other substrates, and the effect of single amino-acid changes in the enzyme (Alkema *et al.*, 2004). Such site-directed mutagenesis may be applied to optimize product yields or selectivity for the wanted reaction over the side-reactions, or may be used to take away the (non-competitive) inhibition of certain chemicals. In Box 1, a calculation is made with the model for Assemblase<sup>®</sup>-catalyzed CEX synthesis (Chapter 7). It illustrates which effects are to be expected from a hypothetical mutant enzyme with other kinetic characteristics.

An alternative parallel ongoing development is in random mutagenesis, or directed evolution (the accelerated mimicked Darwinian evolution in a testing tube). This approach requires no knowledge on the 3-dimensional structure of the enzyme, because a-specific alterations are introduced in the DNA that encodes the enzyme. Upon expression, mutant enzymes are screened by automated high-throughput scanning for new functionalities, and huge numbers of samples can be evaluated for the desired properties. For high-throughput screening, fluorescent or chromogenic reference substrates are particularly useful, because they can be analyzed accurately and quickly.

### Box 1

#### Effect of changes in kinetic properties of penicillin-G acylase on cephalixin synthesis

Genetic alterations may lead to changes in enzyme kinetics, and in changes of rate constants in particular. The reaction rate constants of penicillin-G acylase are declared in Fig. 1. The potential effect on changes in the reference values (Schroën *et al.*, 2002) of each constant is depicted in Table 1.

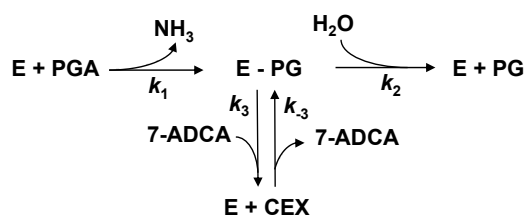


Figure 1. Kinetic model for cephalixin synthesis as adopted from Schroën *et al.* (2002).

Table 1 shows that a fixed increase or decrease in specific rate constants results in different kinetic behaviour. The table shows that not all model rate constants are equally relevant for optimization of output parameters. For instance, a five-fold reduction in the rate constants for E-PG ( $k_2$ ) and CEX hydrolysis ( $k_3$ ) result in an increase of the S/H with a factor 2.6 and 2.0, respectively.

Table 1. Effect of hypothetical alterations in rate constants ( $k$ ; see Fig. 1) on yield ( $Y$ ) of cephalaxin on 7-ADCA, and on synthesis/hydrolysis ratio ( $S/H$ ) at maximum yield. Calculations were done with the model in Chapter 7.

	$k_1$		$k_2$		$k_3$		$k_{-3}$	
	$Y$	$S/H$	$Y$	$S/H$	$Y$	$S/H$	$Y$	$S/H$
ref	0.41	1.19	0.41	1.19	0.41	1.19	0.41	1.19
$5k$	0.56	1.80	0.18	0.40	0.64	2.72	0.21	0.56
$k/5$	0.23	0.78	0.66	3.15	0.48	0.48	0.62	2.34

Therefore, such calculations enable speculation on the desirability of specific changes of the input rate constants. Provided that knowledge is available on the relation between the enzyme conformation and its kinetics behaviour, sensitivity analysis may give clues to specific alterations of the structure (genomic sequence) to optimize the kinetic behaviour. specific alterations in the kinetic behaviour by specific mutations in the genome.

### STRUCTURING OF THE SUPPORT MATERIAL

Membranes and microstructures can be used to produce enzyme carrier particles of uniform size. Recently, Vladisavljevic and Williams (2005) published a review paper on the manufacture of particles with membranes and related structures.

The difference between conventional particle preparation and membranes is rather pronounced. Particles show a pronounced particle-size distribution when prepared by homogenization, but can be fairly monodisperse when prepared by

membrane emulsification. Nakashima *et al.* (2000) illustrate the concept for making emulsions with a Shirazu porous glass (SPG) membrane. For the preparation of solid particles, similar differences in particle size distribution are expected: The same authors report the production of poly-di-vinyl-benzene particles with SPG membranes. The particles are uniform to such an extent that they can be used as spacers in LCD screens. In general, large amounts of particles (or droplets) can be produced with membranes. The SPG membranes seem to be the best choice if uniform particles are required: reported spans,  $(D_{10}-D_{90})/D_{50}$ , are 0.26 – 0.45 for particles that can be as small as 1 micron and as big as 60 micron. For ceramic membranes, recent research shows that relatively narrow spans (1.2) are within reach for the jetting technique (Jing *et al.*, 2005).

Even more uniform particles are reported for microsieves. An example is shown in figure 2. Compared to membranes, microsieves have an exemplary pore size (distribution). Microsieves are produced with techniques from the photolithographic industry and this allows design of pore size and pore shape, unlike membranes. If properly designed, microsieves can give uniform droplets. This is also true for microchannels that make use of the interplay of curvatures imposed by the structure itself in order to reach snap-off of droplets/particles.

Current developments in micro-technology even indicate that meso-structured biocatalysts are within reach. Utada *et al.* (2005) have reported the formation of magic bead particles that consist of a core of one polymer that is covered with a uniform layer of a second polymer. An even more exotic example was published by Nisisako and co-workers (2004), who produced particles that consist of two

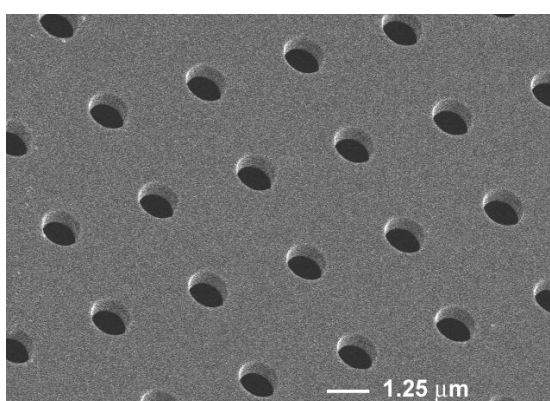


Figure 2. Example of a microsieve. The emulsion is formed by pressing the to-be-dispersed phase through the pores where they form droplets that are taken up by the cross flowing continuous phase (Gijsbertsen-Abrahamse *et al.*, 2004). Picture courtesy of Aquamarijn Micro Filtration B.V..

halves with different properties. Okushima and co-workers (2004) reported the production of multi-phase particles that may consist of more than two areas with different properties each. In parallel, also a lot of research is done in loading the various particles with enzyme (e.g. Omi *et al.*, 1997). It is clear that in the field of structuring, many options have become available in recent years. This is not only true for the particle size as such but also for the construction of regions with different properties within one particle.

## DEVELOPMENTS IN REACTOR OPERATION

### PRODUCT REMOVAL AND FEEDING STRATEGIES

Obviously, product removal is of importance for many processes. The number of options in this field seems to be unlimited; therefore, we don't go into detail here. Also feeding strategies can be of eminent importance for any process, but also in this case we will not go into detail given the numerous options, which mostly are very case-specific.

There is, however, one option relevant to cephalexin synthesis that we would like to mention. It comprises of a combination of feeding strategy and competitive product removal. The total reaction system is simple and consists of a reaction vessel and an adsorption column filled with an ion-exchange resin (XAD-4). The process conditions that were tested are the same as required for the enzymatic synthesis reaction. For simplicity, we will focus on the adsorption column. This column is first loaded with the phenylglycine amide substrate, and subsequently with a solution of 62 mM 7-ADCA, 108 mM cephalexin, 55 mM phenylglycine amide, and 6 mM phenylglycine (Figure 3). The phenylglycine amide is (practically) solely replaced from the column by cephalexin, which is removed this way. The phenylglycine amide that is released is an additional source of substrate that can be fed to the reaction system. Although 7-ADCA has affinity for the XAD-4 adsorbent, it cannot replace phenylglycine or cephalexin from the column. The phenylglycine does not have an affinity for the adsorbent and leaves the column in the same concentration that it entered.

The effects that can be reached in this way are many-fold. First, cephalexin is removed, therewith preventing secondary hydrolysis by the enzyme. Second, the phenylglycine amide that is released will increase the effective substrate



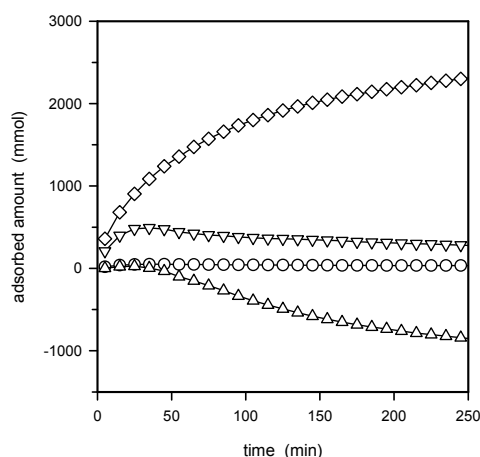


Figure 3. Combined feeding of phenylglycine amide and simultaneous cephalixin removal with the aid of an XAD-4 column as described in the text. Symbols:  $\diamond$ : CEX;  $\nabla$ : 7-ADCA;  $\triangle$ : PGA;  $\circ$ : PG.

concentrations, which leads to higher yields (Schroën *et al*, 2002). Besides this, the reaction can now continue until, in principle, only phenylglycine remains and no further recycling steps are required. The only thing that remains is to effectively remove cephalixin from the column, which can be achieved with an elution gradient with iso-propyl alcohol.

## INTRODUCTION OF OTHER DRIVING FORCES

### *Hydrostatic pressure*

Besides minimization of the diffusive resistance of the matrix material of the biocatalytic particle for all reactants (or one in specific), alternatively a hydrostatic pressure difference may be used to overcome diffusion limitation. For such processes, the enzyme is usually immobilized onto or into a membrane. This can be done by adsorption, although binding may not always be sufficiently strong for industrial applications (Chaplin, 2002). This is not an issue for entrapment, in which the enzyme is added to the polymeric blend before biocatalyst matrix formation and becomes trapped in the polymeric network, and encapsulation, in which the membrane is impermeable to the enzyme, but permeable to the reactants (Mulder, 1996). Covalent attachment is a well-studied method of immobilization; the obvious advantage is the strength of the chemical binding.

After immobilization, the membrane is ready for use. The application of a hydrostatic pressure difference across the membrane is expected to result in convective transport of reactants, provided the pores are not too small. We tested this concept for the enzymatic conversion of PGA and 7-ADCA to CEX and found that it was possible to produce CEX free of diffusion limitations with the membrane bioreactor. In this case, the advantages of an immobilized biocatalyst can be combined with those of the intrinsic enzyme kinetics (higher yields and higher specificity). A more detailed description is given in Box 2.

**BOX 2****A membrane bioreactor (MBR) without diffusion limitation**

The enzyme, penicillin-G acylase was immobilized onto and into several membranes that contained free aldehyde or epoxide groups that allow covalent attachment of the enzyme. Sheets of these activated membranes were tested in a membrane bioreactor (Figure 4). The substrates, PGA and 7-ADCA, were passed through the membrane by application of a hydrostatic pressure difference over the membrane. During membrane passage, the substrates were partially converted into the product CEX and by-product PG. After each passage, the pH of the solution was adjusted to the desired value and this procedure was repeated until the desired degree of conversion was reached. The offline pH regulation during the experiment is a clear advantage over the use of other plug flow reactors (e.g. packed columns), where such online pH regulation generally is very difficult (ref).

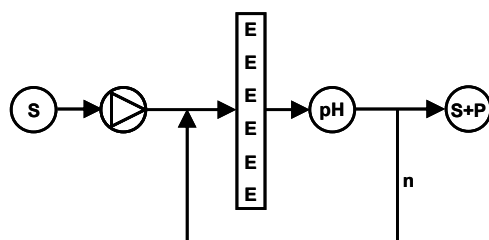


Figure 4. a: Schematic experimental set-up of CEX production with a membrane bioreactor. In each passage, the substrates (S) are partially converted into products (P), and after each passage, the pH is adjusted.

In Figure 4b, the selectivity for CEX formation over PG formation (i.e. the previously declared S/H ratio, defined as the amount of moles produced CEX per mol of produced PG) is plotted as a function of the degree of conversion of

the reaction (defined as the number of moles of CEX produced per mol ADCA initially present. This was compared to the data for reactions carried out with freely suspended enzyme. The Figure indicates that the selectivity of the MBR catalyzed reaction was just as high that of the free-suspended enzyme reaction. Diffusion limitations, which are detrimental for the S/H, were thus absent in the MBR during the conversion. In this configuration, immobilized enzymes can be applied without the negative effects on selectivity and yield described for Assemblase<sup>®</sup> particles.

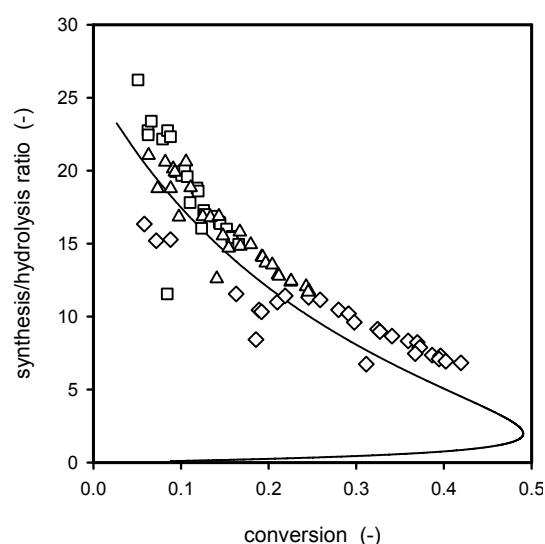


Figure 4. b: The selectivity of the reaction with the membrane bioreactor as function of the conversion for hydrostatic pressure differences of 0.2 ( $\square$ ) and 0.4 bars ( $\diamond$ ) in comparison with that of the free-suspended enzyme reaction (line) intrinsic kinetics. The macroscopic selectivity of the conversion with the immobilized enzyme is equals that of the freely suspended enzyme.

### ***Other driving forces to enhance mass transfer***

Not only concentration gradients or hydrostatic pressure differences can be used as a driving force for the transport of reactants in conversions with immobilized enzymes. When electrolytes are involved in the reaction, another option is to introduce charges onto the support material in order to attract or repulse specific ionic substrates. The resulting electrical gradient may be used as an additional driving force for mass transport of reactants. In the case of weak electrolytic reactants, especially when the pH is near the dissociation constant, the pH can be used as an extra control parameter to adapt the charge of the different substrates

to optimize the electrostatic interaction with the support. This is especially so for components with multiple groups that can dissociate.

Also thermal gradients may be used as a(n) (additional) driving force. In such applications, the enzyme is often immobilized onto a membrane over which a temperature gradient is applied (e.g. Diano *et al.*, 2004 and Eldin *et al.*, 2000). This gradient may be supplemented by a concentration gradient, and therewith an additional driving force. With such application of multiple driving forces, diffusion limitations may be avoided, or the transport of selected reactants may be specifically enhanced or inhibited.

### ***Combinations of driving forces to enhance mass transfer***

Other combinations of driving forces may also be used. When the enzyme is immobilized onto or into a membrane by covalent attachment and contacted with a substrate solution, concentration gradients will develop in the stagnant layer near the membrane surface. These concentration gradients (or chemical potential gradients) may be influenced by the addition of a hydrostatic pressure difference across the membrane. The reactants will drift along with the resulting solvent flux through the membrane. Depending on the friction coefficient of the reactant with the solvent (function of hydrodynamic radius), and e.g. the direction and magnitude of the applied pressure difference, the supply of reactants to and from the membrane can be enhanced or suppressed.

It is also possible to use electrical gradients in combination with concentration gradients. Analogous to the addition of a hydrostatic pressure difference, the driven transport of the, in this case, ionic reactants can be accelerated or suppressed as a function of the pH, salt content, direction and strength of the electrical field, and by imposing an electrical current.

These combinations, where multiple driving forces are simultaneously used in the same or opposite directions, to selectively influence the transport of specific reactants are a fallow area, still much research needs to be done. In many cases, the systems are so complex (and concentrated in the area's of interest) that basic assumptions of ideality are no longer valid. This implies that irreversible thermodynamics, Maxwell-Stephan equations, or meso-scale models, have to be used to describe the systems. This in itself is not a problem, but it may imply that considerable effort has to be put into determining constants for these models,

before these models can actually be used to their fullest potential. With increasing computing power, increasingly difficult theoretical models can be run, therewith opening new options for detailed studies of underlying mechanisms.

At a very basic level, we have made a start with the implementation of multiple driving forces. As an illustration, some results of theoretical calculations for systems with membrane-bound penicillin-G acylase with multiple driving forces are given in BOX 3.

**BOX 3****Multiple driving forces in penicillin-G acylase-catalyzed cephalixin synthesis**

In our model calculations, it was assumed that penicillin-G acylase was immobilized onto an uncharged membrane which was part of a membrane stack i.e. all membranes were placed in parallel (Fig. 5a). Transport of ions through the membrane was neglected, so the membrane only acted as support material for the enzyme. Substrates are transported parallel to the membranes and conversion to (by-) products can take place. We assumed fully developed laminar flow through the channels ( $Sh=3.66$ ) and assumed that the contact time of substrates and products with the enzyme (residence time in the module) is short. In that case, no major composition gradients will arise in tangential direction.

Mass transfer was assumed limited near the membrane (in the stagnant layer), and only component friction with the solvent (water) was taken into account. Maxwell-Stephan equations for mass transfer were used. The system performance was evaluated as a function of the water flux through the membrane. The desired effect is to influence the concentration gradients in the boundary layer, and thus enhance production rates and S/H ratio. Figure 5b shows that both selectivity (S/H) and production speed increase for a water flux from left to right. What exactly happens here is not completely clear. The increased supply of substrates is probably the cause of the improved cephalixin production rate. The reduced cephalixin removal from the membrane, due to the frictional forces with the flowing water may be the cause of the slightly reduced S/H at high water fluxes from left to right: the prolonged residence of cephalixin near the enzyme increases the risk of its hydrolysis.

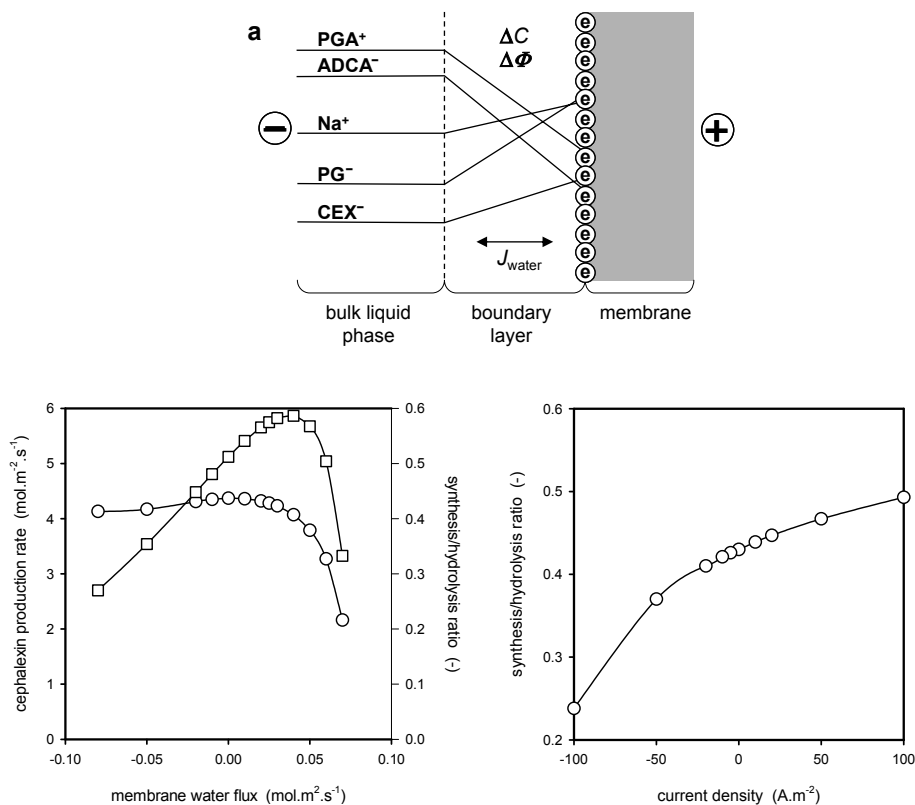


Figure 5. Predicted effects of additional driving forces during steady state cephalixin synthesis with a penicillin-G acylase coated membrane in a semi-infinite bath at 300 K, pH 8.0. Reactant concentrations for total (charged + uncharged) PGA, ADCA, CEX, PG were 100, 200 50, and 25 mM, respectively. The initial Na<sup>+</sup> concentration was 222.5 mM. a: Schematic illustration of the system. Apart from a concentration gradient ( $\Delta C$ ) in the boundary layer, also a water flux ( $J_{\text{water}}$ ) through the membrane can be imposed. Alternatively, an electrical field ( $\Delta \Phi$ ), and possibly an imposed current though the system can be applied (b) Predicted effects of the addition of a water flow ( $\text{mol} \cdot \text{m}^{-2} \cdot \text{s}^{-1}$ ) through the membrane on the selectivity for CEX formation (S/H,  $\circ$ ) and the CEX production rate ( $\square$ ) during the CEX syntheses. The optimum selectivity (S/H) and cephalixin production rate are obtained for approximately 0.01 and 0.04  $\text{mol} \cdot \text{m}^{-2} \cdot \text{s}^{-1}$ , respectively. c: Predicted effect of the imposed current density ( $\text{A} \cdot \text{m}^{-2}$ ) on the selectivity ( $\circ$ ) of CEX formation.

In Figure 5c, an example is given of what could happen in the presence of an electric field (Maxwell-Stephan equations for mass transfer were used). Products are attracted to or repelled by the membrane, depending on their charge and the direction of the applied field. Apparently, a negative current across the membrane is beneficial for the S/H of the process. At pH 8, the 7-ADCA is almost exclusively negatively charged, whereas approximately 14% of the PGA is positively charged. Possibly this enriches the membrane surface in 7-ADCA, relative to PGA (effective component diffusivities and water frictions are in the same order of magnitude), pushing the reaction towards synthesis of CEX rather than by-product (PG) formation (Schroën *et al.*, 2002). Under the applied conditions, this apparently outweighs the disadvantage that at pH 8.0 approximately 80% of the formed CEX will be negatively charged and will be retained near the membrane longer.

Clearly, these calculations are only an initial study to evaluate whether certain driving forces could have an effect and it is obvious that this is the case. To which extend these forces are to be used, either alone or in combination, is still to be investigated in detail. It would be interesting to create such a favorable environment near the enzyme, that the overall reactor performance surpasses that of free enzyme reaction, i.e. surpasses intrinsic enzyme kinetics.

## DEVELOPMENTS IN MICROTECHNOLOGY

In the previous sections, examples were given on possible developments in enzyme kinetics and reactor operation. Recently, micro-technology is coming to growth. It enables the production of well-defined micro-structures with micrometer dimensions. Because of their small size, they offer some specific advantages, such as fast mixing times, and high transfer rates of mass and heat. On this basis, micro-technology may open alternative ways for improvement of bioconversions.

Various microstructures have been reported, most of them made from glass or silicon with technology developed in the semi conductor industry (Jensen, 2001). Biochips have been constructed with covalent attachment of sugar molecules and enzymes to silicon surfaces for specific substrate recognition and conversion (De Smet *et al.*, 2004; Lee *et al.*, 2003). The integration of micro-sieves and biochips

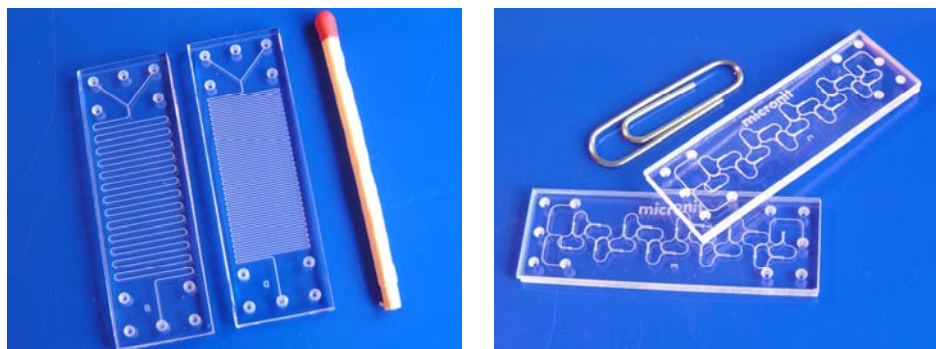


Figure 6. 2 Microchemical reactor chips (courtesy of Micronit Microfluidics B.V., Enschede, The Netherlands). Each chip has 10 storage holes and several mixing / reaction chambers. The maximum number of separate fluids for the chemical reactor depends on the size of the chip, but could be hundreds.

resulted in a lab-on-a-chip, a complete diagnostic device for blood on a credit card size (Van Rijn, 2002). In Figure 6, some examples of microchemical reactor chips are depicted.

Although most applications seem to be related to medical diagnostics and biosensors nowadays, the interest in the chemical industry is growing (Lundgren *et al.*, 2004). Because of the high specificity and high volumetric capacity, micro-reactors could be advantageous for production as well. Further, the micro-structures could be seen as the ultimately designed biocatalyst carriers. So-called Brownian ratchets have been applied for separation purposes, and these devices can be produced in parallel (Matthias and Mueller, 2003). Therewith, the road to large-scale production is open.

The control over various shapes and scales that is possible now within micro-technology may be the ultimate tool for biocatalyst and process design. This may seem farfetched at first sight. Nevertheless, Prof. Takehito Kitamori runs a micro-technological test plant that produces 30 tons of polymers per year (Kitamori, 2003; Kikutani, and Kitamori, 2003; Tokeshi *et al.*, 2003).



## SUMMING UP

A large number of phenomena are involved in biocatalysis that each play at their own level of detail and are functions of different parameters. However, when optimizing existing biocatalysts or developing new ones, the resulting interplay between biological, chemical and physical characteristics must comply with process demands. Because the particle behavior is the result of a complex interplay of the quantities involved, they are preferably studied in coherence. However, the resolution at which information is desired makes simultaneous analysis difficult. In many cases, therefore, parameters are studied individually with dedicated preparation and detection techniques. Because of their multitude, the contribution of each phenomenon in the overall particle performance is not intuitively resolved. Consequently, the overall concept must be integrated in a mechanistic model to allow its validation against experimental data.

With the model, many virtual experiments on differing conditions and configurations can quickly be evaluated at-the-desk. The outcome provides insight in the bottlenecks of the biocatalytic system, and may identify the most promising target areas for improvement.

Some examples of possible developments in enzyme and matrix modification, reactor operation, and micro-technology are given. One or more of these areas should be pursued to develop an optimal biocatalyst for cephalixin synthesis. However, the qualities that the optimal biocatalyst should have are determined by industrial and economic boundary conditions. For this, all costs have to be considered, which is outside the scope of the present research. However, once the optimization criteria are determined, our model will play a central role in the production of the optimal biocatalyst for cephalixin synthesis.

## REFERENCES

- Alkema W.B.L., Hensgens C.M.H., Snijder H.J., Keizer E Dijkstra B.W., and Janssen D.B. (2004). Structural and kinetic studies on ligand binding in wild-type and active-site mutants of penicillin acylase. *Protein Engineering Design and Selection* 17: 473-480.
- Bouwer J.C., Mackey M.R., Lawrence A., Deerinck T.J., Ying Z., Terada M., Martone M.E., Peltier S., and Ellisman M.H. (2004). Automated most-probable

- loss tomography of thick selectively stained biological specimens with quantitative measurement of resolution improvement. *J. Struct. Biol.* **148**: 297-306.
- Centi G., and Perathoner S.** (2003). Integrated design for solid catalysts in multiphase reactions. *CATTECH* **7**: 78-89.
- Chaplin M.** (2002). Methods of immobilization. <http://www.sbu.ac.uk/biology/enztech/immethod.html>.
- Cloix J. F., and Wainer I.W.** (2001). Development of an immobilized brain glutamine synthetase liquid chromatographic stationary phase for on-line biochemical studies. *J. Chromatogr. A* **913**: 133-140.
- De Smet L.C.P.M., Pukin A.V., Stork G.A., De Vos C.H.R., Visser G.M., Zuilhof H., and Sudhölter E.J.R.** (2004). Syntheses of alkenylated carbohydrate derivatives toward the preparation of monolayers on silicon surfaces. *Carbohydr. Res.* **339**: 2599-2605.
- Diano N., Grano V., Rossi S., Bencivenga U., Portaccio M., Amato U., Carfora F., Lepore M., Gaeta F.S., and Mita D.G.** (2004). Hollow-fiber enzyme reactor operating under nonisothermal conditions. *Biotechnology Progress*. **20**(2): 457-466.
- Eijsink V.G.H., Bjork A., Gaseidnes S., Sirevag R., Synstad B., Van den Burg B., and Vriend, G.** (2004). Rational engineering of enzyme stability. *J. Biotechnol.* **113**: 105-120.
- Eldin M.S.M., Santucci M., Rossi S., Bencivenga U., Canciglia P., Gaeta F.S., Tramper J., Janssen A.E.M., Schroën C.G.P.H., and Mita D.G.** (2000) Non-isothermal cephalixin hydrolysis by penicillin G acylase immobilized on grafted nylon membranes. *J. Molec. Catalysis B. Enzymatic.* **8**: 221-232.
- Fuentes M., Maquiese J.V., Pessela B.C.C., Abian O., Fernandez-Lafuente R., Mateo C., and Guisan J.M.** (2004). New cationic exchanger support for reversible immobilization of proteins. *Biotechnol. Progr.* **20**: 284-288.
- Gijsbertsen-Abrahamse A., Van der Padt A., and Boom R.M.** (2004). Status of cross-flow membrane emulsification and outlook for industrial application. *J. Membr. Sci.* **230**: 149-159.
- Jensen K.F.** (2001). Microreaction engineering – is small better? *Chem. Eng. Sci.* **56**: 293-303.
- Jing H., Li X.F., Evans D.G., Duan X., and Li C.Y.** (2000). A new support for the immobilization of penicillin acylase. *J. Mol. Catal. B Enz.* **11**: 45-53.
- Jing W., Wu J., Xing W., Jin W., and Xu N.** (2005). Emulsions prepared by two-stage ceramic membrane jet-flow emulsification. *Part. Technol. Fluid.* **51**: 1339-1345.
- Keusgen M., Glodek J., Milka P., and Krest I.** (2001). Immobilization of enzymes on PTFE surfaces. *Biotechnol. Bioeng.* **72**: 530-540.
- Kitamori T.** (2003). Integrated micro-nano chemical and bio systems. <http://www.unisa.edu.au/promo/2003/micronano.pdf>.
- Kikutani Y., and Kitamori T.** (2003). Micro-Flow reaction systems for combinatorial syntheses. *Macromol. Rapid Commun.* **25**: 158–168.
- Lee M.Y., Srinivasan A., Ku B., and Dordick J.S.** (2003). Multienzyme catalysis in microfluidic biochips. *Biotechnol. Bioeng.* **83**: 20-28.
- Lundgren S., Russom A., Jönsson C., Stemme G., Haswell S.J., Andersson H., and Moberg C.** (2004). Microreactors for the optimization of reaction conditions in asymmetric metal catalysis. In: Micro Total Analysis Systems. The Royal Society of Chemistry, Cambridge, England.

- Ma G.H., Chen A.Y., Su Z.G., and Omi S.** (2003). Preparation of uniform hollow polystyrene particles with large voids by a glass-membrane emulsification technique and a subsequent suspension polymerization. *J. Appl. Pol. Sci.* **87**: 244-251.
- Matthias S., and Mueller F.** (2003). Asymmetric pores in a silicon membrane acting a massively parallel Brownian ratchets. *Nature* **424**: 53-57.
- Modi A.T., Kjonstad, T.A., and White B.J.** (2004). Comparison of EDX and AA to determine distribution of  $\text{Ca}^{2+}$  in *Phaseolus vulgaris* (L.) seed parts following osmopriming. *S. Afr. J. Bot.* **70**: 298-302.
- Moulijn J.A., Perez-Ramirez J., Van Diepen A., Kreutzer M.T., and Kapteijn F.** (2003). Catalysis engineering on three levels. *Int. J. Chem. React. Eng.* **1**: R4 (<http://www.bepress.com/ijcre/vol1/R4>).
- Mulder M.** (1996). Basic Principles of Membrane Technology. Kluwer Academic Publishers Dordrecht The Netherlands.
- Nakashima T., Shimizu M., and Masato K.** (2000). Particle control of emulsion by membrane emulsification and its applications. *Adv. Drug Del. Rev.* **45**: 47-56.
- Nisisako T., Torii T., and Higuchi T.** (2004). Novel microreactors for functional polymer beads. *Chem. Eng. J.* **101**: 23-29.
- Novick S.J., and Dordick J.S.** (2000). Investigating the effects of polymer chemistry on activity of biocatalytic plastic materials. *Biotechnol. Bioeng.* **68**: 665-671.
- Okushima S., Nisisako T., Torii T., and Higuchi T.** (2004). Controlled production of monodisperse double emulsions by two-step droplet breakup in microfluidic devices. *Langmuir* **20**: 9905 -9908.
- Pereira-Filho E.R., Perez C.A., Poppi R.J., and Arruda M.A.Z.** (2002). Metals distribution and investigation of L'vov platform surface using principal component analysis multi-way principal component analysis micro synchrotron radiation X-ray fluorescence spectrometry and scanning electron microscopy after the determination of Al in a milk slurry sample. *Spectrochim. Acta B Atom. Spectrosc.* **57B**: 1259-1276.
- Ragnitz K., Syltatk C., and Pietzsch M.** (2001). Optimization of the immobilization parameters and operational stability of immobilized hydantoinase and L-N-carbamoylase from *Arthrobacter aurescens* for the production of optically pure L-amino acids. *Enzyme Microb. Technol.* **28**: 713-720.
- Schroën C.G.P.H., Fretz C.B., De Bruin V.H., Berendsen W., Moody H.M., Roos E.C., Van Roon J.L., Kroon P.J., Strubel M., Janssen A.E., and Tramper J.** (2002). Modeling of the enzymatic kinetically controlled synthesis of cephalixin: influence of diffusion limitation. *Biotechnol. Bioeng.* **80**: 331-340.
- Tokeshi M., Kikutani Y., Hibara A., Sato K., Hisamoto H., and Kitamori T.** (2003). Chemical processing on microchips for analysis synthesis and bioassay. *Electrophoresis* **24**: 3583-3594.
- Utada A.S., Lorenceau E., Link D.R., Kaplan P.D., Stone H.A., and Weitz D.A.** (2005). Monodisperse double emulsions generated from a microcapillary device. *Science* **308**: 537-541.
- Van Rijn C.** (2002). Nano and micro engineered membrane technology. Aquamarijn Research BV Zutphen The Netherlands.
- Vladisavljevic G.T., and Williams R.A.** (2005). Recent developments in manufacturing emulsions and particulate products using membranes. *Adv. Coll. Interf. Sci.* **113**: 1-20.

- Vertesi A., Simon L.M., Kiss I., and Szajani B.** (1999). Preparation characterization and application of immobilized carboxypeptidase A. *Enzyme Microb. Technol.* **25**: 73-79.
- Wang P., Dai S., Waezsada S.D., Tsao A. Y., and Davison B.H.** (2001). Enzyme stabilization by covalent binding in nanoporous sol-gel glass for nonaqueous biocatalysis. *Biotechnol. Bioeng.* **74**: 249-255.
- Wooley K.L., Moore J.S., Wu C., and Yang Y.** (2000). Molecular to nanoscale order in three dimensions. *Proc. Natl. Acad. Sci. U.S.A.* **97**: 11147-11148.
- Ziese U., Kubel C., Verkleij A.J., and Koster A.J.** (2002). Three-dimensional localization of ultrasmall immuno-gold labels by HAADF-STEM tomography. *J. Struct. Biol.* **138**: 58-62.

---

## Chapter 9 Epilogue



In the previous chapters, one key concept was used throughout, but was not defined: heterogeneity. In this thesis, I have used this term rather intuitively, but the longer I have worked on this topic, the less I understood what heterogeneity really meant. The English Dictionary did not help much. Take the first definition (see below) as an example: “Composed of unrelated or differing parts or elements” Would this make a glass of rainwater heterogeneous?

The Times English Dictionary:

**Heterogeneous** *adj* 1 composed of unrelated or differing parts or elements. 2 Not the same kind or type. 3 *Chem.* Of, compound of, or concerned with two or more different phases. [C17: From Medieval Latin *heterogeneous*, from Greek *heterogenes*, from *HETERO* + *genos* sort] Compare homogeneous.

**Homogeneous** *adj* 1 composed of similar or identical parts or elements. 2b of uniform nature. 3 similar in kind or nature. 4 having a constant property, such as density throughout. 5 *Maths.* 5a (of a polynomial) containing terms of the same degree with respect to all the variables, as in  $x^2 + 2xy + y^2$ . 5b (of a function) containing a set of variables such that when each is multiplied by a constant, this constant can be eliminated without changing the value of the function, as in  $\cos x/y + x/y$ . 5c (of an equation) containing a homogeneous function made equal to 0. 6 *Chem.* Of. Composed of, or concerned with a single phase. Compare heterogeneous.

If we look at it with our naked eye, most of us would probably not classify the liquid in the glass as “composed of unrelated or differing parts or elements”. The definition of the second entry would be more appropriate: the content in the glass would be called a homogeneous liquid. This statement, based on macroscopic observation, however, would be subtler if we looked at the same liquid under a microscope. Here we would probably encounter micro-organisms (e.g. micro algae or bacteria), and the liquid that was previously defined as homogeneous, must now be defined as heterogeneous by the same definition. Suppose we filter-

sterilize the water to remove all micro-organisms. Would this make the filtrate homogenous? Probably it would, if we looked at it with a light microscope. At the nano-scale level of electron microscopy, however, we will most likely encounter cell organelles, protein agglomerates and other very small structures. Consequently, we would once more have to change our classification, this time from homogeneous to heterogeneous.

This line of reasoning ends at the level of quarks, and only so because these currently are the smallest particles that are acknowledged. Evidently, a definition in which everything is classified as heterogeneous except a homogeneous limit situation is not what we mean in our day-to-day usage of heterogeneity, nor what was meant with it in this thesis.

Reading literature on the concept, I immediately ran into the fields of biology and ecology, where I found (partly to my relief) that these issues existed a long time in these fields of expertise. As early as in the beginning of the 19<sup>th</sup> century, Von Humboldt published on the distribution of vegetative zones over a large space (Von Humboldt, 1807). After that, biologists and mathematicians worked on the analysis and characterization of different sorts of heterogeneity. In ecology, efforts to develop methods to quantify spatial heterogeneities began in the 1980's (e.g. Romme, 1982). Although at present hundreds of papers are available on measurement of various aspects of spatial heterogeneity, its quantification remains problematic, because the phenomena are complex (Gustafson, 1998) and because the components of heterogeneity are not well defined (Li and Reynolds, 1994). In the last decennia of the 20<sup>th</sup> century, several authors called for better definition of the concept heterogeneity, and, for lack of better, some tried to give their own (e.g Adler *et al.*, 2001).

To date, I'm still not sure what the definition of heterogeneity is or should be. However, I think the cause for the faulty line of reasoning on the heterogeneity of the rainwater given before had to do with under-definition of the concept. In my opinion, two major additions must be made. One: declare the concept only for a defined quantity of interest. Two: incorporate scale into the definition.

The first addition may sound trivial, but care must be taken to avoid confusing statements. Depending on the property of interest, the answer to the question whether or not the system is heterogeneous may vary. For example: a solution



that contains a concentration gradient but not a temperature gradient is homogeneous in temperature but heterogeneous in concentration. The question if this system is heterogeneous should therefore immediately be replied with: “With respect to what property?” Li and Reynolds (1995) call this “the definition of the system property”. Doing so, heterogeneity itself is implicitly used as a quantity that concerns the changeability of an intensive quantity, which are the only quantities that can vary along a spatial coordinate.

The second addition is more complex and states that heterogeneity is a function of scale. Implicitly, the problems encountered in the example had to do with scale. A property (structure in the case of the example) that appears to be homogeneous at one scale, may appear heterogeneous at a higher magnification. The opposite can also happen. Suppose a person is looking around in the middle of a large forest. To the observer, the distribution of trees may look homogeneous in each direction. If the same observer would look at the tree distribution from a helicopter above the forest, he may see open and dense spots in the forest, or see the adjacent landscapes. At this reduced magnification, the tree distribution of the forest may not be homogeneous at all.

Thus, in the description of spatial and temporal distributions of intensive quantities, scale is a key concept. Scale refers to the dimension of the observed and is associated with both observation and analysis. In some cases the scale of observation may be chosen deliberately to emphasize certain key features of a system, but often it is imposed on us by capabilities of perception, or by technological constraints (Avois-Jacquet and Legendre, submitted). The scale of observation contains three properties (Dungan *et al.*, 2002 and Legendre and Legendre, 1998). The first property is ‘grain size’, which is the size of the elementary unit. It indicates the lowest level of detection, i.e. the resolution. The second property is the ‘sampling interval’, which is the distance between neighboring sampling units. The lowest sampling interval (most samples) is at the grain size. The last element of scale is the ‘extent’, the total length or area included in the study. The extent is determined once the system boundaries have been chosen.

As has become clear from the two previous examples, the scale of observation determines our view of the heterogeneity of the system. In the example of the glass of water, the micro-organisms were below the grain size when observed

with the naked eye. No perturbations larger than the grain size (resolution of the human eye) were within the extent of research, even when sampling (looking in this case) at a grain-size interval. With a light microscope, the grain size became much smaller. In this case, the size of the micro-organism was larger than the grain size and the liquid will determined to be heterogeneous. However, by increasing magnification and resolution, also the extent was reduced. Therefore, if the concentration of micro-organisms was low enough, it might also be possible that no micro-organism was observed within the extent, leading to the conclusion that the liquid was homogeneous. Thus, two opposite conclusions may be drawn on a single system with identical grain, sample size and extent. This indicates that one has to be very careful in formulating conclusions on heterogeneity and that, preferably, many extents on different locations have to be observed at a particular scale.

Here another important question comes about: “What is the proper scale for determination of heterogeneity?” One uniform answer to this question may be impossible to give, because it depends on the information that the observer wants to extract from the system. For instance, if the observer was interested in giving a description of the appearance of the liquid in the glass to somebody unable to see it, he could say that is a clear, homogeneous, colorless liquid. Here the grain is the resolution of the human eye, and this scale is perfectly suited to extract the desired information. However, if the observer wanted to know if there was any microbiological contamination of the liquid, he would have to increase resolution and decrease the grain.

Typically, however, it is not known beforehand at which scale phenomena are important for the overall behavior of a system with predetermined extent. Suppose a researcher wants to study the movement of a school of fish in a defined part of the ocean. It is difficult to say beforehand which processes are determining the heterogeneity in space and time. Are seasonal heterogeneities in ocean currents and temperature gradients, acting over 100's of kilometers the main cause for the spatial variability in the fish schools? Or do processes occurring at much smaller scale, e.g. local nutrient availability, also play a role? In such cases it is necessary to observe phenomena that may be causal for heterogeneity at various levels of scale. Correlation studies will then have to pinpoint the main dependencies of the phenomenon observed and can define the

scale (grain size sampling interval and extent) at which the study on heterogeneity should take place.

For the research described in this thesis, a progressive resolution of analysis was chosen intuitively. In case of Assemblase<sup>®</sup>, light-microscopy had sufficient resolution to elucidate the global enzyme distribution of the biocatalytic particles (Chapter 4). In hindsight, this micro-scale level of detail proved to be sufficient for the model description of Assemblase<sup>®</sup> behavior (Chapter 7). While the nano-scale level of detail (TEM, Chapter 5) was not required for the adequacy of the model, it was found to provide useful information for future particle improvements. The observation that the locally and abruptly increased enzyme concentrations coincided with local deviations in matrix structure led to a thermodynamic reasoning, which may be a future basis for rationally controlled heterogeneity. This result, however, was obtained serendipitously.

The previous section is far from complete. We have not yet begun to divide heterogeneity in subclasses and nothing was said on how to express heterogeneity. These are interesting but difficult subjects, on which the scientific discussion of clarifying and defining is still going on. The interested reader is referred to an excellent overview collected by Peterson and Parker (1998), which covers different kinds of heterogeneity, and its relation to scale in ecological systems. Especially the contribution from Gardner (Chapter 2) is very interesting. Kolasa and Pickett (1991) bundled literature on terminology, multi-scale analysis, kinds of heterogeneity and even on the heterogeneity of heterogeneity. These extensive works illustrate the complexity of the classification of heterogeneity and of expressing it in explicit relations: it involves advanced mathematics (including statistics and fractal analysis).

If you would ask me, therefore: “What *is* heterogeneity?”, I’m afraid my answer would be: “I have no idea.”

## REFERENCES

- Adler P.B., Raff D.A., and Lauenroth W.K.** (2001) The effect of grazing on the spatial heterogeneity of vegetation. *Oecologia* **128**: 465-479
- Avois-Jacquet C., and Legendre P.** Implications of heterogeneity and scale in zooplankton spatial variability. *Oikos* submitted for publication.

- Dungan J.L., Perry J.N., Dale M.R.T., Legendre P., Citron-Pousty S., Fortin M.-J., Jakomulska A., Miriti M., and Rosenberg M. S.** (2002) A balanced view of scale in spatial statistical analysis. *Ecography* **25-5**: 626-640.
- Gustafson E.J.** (1998). Quantifying Landscape Spatial Pattern: What is the state of the art? *Ecosystems* **1**: 143-156.
- Kolasa J., and Pickett S.T.A.,** eds. (1991) Ecological Heterogeneity. *Springer-Verlag* New York USA.
- Legendre P., and Legendre L.** (1998). Numerical Ecology. 2<sup>nd</sup> English ed. *Elsevier Science* Amsterdam The Netherlands.
- Li H., and Reynolds J.F.** (1993). A new contagion index to quantify spatial patterns of landscapes *Landscape Ecol.* **8**: 155-162
- Li H., and Reynolds J.F.** (1995). On definition and quantification of heterogeneity. *Oikos* **72**:280-284.
- Peterson D.L., and Parker V.T.,** eds. (1998) Ecological Scale. Theory and Applications. *Columbia University Press* New York USA.
- Romme W.H.** (1982). Fire and landscape diversity in sub-alpine forests of Yellowstone National Park. *Ecol. Monogr.* **52**: 199-221
- Von Humboldt A.** (1807). Ideen zu einer Geographie der Pflanzen nebst einem Naturgemälde der Tropenländer. Cotta, Tübingen.

## Summary

Assemblase<sup>®</sup> is an industrially applied immobilized penicillin-G acylase. It catalyzes the synthesis of the semi-synthetic  $\beta$ -lactam antibiotic cephalexin (CEX) from 7-amino deacetoxy cephalosporinic acid (7-ADCA) and (D-)(-)-phenylglycine amide (PGA). In addition to the coupling reaction, also two unwanted side-reactions are catalyzed: the hydrolysis of PGA to the inactive by-product phenylglycine (PG) and the hydrolysis of CEX to 7-ADCA and PG. Compared to a free-enzyme reaction, CEX synthesis with Assemblase<sup>®</sup> is sub-optimal, both in terms of selectivity for CEX synthesis over PG hydrolysis (decreased synthesis/hydrolysis ratio, S/H) and of CEX yield on both substrates.

In literature, an extensive body of data was available on Assemblase<sup>®</sup>-catalyzed cephalexin synthesis. However, quantitative information on the Assemblase<sup>®</sup> performance on the basis of the underlying physical and chemical mechanisms was scarce at best. Because the phenomena involved take place at various scales, it was decided to study them at an increasing level of detail (resolution), until an adequate description of the system would be obtained. First, an inventory was made of available techniques for visual inspection of the Assemblase<sup>®</sup> interior, both with respect to intra-particle enzyme distribution and support matrix characteristics (Chapter 2).

Subsequently, the kinetic behaviour of Assemblase<sup>®</sup> was analyzed by external, macroscopic means, i.e. without any intra-particle observations (Chapter 3). The size-dependent quantitative enzyme loading of Assemblase<sup>®</sup> was determined. From macroscopic observations on mass-transfer limited CEX-synthesis experiments, a heterogeneous intra-particle enzyme distribution with most biocatalyst present in the outer 100  $\mu\text{m}$  of the particle was estimated. However,

this could not provide a sufficient description of the particle behaviour in various reaction conditions.

Being an essential characteristic of Assemblase<sup>®</sup>, the size-dependent quantitative intra-particle enzyme distribution was measured (Chapter 4). To this end, multiple particles of different sizes were each cut in multiple sections, which were immunochemically labelled for penicillin-G acylase presence. After enzyme detection with light microscopy (LM), image analysis showed that the intra-particle distributions resembled unsteady-state enzyme-diffusion profiles. These profiles were successfully expressed by a size-dependent Fourier number for (enzyme) mass transport.

The relation between heterogeneity in enzyme concentration and in the structure of the support material was studied at high resolution (Chapter 5). Globally, transmission electron microscopy (TEM) confirmed the size-dependent enzyme gradient observed with light microscopy. Locally, however, abrupt deviations in enzyme concentration were observed at the particle surface (1.4-fold) and in areas (designated halos) that surrounded internal voids (7.7-fold). Cryogenic field-emission scanning electron microscopy (cryo-FESEM) on cryo-planed surfaces related these local heterogeneities to local deviations in the matrix structure. Cryo-FESEM additionally indicated that the matrix was locally enriched in chitosan, which is one of the two matrix polymers of Assemblase<sup>®</sup>. This was supported by a basic thermodynamic line of reasoning on polymer demixing during particle formation.

Although the resolution of TEM and cryo-FESEM analysis is exemplary, these methods each study a single phenomenon and each requires its own sample preparation method. This inevitably complicates the interpretation of the results. Therefore, a technical feasibility study was set up, to evaluate if ambient-temperature FESEM could serve as an integral alternative to study the above-mentioned phenomena in a single sample with a single piece of equipment (Chapter 6). The results were benchmarked against previous results obtained with TEM and cryo-FESEM. Although integration of different measurements with FESEM involved some concessions with respect to resolution, for the Assemblase<sup>®</sup> system this integrated approach proved to be an attractive alternative to the two previously used methods.

From data gathered hitherto, a single, representative Assemblase<sup>®</sup> particle was inferred, with a typical particle size and enzyme distribution. Combined with additional experiments on intra-particle reactant diffusivities, an integrated mechanistic model for Assemblase<sup>®</sup>-catalyzed CEX synthesis was developed (Chapter 7). The model features, among other things, reactions in a heterogeneous enzyme system, electrostatically coupled diffusive mass transfer, and pH-dependent dissociation of reactants.

The model was successfully validated against synthesis experiments for conditions ranging from heavily diffusion-limited to hardly diffusion-limited, including substrate concentrations from 50 to 600 mM, temperatures between 273 and 303 K and pH's between 6 and 9. The pH gradients inside Assemblase<sup>®</sup> during CEX synthesis as reported by others were predicted correctly. The model provides physical insight in the complex interplay between the individual processes leading to the sub-optimal cephalixin synthesis with Assemblase<sup>®</sup>, and may therefore give important clues for future biocatalyst design.

Although the integrated mechanistic model identifies the bottlenecks of the biocatalytic system, it does not determine the scientific area into which future improvements should be made. This depends on the outcome of an economic evaluation, which lies outside of the scope of this work. Therefore, in Chapter 8 an overview is given of promising developments in enzyme biochemistry, material science, reactor engineering and micro-technology that all can become relevant in future biocatalyst design.





## Samenvatting

Assemblase is een industrieel geïmmobiliseerd penicilline-G acylase. Het katalyseert de synthese van het semi-synthetisch  $\beta$ -lactam antibioticum cefalexine (CEX) uit 7-amino deacetoxycephalosporinezuur (7-ADCA) and (D-)(-)-fenyglycine amide (PGA). Naast deze koppelingsreactie worden twee ongewenste nevenreacties gekatalyseerd: de hydrolyse van PGA tot het inactieve bijproduct fenylglycine (PG) en hydrolyse van het eerder gevormde CEX tot 7-ADCA en PG. In vergelijking met de vrij-enzym-reactie verloopt de CEX-synthese met Assemblase<sup>®</sup> suboptimaal, zowel op het gebied van de selectiviteit voor CEX synthese over PG hydrolyse (verlaagde synthese/hydrolyse ratio, S/H), als op het gebied van de CEX-opbrengst op beide substraten.

Hoewel er in de literatuur reeds een aanzienlijke hoeveelheid data beschikbaar was over de Assemblase<sup>®</sup>-gekatalyseerde cefalexinesynthese, was kwantitatieve informatie over het gedrag van Assemblase op basis van natuurkundige en chemische mechanismen schaars. Omdat de betrokken fenomenen zich op verschillende schalen afspelen, werd besloten deze te bestuderen op een progressief detailniveau (resolutie), totdat op basis van die studie een adequate systeembeschrijving mogelijk was. Daartoe werd als eerste een inventarisatie gemaakt van de beschikbare technieken voor visuele inspectie van de intrapartikel-enzymverdeling en van de interne matrixstructuur van Assemblase (Hoofdstuk 2).

Vervolgens werd het kinetische gedrag van Assemblase geanalyseerd op basis van externe waarnemingen (Hoofdstuk 3). Op basis van macroscopische metingen aan massatransportgelimiteerde CEX-syntheseexperimenten werd een heterogene intrapartikel-enzymverdeling geschat: het enzym werd geacht gelocaliseerd te zijn in de buitenste 100  $\mu\text{m}$  van het deeltje. Deze schatting,

echter, kon het gedrag van Assemblase niet afdoende beschrijven voor de verscheidene reactiecondities.

Omdat de enzymverdeling een essentiële deeltjeskarakteristiek van Assemblase is, werd de intrapartikel-enzymverdeling in Assemblase gemeten (Hoofdstuk 4). Daartoe werden meerdere deeltjes elk in meerdere coupes gesneden, die elk immunologisch gelabeld werden op aanwezigheid van penicilline-G acylase. Na lichtmicroscopische detectie werd met behulp van beeldverwerkingsroutines vastgesteld dat de enzymprofielen de gedaante hadden van instationaire diffusieprofielen. De profielen werden wiskundig gekarakteriseerd door een grootte-afhankelijk Fouriergetal voor massatransport van het enzym.

De relatie tussen heterogeniteit in enzymconcentratie en de structuur van het dragermateriaal werd met hoge resolutie onderzocht in Hoofdstuk 5. Met transmissie-electronenmicroscopie (TEM) werd de globale, diameterafhankelijke enzymdistributie, zoals eerder gevonden met lichtmicroscopie, bevestigd. Op een localer niveau, echter, werden abrupte deviaties van de enzymconcentratie waargenomen aan het deeltjesoppervlak (1.4 maal hogere enzymconcentratie dan de omgeving) en in gebieden die de interne makro-holten omsloten (halo's genoemd, tot 7.7 maal hogere enzymconcentraties dan de omgeving). Met cryogene veld-emissie scanning-electronenmicroscopie (cryo-FESEM) op koud-afgevlakte oppervlakken werden deze lokale heterogeniteiten gerelateerd aan locale deviaties in de matrixstructuur. De studie indiceerde tevens dat deze gebieden lokaal verrijkt waren met chitosan, één van de twee polymeren waaruit de Assemblasematrix is opgebouwd. Deze indicatie werd ondersteund door explorerende thermodynamische berekeningen over polymeerontmeling tijdens deeltjesproductie.

Hoewel de resolutie van TEM en cryo-FESEM exemplarisch is, bestuderen ze elk slechts één enkel fenomeen en hebben daartoe elk een specifieke preparatiemethode nodig, wat de interpretatie van de resultaten compliceert. Daarom werd een technische haalbaarheidsstudie gestart naar het gebruik van FESEM op kamertemperatuur, als geïntegreerd alternatief voor beide bovenstaande methoden (Hoofdstuk 6). De aldus verkregen resultaten werden getoetst aan die eerder verkregen met TEM en cryo-FESEM. Hoewel deze detectiemethode enig negatief effect bleek te hebben op de resolutie, bleek deze

voor het geval van Assemblase<sup>®</sup> een attractief alternatief voor beide eerder gebruikte methoden.

Uit de tot dan toe verkregen resultaten werd een enkel representatief Assemblasedeeltje afgeleid, met een typische deeltjesgrootte en een typische enzymdistributie. In combinatie met metingen aan de diffusiecoëfficiënten van de reactanten werd een geïntegreerd mechanistisch model voor de Assemblase-gekatalyseerde CEX-synthese ontwikkeld (Hoofdstuk 7). Het model incorporeert onder andere reacties in een heterogeen enzymstelsel, elektrostatisch gekoppeld diffusief massatransport en pH-afhankelijke dissociatiereacties.

Het model werd succesvol gevalideerd tegen synthese-experimenten voor condities variërend van nauwelijks tot zeer diffusielimiteerd, inclusief substraatconcentraties van 50 tot 600 mM, temperaturen tussen 273 and 303 K en pHs tussen 6 and 9. Het gevalideerde model bleek de door anderen gemeten pH-gradiënten die tijdens de CEX-synthese in Assemblase<sup>®</sup> optreden goed te voorspellen. Daar het model inzicht verschaft in het complexe samenspel van de individuele processen dat leidt tot het suboptimale gedrag van Assemblase<sup>®</sup> tijdens de CEX-synthese, levert het mogelijk interessante aanwijzingen op voor toekomstig biokatalysatorontwerp.

Hoewel het model de limitaties van het huidige systeem kan identificeren, voorspelt het niet in welke specifieke richting vervolgonderzoek gedaan zou moeten worden. Dit hangt af van de uitkomst van een economische evaluatie welke buiten het doel van dit onderzoek valt. In Hoofdstuk 8 is daarom volstaan met het geven van een overzicht van een aantal mogelijke ontwikkelingen op de vakgebieden enzymbiochemie, materiaalkunde, reactorkunde en microtechnologie, die alle relevant kunnen zijn voor toekomstige ontwikkelingen in biokatalysatorontwerp.



## List of publications

**Van Roon J.L., Beftink H.H., Schroën C.G.P.H., and Tramper J.** (2002). Assessment of intraparticle biocatalytic distributions as a tool in rational formulation. *Curr. Opin. Biotechnol.* 13: 398-405.

**Van Roon J.L., Joerink M., Rijkers M.P.W.M., Tramper J., Schroën C.G.P.H., and Beftink H.H.** (2002). Enzyme distribution derived from macroscopic particle behavior of an industrial immobilized penicillin-G acylase. *Biotechnol. Progr.* 19: 1510-1518.

**Van Roon J.L., Groenendijk E., Kieft H., Schroën C.G.P.H., Tramper J., and Beftink H.H.** (2005). Novel approach to quantify immobilized-enzyme distributions. *Biotechnol. Bioeng.* 89: 660-669.

**Van Roon J.L., Boom R.M., Paasman M.A., Tramper J., Schroën C.G.P.H., and Beftink H.H.** (2005). Enzyme distribution and matrix characteristics in biocatalytic particles. *J. Biotechnol.*, <http://dx.doi.org/10.1016/j.jbiotec.2005.04.012>.

**Van Roon J.L., van Aelst A.C., Schroën C.G.P.H., Tramper J., and Beftink H.H.** (2005). FESEM analysis of morphology and enzyme distribution within an industrial biocatalytic particle. *Scanning* 27: 181-189.

**Schroën C.G.P.H., Fretz C.B., De Bruin V.H., Berendsen W., Moody H.M., Roos E.C., Van Roon J.L., Kroon P.J., Strubel M., Janssen A.E., and Tramper J.** (2002). Modeling of the enzymatic kinetically controlled synthesis of cephalixin: influence of diffusion limitation. *Biotechnology and Bioengineering* 80:331-340.

**Van Roon J.L., Beeftink H.H., Schroën C.G.P.H., and Tramper J.** (2002). The role of the quantitative biocatalyst distribution in the design of biocatalytic particles. Lecture on the European Symposium on Biochemical Engineering Science (ESBES-4). In ESBES-4 Symposium – Life: Science and Technology, Book of abstracts, 32

**Tramper J, Beeftink H.H., Janssen A.E.M., Ooijkaas L.P., Van Roon J.L., Strubel M., and Schroën C.G.P.H.** (2001). Biocatalytic production of semi-synthetic cephalosporins: process technology and integration. In Synthesis of  $\beta$ -lactam antibiotics: Chemistry, Biocatalysis & Process Integration. Edited by Bruggink A. Dordrecht: Kluwer Academic Publishers 207-250.

**Schroën C.G.P.H., and Van Roon J.L.** (2003). Groene routes voor de antibiotica-productie. Resultaat van een levendige synthese tussen universiteiten en het bedrijfsleven. *NPT procestechnologie* 10-4:16-20.

Submitted for publication:

**Van Roon J.L., Arntz M.M.H.D., Kallenberg A.I., Paasman M.A., Tramper J., Schroën C.G.P.H., and Beeftink H.H.** (2005). A multi-component reaction-diffusion model of a heterogeneously distributed immobilized enzyme. *Appl.Microbiol.Biotechnol.*

## Nawoord

Met de eindstreep in zicht, is het – na ruim 200 pagina's – toch echt de hoogste tijd om mensen te bedanken voor hun niet geringe bijdrage aan de totstandkoming van dit proefschrift.

Hans (Tramper), in 1998 begon ik in jouw groep als afstudeerstudent. Na een stage mocht ik bij jou terugkeren als AIO: bedankt voor het door jou in mij gestelde vertrouwen. Hoewel je niet altijd de kracht had mij van dichtbij te begeleiden, zal ik je passie voor het vak en je rechtvaardigheidsgevoel niet vergeten.

Niet alleen in je hoedanigheid als copromotor, Rik (Beeftink), wist je altijd de goede vragen te stellen en door te dringen tot de kern van de zaak. Je oprechte belangstelling voor het werk en voor persoonlijke en maatschappelijke zaken die zich daarbuiten afspelen, maakt dat ik enorm veel van je geleerd heb. Het was heel bijzonder om met jou samen te mogen werken de afgelopen jaren. Ik zal het zeker missen.

Copromotor, projectleider, kamergenoot, je was het allemaal Karin (Schroën). In het begin van mijn project wist je me met jouw ervaring een vliegende start te geven. Je vakkennis is gedurende het hele project een belangrijke factor geweest. Bedankt voor je altijd snelle 'service' en je bijdrage aan de manuscripten.

Nauw betrokken bij het werk waren een tweetal begaafde collega's van Plantencelbiologie. Henk (Kieft), zonder jouw ervaring en flexibiliteit hadden we onze 'biocatalytische skippyballen' nooit kunnen labelen en detecteren. Ongelooflijk, hoe goed jij coupes maken kan. Veel van elektronenmicroscopie heb ik mogen leren van jou, Adriaan (van Aelst). Je passie om immer het beste beeld onder nimmer ideale omstandigheden te produceren heeft geleid tot een

mooie publicatie waarin we immunolabels en matrixstructuur in hetzelfde preparaat konden bestuderen (hoofdstuk 6). Remko (Boom), je enthousiasme straalt over de gang. Ik zal niet vergeten dat je, toen je met mij door een oculair van een microscoop stond te turen, door het secretariaat van het lab werd gehaald om je naar je afspraak te sturen. Bedankt voor je thermodynamische bijdrage in hoofdstuk 7.

Kundige en positief-kritische begeleiding kreeg ik van onderzoekspartner DSM. Sander (Arendsen), bedankt voor je scherpe, motiverende begeleiding. Later, Marten (Paasman), volgde jij Sanders taken kundig op. Zeker naar het einde toe werd onze samenwerking intensiever, getuige ook onze gemeenschappelijke publicaties. Alle (Bruggink), dank voor je enthousiaste, maar kritische houding tijdens de werkbesprekingen. Hartelijk dank ook, Marijn (Rijkers), voor je belangstelling en voor het lezen van verschillende manuscripten.

Vrachten werk werd verzet door de studenten, die ik allen zeer erkentelijk ben. Michiel (Joerink): enorme hoeveelheden PGA-hydrolyses vielen je ten deel. De beloning – lekker programmeren in Matlab – was de basis voor de beeldverwerking die we nodig hadden om de enzymgradiënten te kwantificeren. Esther (de Graaf): dankzij jouw metingen aan massa's gelabelde Assemblasecoupes en de beeldverwerking die je verder uitbreidde, hebben we de enzymdistributie zo goed kunnen bepalen. Sander (Thijssen), bedankt voor het bepalen van de reactantdiffusiecoëfficiënten. In jullie afstudeerprojecten maakten jullie, Claartje (Hengeveld), Jolanda (Peeters) en Ruurdje (Anema), het mogelijk om penicilline-G acylase covalent te binden aan verschillende membraantypen en verzorgden jullie een proceskundige modelbeschrijving van het systeem. Delen van jullie werk vinden jullie terug in hoofdstuk 8. Dank jullie wel! Marleen (Arntz), een jaar lang brak je je het hoofd over elektrostatische interacties en elektrolyse. Mede dankzij jouw werk, hebben we een prachtig model kunnen maken. Succes met je eigen promotie!

De collega's bij proceskunde zorgden ervoor dat het werk gedaan werd in een fijne sfeer. Lydia (de Moes), het was een genoegen jouw kamergenoot te zijn de afgelopen jaren. Ondanks onze verschillen hebben we denk ik veel van elkaar opgestoken. Maurice (Strubel), kamergenoot vanaf de eerste dag, bedankt voor je technische ondersteuning bij de diverse HPLC-analyses. Met vragen over welk onderwerp dan ook kon ik bij jou, Mark (van der Veen), altijd terecht. Als



collega-AIO gaf je mij vanuit jouw goede totaalbeeld altijd wel weer een nieuw idee. Wat hebben we het gaaf gehad tijdens de AIO-reizen in Polen en Zuid-Afrika. Ik ben blij dat je mijn paranimf wilt zijn. Geen meestal niet werkgerelateerde (Linux-) vraag was gek genoeg, of jullie, Hylke (van der Schaaf) en Olivier (Sessink), doken vol enthousiasme op het “probleem”. De afgelopen jaren hebben we talloze discussies gevoerd over zeer zinnige, maar ook over zeer onzinnige onderwerpen, en ik hoop dat we die discussies in de toekomst zullen blijven voeren. Wat moest proceskunde toch zonder jouw IT-ondersteuning, Gerrit (Heida), dacht ik toen ik jouw beeldscherm van je bureau jatte, om mijn modellerwerk te vergemakkelijken. Jos (Sewalt) en Arjen (Rinzema), jullie waren fijne collega’s. Hedy (Wessels), wat hebben we geklept over vakanties en wintersport. Bedankt ook voor alle hulp. Joyce (Krauss), je tennis- en kooklessen waren een feest.

Ik ben veel dank verschuldigd aan mijn beste vrienden, die er altijd waren, maar mij nooit iets verweten wanneer ik er weinig was. Herman (de Grijs), wat jammer dat ik de laatste tijd niet veel in Breda kon zijn – Highstreet wacht nog steeds! Bedankt voor je oprechte belangstelling. Raymond (Bastiaansen), ik kan niet wachten tot we weer naar Heilbachsee gaan. Marcel (Hendriks), schandalig dat we dat partijtje squash nu nog steeds niet gespeeld hebben. Bert (Wijnholds), sinds we in 1994 startten als jaargenoten, hebben we heel wat meegemaakt – bedankt!

Oma (van Roon), toen ik 11 jaar geleden ging studeren mocht ik – bij gebrek aan een kamer – bij u en opa wonen. Jullie enthousiasme en geïnteresseerdheid waren fantastisch. Wat hadden we graag gewild dat opa dit nog had mogen meemaken. Jan (Wijnholds), als directeur van Nutrac B.V. was jij drie jaar mijn part-time-baas en gedurende die tijd heb ik enorm veel van je mogen leren en zien (“Ja jongen, zo maak je nog eens wat mee”). Daarnaast ben je als mijn schoonvader een goede raadgever. Greet (Wijnholds), bedankt voor alle hulp en belangstelling; ik ben blij dat ik het met jou en Jan zo goed kan vinden.

Pa en ma, jullie onvoorwaardelijke steun staat aan de basis van alles. Ik ben jullie dankbaar dat jullie me de ruimte gaven dit te doen, en tegelijkertijd zo betrokken wilden zijn. Geniet samen van jullie welverdiende vrije tijd! Daniëlle, hoewel je voor mij altijd mijn kleine zusje zult blijven, ben ik hartstikke trots op je. Ik vind het geweldig dat jij mijn paranimf wilt zijn.

Lieve Janet, sinds ik je voor het eerst zag, meer dan 10 jaar geleden, wil ik bij je zijn. Zonder jou lag dit werk er zeer waarschijnlijk niet. Jij bent de enige die altijd weer in no-time een lach op mijn gezicht weet te toveren. Laten we genieten van de vrije tijd die we nu samen krijgen.

## Curriculum vitae

Jeroen Louis van Roon was born in Eindhoven, The Netherlands on April 29, 1976. In 1994, he completed secondary grammar school in Breda, The Netherlands. Shortly after, he started with the MSc curriculum in Bioprocess Engineering at the former Wageningen Agricultural University, The Netherlands. After a specialization in Biochemical Reactor Engineering, a thesis project in Process Engineering, and an internship at DSM Deretil in Villaricos, Spain, he graduated in January, 2000. In the same month, he started a Ph.D. project at the Food and Bioprocess Engineering Group of Wageningen University, The Netherlands, of which the results are summarized in this thesis. From January, 2002 until January, 2005, he additionally worked part-time as a researcher for Nutrac B.V. in Hoogerheide, The Netherlands. From February, 2005, he is employed as scientist Biochemistry by DSM Food Specialties in Delft, The Netherlands.

Jeroen Louis van Roon werd op 29 april 1976 te Eindhoven geboren. In 1994 behaalde hij het Atheneumdiploma aan de Scholengemeenschap Graaf Engelbrecht te Breda. Aansluitend werd begonnen met de studie Bioprocestechnologie aan de toenmalige Landbouwniversiteit Wageningen. Na een specialisatie in de Biochemische Reactorkunde, een afstudeervak in de Proceskunde en een stage bij DSM Deretil in Villaricos, Spanje, behaalde hij in januari 2000 het ingenieursdiploma. In diezelfde maand werd gestart met een promotieonderzoek bij de sectie Proceskunde aan Wageningen Universiteit, waarvan het resultaat beschreven staat in dit proefschrift. Daarnaast was hij van januari 2002 tot en met januari 2005 in deeltijd werkzaam als onderzoeker bij Nutrac B.V., gevestigd te Hoogerheide. Vanaf februari 2005 is hij werkzaam als onderzoeker Biochemie bij DSM Food Specialties in Delft.



---

---

---

---

---

---